

Optimisation of large-scale offshore wind farms  
considering turbine layout, cable layout, and co-located  
energy storage systems

PhD Thesis

Peter John Taylor

EPSRC Centre for Doctoral Training in Wind & Marine Energy Systems

Department of Electronic & Electrical Engineering

University of Strathclyde, Glasgow

August 25, 2024

This thesis is the result of the author's original research. It has been prepared and written by the author and has not been previously submitted for examination which has led to the award of a degree.

The copyright of this thesis belongs to the author under the terms of the United Kingdom Copyright Acts as qualified by University of Strathclyde Regulation 3.50. Due acknowledgement must always be made of the use of any material contained in, or derived from, this thesis.

# Abstract

This thesis aims to explore two ways in which the electrical infrastructure of a gigawatt-scale offshore wind farm may be optimised to reduce costs and aid the increasing deployment of renewable energy capacity. The two areas considered are (1) the integration of a cable layout optimisation with a turbine layout optimisation forming a novel concurrent optimisation framework, and (2) the integration of energy storage systems into a cable layout optimisation for the purpose of peak-shaving power in the cables enabling alternative cable sizes to be used and reducing peak electrical losses.

While there are a wide variety of approaches to turbine layout optimisation, the particle swarm optimisation (PSO) method offers a good balance between accuracy and computational expense, enabling large-scale problems to be handled by standard desktop PCs. The turbine layout problem is formulated as a grid-based layout, fully defined by eight variables, to comply with maritime navigation and search and rescue regulations, while allowing some deviation to maximise energy capture. The eight variables defining the grid are optimised by means of PSO, followed by a novel micro-siting function to move individual turbines and increase energy yield. The method was compared to SSEs in-house method, matching the energy capture of a case study of their Berwick Bank site to within 0.3%.

Two cable layout optimisation methods from the literature are selected, which are the widely used mixed-integer linear programming (MILP) method, and ant colony optimisation (ACO) representing the increasing use of heuristic approaches. These are compared to a novel ACO-based method, ACOsp, that employs a decomposition strategy. The ACOsp method is shown to maintain the good quality solutions of the MILP approach, with solutions 0.0-1.4% more expensive than optimal, while also demonstrat-

ing the computational efficiency of heuristic approaches, useful for large-scale problems.

An optimisation framework considering the concurrent optimisation of turbine and cable layouts is proposed, with comparison made to a sequentially optimised solutions, isolating the impact of this integration. Solutions of the integrated, concurrent, approach show improved objective values where the increase is statistically significant. For a case study site with 164-165 turbines, the approach increases the objective value (for this maximisation problem) by 0.45%, which is slightly less than the increase found by the addition of one further turbine at 0.55-0.57%.

Considering the limitations of the investigated cable layout optimisation approaches, a following study proposed a MILP-based optimisation in combination with a decomposition strategy, MILPsp. The MILPsp method maintained the accuracy of the MILP method and reduced computational expense, improving on the earlier ACOSp method. Variables describing ESS are integrated into the MILPsp algorithm to determine the impact of using co-located ESS on the array cable network. It was found that very few charging strategies were able to deliver meaningful peak shaving to the power in the array cables and those that did required a very large ESS capacity to do so (3MW/64MWh for a site using 8MW turbines). Further, the required cost of the co-located ESS was prohibitively low, at <£1,800, compared to real ESS prices at the time of writing. Ignoring cost restrictions, using ESS within the cable layout optimisation, for a site containing 122 8MW turbines, was able to reduce cable network costs by 0.22-1.85%.

## Publications

Parts of the work outlined in this thesis have been published:

### **Journal of Physics: Conference Series (2020)**

Taylor, P., Campos-Gaona, D., Yue, H., Anaya-Lara, O., Jia, C., & Ng, C. (2020). Sequential heuristic optimisation of a real offshore wind farm site considering turbine placement and cable layout. *Journal of Physics: Conference Series*

<https://doi.org/10.1088/1742-6596/1669/1/012024>

- This paper covers an initial high-level study of the work presented Chapters 3, 4, and 7.

### **IET Renewable Power Generation (2021)**

Taylor, P., Yue, H., Campos-Gaona, D., Anaya-Lara, O., & Jia, C. (2021). Turbine layout optimisation for large-scale offshore wind farms - a grid-based method. *IET Renewable Power Generation* <https://doi.org/10.1049/rpg2.12295>

- This paper covers the work presented in Chapter 3.

### **IET Renewable Power Generation (2022)**

Taylor, P., Yue, H., Campos-Gaona, D., Anaya-Lara, O., & Jia, C. (2022). Wind farm array cable layout optimisation for complex offshore sites - A decomposition based heuristic approach. *IET Renewable Power Generation*

<https://doi.org/10.1049/rpg2.12593>

- This paper covers the work presented in Chapter 4.

# Contents

<b>Abstract</b>	<b>ii</b>
<b>List of Figures</b>	<b>x</b>
<b>List of Tables</b>	<b>xiv</b>
<b>List of Algorithms</b>	<b>xvii</b>
<b>Acknowledgements</b>	<b>xx</b>
<b>1 Introduction</b>	<b>1</b>
1.1 The Offshore Wind Farm Layout Problem . . . . .	2
1.2 Thesis Aims & Research Questions . . . . .	4
1.3 Novel Contributions . . . . .	5
1.3.1 Turbine Layout Optimisation . . . . .	6
1.3.2 Cable Layout Optimisation . . . . .	6
1.3.3 Integrated Turbine & Cable Layout Optimisation . . . . .	7
1.3.4 Integrated ESS & Cable Layout Optimisation . . . . .	7
1.4 Layout of the Thesis . . . . .	8
<b>2 Background</b>	<b>11</b>
2.1 Turbine Placement Optimisation . . . . .	12
2.1.1 Wind Turbine Wakes . . . . .	13
2.1.2 Problem Formulations . . . . .	16
2.1.3 Optimisation . . . . .	18

## Contents

2.2	Cable Layout Optimisation . . . . .	24
2.2.1	Costs & Electrical Losses . . . . .	24
2.2.2	Collector Network Topologies & Attributes . . . . .	25
2.2.3	Optimisation . . . . .	26
2.3	Integration of Turbine & Cable Layout Optimisation . . . . .	32
2.3.1	Early approaches . . . . .	33
2.3.2	Degrees of integration . . . . .	34
2.3.3	Grid-based turbine layouts . . . . .	35
2.3.4	Heuristic methods . . . . .	36
2.3.5	Increasing the number of turbines . . . . .	37
2.4	Energy Storage Systems . . . . .	38
2.4.1	ESS in Grids with High Renewable Energy Penetration . . . . .	39
2.4.2	Co-located ESS and Wind Turbines . . . . .	40
2.4.3	ESS for Power Smoothing Applications . . . . .	42
2.4.4	Ancillary Service Provision . . . . .	43
2.4.5	Types of ESS . . . . .	45
2.5	Identifying Research Gaps . . . . .	46
2.5.1	Integrated Turbine & Cable Layout Optimisation . . . . .	46
2.5.2	Integrated Cable Layout and ESS Optimisation . . . . .	49
2.6	Thesis Objectives . . . . .	50
<b>3</b>	<b>Turbine Placement Optimisation</b>	<b>51</b>
3.1	Wind Farm Model . . . . .	51
3.1.1	Larsen Wake Model . . . . .	52
3.1.2	Summation of Multiple Wake Effects . . . . .	54
3.1.3	Rotor Effective Wind Speed . . . . .	55
3.2	Formulation of the Turbine Layout . . . . .	55
3.3	Optimisation Methodology . . . . .	58
3.3.1	Problem Formulation . . . . .	58
3.3.2	Algorithm Selection & Implementation . . . . .	61
3.3.3	Additional Improvements . . . . .	63

## Contents

3.3.4	Summary of Optimisation Process . . . . .	69
3.4	Validation . . . . .	71
3.4.1	Wind Farm Model Validation . . . . .	71
3.4.2	Implementation of the Algorithm . . . . .	75
3.4.3	Real Site Case Study . . . . .	76
3.5	Case Studies . . . . .	78
3.5.1	Hypothetical Offshore Wind Farm . . . . .	78
3.5.2	Berwick Bank Offshore Wind Farm . . . . .	81
3.5.3	Summary of Optimisation Process Amendments . . . . .	85
3.6	Results & Discussion . . . . .	86
3.6.1	Hypothetical Offshore Wind Farm Case Study . . . . .	86
3.6.2	Berwick Bank Offshore Wind Farm Case Study . . . . .	90
3.7	Summary . . . . .	92
<b>4</b>	<b>Cable Layout Optimisation</b>	<b>96</b>
4.1	Formulation of the Cable Layout Problem . . . . .	96
4.2	Optimisation Design Methodology . . . . .	98
4.2.1	Algorithm Selection . . . . .	99
4.2.2	Pre-Processing . . . . .	100
4.2.3	Mixed-Integer Linear Programming (MILP) . . . . .	103
4.2.4	Classical Ant Colony Optimisation (ACO) . . . . .	109
4.2.5	ACO with Decomposition into Sub-Problems (ACOSP) . . . . .	112
4.3	Case Studies . . . . .	117
4.3.1	Hypothetical Offshore Wind Farm . . . . .	118
4.3.2	Definition of the Six Case Studies . . . . .	119
4.3.3	Cost Components & Parameters . . . . .	121
4.3.4	Berwick Bank Offshore Wind Farm . . . . .	122
4.4	Results & Discussion . . . . .	125
4.4.1	Hypothetical Offshore Wind Farm . . . . .	125
4.4.2	Berwick Bank Offshore Wind Farm . . . . .	131
4.5	Summary . . . . .	133

<b>5</b>	<b>Integrated Turbine &amp; Cable Layout Optimisation</b>	<b>138</b>
5.1	Integration of Turbine & Cable Layout Optimisation . . . . .	138
5.1.1	Integration into Solution Seeding for the PSO . . . . .	139
5.1.2	Integration into the PSO Algorithm Phase . . . . .	140
5.1.3	Integration into the Micro-siting Phase . . . . .	141
5.1.4	Updating the Cable Routing . . . . .	148
5.1.5	Substation Positioning . . . . .	149
5.1.6	Extending the Model . . . . .	150
5.1.7	The Integrated Optimisation Algorithm . . . . .	150
5.1.8	Turbine Selection Probability . . . . .	152
5.2	Comparison of Sequential & Integrated Optimisations . . . . .	154
5.2.1	Sequential Optimisation Algorithm . . . . .	155
5.3	Results & Discussion . . . . .	156
5.4	Summary . . . . .	162
<b>6</b>	<b>Advanced Cable Layout Optimisation</b>	<b>164</b>
6.1	Methodology . . . . .	165
6.1.1	The Original MILP Model . . . . .	166
6.1.2	Route Finding Algorithm . . . . .	166
6.1.3	Electrical Losses . . . . .	171
6.1.4	Substation Connection Costs . . . . .	174
6.1.5	Cable Crossing Constraint . . . . .	175
6.1.6	Jack-up Vessel Exclusion Zone . . . . .	177
6.1.7	Limiting the Number of Cable Sizes . . . . .	178
6.1.8	Updating the Objective Function . . . . .	180
6.1.9	The MILPsp Algorithm . . . . .	180
6.2	Case Studies . . . . .	187
6.2.1	Hypothetical Offshore Wind Farm . . . . .	187
6.2.2	Expanding the Hypothetical Offshore Wind Farm Case . . . . .	188
6.3	Results & Discussion . . . . .	190
6.3.1	Hypothetical Offshore Wind Farm . . . . .	191

## Contents

6.3.2	Expanded Hypothetical Offshore Wind Farm Case . . . . .	195
6.4	Summary . . . . .	200
<b>7</b>	<b>Influence of Energy Storage Systems</b>	<b>204</b>
7.1	Methodology . . . . .	206
7.1.1	Adapting the MILP Model . . . . .	207
7.1.2	Adapting the MILPsp Algorithm . . . . .	211
7.2	Case Study . . . . .	214
7.2.1	ESS Sizing & Charging/Discharging Strategy . . . . .	214
7.2.2	ESS Costing . . . . .	215
7.2.3	ESS Placement . . . . .	216
7.3	Results & Discussion . . . . .	216
7.3.1	ESS Sizing . . . . .	216
7.3.2	ESS Costing . . . . .	219
7.3.3	ESS Placement . . . . .	227
7.3.4	Limitations . . . . .	237
7.4	Summary . . . . .	238
<b>8</b>	<b>Conclusions</b>	<b>242</b>
8.1	Thesis Summary . . . . .	242
8.1.1	Turbine Placement Optimisation . . . . .	242
8.1.2	Cable Layout Optimisation . . . . .	243
8.1.3	Integrated Turbine & Cable Layout Optimisation . . . . .	244
8.1.4	Advanced Cable Layout Optimisation . . . . .	245
8.1.5	Influence of Energy Storage Systems . . . . .	246
8.2	Conclusions . . . . .	247
8.2.1	Research Question 1 . . . . .	247
8.2.2	Research Question 2 . . . . .	248
8.3	Future Research . . . . .	250
8.4	Application for Industry . . . . .	253
8.4.1	Turbine Layout Optimisation . . . . .	253

## Contents

8.4.2	Cable Layout Optimisation . . . . .	254
8.4.3	Integrated Turbine & Cable Layout Optimisation . . . . .	254
8.4.4	Integrating Energy Storage . . . . .	255
	<b>Bibliography</b>	<b>256</b>
	<b>Appendix A: Industry Engagement</b>	<b>278</b>
A.1:	Turbine Layout Optimisation . . . . .	278
A.2:	Cable Layout Optimisation . . . . .	280
	<b>Appendix B: ESS &amp; Ancillary Services</b>	<b>283</b>
	<b>Appendix C: Turbine Layout Optimisation Case Studies</b>	<b>287</b>
C.1:	Case Study 1: Hypothetical Wind Farm . . . . .	287
C.2:	Case Study 2: Berwick Bank Offshore Wind Farm . . . . .	289
	<b>Appendix D: Cable Layout Optimisation Comparison</b>	<b>293</b>
D.1:	Hypothetical Wind Farm Turbine Positions . . . . .	293
D.2:	Berwick Bank Offshore Wind Farm Turbine Positions . . . . .	295
D.3:	Full Set of Results . . . . .	297
	<b>Appendix E: Advanced Cable Layout Optimisation</b>	<b>301</b>
E.1:	Expanded Hypothetical Offshore Wind Farm Site . . . . .	301

# List of Figures

1.1	Key components of an offshore wind farm. . . . .	2
1.2	Schematic of key components of an offshore wind farm. . . . .	3
1.3	Thesis structure . . . . .	8
2.1	Wake model comparison. . . . .	15
2.2	Example of use of Steiner nodes. . . . .	29
3.1	Illustration of the eight variables describing the grid layout . . . . .	57
3.2	Decision block for wind farm model evaluation. . . . .	66
3.3	Example look-up data set of wind farm power against number of turbines. . . . .	68
3.4	Flowchart of the key optimisation processes. . . . .	70
3.5	Capacity factor comparison between Lillgrund SCADA data and the proposed wind farm model. . . . .	73
3.6	Capacity factor comparison between Lillgrund SCADA data and the proposed wind farm model across wind directions. . . . .	75
3.7	Objective values in the particle swarm optimisation evolving over iterations. . . . .	76
3.8	Turbine positions of the Lillgrund site and the optimisation result. . . . .	77
3.9	Proposed hypothetical offshore wind farm site. . . . .	79
3.10	Non-uniform distribution of wind speed and direction. . . . .	80
3.11	SSE's Berwick Bank offshore wind farm site. . . . .	82
3.12	Wind rose for SSE's Berwick Bank offshore wind farm site. . . . .	83
3.13	Flowchart of the amended optimisation processes. . . . .	86
3.14	Turbine layouts of intuitively designed and optimised solutions. . . . .	87

## List of Figures

3.15	Solution fitness for intuitively designed, and optimisation, solutions. . . . .	89
3.16	Optimised turbine layouts for Berwick Bank. . . . .	90
4.1	Examples of different array cable layout typologies. . . . .	97
4.2	Possible cable connections between 12 turbines and a substation. . . . .	102
4.3	Illustrative example of ACO algorithm evolution. . . . .	110
4.4	Illustrative example of sub-problem handling in the ACOsp algorithm. . . . .	115
4.5	Hypothetical GW-scale offshore wind farm test case. . . . .	119
4.6	Six test cases of the hypothetical offshore wind farm site. . . . .	120
4.7	The Berwick Bank site with turbine and substation positions. . . . .	123
4.8	Optimised cable layouts from the three optimisation algorithms. . . . .	128
4.9	Optimal cable layout for the 25 turbines case. . . . .	129
4.10	Optimised cable routings for Berwick Bank using different conductor materials. . . . .	132
4.11	Optimised cable routing for Berwick Bank using all conductor materials. . . . .	134
5.1	Approximation of the total cable network cost. . . . .	141
5.2	Flowchart of the integrated cable and turbine micro-siting phase. . . . .	142
5.3	Cost surface for the change in the NPV lifetime energy capture of the wind farm. . . . .	145
5.4	Cost surface approximation and true values for the change in the NPV lifetime energy capture of the wind farm. . . . .	146
5.5	Cost surface for the change in cable costs and NPV lifetime electrical losses. . . . .	147
5.6	Cost surface for the combined change in NPV energy capture and cable costs. . . . .	148
5.7	Cost surface for the combined change in NPV energy capture and cable costs (valid positions only). . . . .	148
5.8	Probability density function of a turbine being selected for the micro-siting iteration. . . . .	153
5.9	Comparison of objective values of optimised layouts. . . . .	158

## List of Figures

5.10	Comparison of objective values of optimised layouts against number of turbines. . . . .	159
5.11	Layout solutions of the sequential and integrated optimisations. . . . .	160
6.1	Identifying the gap in optimisation approaches. . . . .	165
6.2	Generation of Steiner nodes for obstacle avoidance. . . . .	168
6.3	An example cable routing using the additional cable corridor constraint. . . . .	178
6.4	Flowchart showing the four phases of the MILPsp algorithm. . . . .	181
6.5	MILPsp Phase 1 flowchart. . . . .	182
6.6	MILPsp Phase 2 flowchart. . . . .	183
6.7	MILPsp Phase 3 flowchart. . . . .	185
6.8	MILPsp Phase 4 flowchart. . . . .	186
6.9	The updated hypothetical GW-scale offshore wind farm test case. . . . .	189
6.10	Layout solutions of the MILP algorithm and the MILPsp algorithm. . . . .	194
6.11	MILPsp solutions for the expanded hypothetical offshore wind farm site. . . . .	199
7.1	Example of ‘peak-shaving’ power using energy storage. . . . .	205
7.2	Peak output power of co-located turbine/ESS over a range of charging levels. . . . .	217
7.3	Peak output power of co-located turbine/ESS over a range of power/energy capacities. . . . .	219
7.4	Optimised cable selection and ESS sizing/location for an ESS cost of £0. . . . .	220
7.5	NPV lifetime electrical losses in the presence of varying ESS capacity. . . . .	221
7.6	Optimised cable selection and ESS sizing/location for a fixed ESS jointing cost of £13,800. . . . .	222
7.7	Optimised cable selection and ESS sizing/location for a range of variable costs (£/MWh). . . . .	224
7.8	Cable layout solutions for 10 turbines with/without ESS. . . . .	228
7.9	Cable layout solutions for 15 turbines with/without ESS. . . . .	229
7.10	Electrical losses for a varying number of ‘upstream’ ESS units. . . . .	231
7.11	Cable layout solutions for 25 turbines with/without ESS. . . . .	233

List of Figures

7.12 Cable layout solutions for 40 turbines with/without ESS. . . . .	234
7.13 Cable layout solutions for 60 turbines with/without ESS. . . . .	235
7.14 Cable layout solutions for 122 turbines with/without ESS. . . . .	236

# List of Tables

1	Summary of algorithms proposed in this thesis, with location and description. . . . .	xix
3.1	Capacity factor and energy capture error between model evaluation and SCADA data. . . . .	73
3.2	Mean absolute error of capacity factor between the model evaluation and SCADA data for three turbines, with original and shifted SCADA data. . . . .	74
3.3	Objective value of intuitively generated and optimised solutions. . . . .	88
3.4	Annual energy yield for the SSE solution and proposed model solution. . . . .	91
4.1	Example set of cable types. . . . .	101
4.2	Example of a reduced set of cables types. . . . .	101
4.3	Key cable parameters. . . . .	121
4.4	Key parameters used in the cable layout optimisation algorithms comparison. . . . .	122
4.5	Representative key cable parameters provided by SSE. . . . .	124
4.6	Key parameters used in the Berwick Bank cable layout case study. . . . .	124
4.7	Average results of the three optimisation methods for the six hypothetical test cases. . . . .	126
4.8	Objective value of the three optimisation methods with and without the cable crossing penalty. . . . .	130
4.9	Objective value for Berwick Bank using different conductor materials. . . . .	132

## List of Tables

5.1	Key parameters used in the comparison of the sequential and integrated optimisations. . . . .	155
5.2	Full results for the sequential vs integrated optimisation methods (wind rose 2). . . . .	157
6.1	Representative cable parameters for hypothetical site. . . . .	188
6.2	Representative copper cable parameters. . . . .	190
6.3	Representative aluminium cable parameters. . . . .	191
6.4	Objective values and optimality ratio of the four cable layout optimisation algorithms. . . . .	193
6.5	Computational time of the four cable layout optimisation algorithms. . .	194
6.6	Objective values of the MILPsp algorithm on the copper cable case study.	196
6.7	Objective values of the MILPsp algorithm on the aluminium cable case study. . . . .	198
7.1	Objective values of cable and ESS selection over a range of costs per MWh.	223
7.2	Objective values of the MILPsp cable layout solutions with/without ESS.	227
A.1	Revenue streams for energy storage projects in the UK. . . . .	284
A.2	Comparison of ESSs (part 1). . . . .	285
A.3	Comparison of ESSs (part 2). . . . .	286
A.4	Coordinates for the hypothetical wind farm boundary and obstacles. . .	287
A.5	Non-uniform distribution of wind speed and direction probabilities. . . .	288
A.6	Coordinates for the Berwick Bank offshore wind farm boundary. . . . .	289
A.7	Representative wind speed and direction probabilities for the Berwick Bank offshore wind farm site (part 1). . . . .	290
A.8	Representative wind speed and direction probabilities for the Berwick Bank offshore wind farm site (part 2). . . . .	291
A.9	Power output and thrust coefficients of the representative turbine. . . .	292
A.10	Turbine positions for cable layout optimisation comparison. . . . .	294
A.11	Turbine positions for the Berwick Bank cable layout study. . . . .	296

List of Tables

A.12 Full results of the 3 cable layout optimisation methods for the hypothetical site (part 1). . . . .	298
A.13 Full results of the 3 cable layout optimisation methods for the hypothetical site (part 2). . . . .	299
A.14 Full results of the 3 optimisation methods for 25 turbines, including the cable crossing constraint. . . . .	300
A.15 Coordinates for the existing features in the expanded hypothetical site. .	301
A.16 Full set of results for the MILPsp cable layout optimisation of the hypothetical site. . . . .	302

# List of Algorithms

1	Particle swarm optimisation algorithm . . . . .	63
2	Pattern search algorithm . . . . .	65
3	Improved solution seeding . . . . .	85
4	Ant colony optimisation algorithm. . . . .	113
5	Ant colony optimisation algorithm with decomposition strategy. . . . .	117
6	k-means clustering algorithm for initial substation positions. . . . .	150
7	Integrated turbine and cable layout optimisation algorithm. . . . .	151
8	Sequential turbine and cable layout optimisation algorithm. . . . .	156
9	A* route finding algorithm. . . . .	169
10	MILPsp Phase 1: Creating a seed solution. . . . .	182
11	MILPsp Phase 2: Recursive decomposition. . . . .	184
12	MILPsp Phase 3: Cable selection. . . . .	185
13	MILPsp Phase 4: Recursive decomposition with reduced cable set. . . . .	186
14	ESS (dis)charging strategy. . . . .	212

## Summary of Main Proposed Algorithms

Table 1: Summary of algorithms proposed in this thesis, with location and description.

Algorithm	Location in Thesis	Description
<i>PSO-based method</i>	Section 3.5.1	A grid-based turbine layout, optimised by means of PSO, and second phase allowing some deviation away from original grid positions. Uses the wind farm model presented in Section 3.1.
<i>PSO-based method v2</i>	Section 3.5.2	As <i>PSO</i> , with amendments made for application to Berwick Bank offshore wind farm, and improved solution seeding method. Uses the wind farm model presented in Section 3.1.
<i>MILP</i>	Section 4.2.3	Replication of the widely used MILP algorithm from academic literature. Uses the array cable model presented in Section 4.2.2.
<i>Classical ACO</i>	Section 4.2.4	Replication of the ACO algorithm from academic literature. Uses the array cable model presented in Section 4.2.2.
<i>ACO with decomposition</i>	Section 4.2.5	As <i>Classical ACO</i> , with the integration of a novel decomposition strategy. Uses the array cable model presented in Section 4.2.2.
<i>Integrated optimisation</i>	Section 5.1	Novel concurrent optimisation, using a combination of <i>PSO-based method v2</i> and <i>ACO with decomposition</i> .
<i>MILPsp</i>	Section 6.1.9	As <i>MILP</i> , with the integration of a novel decomposition strategy. Uses the array cable model presented in Section 6.1.
<i>MILPsp with ESS</i>	Section 7.1.2	As <i>MILPsp</i> , with the integration of ESS variables. Uses the array cable model presented in Section 7.1.1.

# Acknowledgements

This thesis would not have been possible without the help and support of countless people and organisations. But to name a few...

My supervisors Prof. Olimpo Anaya-Lara, Dr David Campos-Gaona, Dr Hong Yue, Dr Chunjiang Jia, and everyone at the Offshore Renewable Energy Catapult's Electrical Infrastructure Research Hub for all their help with my PhD, papers, and projects. The staff and students at the EPSRC Centre for Doctoral Training in Wind & Marine Energy Systems. Everyone involved in the University of Strathclyde's Low Carbon Power & Energy programme, SSE, and ScottishPower Renewables whom I was able to work with. My friends and family who put up with endless wind-energy-related conversations and ramblings over the last several years.

Thanks to all for their help, support, and encouragement - and to everyone else who supported me along the way that I wasn't able to include in the above.

Some of the results in this thesis were obtained using the ARCHIE-WeSt High Performance Computer ([www.archie-west.ac.uk](http://www.archie-west.ac.uk)) based at the University of Strathclyde. This work was supported by the Engineering and Physical Sciences Research Council (Grant/Award Number: EP/L016680/1).

# Chapter 1

## Introduction

It is now widely accepted that anthropological climate change due to emissions of greenhouse gases is a global problem in need of a myriad of solutions. These solutions all centre around emissions reductions with many countries around the world setting targets to reach net zero emissions by 2050 [1–3]. Wind energy has, and will continue to have, a significant role to play in de-carbonising the energy production of the world, with offshore wind energy providing an increasing contribution to this [4–7]. Wind energy is now also crossing the threshold to become one of the cheapest sources of new energy generation in many parts of the world when prices are calculated without financial support mechanisms [8], however there is still plenty of scope for further reduction in the cost of energy. Typically, energy projects use the levelised cost of energy (LCOE) as the key metric for comparison. LCOE is the sum of the total lifetime costs of a project, discounted into net-present-value (NPV), divided by the total lifetime energy capture (also discounted to NPV). Reducing LCOE and providing affordable clean energy to the world’s poorest countries is also essential in ensuring a ‘just-transition’ away from conventional fossil-fuel-based energy generation. To achieve these cost reductions, it is important to design wind farms as efficiently as possible - with layout optimisation being at the heart of this problem.

## 1.1 The Offshore Wind Farm Layout Problem

The key components of an offshore wind farm are the turbines, array cable network, offshore substation, export cable, and onshore substation and grid connection, as shown in Figure 1.1. Turbines are sited offshore with several factors influencing their positions such as predominant wind direction, bathymetry conditions, visual impact, and navigational regulations. The energy generated by each turbine must be carried to the offshore substation via the array cable network. At the substation, the voltage may be increased to reduce electrical losses during transmission via the export cable to the shore and electrical grid connection.

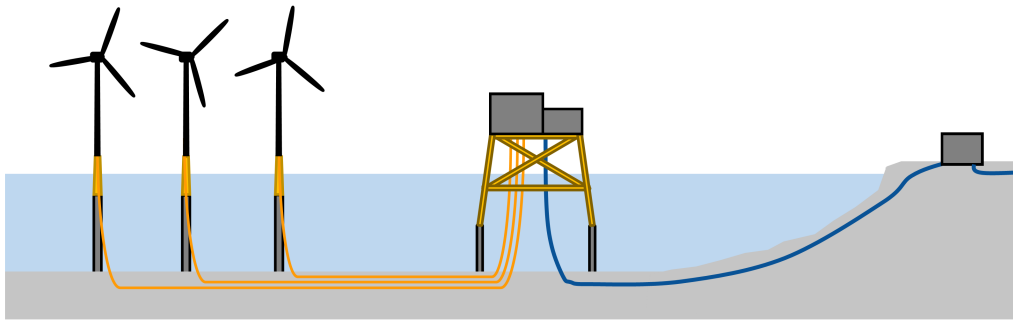


Figure 1.1: Key components of an offshore wind farm including turbines, array cables (orange), substation, export cable (blue), and onshore grid connection.

Figure 1.2 shows a schematic representation of the major components in an offshore wind farm. As can be seen, multiple turbines may be connected to a single cable or ‘string’, and a typical wind farm may have many strings connecting to the substation [9]. The number and length of these strings depends on the power rating of the turbines, the ratings of the available cables, the wind conditions (since this will affect power generation and therefore electrical losses), and the number of allowable connections into the substation.

Different topologies of the collector network have been proposed and will be covered in more detail in the following chapters. Some of these connect the ends of strings together to create a looped structure, while others connect a redundant cable from the end of a string straight to the substation. Another topology allows multiple cable

connections into a turbine creating a ‘branched’ collector network structure.

Further, since the cables connect turbines and substations, the positions of turbines and substations greatly influences the final cable routing. As mentioned previously, turbine positions are subject to many constraints, but from the perspective of the wind farm developer and/or operator, it is of the utmost importance to position turbines to maximise the potential energy capture from the site [10]. When air passes through the rotor of a wind turbine, energy is extracted and the turbulence increases downstream of the rotor in the wake of the turbine. Should another turbine be situated in the wake of an upstream turbine, the power generation of the downstream turbine will be lower. As such, developers consider the distribution of wind direction and wind speed of the site to position turbines to minimise these interactions and losses [10]. Other factors will influence the turbine positions, not least regulations on navigational safety that sometimes stipulate turbines must be placed in a regular grid layout, even if this compromises energy capture. For larger sites with more turbines, it may be necessary to have more than one substation to collect the power of the wind farm [11]. This adds an additional layer of complexity to the offshore wind farm layout problem that would need to determine how many, and which, turbines connect to which substations.

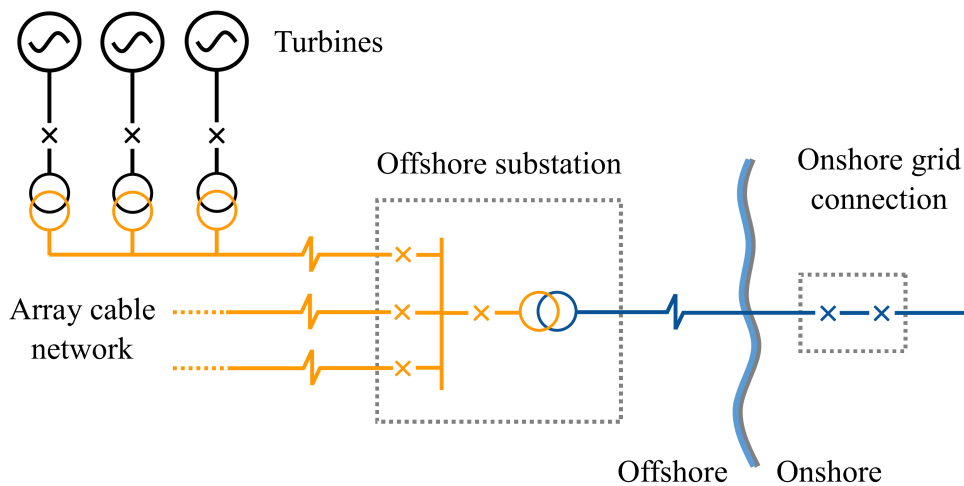


Figure 1.2: Schematic of key components of an offshore wind farm including turbines, array cables (orange), substation, export cable (blue), and onshore grid connection.

As alluded to, two major optimisation problems can be extracted from consideration of the offshore wind farm layout problem. These are the turbine layout optimisation and the array cable routing optimisation (which may also include substation position optimisation). These two problems are clearly inextricably linked since the optimal cable routing must connect to and from optimal turbine positions. The individual problems themselves are not trivial and so the degree to which they can be optimised together is not yet clear. Typically, in real world applications these problems are considered separately, in a sequentially optimised manner starting with turbine layout optimisation and then the collector network layout [10].

One obvious constraint of the cable layout optimisation that may be considered is that the cables must have a rating sufficient to carry the rated power from the number of turbines that the given connection is supporting. However, as wind energy is a variable resource, the cable will not experience the rated power for a large proportion of the operational lifetime. Since larger cables use more material and are more expensive, there may be scope to ‘peak-shave’ the power experienced by a cable and therefore reduce the required rating and cost, sometimes referred to as "under-planting". Co-locating energy storage in the offshore wind farm could provide this peak-shaving service and may allow this constraint on the cable layout optimisation problem to be ‘loosened’. An alternative to achieve peak-shaving would be to curtail the power output of turbines, however this would reduce the energy delivered to the grid (and wind farm revenue) and is beyond the scope of this work.

The size of offshore wind farm projects is increasing [12] and so too is the complexity of the wind farm layout problem. Therefore, developments in the field of layout optimisation must be capable of handling these large wind farms of the order of gigawatts (GW).

## 1.2 Thesis Aims & Research Questions

The aim of this thesis is to explore how taking a more holistic approach to offshore wind farm layout optimisation, relative to that which is currently used in industry [10], may result in improved solutions compared to sequentially optimising the constituent

parts of a wind farm, as is the standard approach within the industry. This is achieved by using the same constituent parts for turbine layout and cable layout optimisation, and isolating the difference between the sequential and integrated approaches. Project costs are centered around turbine and cable CAPEX and also the net present value of electrical losses and revenue generated by energy capture (discussed further later). Further, with developments and cost reductions in ESS, a secondary aim is to explore how ESS may be included in cable routing optimisation to further improve the quality of solutions produced in array cable routing design. Improvements will be considered in the context of cable CAPEX and the reduction in the net present value of electrical losses. Both aims, focusing on potential improvements to offshore wind farm electrical infrastructure, will be conducted in the context of large-scale (in the order of giga-watts) offshore wind farms, and can be summarised by the following two research questions:

- (1) What is the potential impact, in terms of project costs, of considering array cable network costs during early turbine layout design optimisation phases of GW-scale offshore wind farms?**
- (2) What is the potential impact of using energy storage at the wind farm level to reduce the cable rating and lifetime losses in offshore wind farm array cable networks?**

### **1.3 Novel Contributions**

This work provides novel contributions to knowledge, both in the academic literature and industry approaches, through the remaining chapters of work. These contributions are provided in the fields of turbine layout optimisation, cable layout optimisation, integrated turbine and cable layout optimisation, and integrated ESS and cable optimisation. Contributions in these fields is of value to the industry in providing effective and computationally efficient tools for the optimisation of turbine and cable layout optimisation. Additionally, the integrated concurrent optimisation approach aims to

determine what, if any, benefits (in terms of project costs, energy capture, and electrical loss reduction) can be attained by considering cable layout optimisation in earlier design phases of an offshore wind farm. This will enable decision makers to adapt their design workflow, if necessary, or provide confidence in current approaches. Further, contributions in ESS optimisation will allow offshore wind farm developers to begin to quantify what potential cable cost and loss reductions might be achievable through using co-located energy storage in an offshore wind farm.

### **1.3.1 Turbine Layout Optimisation**

For turbine layout optimisation, four contributions are highlighted. (1) An eight-variable formulation for grid-based turbine layouts is proposed that is applicable to a wider range of sites than similar existing formulations in the literature (existing formulations discussed further in Chapter 2). (2) A simple pattern-search-based approach is proposed for seeding some particles (for particle swarm optimisation), using the eight-variable formulation mentioned, that quickly finds very good solutions for grid-based turbine layouts. (3) A look-up function is proposed that reduces computational time, using the number of wind turbines as the key metric. And (4) a turbine micro-siting function is proposed that is shown to improve the quality of solutions beyond that of the PSO. The solutions generated using these approaches are shown to closely match those generated by SSE plc in both layout and objective value. These contributions are presented in Chapter 3 and are published in IET Renewable Power Generation [13].

### **1.3.2 Cable Layout Optimisation**

Novel contributions in cable layout optimisation methods are also contained in this work. (1) A cable layout optimisation algorithm based on ACO is proposed including a decomposition strategy that is informed by the incumbent solution. This proposed algorithm, ACOSP, demonstrates improved solutions relative to the classical ACO approach and reduced computational complexity compared to the ubiquitous MILP-based methods in academic literature. (2) With the decomposition strategy of the aforementioned ACOSP algorithm, a second algorithm is proposed combining this with a standard MILP

approach. This second proposed algorithm, MILPsp, maintains the effectiveness of the classical MILP approach but reduces the computational complexity and time. (3) The capabilities of the MILPsp method are expanded to include additional features such as cable corridors for avoiding jack-up vessel operations, existing site features that must be crossed with cables, and limiting the number of cable sizes used in the array. These contributions are presented in Chapter 4 and Chapter 6, with the thesis structure explained further in Section 1.4, and the ACOsp method also published in IET Renewable Power Generation [14].

### **1.3.3 Integrated Turbine & Cable Layout Optimisation**

Rather than sequentially optimising the turbine layout and then using those turbine positions as an input for a separate cable layout optimisation phase, this work proposes a novel method for the integration of both turbine and cable layouts into a single concurrent optimisation framework. The novel contributions of this section of work therefore includes (1) a framework using a stepped approach to the integration of the cable layout optimisation into the turbine layout optimisation, reducing the computational complexity of co-optimising two already-complex optimisations. Additionally, (2) a turbine selection probability method is proposed for the selection of turbines to be considered in the integrated co-optimisation approach, reducing the number of iterations with no improvements made to the objective value. These contributions are presented in Chapter 5.

### **1.3.4 Integrated ESS & Cable Layout Optimisation**

The final section of work introduces novel approaches for the integration of ESS optimisation (co-located with turbines in an offshore wind farm) with a cable layout optimisation into a concurrent integrated optimisation framework. The novel contributions include (1) discretisation of the ESS and a location-agnostic formulation for calculating cable losses and peak power in the presence of ESS, and (2) an expanded formulation of a MILP optimisation to enable the optimisation of ESS locations and sizing throughout an offshore wind farm. These contributions are presented in Chapter 7.

## 1.4 Layout of the Thesis

The layout of the main chapters of this thesis are described pictorially in Figure 1.3. It can be seen that Chapter 3 to Chapter 5 address Research Question 1; these aim to isolate the effect (on the objective value and quality of solutions) of an integrated concurrent optimisation relative to a sequentially optimised approach. Chapter 3 develops the turbine layout optimisation to be used, while Chapter 4 develops the cable layout optimisation approach. Both approaches are then provided to Chapter 5 where they are used in a sequential manner (optimising turbine layout followed by cable layout) and in an integrated concurrent optimisation approach.

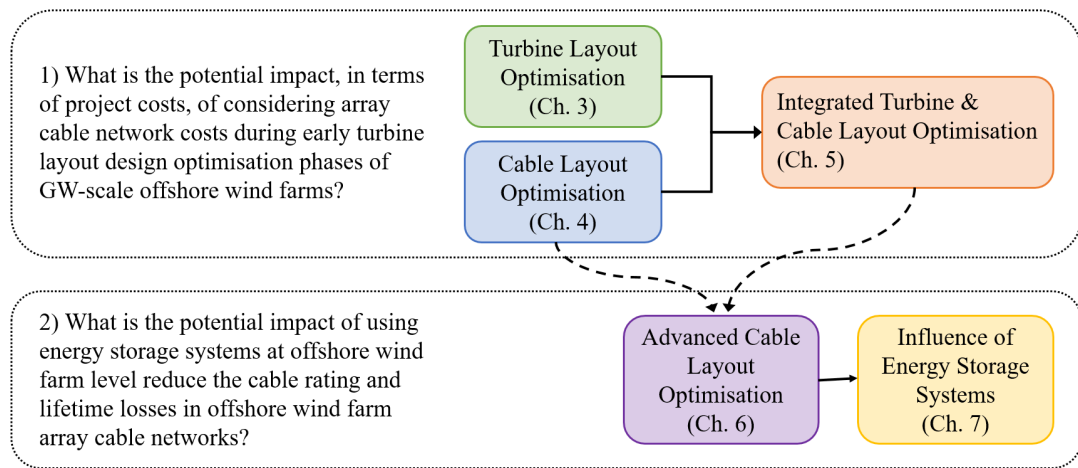


Figure 1.3: Thesis structure

Research Question 2 is then addressed through Chapter 6 and Chapter 7. Upon completion of Chapter 5, a gap was identified for combining the benefits of the MILP-based approaches and decomposition methods from Chapter 4. This work was largely conducted through an additional research project by the author and included further industry engagement, with SSE and Iberdrola/Scottish Power Renewables, developing a more comprehensive cable layout optimisation tool for commercial use. The developed optimisation framework is then provided to Chapter 7 to determine the potential impact of co-locating ESS within the offshore wind farm.

Following this introductory chapter, the remaining thesis is comprised of seven fur-

ther chapters.

**Chapter 2** provides background information on the state of the art of turbine layout and cable layout optimisation through a review of the literature. This is extended to consider to what extent these two sections have been integrated and how effective this has been. The state of the art for co-located energy storage in offshore wind farms is also presented, with consideration of the different functions of the storage systems.

**Chapter 3** presents the development of an approach to turbine layout optimisation. Using particle swarm optimisation as a base, novel aspects developed around the algorithm are presented including a look-up function for computational efficiency and a solution seeding algorithm based on a ‘pattern-search’ method. Two case studies are carried out to assess the performance of the algorithm. The first considers a large scale hypothetical site and the second compares the algorithm with an industry standard tool used by SSE.

**Chapter 4** presents the development of a cable routing optimisation algorithm. A new algorithm is proposed based on the ant-colony optimisation algorithm with a decomposition strategy integrated to improve the quality of solutions. The adapted ACO algorithm is compared to a classical ACO approach and a mixed-integer linear programming approach widely used in the literature. Cases are run on the hypothetical site proposed in Chapter 3, with an additional case study investigating cable conductor material which is run on a real site with representative data from SSE.

**Chapter 5** considers the previous two chapters, integrating these into a single optimisation approach. Comparison of this integrated method with a sequential optimisation is conducted on the large hypothetical site mentioned previously. Wind conditions from turbine layout optimisation literature are used in a first comparison study and representative wind conditions from SSE are used in a second case study of the hypothetical site. Analysis of the comparison is presented to determine if integrating the cable layout optimisation into earlier stages of wind farm design can result in meaningful improvements in the overall wind farm layout and cost of energy.

**Chapter 6** considers an advanced approach to cable layout optimisation with a more comprehensive set of real-world constraints by using a classical MILP algorithm

## Chapter 1. Introduction

(rather than heuristic methods as in Chapter 4) in conjunction with the decomposition strategy proposed in Chapter 4. While not directly comparable to the previous cable layout optimisation methods, analysis of the algorithm is conducted through case study simulations using the same hypothetical site as mentioned previously.

**Chapter 7** presents further additions to the cable layout optimisation method from Chapter 6 by introducing decision variables for energy storage systems co-located within an offshore wind farm for the purpose of peak-shaving the power output of turbines. An initial study determines the size and charging strategy necessary to provide any peak-shaving for the specific hypothetical site scenario. A second study determines at what cost any ESS may be used, with the additional cost of ESS offset by cost savings from either cable de-rating or electrical loss reduction. A final study investigates what the impact is to the cable layout and selection by integrating the ESS into the cable layout optimisation and considering the hypothetical site used previously.

**Chapter 8** concludes the findings of the work presented in this thesis and discusses the effectiveness of the approaches taken. Recommendations are made for wind farm layout optimisation and future investigations are proposed for this area of research.

Additionally, key findings and recommendations are provided in an “Applications for Industry” section, **Section 8.4**. This chapter aims to guide the implementation of the work presented in this thesis and maximise the impact of the research.

## Chapter 2

# Background

This section provides a background to the research presented in this thesis to frame the work in the context of current knowledge, to highlight gaps, and to identify areas to target for contribution to knowledge. Factors affecting offshore wind farm layout optimisation are considered and a review of the literature for each factor is presented. Different optimisation algorithms and methodologies are explored and the extent to which they have been utilised in academic research is discussed. Finally, in the context of the literature review, thesis objectives are proposed in order to meet the aims of the thesis, presented in Section 1.2.

When considering offshore wind farm layout optimisation, perhaps the most obvious aspect is the turbine layout. This is certainly one of the most significant components, however - as mentioned in the previous chapter - the routing of the electrical collector network must be considered too. Further, due to the interconnected nature of these problems, the level to which they are integrated (considered concurrently) will influence the overall layout of the wind farm with the solution of one affecting the solution of the other. While these two factors (and their level of integration) is a focus of the following literature review, another hypothesis is presented in Section 1.2. Energy storage as a means to reduce peak power carried by a cable - and therefore reduce the required cable rating - is explored and a review of the academic literature to date is presented.

## 2.1 Turbine Placement Optimisation

When a turbine extracts energy from the wind, it leaves behind it a wake, which is a region characterised by lower wind speed and increased turbulence [15]. If another turbine is operating in this downwind region, several effects will be experienced by the downwind turbine. Firstly, it will generate less energy as a result of the decreased mean wind speed, and secondly, the increased turbulence (fluctuations in wind speed about the mean) will increase the fatigue loads on the structure, potentially reducing the wind turbine's usable life. One study by Kim et al. [16] showed that, for a specific case, the reduction in mean wind speed in the wake reduced energy capture of the downwind turbine by approximately 7%, while the increase in turbulence was responsible for a further reduction of 0.4%. While the energy capture decrease appears to be dominated by the reduction in mean wind speed, the increased turbulence can drastically increase fatigue loading. Thomsen et al. [17] found that the increase in fatigue loading in a wake can be between 5-15% greater than that for a turbine in free stream (non-waked) wind. More recent studies, such as that by Stanley et al. [18], have shown that the problem of fatigue is more nuanced than a simple increase in fatigue loading. The authors showed that the side of the rotor on which a wake partially impinges can also significantly change the fatigue loading. Blades experience cyclical loading as they rotate due to gravity and aerodynamic lift and drag forces. A rotor impinged upon by a wake will experience a lower mean wind speed and therefore generate lower lift and drag forces, but the gravity loading will remain the same. Stanley et al. [18], showed that this can exacerbate fatigue loading when a wake partially impinges one side of a rotor, but can actually lead to more favourable loading if a wake partially impinges on the other side of the rotor. The study only considers edgewise blade root bending moments and turbine proximity was constrained to two or more rotor diameters (much less than typical real sites), so further work is required to determine the validity of this result.

The interactions between turbines due to the wake effect, therefore means that individual turbine positions cannot be considered in isolation when trying to maximise energy capture of a wind farm. Variable wind direction and speed further complicate

this problem affecting the strength and/or direction of wind turbine wakes. This non-trivial optimisation problem has only increased in complexity in recent decades, as wind farms have more and more individual wind turbines in them [19]. Firstly, this means that there are an increasing number of turbines for an optimisation study to determine the positions for. Secondly, when determining the quality of turbine layouts, this means that not only are there more turbines for which to calculate the energy capture, but also more wakes impacting each of these turbines (from every other turbine).

### 2.1.1 Wind Turbine Wakes

Since the early 1980's researchers have been trying to model the interactions between turbines due to wakes. Jensen et al. [20] was one of the first, describing a model for calculating wind speed at a point in space in a wake at a given downstream and cross-stream distance and is still one of the most widely used wake models in academic studies [21]. In the Jensen model, the velocity deficit within the wake decreases with downstream distance, but is uniform across the wake region which is not representative of reality, Figure 2.1. It is an analytical model, based on mass conservation, that assumes a linear wake expansion using the diameter of the wind turbine rotor and a wake decay factor to define the wind speed deficit in the wake [20,22]. The Jensen wake model was expanded upon by Katic et al. [23] to allow for the aggregation of multiple wake effects and to calculate cluster efficiency, and although this approach was believed to be sufficient for mean energy production, it is not sufficient for considering turbine loading or the economics of projects [23]. The Jensen model has been shown to overestimate wake losses by up to 1.91%, compared to Gaussian wake models that overestimated losses by up to 0.95% [21]. The Larsen model is one such Gaussian wake model, describing a wake-affected region that expands non-linearly with a Gaussian velocity deficit [24], Figure 2.1. Other models take into account other significant parameters, such as the Frandsen model that considers two-way interaction with the atmosphere, and neighbouring wakes to calculate wake expansion horizontally and vertically [25]. There are also more recent studies that extend the simple Jensen model and apply a Gaussian

velocity deficit over the linearly expanding wake region. Compared to large eddy simulation, physical experiments, and field observation, this Jensen-Gaussian approach was found to offer improved accuracy but maintain model simplicity [26] and was improved further by ensuring mass conservation and consideration of the pressure recovery region [27]. Bastankhah et al. [28] also proposed a Gaussian-based wake model that requires one parameter to determine the velocity deficit within the wake, matching well with large-eddy simulations (LES) and wind tunnel data. Compared to the Jensen and Frandsen models, the Bastankhah model was shown to be more accurate at predicting the velocity deficit in the wake.

In addition to the widely used Jensen and Larsen models, several other wake models have been developed at the Technical University of Denmark (DTU), including the infinite wind farm boundary layer model, the dynamic wake meandering model (DWM), Fuga, and EllipSys3D [29]. Many of these models have been adopted as standard approaches in tools such as PyWake, an open-source wind farm simulation tool developed by DTU [30]. Instead of considering the effect of a single wind turbine wake, the infinite wind farm boundary layer model determines the reduction in wind speed at the centre of a large wind farm [31]. It does so by assuming that the wind turbines in the farm act as a surface roughness, reducing the wind speed in the resulting boundary layer. Compared to existing models at the time of publication, the author claims good agreement was found in the efficiency reduction of wind turbines in the centre of a large wind farm. However, the approach is only able to predict this wind speed reduction effectively for turbines three to four rows into the wind farm array. The Fuga model is a linearised CFD model [32] using linearised Reynold's-Averaged Navier-Stokes (RANS) equations to build look-up tables of downstream wind velocity in a wake [29,33]. The initial model was improved in 2014 to include different types of turbines in the same simulation, effects of stability, and wake meandering [32]. While the model was validated against a number of real world data sets, the authors point out that the model seems to over predict the measured efficiencies of wind turbines by a few percent and the that results in stable conditions are questionable [32]. EllipSys3D is a CFD solver which can use a RANS or large-eddy simulation (LES) model [29]. Rather than solving a full complex

CFD simulation, an actuator disc model can be used. This avoids the need to mesh the blade geometry and resolve the local boundary layer at the blades, saving computational time [29, 33, 34]. Despite this computational time saving, a study by Göçmen et al. [29] highlighted the computational cost as a prohibitive factor for using the model on anything more than a small number of academic cases, when compared to other wake models such as Jensen, Larsen, and Fuga. The DWM model builds on traditional wake models by including a wake transportation effect caused by turbulent components in the atmospheric boundary layer [35]. These lateral and vertical turbulence components (eddies larger than two rotor diameters [29]) lead to the development of a meandering frame of reference in which a wake can be considered. Three core components are considered in this model, a velocity deficit, the meandering of the wake, and rotor added turbulence. The model is also capable of considering the loading on a downstream turbine, however, a relatively highly resolved turbulence field is required to feedback to an aeroelastic code [29].

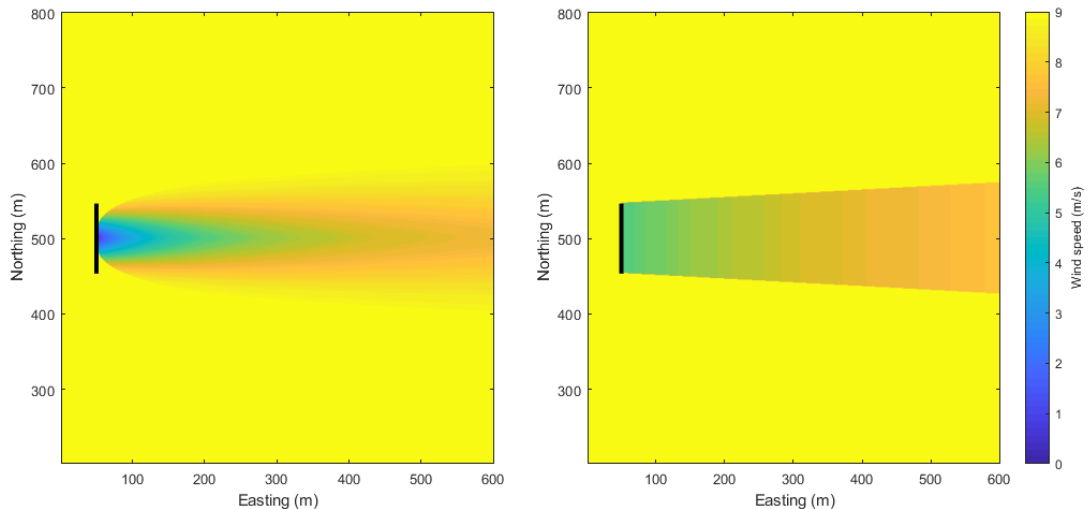


Figure 2.1: Comparison of wake models, showing wind speed in the wake-affected region using (left) the Larsen wake model, and (right) the Jensen wake model.

Pillai et al. [36] conducted a comparison of wake models considering accuracy and computational time, including: the Jensen model, the Larsen model, the Ishihara model, and the Ainslie Eddy-Viscosity (AEV) model. It was found that, while the Jensen and

AEV models were the most accurate for a few wind scenarios, the Larsen model by far offered the best trade-off between accuracy and computational time. Figure 2.1 shows the wind speed in the wake-affected region using the Larsen (left) and Jensen (right) wake models. While the Larsen wake model exhibits a Gaussian velocity deficit over the wake and a non-linear wake expansion, the Jensen model shows a linear wake expansion with uniform velocity deficit over the width of the wake.

### 2.1.2 Problem Formulations

#### Early Grid-Based Approaches

One of the earliest formulations of a wind farm layout optimisation study was by Mosetti et al. [37] where a 10x10 grid is proposed as possible locations for turbines. Many studies have since used this 10x10 grid formulation of the wind farm layout problem changing either the optimisation algorithm or objective function to be assessed [38–40]. In these studies, turbines are placed within the defined 100 discrete grid positions to maximise energy capture by assessing wake interactions across the site. This approach of using a discrete set of positions can be computationally efficient and require a small number of variables to be optimised. For small cases such as a 10x10 grid, it is also possible to find and prove the optimal solution to enable benchmarking for alternative optimisation algorithms. While this is valuable to determine the efficacy of the algorithms, the 10x10 test case is far from representative of a real offshore wind farm site [37]. Modern offshore wind farms now often have very large numbers of turbines (close to, or greater than, 100) placed in sites with more irregular (non-square) boundaries. They also set the rows and columns of turbines depending on the predominant wind direction (rather than a perfect north-south, east-west set up of the 10x10 grid cases) and may sometimes have non-perpendicular rows and columns and/or non-parallel rows of turbines. Another study based on the work by Mosetti et al. is that by Huang et al. [41] which uses both the 10x10 grid and the wind conditions of Mosetti et al. Huang et al. focuses on a change to the objective function and optimisation algorithm, claiming that GAs are good for global searches (identifying regions in the solution space with relatively good objective values) but not for local searches (detailed searches within a

region of the solution space to identify the optimal solution). The paper proposes the addition of a local search algorithm (steepest ascent hill-climbing) to the GA base, and adapting the GA into a distributed GA (DGA). A DGA approach uses sub-populations with some individuals exchanging between sub-populations every few iterations. The combination of DGA and local search algorithm shows improvements over the GA approach, such as that used by Mosetti et al., (especially in computational time, with a reduction of 88-92%) and also a stand-alone DGA approach. However, while the approach is shown to be effective on a 10x10 grid-based problem, it is unclear if this is a practical approach for more realistic wind farm sites. This is because large offshore sites will require a much greater level of resolution of possible turbine positions to achieve a reasonable layout solution (i.e. changing the angle of rows of turbines). They also have additional constraints relating to search and rescue (SAR) operations that require a regular, grid-based layout of turbines [42] rather than the irregular layouts generated with this method.

### **Irregular vs Grid-Based Layouts**

Turbine layout optimisation studies optimise turbine positions in a variety of ways, but some result in layouts that are irregular and unstructured. Studies by Wu et al. [43], Gonzalez et al. [44], and Kunakote et al. [45] use many discrete positions as possible turbine locations, but prescribe no regular pattern constraint, resulting in irregular layouts. Lackner et al. [46] and DuPont et al. [47] optimise turbine positions in continuous space (i.e. no pre-determined set of discrete possible turbine positions) but also do not require the solutions to be in the form of any discernible regular pattern. Irregular layouts can face difficulty and delays in consenting due to the negative impact on maritime navigation, SAR operations, and – when close to the shore – visual impact [42]. Therefore, given that they do not meet many of the real world constraints and considerations, especially in the UK [42], these tools are not currently suitable for design of real large-scale offshore wind farms. A small number of studies utilise a grid-based problem formulation, however these often leave the majority of grid spaces unoccupied

resulting in layouts that appear to be essentially irregular [48], or are overly constrained in the solutions that they are able to generate, i.e. requiring rows of turbines to be parallel [49]. Although some grid-based algorithms are capable of generating reasonable solutions, no deviation from the described grid positions is considered in those techniques [49, 50] limiting the potential energy capture of the farm. To better understand the degree to which the industry aims to keep to a grid-based layout, a short series of industry interviews were also conducted by the thesis author [10], more detail provided in the Appendix. This revealed that there is some difference throughout the industry, with some adhering to reasonably strict grid layouts and others allowing some flexibility in the design. ‘Perimeter and grid’ layouts are also increasingly of interest in order to abide by maritime regulations (particularly in the UK) and also to maximise the number of wind turbines on the edge of the site (in an attempt to minimise wake losses). ‘Perimeter and grid’ layouts (sometimes referred to as ‘boundary-grid’ layouts) place many turbines along the boundary of the wind farm (in no regular pattern) and place the remaining turbines within the wind farm in a grid pattern [51]. While individual interview responses cannot be shared, the companies engaged with included K2 Management, SSE (two interviews), Atkins (group interview of three individuals), Orsted, Fraser Nash (two interviews), and UL Openwind between April 2020 and April 2021. These interviews also aided the development of the models in the following chapters, providing a ‘sounding board’ and ensuring the work conducted was in line with industry interests and research. As much information as is possible to provide, regarding the interview process and use of the feedback, is presented in the Appendix.

### 2.1.3 Optimisation

With a variety of approaches to the problem formulation of wind turbine placement optimisation and the modelling of wind turbine wakes, it is useful to understand the constituent parts of an optimisation problem and some of the approaches taken to apply this to turbine placement.

A mathematical optimisation problem typically takes the form [52, 53]:

$$\begin{aligned} & \text{minimise } f_0(x) \\ & \text{subject to } f_i(x) \leq b_i, \quad i = 1, \dots, m \end{aligned}$$

where the vector,  $x$ , is the optimisation variable;  $f_0$  is the objective function; and the functions,  $f_i$ , are inequality constraint equations which must be satisfied [52, 53]. Constraint equations may also take the form of equality constraints, where  $f_i(x) = b_i$ . The optimisation problem can be said to be a linear problem, if it satisfies:

$$f_i(\alpha x + \beta y) = \alpha f_i(x) + \beta f_i(y)$$

where  $x, y \in \mathbb{R}^n$  and  $\alpha, \beta \in \mathbb{R}$  [52]. Optimisation problems can be altered from a minimisation problem, presented here, to a maximisation problem, by multiplying both sides of the objective function by  $-1$ . In the optimisation of turbine layouts for offshore wind farms, there has been a variety of approaches in the academic literature. The following highlights some of the objective functions and constraint equations used to tackle this complex problem.

### Objective Functions

There are a range of objective functions used to determine the effectiveness of solutions in wind turbine layout optimisation. Kunakote et al. [45] focuses on minimising the capital cost of turbines divided by the wind farm power output. While this captures the major factors associated with the cost of energy, it uses only the mean wind farm power output rather than the lifetime energy capture (in NPV) and does not consider other additional costs such as the collector network cost. Al Shereiqi et al. [54] extends this perspective by considering turbine CAPEX and wind farm power production as Kunakote et al. [45], but with the addition of cable CAPEX and lifetime electrical losses, enabling a more complete picture of wind farm costs. Gagakuma et al. [55] considers only wind farm power output in the first phase of the work, missing critical cost elements such as turbine CAPEX, followed by minimising power variance in a second

phase. The authors do this through a two-phase multi-objective optimisation where the first optimisation aims to maximise mean energy yield from the wind farm, and the second optimisation aims to reduce power variance from the different wind directions (using the result of the first objective, mean power, as a constraint for the second optimisation i.e. mean power must be greater than or equal to the solution of the first optimisation). While this is an elegant solution to a multi-objective optimisation problem (based on the  $\epsilon$ -constraint method), it relies on a hierarchy of objectives with the first being of primary importance (i.e. maximising mean power is more important than minimising power variance). Croonenbroeck et al. [56] considers profit as the objective function through revenue minus costs. The authors point out, that for their formulation, this is essentially equivalent to energy capture maximisation, however, there is value in using economically driven cost functions due to things such as time-dependent sales price and discount rate forecasts [56]. The assumption that profit maximisation is the same as energy capture maximisation is reasonable if the objective only considers fixed turbine CAPEX and a fixed number of turbines. This overlooks the variable cost of cables and electrical losses that vary with turbine positions and so a more complete objective function would be preferable. Gu et al. [57] considers a fixed turbine layout, using the Horns Rev wind farm as a case study, optimising the set point (axial induction factor) of turbines to maximise wind farm power production for a single wind speed and direction. While useful for the specific test case, further work would be required to optimise the set points for different wind speeds and directions and could be very complex for considering during the turbine layout design phase of a project. Park et al. [58] also focuses on maximising wind farm power, while Ulku et al. [59] considers both a wind farm power maximisation approach and a cost per unit power approach. The authors did not include all cost factors and highlight that future work may benefit from including the cost of the array cable network in the turbine layout optimisation phase.

### Constraints

Constraint equations may depend on the problem formulation of the wind turbine layout optimisation study. One popular formulation is to use a set of 100 discrete turbine positions in a 10x10 grid, constraining turbines to only those possible positions [45,54]. This approach of using a discrete set of turbine positions can be useful for small benchmarking cases, but is not representative of real offshore wind farm sites [37]. An alternative approach is taken by Croonenbroeck et al. [56] where the authors consider a turbine proximity constraint. This ensures turbines have sufficient spacing between them to allow for some wake recovery to occur and avoid the worst of the turbulent wake from the upstream turbine. However, using only this constraint within turbine placement can lead to highly irregular layouts. In a real-world application, it could be the case that these irregular layouts do not comply with SAR guidelines and/or may suffer from a more significant visual impact, delaying projects. Gu et al. [57] doesn't consider turbine placement at all, focusing only on optimising the set point of turbines for power maximisation. Although not mentioned by the authors it seems appropriate that the variables describing the set points of turbines be constrained at extreme values. This approach of maximising power ignores other effects such as electrical losses, drivetrain losses, and fatigue loading on turbines. A more complete objective function (including considerations such as losses) would allow the authors to apply constraints to these aspects and possibly deliver solutions with a more comprehensive considerations of the various costs and benefits. Park et al. [58] constrains the number of turbines to 49, ensuring exactly that number of turbines are built within the farm. This can be a useful approach providing a reasonable number of turbines is selected for the site under consideration, although determining this number may be an optimisation study in-and-of itself. Ulku et al. [59] also constrains the number of turbines in the site. The authors also define a binary constraint on the variables describing turbine positions, where the variable is equal to one if a turbine is built, and zero if not.

### Recent Approaches

Optimisation algorithms can largely be classified as exact methods or heuristic methods. An exact method refers to an approach or algorithm designed to find the optimal solution to a given problem with a guarantee of mathematical correctness. Exact methods are employed when it is essential to obtain the best possible solution according to the objective function and constraints, and approximation or heuristic methods are not acceptable. These methods are typically used when the problem size is small enough to permit an evaluation of all possible valid solutions [53]. A heuristic optimisation algorithm is a problem-solving approach that uses a practical, rule-of-thumb, or ‘good enough’ strategy to find approximate solutions to complex optimisation or search problems, often in situations where finding an exact solution is impractical or too time-consuming [53]. Of note, interior point methods are a class of optimisation algorithm used to solve linear programming and other convex optimisation problems [52]. They are characterised by their approach to finding solutions by moving through the interior (feasible region) of the convex solution space, as opposed to traditional methods, such as the Simplex Method [60], which operate on the boundary of the feasible set/region.

There are a wide variety of methods in the literature for wind farm layout optimisation [61], employing various methods such as gradient-based algorithms [46], genetic algorithms (GA) [37, 48, 62] and particle swarm optimisation (PSO) algorithms [63, 64]. A review of layout optimisation algorithms by [33] reveals yet more approaches that have been taken in solving this complex optimisation problem, including: simulated annealing, ant-colony optimisation, definite point selection and binary artificial algae algorithm. Additionally, Wilson et al. [65] describes the top four methodologies of eight teams in the second edition of the Wind Farm Layout Optimisation Competition held at the 22nd Genetic and Evolutionary Computation Conference, where all teams employed evolutionary algorithms. Evolutionary algorithms are heuristics which, as mentioned, can provide good quality solutions relatively quickly, but can suffer from getting ‘stuck’ in local optima (and therefore not finding the global optimal solution). Pillai et al. [66] compared a GA with a PSO algorithm (two evolutionary algorithms) and found that both methods perform well, with the PSO expected to offer savings in computational

time due to the typically smaller population and constant number of function calls per iteration. The authors highlight that the PSO produced better solutions, but also that the simplicity of the 10x10 grid cases used in the study made it difficult to determine if additional cost considerations (such as electrical infrastructure) affected the solutions at all. Other studies employ a two-part optimisation process, for example Park et al. [58] firstly site turbines within a set of available grid positions using a GA, and secondly split the chosen grid spaces into four smaller sections to allow for turbine micro-siting (also using a GA). This approach was applied to the Daegwallyeong wind farm and was able to reduce wake losses by 2.3% compared to real site measurements. The staged approach appears to offer a good compromise between heuristic approaches generating good solutions quickly and the ability to further refine the search in the locality of the solution space. However, the heuristic method would still be susceptible to getting stuck in local optima. Given the complexity of the wind turbine layout optimisation problem, many studies are clearly focusing on the use of heuristics to tackle the problem [45, 65, 66]. The number of heuristics being developed highlights the relative ease with which the methods can be designed compared to exact methods, with many heuristics having only subtle differences between them. As with all heuristics, care must be taken when considering the trade-off between global search efficiency (sufficient exploration of the solutions space) and local search completeness (level of fidelity when searching in near-optimal regions).

### **Commercial Tools**

In addition to academic studies there are several commercial tools that include turbine layout optimisation as a package within the tool. Many of these tools are developed for energy yield estimation but sometimes include additional features such as cable routing design. Detail on the exact methods and algorithms used within the tools is often not publicly available.

Notable tools in this category include the energy yield calculation tool WAsP, which employs the Jensen/Park model with root-sum-square superposition [23, 67] of wakes. WindPRO is primarily designed for annual energy production estimation and capable of

layout optimisation based on noise levels. modeFRONTIER is an optimisation framework and has been used for simulation process automation and design optimisation, including studies on monopile design optimisation. DNV's WindFarmer, commonly employed by wind farm developers, uses a wake model based on the Ainslie Eddy-Viscosity model. Openwind, another popular choice among developers [68,69], offers various wake models and can optimise for LCOE while considering electrical losses, noise impacts, shadow flicker, and GIS constraints. WindSim is built on a computational fluid dynamics approach to address wake effects in detail. These tools provide a range of features and capabilities for optimising wind turbine layouts [70] and assessing wind farm performance, though the specifics of their underlying optimisation algorithms may not always be publicly disclosed.

## 2.2 Cable Layout Optimisation

The electrical infrastructure of offshore wind farms contributes a very large capital cost to projects, at approximately 15-30% total initial investment costs [61,71]. In the UK, the Offshore Transmission Owner has some of this cost, meaning the inter array cable network constitutes approximately 1.6% of capital costs for wind farm developers [9]. Additionally, since most of this infrastructure (long sub-sea array cables) is sub-sea, it is more difficult and expensive to access than in an onshore wind farm, with access far more subject to weather conditions and favourable sea states. This high cost and difficult access means projects could benefit greatly from incremental improvements to the electrical infrastructure, found through optimisation techniques, minimising performance indices such as the total network length, capital costs, and associated electrical losses.

### 2.2.1 Costs & Electrical Losses

The primary considerations of a cable layout optimisation are the capital costs and the electrical losses. The layout topology heavily influences electrical losses of the system [72, 73], therefore, most studies in the literature include electrical losses as a key component of their objective function in addition to capital costs [54, 71, 74, 75]. Some

studies simplify this calculation to limit the impact on computational time, for example by assuming that the current experienced by a cable is half of the current at rated power [76]. This proxy for the true current profile of a cable connection may be computationally quicker, but introduces significant assumptions about the non-linear electrical losses of the cables. Typically, studies that compute electrical losses for cables do so in a pre-optimisation phase, where losses are calculated for each cable under different scenarios (supporting different numbers of turbines) [77, 78]. The losses then can be appropriately considered for each cable in a given layout, considering the losses for the correct scenario/electrical-loading. Since the cost of electrical losses is a function of the price of energy, some consideration has been given to the effect of a changing price of energy in the future. It has been shown that, for a realistic fluctuation in the energy price, the optimal layout of the collector network was not significantly affected [78].

### **2.2.2 Collector Network Topologies & Attributes**

Various recent studies, particularly since 2010, have investigated collector network topologies to reduce the cost of the array cables through cost comparisons, modelling, and redundancy measures. A chosen topology heavily influences the electrical losses of the cable network, however has little impact on the voltage levels throughout the collector system [72]. Detailed cost modelling of the system, and the different topologies, is necessary to accurately assess the quality of proposed layouts, which can have significant impacts on decisions such as whether or not a substation is required. For example, one study, considering a small 150 MW wind farm, showed that a substation was necessary only when the wind farm was further than 3km from the shore [79]. Reliability assessments and consideration of strategically placed breakers and redundant cables have been shown to improve solutions, when compared to real wind farm sites such as the Lillgrund offshore wind farm [72, 80]. Real projects typically use multiple cable sizes, which is an important factor influencing the cost, so selecting the most suitable cable rating for each section is essential for the whole infrastructure optimisation. While most approaches identify the peak current of a given connection and size the cables accordingly, it has been shown that considering equivalent cyclical loading and

temperature limits of cables can greatly reduce the necessary cable rating [81]. One such study demonstrated that only two of the original three export cables were necessary for a real site case study, however, noted that lost revenue may need to be taken into account during long periods of high wind speeds [81]. Larger cables tend to be favoured in routing and optimisation studies that consider lifetime costs and electrical losses, compared to real world networks [82, 83]. However, the trend of increasing cable ratings to reduce the electrical losses has been shown to be a valid strategy with limitations. One study demonstrated that sizing cables to carry the total power of a string and the total power of a neighbouring string - during a fault, through a redundant connection - was not cost effective [83].

### 2.2.3 Optimisation

#### Classical Methods

Classical methods for cable layout optimisation have centered around mixed-integer linear programming (MILP) [54, 71, 74, 77], where a combination of binary and non-binary variables are employed to describe the location and size of cables [77]. MILP problems are categorised by a linear objective function and contain some decision variables that are allowed to assume only integer values, while others are allowed to assume continuous values [84]. Studies taking this approach have shown that branched layouts outperform non-branched radial layouts and that using offshore transformer modules at selected turbines instead of a dedicated substation can greatly reduce lifetime costs [85]. The MILP formulation is also capable of considering looped cable layouts and branching connection costs [86, 87], as well as utilising Steiner (non-turbine or empty) nodes for obstacle avoidance [71]. Steiner nodes are ‘empty’ nodes that do not relate to anything in reality, but offer a point in space through which cables may pass to avoid obstacles [88]. MILP can be used to solve problems of a capacitated minimum spanning tree (CMST) formulation and has been used in conjunction with path-finding algorithms, substation positioning [89], and turbine layout optimisation [48]. A CMST is a graph optimisation problem that extends the classic minimum spanning tree (MST) problem by introducing capacity constraints on the edges of the graph. In a CMST problem,

the algorithm is tasked with finding a spanning tree (a sub-graph that connects all the vertices of the original graph without creating cycles), while considering the capacities of the edges. The goal is to minimise the total weight (or cost) of the tree while ensuring that the total weight of edges incident to each vertex does not exceed its given capacity [71, 89, 90].

The MILP method though, can be very computationally expensive, particularly in terms of its memory requirements. This means the algorithm is not a sufficient solver when the underlying MILP model is very large and the formulation is weak [75] and may need ‘warm-starting’ by providing a reasonable starting solution [75]. For example, one study optimised sub-problems of a larger cable layout problem, to seed the final MILP solver with a sufficiently good quality initial solution [71]. Using this method, the solver was able to find the optimal solution to approximately half of the case study scenarios within 24 hours. Furthermore, an earlier integer linear programming (ILP) study employed a model strengthening and additional cutting-planes method to improve the performance of its ILP solver, but suggested that heuristics may be a good approach for Steiner tree problems such as offshore wind farm cable layout optimisation [91]. A more recent ILP study considered wind farms with several substations and allowed connections to another local wind farm. The largest case study considered contained 102 turbines and generated solutions quickly, but lacked several key constraints. Constraints that were in the study included ensuring all turbines were connected by a cable, a maximum number of feeder cables to the substation, and power flow conservation constraints [92]. Constraints not in the study included a wind farm boundary, obstacle regions, and cable crossing constraints [92].

### **Heuristics Methods**

Other approaches have been taken in the cable layout optimisation literature, with heuristics offering a good alternative to MILP-based solvers. Heuristics, although not guaranteed to find the optimal solution, have been shown to produce good quality solutions for a global search [93–95]. One study on a no-branching layout demonstrates that the cost of the heuristic designed layouts is only 2% more than the optimal solution

[93]. Another study demonstrated that a Voronoi diagram based adaptive PSO method with additional local search heuristic could produce a 12.74% cost reduction compared to a benchmark case [96]. A Voronoi diagram is a metric space decomposition method, whereby the ‘nearest-neighbour’ rule is used on each discrete point in the diagram to ascertain the region of the plane to which it belongs [96]. While PSO is considered by some studies for cable layout optimisation, it seems that alternatives such as GAs and route-finding algorithms such as ACO (discussed further later) are more widely used in the literature (with PSOs more widely used in turbine layout optimisation, as discussed previously). The study by Pillai et al. [66] does consider PSO in a comparison to a GA, finding that in some cases the PSO delivered better solutions, and for other cases the GA produced the best solutions. Serranno Gonzalez et al. [49] conducted a similar study comparing a GA and PSO method and similarly found good results from both the GA and PSO, with very small cases-specific differences between the objective values of solutions from the two algorithms. Clustering-based algorithms, such as quality threshold (QT) clustering, optimise solutions that reduce electrical losses and improve reliability, but increase the capital expenditure. These QT algorithms, despite generating good quality solutions, can lead to a high degree of cable connections at turbines, with one study’s proposed layout having 13 cables entering a turbine node [97] which is not a feasible solution in reality. Similar approaches have been taken focusing on optimising the grouping of turbines to be connected in strings, for example, grouping turbines using k-means clustering and a GA, while relying on a simple minimum spanning tree (MST) algorithm to compute the shortest cable routing for each group [98]. Similarly, a Euclidean minimum Steiner tree approach has been explored, utilising a ‘GeoSteiner’ algorithm solver. This method was able to generate solutions to small problems (e.g., approx. 30 turbines) in less than 1 hour, however the computational time quickly increased to around 10 hours for larger cases (e.g., approx. 50 turbines). Additionally, the proposed layout solutions contained many branching connections at the Steiner nodes, which again is not a practical solution for real offshore cases [43]. While minimum Steiner trees are very similar to MSTs, in an MST the arcs may only branch at turbine nodes, whereas the arcs in a Steiner tree may also branch at empty Steiner nodes

(or anywhere along the arc) [22]. To make this formulation more applicable to offshore array cable layout optimisation problems many studies introduce additional constraints to limit the number of cables that may enter/leave a Steiner node [71,85,95]. In limiting the number of cables into/out of a Steiner node to one, this avoids branching at these empty nodes where it would be impractical for real applications, Figure 2.2.

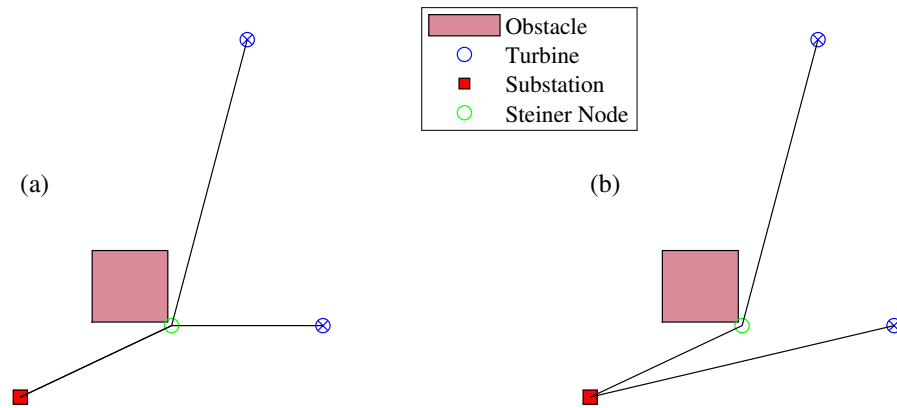


Figure 2.2: Example of use of Steiner nodes.

Figure 2.2 (a) shows the Steiner node being used to navigate around the obstacle to connect the turbine at the top of the figure to the substation. A branched section of cable also connects at the Steiner node to connect the second turbine. Since the Steiner node only represents an empty point in space (on the seabed in the context of offshore wind farms), this is an unrealistic layout for offshore cases due to the impracticality of connecting cables at the seabed location described by the Steiner node (rather than at a turbine or substation). A more realistic layout is proposed in Figure 2.2 (b), where the Steiner node is still used to navigate around the obstacle, but the second turbine is connected with a second string. In an unconstrained Steiner tree where Steiner nodes can be placed anywhere, these nodes are often placed at Fermat points to minimise the distance between vertices. For triangles (with a maximum internal angle of less than  $120^\circ$ ), this is an internal point minimising the sum total distance to all vertices or (if an internal angle is greater than  $120^\circ$ ) it would be located at one of the triangle vertices [22]. Several studies in the academic literature use Steiner nodes, placed

strategically rather than at Fermat points, to facilitate the avoidance of obstacles, as in Figure 2.2. Fagerfjall et al. [99] uses a grid of Steiner nodes for the optimisation to use. This offers great flexibility in the available routes for cables but increases the number of arcs and therefore the computational complexity of the problem. The authors suggest that more motivated positioning should be used for Steiner nodes, proposing that the number of Steiner nodes can be reduced when the turbine positions are fixed. While the authors don't employ a constraint to limit the number of connections in the Steiner node, the same study introduces a constraint to split Steiner nodes that have branched connections, creating multiple nodes at each location and allowing multiple cable routes to use the node without actually connecting/branching there. Several studies by Fischetti et al. [71, 85, 87] and one by Cazzaro et al. [95] present formulations with Steiner nodes located at obstacle vertices for improved obstacle avoidance, without a significant increase in the number of nodes and computational complexity.

Other heuristic methods have been shown to be computationally fast with one study utilising a large neighbourhood search algorithm, followed by swapping and re-partitioning heuristics, claiming two orders of magnitude reduction in time-to-solutions [95]. GAs are promising heuristic methods, capable of handling large numbers of turbines to connect through the collector network, with one study considering 280 turbines [11]. GAs are not without limitations, however, and it is important to ensure the parameters are well tuned to the problem under consideration. For example, in the mentioned case of 280 turbines, the resulting solution contained many crossing cables, one string that was not connected to a substation, and a few strings that could be seen through visual inspection to be non-optimal [11]. Combining a GA approach with clustering techniques and Clark and Wright's saving algorithm was shown to provide consistent and economically efficient layout solutions [94].

An interesting heuristic of note, the ACO algorithm was introduced in 1999 as a common framework for the many ant-system algorithms of the time [100], presenting applications of the algorithm to travelling salesman problems (TSP) and network routing problems. The general principle of the algorithm is that a colony of ants traverses the arcs in a graph, aiming to connect the start node and destination node via the

shortest route. Information about each of the explored routes is stored as a pheromone deposit on some or all of the arcs taken in the route (with shorter routes resulting in a greater pheromone deposit). Pheromones from previous routes/ants incentivise future ants to take a given arc, while an evaporation of the pheromone at each iteration prevents premature convergence on a non-optimal solution [100]. Although the method clearly has applicability to cable layout optimisation problems, ACO has only been used in a few promising cable routing optimisation studies. One of the earliest studies to use ACO in this application was that by Wu et al. [40]. In this study, the authors use ACO for the cable layout optimisation considering 32 turbines and three cable sizes, but limiting string lengths to a maximum of three turbines. While the implementation in the paper seems to be sensible, the resulting cable routing presented by the authors is clearly non-optimal by visual inspection [40]. As a heuristic approach, it is important to ensure that the parameters are reasonably tuned for the problem. If the presented route is identified as the optimal (or final) route by the algorithm, it is likely that the pheromone deposit was too low and/or the evaporation constant was too high. The ACO algorithm has also been demonstrated on very large cases containing 280 turbines [101], optimising cable routing for different substation positions and considering several cable sizes. This scale of problem is more in-line with modern wind farm sizes, where large numbers of turbines ( $>100$ ) need to be connected by the array cable network. Optimisation methodologies for real offshore wind farm array cable networks will need to be able to consider not only large numbers of turbines, but also different cable sizes, obstacles, and varying electrical losses [10]. A more recent study by Wu et al. [102] goes further by not only considering obstacles, different cable sizes, and electrical losses, but also three-dimensional bathymetry to influence the cable routes. The case study in the paper considers only a very small number of turbines to be connected, but does so in a two-layer optimisation with turbine layout considered in the outer layer. This shows the applicability of the ACO algorithm to cable layout optimisation and integration with other aspects of offshore wind farm design. Comparison with classical methods such as MILP, will be useful in determining if this approach is reliable, quick, accurate enough for use within a larger scale integrated optimisation with turbine layout.

### **Decomposition Strategies**

As modern wind farms increase in size - both in terms of power generation and the number of turbines - the complexity of cable layout problems increases dramatically, and even more so for integrated optimisation of cable and turbine layouts [103]. It is also increasingly important to optimise the cable layout, rather than restrict it to any given topology in advance [103]. Therefore, cable layout optimisation algorithms must be robust and computationally efficient, a challenging issue for which decomposition strategies may be able to provide a solution. Many optimisation algorithms use branch-and-bound (B&B) techniques within the solver. Hendrix et al. (2010 pg.159) highlighted the similarity of this process to problem decomposition as “The basic idea in B&B methods consists of a recursive decomposition of the original problem into smaller disjoint sub-problems until the solution is found” [53]. The decomposition of a problem can be considered as the isolation of a subset of the decision variables for optimisation, while all other variables remain fixed. Recursively decomposing a problem into different subsets of the decision variables allows solvers to reach optimal solutions more quickly. Several studies have employed decomposition techniques (beyond the B&B algorithm in solvers) to improve the performance of their MILP algorithms [88], in some cases reducing computational time by up to 98% [104]. Such studies [88,104] typically apply decomposition strategies to classical MILP methods, but not to heuristics which may also benefit from the decomposition approach.

### **2.3 Integration of Turbine & Cable Layout Optimisation**

As shown in the previous sections, there are many academic studies that focus on the optimisation of the turbine and cable layouts separately. However, the cable layout of a wind farm is inherently linked to the positions of the turbines and sub-stations. Integrating these aspects into a more holistic concurrent optimisation process has increasingly been the focus of investigations in the literature. This section aims to provide an overview of the studies concerned with a combined optimisation of both the turbine and cable layouts. For the purpose of this thesis, optimisation approaches that consider

both turbine layouts and cable layouts are termed *sequential optimisations* if they are considered in two distinct optimisation steps independent from one another, or *integrated optimisations* if they are considered concurrently in a single optimisation framework.

### 2.3.1 Early approaches

One of the earliest studies to consider an integrated approach is by Gonzalez et al. [44] where two nested EAs are used to optimise the turbine layout and the electrical infrastructure layout. The study compares solutions to a sequentially optimised method and performs a sensitivity study on the interest rate and price of energy. However, only up to eight onshore turbines are considered which is far from a large-scale offshore wind farm. Wu et al. [40] also use heuristic algorithms, with a GA for turbine placement and an ACO algorithm for the cable layout. This study uses the discrete grid-based set of possible turbine positions discussed previously (with no preset number of turbines) resulting in a site of around 32 turbines. Only strings of a fixed length (supporting three turbines, and one supporting two turbines) are used in the site and the resulting cable layout can be seen to be far from optimal. Another early study by Fagerfjall [99] also considered both the turbine layout optimisation and cable layout optimisation using a MILP approach. The study developed two models, the *Production Optimization* model and *Infrastructure Optimization* model. Considering each section of the wind farm layout optimisation problem separately (turbine layout and cable layout), this early study showed the benefits of optimisation of these two key aspects of wind farm design, but did not determine if an integrated approach (as defined in this thesis) would yield improvements over a sequential optimisation of the turbine layout followed by the cable layout. Pillai et al. [22] develops, validates, and integrates three optimisation modules into a single integrated optimisation framework to determine if an integrated approach can generate improved solutions. The three modules consider electrical infrastructure, annual energy production, and wind farm cost assessment. The single integrated optimisation framework is applied to several benchmark cases from the literature with comparison made to the original study. The approach shows improvements in the solutions compared to the original studies suggesting there could be benefits from taking a

more holistic approach to wind farm layout optimisation. However, the comparison between the original studies and the new optimisation framework leaves some uncertainty as to where the benefit is coming from (i.e. from the new implementation of the individual optimisation modules/algorithms, or from the act of integrating several modules into a single optimisation framework).

### 2.3.2 Degrees of integration

Some studies consider both the turbine layout and cable layout but integrate only aspects of these into the full algorithm. For example, the study by Amaral et al. [105] uses the electrical losses of the cable layout to influence the turbine positions, however, the cable routing itself is predefined in a looped structure connecting specific turbines. A GA and PSO algorithm is used for the optimisation of turbine positions but no optimisation of the cable routing is presented. Shin et al. [98] uses a pattern search (PS) algorithm to offer a simple, yet effective approach to the concurrent optimisation of the substation positioning with the cable routing, as this is more heavily affected by cable layout than turbine positions. The optimisation of turbine positions is omitted from this study, instead taking the turbine layout as an input. Fischetti et al. [75] includes a greater number of components to be optimised, covering the turbine layout optimisation, cable layout optimisation, and jacket design optimisation. The proposed methodology [75] considers these in a three-step sequential optimisation, which does not affect the solutions of the previously optimised step. Large improvements over real world sites are demonstrated though and the study suggests a truly integrated approach (of at least the turbine and cable layouts) as a valuable area of future research. Marge et al. [106] present a concurrent turbine and layout optimisation, considering a site of 30 turbines. However, the inputs to the model are a discrete set of turbine layouts which are assessed for wake effects before having the cable layouts optimised. Rather than necessarily optimising the turbine layout, these discrete solutions are used in post-processing to form continuous curves of the objective value from which an optimal turbine and cable layout can be determined. Serrano-Gonzalez et al. [49] claims that the electrical infrastructure represents around 2-5% of the total offshore wind farm cost and

so is negligible and therefore does not calculate electrical losses of the cable network. The study focuses mostly on grid-based layout optimisation of turbine positions and only includes cable capital costs for the turbine layout solutions in order to assess them based on LCOE. A simple approach is used to cable routing, Prim's algorithm, which finds the shortest path cable connections and doesn't explore to what extent this might affect turbine positions. Srikakulapu et al. [101] optimises the angle between rows of turbines, however the turbine layout optimisation method is not clear, nor present in the objective function. The turbine layout is formulated as columns of turbines with a given row and column spacing and a repeating pattern, and cable routing is handled by an ACO-MTSP to minimise cable lengths. Although very large numbers of turbines (280) are considered, it is not clear what level of integration these turbine and cable layout optimisations have and it appears that no significant improvement is found over the reference case.

### 2.3.3 Grid-based turbine layouts

Many studies that do integrate the turbine layout and cable layout optimisations more comprehensively, do so with a limited solution space. They do this, for example, by using a discrete set of possible turbine positions similar to that of Mosetti et al. [37], as discussed previously. Wu et al. [43] uses a 10x10 grid of possible positions for the turbine layout optimisation, testing a fixed and variable number of turbines and four different objective functions. The cable routing comprises straight-line connections set up using a Euclidean minimum Steiner tree (EMST) and solved by a GeoSteiner algorithm. The resulting solution relies on multiple cables connecting at a Steiner (empty) node, which for an offshore site is an unrealistic assumption. Further, the computational time for a case containing 30 turbines is approximately one hour but increases quickly to up to ten hours for cases of 50 turbines, which demonstrates issues with the scalability of the approach. Another study utilising a 10x10 grid of possible turbine positions is that by Al Shereiqi et al. [54]. Turbine positions, cable layout, and electrical losses are optimised by means of a GA and a comparison is carried out between a sequentially optimised approach and the proposed integrated approach. The authors claim that the

integrated approach is able to provide small reductions in the cost of energy (approximately 0.65%), however the small discrete grid of turbine positions means that it is not an approach that is currently sufficient for real world applications, particularly for large wind farms. A third study in this space is by Tao et al. [107]. This study uses a bi-level multi-objective optimization framework where there is an outer layer optimisation concerned with maximisation of the wind farm's daily profit and capacity factor, and the two inner layers concerned with cable layout optimisation and generation scheduling of other generators. The outer layer is solved by the Non-dominated Sorting Genetic Algorithm-III (NSGA-III) while the inner layers utilise Binary Particle Swarm Optimization (BPSO) and quadratic programming (QP) methods respectively. The study claims that the joint optimisation provides better solutions than a sequentially optimised solution, however this is all based within a discrete set of 12x12 possible turbine positions which is a large simplification of real sites.

### 2.3.4 Heuristic methods

Since the formulations of the turbine layout and cable layout optimisations can be computationally complex individually, it is no wonder that an integrated approach must consider computational efficiency. It is for this reason that many studies in this space continue to use heuristic methods to tackle the integrated design problem. The study by Pillai et al. [66] optimises turbine placement, substation placement, and cable layout in a coupled process, testing both GA and PSO approaches for comparison. It is found that the cable layout and cost modules considered do not greatly affect the results due to the simplicity of the test cases. In this study [66], turbines are restricted to a discrete set of positions in a 10x10 grid, and no limit is imposed to the number of turbines supported by a cable, resulting in a solution with two strings, one supporting one turbine and the other supporting 38 turbines. The GA and PSO algorithms are both found to perform well, with the results suggesting that the PSO offers significant computational time savings. The same authors propose another study [48] in which a GA approach is used exclusively for the combined turbine and cable layout optimisation in order to minimise LCOE. The study includes many real world constraints such as a grid-based layout of

turbines to ensure regularity for shipping and search and rescue (SAR) operations. Wu et al. [102] focuses on adding a high degree of detail to the real world constraints but for very small numbers of turbines. The study considers three-dimensional wind turbine layout and three-dimensional cable network routing based on meta-heuristic algorithms and geographic information systems using a two-layer model. The outer layer of the model is for site selection, while the inner model is for the obstacle-avoiding cable routing optimisation. The two layers are solved using an ACO combined with a GA for the outer layer, and a dual-simplex method and Kruskal algorithms are used for the inner layer. A simple wake model is used - the PARK model - based on the Jensen model and the improvements by Katic et al. [23] for the representative offshore wind farm site (Skipjack), where solutions contained between 10-12 turbines. Another study by Pillai et al. [64] integrates the turbine layout and cable layout optimisations, using a PSO for the turbine layout and CMST solved by a MILP solver for the cable layout. The study considers eight key cost centres including turbine cost and installation, foundation cost and installation, array cables cost, O&M, decommissioning, and offshore transmission cost. The computational time of the algorithm is between 1-3 days which is likely because of the MILP solver section. Without constraining the cable layout solutions sufficiently, some solutions appear unrealistic. For example, one layout solution contains two strings, with one string supporting one turbine and the other string supporting 38 turbines.

### **2.3.5 Increasing the number of turbines**

More recent studies have looked to increase the number of turbines considered in the integrated optimisation of turbine and cable layouts. Fischetti et al. [108] still use a modest number of 10-20 turbines but with 40 nodes for cables to connect through. The authors state that for a cable layout optimisation this number of nodes is quick to optimise but computational time will increase quickly as the number of nodes in the problem increases. The study is developed on a MILP based formulation that does not scale well with problem size, so the authors suggest using heuristics in future works. Another study, by Perez-Rua et al. [109], considers up to 74 turbines for an integrated

turbine layout and cable layout optimisation. The authors use the Bastankhah wake model and a gradient-free algorithm that optimises turbine layout and calls a heuristic algorithm in every iteration to perform the cable layout optimisation. As the algorithm progresses, the heuristic algorithm is replaced by a MILP algorithm to provide a more accurate and reliable optimisation of the cable layout. The study claims to provide up to 6% improvement in the internal rate of return of the fully feasible solutions and that the results are broadly statistically significant. The method considers irregular turbine layouts and linear and branched strings for the cable routing optimisation. Additionally, the authors discuss the difference between the heuristic- and MILP-based approaches to cable layout optimisation, stating that the heuristic approach produces solutions that are up to 8% more expensive. While this seems like a significant increase, the heuristic approach could be limited by the maximum computational time constraint applied within each function call as the overall algorithm is run, and so may be less significant if allowed to run for longer. An earlier study by Hou et al. [110] increased the number of turbines in the site to 80, again concurrently optimising both the turbine and cable layouts. The wind turbine locations are optimised through an adaptive PSO algorithm and the cable layout through an adaptive PSO-MST method. The study performs several case studies on the NORCOWE reference wind farm, showing reductions in levelised production costs of up to 1.45% and 5.00% for a sequential and integrated optimisation process respectively. The set of integrated design results vary by approximately 2% in their objective values and no details about computational time are provided, however the study does select the simple Jensen wake model in an attempt to minimise computational time.

## 2.4 Energy Storage Systems

Beyond layout optimisation, energy storage systems (ESS) offer potential to loosen the constraints of the cable routing and selection algorithms by integrating the optimisation of offshore ESS location and cable layout optimisation. ‘Peak shaving’ the power carried by a connection may offer opportunities to reduce the required cable rating (and therefore cost) or reduce the electrical losses [111]. To date, many studies that consider

ESS with wind energy do so for varying objectives such as using ESS to support a grid containing a high penetration of renewable energy or to provide benefits to the accuracy of the output of a wind farm relative to predicted output [111,112] .

#### **2.4.1 ESS in Grids with High Renewable Energy Penetration**

Dagdougui et al. [113] presents a dynamic model of a hybrid system, integrating a hydro-electric plant, fuel cells, and a wind farm. The focus of the study is not the optimisation of the ESS sizing or location but rather the optimal control/operational management of the distributed hybrid system. Considering real sites in Morocco, the aim of the study is to satisfy the hourly electric, hydrogen, and water demands, however the authors highlight that the many simplifying assumptions may make their approach inadequate for real application.. Similarly, a study by Dvijotham et al. [114] considers the use of ESS within a grid containing a high penetration of renewables, however unlike Dagdougui et al. it does optimise the size and location of the ESS within the network. An optimal energy storage control algorithm is used to develop a heuristic procedure for ESS sizing and placement. Initially, the study allows infinite amounts of ESS capacity in the solutions at all nodes in the network, then begins to restrict the number of ESS units in a staged procedure to find the minimum number of units that can still mitigate the effects of renewable fluctuations. Comparisons are made to ‘intuitively’ designed solutions, showing that the optimal solution does not preferentially place ESS at the nodes with renewable generation as was expected by the authors. Rather, the optimal solutions favour nodes at critical junctions between major sub-components of the network, but the control system proposed in the study requires perfect forecasting of renewable energy generation, which is not necessarily realistic. Le et al. [115] present an ESS application design for regulating wind power variation and increasing grid voltage stability. The study considers compressed-air energy storage (CAES) within a 27-bus transmission grid containing 14 wind farms. Optimal ESS rating and charge-discharge strategy are determined using an exhaustive search method, with results showing that the ESS is effective in raising both the wind energy revenue (1.7-8.0%) and the grid voltage stability (8.3-18.3%). Wang et al. [116] considers how ESS may be utilised

in a transmission network in the context of slow ramp up (or down) of conventional energy generation leading to a potential energy shortage (or surplus) in power systems with a high degree of wind power penetration. Similar isolated micro-grids with limited dispatchable capacity are also considered. The study’s simulation results show the ramp rates of the conventional generation have large impacts on energy not used and energy not supplied. The authors claim that the incorporation of wind farms without ESS has very limited system reliability improvement and can lead to a large amount of energy surplus. While grid considerations are very important for the wider system and may well affect future wind farm developments, this thesis aims to determine the potential benefits of co-located ESS and wind energy that may be owned and operated by the wind farm operator.

#### **2.4.2 Co-located ESS and Wind Turbines**

Castronuovo et al. [117] consider the siting of a pumped-hydroelectric power plant with an onshore wind farm to be used for a process similar to energy price arbitrage. Energy from the wind farm is used to ‘charge’ the pumped-hydroelectric component at times of low price and energy is discharged from the store during times of high energy price. While this isn’t suitable for large offshore wind farms (or many other onshore sites that do not have the required topographical features necessary for pumped-hydroelectric storage), co-locating such facilities can provide added benefit to operators of hybrid wind-ESS sites. Barton et al. [118] present a probabilistic method for ESS sited with wind and solar generation that estimates the fraction of time that the ESS spends at empty or fully charged states. The method is validated against a standard time-stepping approach and intends to improve the use of distributed generation for small local loads. The study only considers very small installations, up to 3MW rated power, so may not be highly relevant for the large offshore wind farms under investigation in this work. Pairing wind with ESS for improving the dispatched power, the study by Abbey et al. [119] focuses on an ESS management algorithm. The knowledge-based algorithm proposed schedules power from a two-level ESS and is shown to require 20% less ESS capacity than a base case alternative. The aim of the study is to use short-term storage

devices for the constrained integration of wind energy to serve a local load in islanded operation. Yao et al. [120] uses a two battery energy storage systems (BESS) approach where the generated wind power charges one BESS while, concurrently, the second BESS is used to discharge power to the grid. The objective of the study is to use the two-BESS set up to enable short-term dispatch commitment from grid connected wind generation. Forecasting is used to predict wind power output and BESS state-of-charge a few hours ahead. The dispatch scheme aims to maximise the harnessed wind energy with the minimum number of BESS switch-overs to help prolong the operational life of the BESS. The authors claim that this approach allows the hybrid system to operate as a power generation station and to participate in some degree of short-term power dispatch markets. However, concurrently charging one ESS while another discharges to the grid, introduces unnecessary losses that could be avoided with an improved approach to control. Kim et al. [121] consider different benefits of co-located ESS by using BESS and super-capacitors connected to a doubly-fed induction generator (DFIG) wind turbine. The study aims to reduce the total harmonic content, improving power quality from the turbine. Using a 1.5MW turbine (connected to a 60Hz grid), the ESS was able to clearly improve power quality and had a payback time of 3.5 years and 15.8 years for the BESS and super-capacitor respectively. Venkataraman et al. [122] propose that integrating wind, solar, and ESS into a hybrid generation station is particularly suitable for regions that have set high targets for wind and solar generation but have limited land available for project development. The study uses ESS for several functions, a primary application of reducing the financial penalty in the deviation settlement charge, and a second application of ancillary service provision. Also investigated is the shifting of renewable energy to peak demand hours while including the forecast deviation reduction for wind and solar plants. The authors claim that including ESS for these functions can also provide cost savings in terms of delaying transmission system upgrades. Moghaddam et al. [123] introduce a novel BESS control strategy to manage the energy exchange between a wind farm and the transmission grid using a receding horizon control approach. The ESS is used to maximise profits for the wind farm operator through utilising short-term wind and price forecasts which are provided as

inputs to the control strategy and can determine the best times to charge and discharge the BESS, including the option of purchasing energy from the day ahead market. When the wind power output exceeds the day ahead scheduled power, the extra power must be curtailed or used to charge the BESS. Alternatively, if the wind power is below that scheduled, the BESS can provide energy (or purchase it from the real time market) to increase the total power to the scheduled amount. This type of benefit to the operator of a hybrid wind-ESS development may be a suitable mode of operation to be undertaken concurrently with another providing benefits to the wind farm's array cable network, if the ESS is positioned throughout the site to do so.

### **2.4.3 ESS for Power Smoothing Applications**

Several studies consider the use of ESS for smoothing the power output of wind turbines and/or farm. Jiang et al. [124] integrate ESS into the DC link of a back-to-back converter of a 2MW DFIG wind turbine, with the ESS controlled to smooth the total power output of the turbine. Control algorithms are proposed that use pulse width modulation (PWM) for the grid side converter, generator side converter, and battery converter. The authors suggest that ESS can provide steady power output however no information is presented on the required size or cost of the ESS. Li et al. [125] presents a method on the design of a wind farm level BESS used in order to realise improved power dispatching. The method uses statistical long-term wind speed data from the site and proposes a dispatch strategy to help determine battery size and maximise the service life of the BESS. The study shows that, in order to increase the confidence level of the short-term power delivery commitment, the lifetime of the BESS is reduced. Tested on a 100MW wind farm, the size of ESS required is found to be between 10-90MWh depending on the cost of the specific BESS type. A very similar study is conducted by Luo et al. [126] where a coordinated dispatch scheme is proposed for a wind farm level BESS. The paper aims to reduce the impacts of wind power forecast errors while prolonging the lifetime of the BESS. The scale of BESS capacity required is proportionally similar to the lower end of the range provided in the study by Li et al., with 5MW/20MWh required for the test wind farm site of 25.5MW. A third study also takes a similar approach to

wind farm level ESS, using the storage capabilities to smooth the real power and reduce the error compared to the forecasted power and/or power delivery commitment. This study, by Xinda et al. [127], proposed three ESS control algorithms to achieve the goal of power-smoothing/error-reduction which are (1) tracking the minute-by-minute power imbalance, (2) post-compensation, and (3) pre-compensation. Tracking minute-by-minute provides the lowest power imbalance but results in an oversized ESS capacity, whereas the post-compensation approach reduces ESS size at the cost of non-zero power imbalance. The authors determine that it is important to consider the trade-off between the lifetime and the size of the ESS which will differ across operating strategies. While not presented in this work, the authors also claim that the charging algorithms are suitable for higher frequency (intra-hour) energy balancing and multiple-hour applications. Bataglioli et al. [128] integrates ESS into the DC link of a back-to-back converter similarly to some of the aforementioned studies. The integrated ESS is used to smooth the power output of the turbine and make it strong enough to operate in an island mode. The paper focuses on several fault types to investigate the wind turbine behaviour in such conditions, considering the operation in a smart grid context. None of these studies explore the effect on the array cables within the wind farm and if the smoothed power has a peak power low enough for cable de-rating. Impacts to the electrical losses would also be a valuable consideration to these approaches.

### **2.4.4 Ancillary Service Provision**

For ESS that is integrated with a wind farm, it is still possible to provide benefits to the grid through participating in ancillary service provision. Berrada et al. [129] used ESS to maximise the revenues of the wind farm by optimising the charging strategy. The study aimed to minimise the capacity of the ESS while meeting ancillary service requirements. The results indicated that more revenue is generated when storage is permitted to participate in both energy arbitrage and regulation services. Pumped-hydroelectric systems were shown to be most cost effective for generation applications (arbitrage), whereas CAES was found to be best for services relating to transmission and distribution applications (regulation services). While the study does include a simple

consideration of ESS lifetime, the authors highlight that a more detailed consideration of ESS lifetime could be valuable. Similarly to other referenced studies, the authors also suggest the approach would be suitable to other time frames, for example intra-hour balancing, however there is no investigation into this application in the study. Fan et al. [130] also consider multiple functions for the ESS, from time-shifting the wind energy generated to providing enhanced frequency response (EFR). The authors develop a simulation model in which the wind farm level BESS is connected to the grid at the wind farm connection point and also connected to the wind farm through an additional converter. While it is shown that the revenue from the four-year EFR contract is lower for the wind-BESS hybrid system than that of a stand-alone BESS (by  $<1\%$ ), the avoidance of charges associated with new assets and/or reinforcements needed for an independent connection greatly increases the project profitability. It is also found that, with the additional converter placed between the wind farm and BESS, the revenues generated by the time shift of wind energy is the highest final NPV among the different scenarios modelled, despite the increase in capital costs. The authors propose that the work should be extended to consider additional revenue streams such as black start and the stacking of multiple revenue streams. The paper by Campos-Gaona et al. [131] provides a good summary of the modern trends in ESS in the UK and reviews its application in the context of wind energy. The research takes into account the advantages and disadvantages of different options of ESS technology based on government and industry projects. Revenue streams and their approximate values are identified for the UK markets and the study also discusses the current UK regulatory framework regarding the implementation of hybrid wind-ESS projects partaking in the ancillary service markets. Key ancillary service revenue streams from the study by Campos-Gaona et al. are presented in the Appendix in Table A.1, however limited information is available for some revenue streams, and for others, such as frequency response, the battery-led competition is beginning to drive prices down [131].

### 2.4.5 Types of ESS

Many different types of ESS are available but not all will be suitable for the integration into wind farms, particularly offshore. While the majority of aforementioned studies have considered either pumped-hydroelectric or battery systems, some studies have also considered other approaches. Banham-Hall et al. [132] used a vanadium redox flow battery (VRFB) for supporting the DC link under grid faults and developed a control method for the storage system. The hybrid wind-ESS system is also controlled to allow the time shift of wind energy and to provide frequency response services which is shown to be effective. Zhang et al. [133] use a combination of ESS types for providing different services and improve the profits of the co-located wind farm project. A first stage uses a lead-acid battery to improve the wind energy revenue in the day ahead market; a second stage uses a lithium-ion battery to eliminate day ahead forecasting error and smooth the power fluctuations; and a third stage uses a hydrogen combined cycle ESS for ancillary service provision. The authors show that the profit of the wind farm can be increased by a very large 20.62% through using the multi-level integrated ESS and an optimised dispatch strategy. The review paper by Mahmoud et al. [134] considers the use of mechanical ESS (MESS) integrated with wind and/or solar projects and whether a series or parallel connection is best. Three main categories of MESS are investigated including flywheels, pumped-hydroelectric, and compressed air. The study determines that a series connection is preferable as it provides an automatic control to reduce any sudden increase/decrease in wind power output as power must first flow through the storage device (however this will introduce additional losses). Flywheels are found to be useful for short-term storage and have both the fastest response and the lowest system cost. Pumped-hydroelectric requires an elevated reservoir and so is often not an option for many wind farm installations. However, pumped-hydroelectric did offer the best long-term storage solution. CAES has a fast start up time but relies on having a compressed air system and in some cases a thermal store. Overall, the systems with the lowest capital cost per kWh are CAES and LAES at \$2-50/kWh and \$3-30/kWh, respectively [135–138]. In the Appendix, Tables A.2 and A.3 contain a summary of the key performance metrics of different types of ESS. Table A.2 includes typical power

ratings, response times, energy densities, and capital cost, while Table A.3 contains information regarding storage duration, lifetime, and environmental impact.

## 2.5 Identifying Research Gaps

The research questions initially posed at the start of the thesis consider what the impact might be of (1) integrating cable layout optimisation with a turbine layout optimisation and (2) utilising energy storage within a cable layout optimisation. A review of the literature regarding aspects of these two questions has been considered in this chapter covering: the current approaches to turbine layout design and optimisation; array cable layout design and optimisation techniques; the degree to which these have been combined into an integrated approach; and the applications of energy storage at wind farm level.

### 2.5.1 Integrated Turbine & Cable Layout Optimisation

It is shown in the literature, that a more integrated approach to wind farm layout optimisation may be desirable to produce improved solutions from a more holistic perspective [22] and that for most of the studies that consider such an integrated optimisation approach (as defined in this thesis) [40, 108], they typically do so under very restricted conditions such as limiting turbines to a discrete set of 10x10 positions [43, 66], using a very small number of turbines [102, 108], or limited consideration of real world cable constraints [40, 107]. Fischetti et al. [75] demonstrates large improvements in solutions when sequentially optimising turbine layout, cable layout, and turbine jacket design, and suggests a truly integrated approach (of at least the turbine and cable layouts) as a valuable area of future research. While Pillai [22] does show some improvements through an integrated approach of the turbine and cable layout optimisations relative to previous studies in the literature, some uncertainty remains as to the source of the improvements, i.e. if this is found from the integration of optimisation modules itself or from the new implementations/algorithms used. Isolating the effect of an integrated approach compared to a sequential one would help develop and influence future works in

the field of wind farm layout optimisation. This integration of the turbine and cable layout optimisations into a single framework, and isolating the effect through a sequential versus integrated comparison (using the same optimisation modules), therefore forms one of the key objectives of this thesis.

In order to address the first research question, and isolate the impact of an integrated optimisation approach, turbine layout and cable layout optimisations must be used independently in a sequential manner (as is the current standard in the wind industry) and as a combined concurrent integrated optimisation. Appropriate algorithms/tools must be selected for the turbine layout and cable layout optimisations. Several areas of interest are proposed in the literature concerning the requirements of future turbine layout optimisation algorithms. Azlan et al. [21] highlights some of these as: the need for developing an efficient optimisation approach for larger, more complex sites; the use of more accurate wake models; and a standard benchmark wind farm with data on the wind profile, turbines, and realistic boundary shape. In addition, interviews and conversations with industry experts conducted as part of this thesis, Appendix A, highlighted the need for a largely grid-based approach to turbine layout optimisation with the ability to slightly deviate from grid positions to increase energy capture (while observing SAR guidelines) [10,42]. Such a tool must be capable of running on a standard desktop PC in reasonable time [10] to enable its use as a practical engineering design tool. This will enable wind farm developers to more quickly assess different sites, technologies, and configurations, and in doing so will support early phase design decisions in turbine layout. Since the tool must also enable a cable layout optimisation to be integrated within it, it is imperative that the model is transparent and that a good understanding of the approach can be gained, rather than using a ‘black-box’ approach. A widely used algorithm in the literature [22, 57, 63, 66, 105], the PSO approach is selected as an appropriate algorithm for a grid-based turbine layout optimisation as it meets the above requirements of the tool and is a computationally efficient, iterative approach (facilitating easy integration with a cable layout optimisation). Additional micro-siting functionality is desirable, with turbines being able to move away from initial grid positions. This functionality is proposed to be a post-processing step after the initial

PSO optimisation is complete, similar to other studies in the literature [41,58], avoiding relatively complex micro-siting at each iteration of the PSO.

The cable layout optimisation algorithm must be computationally efficient, while also providing sufficiently good (close to optimal) results to influence turbine positions effectively. While many studies are investigating the use of MILP approaches to cable layout optimisation [54,71,74,77], several heuristic approaches, such as ACO, are gaining interest for this application which may offer improved computational efficiency for large-scale problems [93–95]. A direct comparison between the widely used MILP approach and a heuristic method would provide useful insight into the different methods, however, to go beyond the existing comparisons between heuristics and optimal solutions, a third approach should be taken utilising decomposition strategies to improve the performance of the ACO method. All methods should include a comprehensive set of constraints including, but not limited to, a wind farm boundary, obstacles in the site, avoiding cable crossings, and limiting the number of cables joints into turbine/substations. Interviews with industry [10] highlighted the need to include electrical losses, as is considered in many studies in the literature [54,71,74,75]; to be able to select both the cable routes and cable sizes; and the resulting framework must be capable of handling large-scale problems efficiently on standard desktop PCs. The layout topologies of interest for the tool to consider should include radial strings and allow for branched connections at turbine nodes; looped structures to the array cable layout need not be considered [10]. While there are many heuristics that could be used, the ACO method is an algorithm specifically designed for route finding problems [100] and has been demonstrated in one study on a very large wind farm [101] so is chosen as a suitable heuristic. The comparison of the three highlighted approaches (MILP, heuristic ACO, and ACO with a decomposition strategy) and the development of an efficient cable layout optimisation framework form the basis of the second objective of this thesis, outlined at the end of the chapter. The most appropriate algorithm, that is both computationally efficient and produces sufficiently near-optimal solutions, will be taken forward for the integration with the turbine layout optimisation.

### 2.5.2 Integrated Cable Layout and ESS Optimisation

One of the most significant constraints in cable layout optimisation for offshore wind farm array cable networks, is that the cable ratings must be sufficient to support the rated power of all the turbines that that cable connects [22,88]. However, as wind energy is a variable resource, the cable will not experience the rated power for a large proportion of the operational lifetime. Since larger cables use more material and are more expensive, there may be scope to ‘peak-shave’ the power experienced by a cable and therefore reduce the required rating and cost, sometimes referred to as "under-planting". Co-locating energy storage in the offshore wind farm could provide this peak-shaving service and may allow this constraint on the cable layout optimisation problem to be ‘loosened’. If practicable, this approach could reduce a significant source of both capital (cables) and operational (electrical losses) costs for offshore wind farms.

Considering ESS in the context of renewable energy generation, several studies focus on hourly balancing mechanisms with varying approaches, and only some optimising the ESS capacity [113,114]. A subset of ESS studies do consider ESS co-located with wind energy generation [117,118,130], however, these studies typically focus on energy price arbitrage or improving power dispatch. Peak-shaving using ESS has been demonstrated as an effective solution for other applications, such as finding cost reductions for an industrial customer [139], deferring infrastructure upgrades in residential areas [140], and energy loss minimisation [141]. However, with no studies meaningfully integrating ESS into a cable layout optimisation framework, the academic literature currently has a gap in determining the extent to which ESS may be able to influence the array cable layout of large offshore wind farms when used in a peak-shaving capacity. This integrated ESS-cable layout optimisation builds upon the cable layout optimisation approaches discussed in the previous chapters, and advances the current understanding of ESS utility in offshore wind farms, forming the final objective of the thesis.

## 2.6 Thesis Objectives

In order to achieve the aims of this thesis and answer the two main research questions, the following objectives are proposed with reference to the relevant chapters:

1. Develop a turbine layout optimisation method capable of considering modern large-scale offshore wind farms (over 100 turbines) using a standard desktop computer (Chapter 3).
2. Develop an array cable layout optimisation capable of considering large-scale problems of the same size as the turbine layout optimisation in a computationally efficient manner (Chapter 4).
3. Integrate these two previous optimisation models into a single optimisation framework and compare the integrated design to sequentially optimised layouts (Chapter 5)
4. Integrate energy storage as a decision variable into the cable routing optimisation to determine to what extent energy storage may be able to change (or ‘loosen’) constraints and provide more cost-effective cable routing solutions (Chapter 7)

## Chapter 3

# Turbine Placement Optimisation

This chapter considers the turbine layout optimisation problem of large offshore wind farm design. With the importance of a regular layout (for considerations such as SAR operations highlighted in Chapter 2), and conversely the proclivity of developers to allow some deviation to maximise energy capture [10], the problem is formulated as a grid-based layout with the first phase optimising the parameters describing the grid and a second phase allowing some deviation away from original grid-based turbine positions. A wind farm model is proposed using a Gaussian wake model and common wake deficit summation method. A PSO optimisation methodology is described and several novel aspects are proposed for cases with a variable number of turbines. The model is validated using real data from the Lillgrund offshore wind farm and two cases studies are presented. The first considers a large - approximately giga-watt scale - wind farm and the second compares the proposed design method to SSE's in-house turbine layout optimisation tools.

### 3.1 Wind Farm Model

The wind farm model considers only the effect of turbine wakes on the power production of the offshore wind farm, given the wind conditions described by a wind rose for the site. Several studies, including those by Pillai et al. (2014) [36] and Göçmen et al. (2016) [29] compare the accuracy and computational time of several wake models.

Although slower than the more widely used Jensen wake model, the Larsen model more accurately predicts the wake behaviour and offers the best compromise between accuracy and computational time. The Larsen wake model [24] calculates a point wind speed as influenced by an upstream wake. There is no one definitive method for the summation of multiple wake effects on a given point in space and so the well-known *energy-balance* method is used [29], also known as the *root-sum-square* method [36]. Point wind speeds are evaluated in this way at multiple locations across the downstream rotor and are used to generate a rotor effective wind speed. This may then be used to generate the wake effect of the rotor on turbines further downstream. It is desired that the model not only be accurate in its assessment of wind farm power production but also be computationally efficient. This is because some optimisation methodologies require large numbers of iterations - and therefore many evaluations of the model - which can make the optimisation process very slow if the evaluation of the wind farm model is not sufficiently quick.

### 3.1.1 Larsen Wake Model

The Larsen wake model was first proposed in Larsen (1988) [24] and is a simple and quick, yet efficient, wake calculation procedure. For this study the wake model (Equations (3.1)-(3.7)) were coded by the author using Matlab R2018b.

The model calculates a point wind speed at a downstream location that is impacted by the wake of an upstream rotor, and is a function of the thrust coefficient of the upstream turbine, downstream distance, and radial distances from the centre of the wake. Improvements to the model were proposed in Larsen (2009) [142] which included a correction term for the ground effect on the wake using an empirically found relationship related to ambient turbulence.

The main calculations of the Larsen wake model are described in this section. The wind speed,  $u$ , at a point,  $n$ , on a downstream rotor,  $i$ , within the wake of an upstream turbine,  $j$ , can be given by:

$$u_{inj} = u_{\infty} \left[ 1 - \frac{1}{9} \left[ C_{T_j} A_i (x + x_0)^{-2} \right]^{\frac{1}{3}} \left( r^{\frac{3}{2}} \left( 3c_1^2 C_{T_j} A_i (x + x_0) \right)^{-\frac{1}{2}} - \left( \frac{35}{2\pi} \right)^{\frac{3}{10}} \left( 3c_1^2 \right)^{-\frac{1}{5}} \right)^2 \right] \quad (3.1)$$

where:  $u_{\infty}$  is the free-stream wind speed ( $m/s$ );  $C_{T_j}$  is the thrust coefficient of turbine  $j$ ;  $A_i$  is the rotor swept area of turbine  $i$  ( $m^2$ );  $x$  is the distance between turbines, parallel to the wind direction ( $m$ );  $r$  is the distance between turbines, perpendicular to the wind direction ( $m$ ); and  $x_0$  and  $c_1$  are parameters that describe the wake expansion.

$$x_0 = \frac{9.5d}{\left( \frac{2R_{9.5}}{d_{eff}} \right)^3 - 1} \quad (3.2)$$

$$c_1 = \left( \frac{d_{eff}}{2} \right)^{\frac{5}{2}} \left( \frac{105}{2\pi} \right)^{-\frac{1}{2}} \left( C_{T_j} A_i x_0 \right)^{-\frac{5}{6}} \quad (3.3)$$

where:  $d$  is the rotor diameter ( $m$ );  $R_{9.5}$  is the radius of the wake at a distance of  $9.5d$  downstream ( $m$ ); and  $d_{eff}$  is the effective rotor diameter ( $m$ ).

$$R_{9.5} = 0.5 (R_{nb} + \min(H, R_{nb})) \quad (3.4)$$

$$d_{eff} = d \sqrt{\frac{1 + \sqrt{1 - C_{T_j}}}{2\sqrt{1 - C_{T_j}}}} \quad (3.5)$$

To capture the ground effect on the wake, Equation (3.4) contains a correction term,  $R_{nb}$ , requiring the hub height,  $H$ , and an empirically found relationship related to ambient turbulence.

$$R_{nb} = \max[1.08d, 1.08d + 21.7d(I_a - 0.05)] \quad (3.6)$$

where  $I_a$  is the ambient turbulence intensity. The wake effect at a downstream point need only be considered if it is within the area experiencing a wake effect from an upstream turbine. To evaluate if this is the case for a given point, the wake radius at the downstream distance must be calculated. Equation (3.7) describes the wake radius

as a function of the downstream distance  $x$ , the thrust coefficient  $C_T$ , the rotor area  $A_i$  and the wake expansion factor  $c_1$ .

$$R_w = \left(\frac{35}{2\pi}\right)^{\frac{1}{5}} (3c_1^2)^{\frac{1}{5}} (C_T A_i x)^{-\frac{1}{5}} \quad (3.7)$$

For a given point,  $n$ , on a downstream rotor,  $i$ , if the distance,  $r$ , between the point and the centre of the wake is less than  $R_w$  then the point lies within the wake-affected region and Equations (3.1)-(3.7) must be evaluated to determine the wind speed as a result of the wake effect. If  $r > R_w$ , then the point lies outside of the wake and no wake effect needs to be calculated.

### 3.1.2 Summation of Multiple Wake Effects

For a given point, the summation of multiple wake effects can be achieved through the root-sum-square (or energy-balance) of the deficit factor,  $D$ , a non-dimensional description of the velocity deficit caused by the wake [23, 29]. The deficit factor can be calculated for each point,  $n$ , on the downstream rotor,  $i$ , for each of the wakes of upstream rotors,  $j$ , from the point wind speeds calculated by the Larsen wake model. Summing these using the energy balance equation [29], the resulting total deficit factor can be returned to a point wind speed as a fraction of the free-stream wind speed,  $u_\infty$ , [23].

$$D_{ijn} = 1 - \frac{u_{ijn}}{u_\infty} \quad (3.8)$$

The total deficit factor experienced by a point as a result of multiple wakes is:

$$D_{in} = \sqrt{\sum_j (D_{ijn})^2} \quad (3.9)$$

This can be returned to a point wind speed, now considering all wake effects, through:

$$u_{in} = u_\infty (1 - D_{in}) \quad (3.10)$$

where the point wind speed,  $u_{in}$ , is equal to the free stream wind speed,  $u_\infty$ , multiplied by one minus the total deficit factor,  $D_{in}$ , experienced at the point,  $n$ .

### 3.1.3 Rotor Effective Wind Speed

The rotor effective wind speed equation [143] is used to calculate the wind speed experienced by the rotor from the individual point wind speeds calculated by the Larsen wake model. As the power coefficient ( $C_P$ ) varies along the blade, the distribution of  $C_P$  must be known and used to weight the influence on power production for each point wind speed. This captures the effects of tip losses and low power production from the root of the turbine blades (however some studies suggest a single point measurement of the hub height wind speed is sufficient [144]). The rotor effective wind speed can then be used to look up the power and the thrust coefficient of the turbine, through the known power curve and thrust curve. These are then used to determine the wake effect of the current turbine on further downstream turbines. Sorting the turbines into upstream-to-downstream order (for each wind direction) and calculating the wind speeds as described, allows the model to estimate the aggregate effect of all the wakes on all of the affected turbines.

$$u_i = \left( \left( \int_0^{2\pi} \int_0^R u_{i_n}^3(r, \theta) \frac{\partial C_P}{\partial r} r dr d\theta \right) / \left( \int_0^{2\pi} \int_0^R \frac{\partial C_P}{\partial r} r dr d\theta \right) \right)^{1/3} \quad (3.11)$$

Equation (3.11) integrates the point wind speed values with respect to radial distance, from the rotor centre ( $r = 0$ ) to the blade tip ( $r = R$ ), and with respect to the azimuth angle (from  $\theta = 0$  to  $\theta = 2\pi$ ).

## 3.2 Formulation of the Turbine Layout

In this work, the grid for turbine positions is fully described by eight variables independent of the size of the site and the number of turbines. Compared to most other methods that have an (x, y) variable for each turbine, this formulation makes it much more efficient when scaling to larger, GW-scale wind farms due to the low number of

### Chapter 3. Turbine Placement Optimisation

variables included in modelling and optimisation. The eight variables are defined as follows:

1.  $\mathbf{m}_1$  - Angle of the central row of turbines (*radians* from north)
2.  $\Delta\mathbf{m}_1$  - Change in angle of two neighbouring rows of turbines (*radians*)
3.  $\mathbf{s}_1$  - Spacing between the rows of turbines along the central column (*m*)
4.  $\mathbf{m}_2$  - Angle of the central column of turbines (*radians* from north)
5.  $\Delta\mathbf{m}_2$  - Change in angle of two neighbouring columns of turbines (*radians*)
6.  $\mathbf{s}_2$  - Spacing between the columns of turbines along the central row (*m*)
7.  $\mathbf{x}$  - x-coordinate of the crossing point of the central row and the central column (*m* from datum in coordinate system used to define the offshore site)
8.  $\mathbf{y}$  - y-coordinate of the crossing point of the central row and the central column (*m* from datum in coordinate system used to define the offshore site)

Figure 3.1a is a graphical representation of the eight variables with turbines placed at the intersection of the rows and columns, with the central row and column indicated by the thicker blue dashed lines. Turbines can be seen marked by the red, filled circles. Figures 3.1b and 3.1c show two layouts, one with no change in the angles between rows or columns ( $\Delta\mathbf{m}_1 = 0$ ,  $\Delta\mathbf{m}_2 = 0$ ) and one with a change in angle between the columns of turbines ( $\Delta\mathbf{m}_1 = 0$ ,  $\Delta\mathbf{m}_2 = -0.1$ ) respectively. The grid is automatically generated with a sufficient number of rows and columns to cover the entire wind farm site being considered, by finding the largest dimension of the wind farm boundary and calculating the maximum number of rows possible assuming the closest allowable spacing of turbines. Each grid point is checked to determine if it falls within the wind farm area, excluding those grid points within an obstacle (user-defined region(s) where turbines cannot be built). Only the grid points within the buildable area have turbines built at that location which are then passed to the wind farm model to be evaluated.

This grid-based formulation allows for addressing of large-scale optimisation problems with a fixed number of variables. Compared to other studies such as that by

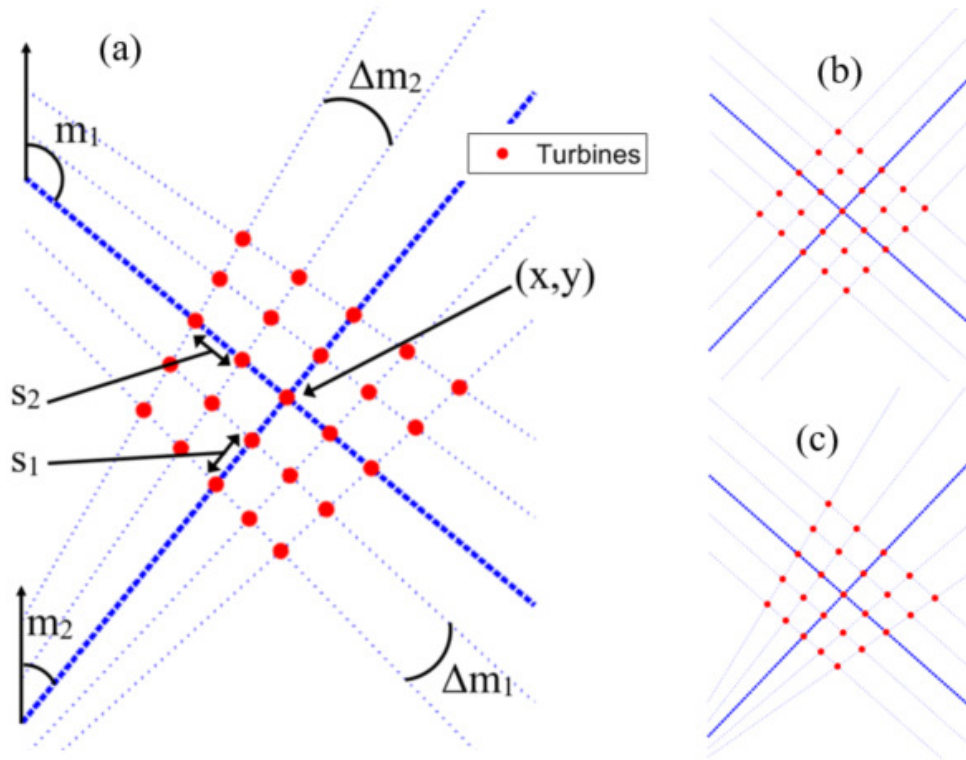


Figure 3.1: Turbines in a grid layout (a) Illustration of the eight variables describing the grid layout (b) Layout with  $\Delta m_1 = 0$ ,  $\Delta m_2 = 0$  (c) Layout with  $\Delta m_1 = 0$ ,  $\Delta m_2 = -0.1$

Serrano-Gonzalez et al. (2017) [49] with similar formulations, the set-up proposed here is suitable for wider wind farm sites and shapes given the inclusion of the two variables that describe the change in the angles of rows and columns.

In order to calculate the coordinates of individual grid points from the eight variables, the gradient ( $m$ ) and y-intercept ( $c$ ) are calculated for the straight lines representing each row and column from the eight decision variables. Equations for the straight lines describing the rows and columns, in the form  $y = mx + c$ , can then be solved as simultaneous equations to yield the  $x$ - and  $y$ -coordinates of each grid point at the intersection of row  $i$  and column  $j$ , through:

$$x_{i,j} = (c_j - c_i)/(m_i - m_j)$$

and

$$y_{i,j} = m_i \cdot x_{i,j} + c_i$$

where the gradient of the line,  $m$ , can be found through  $m_1 \pm k * \Delta m_1$  (or  $m_2 \pm k * \Delta m_2$ ) with  $k$  equal to the number of rows (or columns) away from the central row or column (i.e. for the central row,  $k = 0$ , and for 2 rows away from the central row,  $k = 2$ ). Grid points along the central row and column are equally spaced by  $s_1$  and  $s_2$  respectively, and so these known positions can be used to calculate the y-intercept values ( $c_i$  and  $c_j$ ) of the remaining rows and columns.

### 3.3 Optimisation Methodology

This section provides more detail into the selection and implementation of the chosen algorithm and other key components in the optimisation process.

#### 3.3.1 Problem Formulation

The decision variables, described previously, are considered in vector form,  $\phi$ , for the optimisation problem:

$$\phi = [m_1 \ \Delta m_1 \ s_1 \ m_2 \ \Delta m_2 \ s_2 \ x \ y]^T \quad (3.12)$$

The objective function of the maximisation problem can be written as:

$$\max J(\phi) \quad (3.13)$$

$$\text{where } J(\phi) = J_{rev} - C_{turbines} - P_{distance} \quad (3.14)$$

and  $J_{rev}$  is the net present value of the lifetime revenue from wind farm energy capture;  $C_{turbines}$  is the capital cost of wind turbines; and  $P_{distance}$  is the penalty cost associated with turbines built less than a given proximity distance apart. The levelised cost of energy could also be used as an alternative objective function, and is often used in similar studies [54, 64, 145]. While LCOE is a valid objective to minimise, additional cost parameters required to calculate LCOE - such as operation and maintenance cost

modelling - is beyond the scope of this research. As such, a simplified objective is used that includes the two key cost components presented in this section, with lifetime revenue being of particular interest to wind farm developers [10]. Later chapters expand on this to include array cable costs and lifetime electrical losses. The penalty function,  $P_{distance}$ , is also included; this term will be equal to zero for all layouts that do not violate the proximity constraint, described later, Equation (3.16).

The optimisation problem can then be described by the following:

$$\phi^* = \arg \max J(\phi) \quad (3.15)$$

where  $\phi^*$  is the set of values corresponding to the variables,  $\phi$ , that result in the maximisation of the function  $J(\phi)$ .

The three terms in Equation (3.13) cannot be directly written as functions of  $\phi$ , however all are dependent on all eight variables because the eight variables fully describe the grid of turbine positions. Firstly,  $J_{rev}$  requires the wind farm power from an evaluation of the wind farm model, the result of which is heavily dependent on the angles, spacing and location of the grid. This wind farm power result is assumed to be approximately correct for all years of operation of the wind farm, multiplied by a defined cost of energy and summed over the lifetime of the project at a given discount rate. Given that the wind farm lifetime revenue will vary with layout solutions, the ratio between turbine capital costs and lifetime revenue may not always be the same and so must be considered in this way. If wake losses were not considered, the term  $J_{rev}$  would simply be a function of the number of turbines.

Secondly,  $C_{turbines}$  is the capital cost of turbines. This cost is dependent on the number of grid points that lie within the buildable area and is simply a multiplication of the number of applicable points by a specified turbine capital cost. Further costs, such as the cost of turbine transportation and installation could be included in this term, however have not been considered in this study.

Finally,  $P_{distance}$  is the penalty cost function. As an alternative to a hard constraint formulation, the purpose of this penalty function is to disincentivise solutions where turbines are built too close to each other. During the evaluation of the wind farm

model, turbine positions are recorded and the distances between the turbines and their respective nearest neighbours are calculated. If the distance between a pair of turbines is found to be below a defined minimum spacing (specific to the type of turbines) then a penalty cost is applied, otherwise  $P_{distance} = \mathcal{L}0$ , Equation (3.16). The penalty cost applied for a violation of the minimum spacing is a large cost which is a function of the size of the site and the size of the turbines, however a value of infinity would also suffice. To avoid values of infinity, this algorithm defines the penalty cost to an arbitrary but sufficiently high penalty value, equal to the un-discounted annual revenue of a whole row of turbines.

$$P_{i,j} = \begin{cases} N \times Rev_{AEP} & \text{if dist. between turbines } i \text{ and } j < \text{min. spacing} \\ 0 & \text{if dist. between turbines } i \text{ and } j \geq \text{min. spacing} \end{cases} \quad (i, j \in T) \quad (3.16)$$

where  $N$  is the maximum possible number of turbines in a row, for the given wind farm;  $Rev_{AEP}$  is the revenue of one turbine operating at rated power continuously for one year; and  $i$  and  $j$  are real numbers representing each of the grid points to be considered in the set of  $T$ , where  $T$  is the subset of grid points containing turbines in the current solution. The distance between each turbine  $i$  and every other turbine  $j$  is measured for all grid points in the set  $T$ .  $P_{distance}$  is the summation of the individual penalty costs considered for every pair of built turbines, however one violation of the minimum turbine spacing should provide an effectively-infinite disincentive.

$$P_{distance} = \sum_{i,j \in T} P_{i,j} \quad (3.17)$$

The exact value of the penalty cost is not critical providing it is relatively large compared to the annual revenue of a row of turbines - the number of which will vary with the site dimensions. Formulating the penalty function in this way ensures that this will always be the case.

Constraints - or limits - can be applied to the variables being considered in order

to bound the solution space to create a region of feasible solutions resulting in a constrained optimisation problem. A reformulation of the objective function allows for these complex constraint equations to be considered in the objective function as implicit constraints through the implementation of Lagrange multipliers [52] (similar to the penalty function term,  $P_{distance}$ , in Equation (3.13)). In this style of formulation, the objective function is modified to be negatively infinite, or a very large negative, when these inequality constraints are violated. The problem can then be solved as an unconstrained optimisation problem. These penalties can be thought of as a type of soft-constraint that disincentivises solutions in these regions. In the case of a PSO algorithm, particles may enter this region but will be penalised in the objective function. As such, the particles are likely to move back towards the areas where good solutions have previously been found. This method has two major benefits: firstly, it avoids complex constraint equations and replaces these constraints with a simple evaluation of the specific solution; and secondly it allows particles to enter a region that is penalised and re-enter the un-penalised region in a new location that might otherwise have been difficult or impossible to reach with hard constraints.

This penalty approach is used in the optimisation process instead of hard constraints. The problem is therefore treated as an unconstrained optimisation problem. The PSO algorithm is seeded with an un-penalised solution to guarantee that there is a good quality global best solution for particles to move towards. This ensures that particles, even if initialised in a penalised region, will not deviate far from the un-penalised region. The seeding process is described in more detail in Section 3.3.3.

### 3.3.2 Algorithm Selection & Implementation

The wind farm power found through evaluation of the wind farm model can vary greatly for a small change in some or all of the eight variables. Non-uniform wind distribution, irregular wind farm boundaries and obstacles all contribute to the irregular nature of the objective function values in the solution space. Further, constraints and/or penalties can create regions in the solution space with a step-change in the objective value, Section 3.3.1. It is impractical to rely upon gradient-based search algorithms that require the

objective function to be differentiable. An exhaustive search method could be used, however to achieve a satisfactory level of accuracy would require the evaluation of an impractically large number of possible solutions.

When hard constraints are used, some optimisation methods are able to take advantage of these to reduce the number of required searches to find the optimal solution; either by searching along the vertex edges of the constrained solution space (Simplex Method), or by systematically applying ‘cuts’ (additional constraints) to the solution space (Cutting Plane Method) [60]. However, the problem formulation suggests that an analytical solution is unlikely to exist on a vertex edge when constraints are used to define the feasible region. For example, if the variables  $s_1$  (row spacing) and  $s_2$  (column spacing) have a lower bound constraint applied of some minimum turbine spacing, there is no guarantee that the optimal solution will exist along that vertex. At these locations in the solution space, the wind farm power may be greater due to more turbines fitting into the site, but may be reduced due to greater wake effects. As the row and column spacing increases, the wind farm power increases due to reduced wake effects, therefore a better solution may be found at values not equal to the constraint value. Methods such as the Simplex Method require a bounded linear programme which this problem formulation is not [52, 60]. For this reason, these algorithms may not be suitable for this application.

Evolutionary algorithms, such as Genetic Algorithms (GA) or Particle Swarm Optimisation (PSO), offer a promising alternative. These algorithms generate a range of solutions distributed within the solution space and - through different processes depending on the algorithm - move the initial solutions through the solution space to attempt to find increasingly better solutions. The GA method selects the best quality solutions from the population and, considering pairs at a time, ‘breeds’ the solutions by swapping some of their values (of the 8 variables) to generate new potential solutions for the next ‘generation’. Swapping variables in this way may lead to the generation of grids with highly acute angles and overly-close positioned turbines. A PSO algorithm is analogous to a swarm of bees. Each particle - or solution - moves through the solution space through a combination of vectors: the direction of the individual’s momentum, the di-

rection to its previous personal best solution, and the direction towards the swarm's global best solution [53]. It is found by Balasubramanian et al. [145] that the PSO algorithm requires simpler implementation and faster convergence than the GA algorithm. This could be due to the cooperative nature of the PSO algorithm whereby solutions share knowledge of the solution space and iteratively improve all solutions in the swarm, as opposed to the competitively organised GA [64]. Therefore the PSO method was chosen for this study.

Algorithm 1 outlines the key processes taking place in the PSO, where  $\phi$  is the set of independent variables, described in Equation (3.12).

---

**Algorithm 1** Particle swarm optimisation algorithm

---

Particles randomly distributed in solution space,  $\phi \in \mathbb{R}^8$   
**while**  $max(\phi) - min(\phi) > \phi_{threshold}$  **do**  
  **for** Each particle,  $i$  **do**  
    Update particle velocity  $v_i = X * v_i + Y * (\phi_{PB} - \phi_i) + Z * (\phi_{GB} - \phi_i)$ , where  
       $\{X, Y, Z \in \mathbb{R} \mid 0 < X, Y, Z < 1\}$   
    Update particle position,  $\phi_i = \phi_i + v_i$   
    Evaluate  $J(\phi_i)$   
    **if**  $J(\phi_i) > J(\phi_{PB_i})$  **then**  
      Update personal best solution,  $\phi_{PB_i} = \phi_i$   
    **end if**  
    **if**  $J(\phi_i) > J(\phi_{GB})$  **then**  
      Update global best solution,  $\phi_{GB} = \phi_i$   
    **end if**  
  **end for**  
**end while**  
Output  $\phi_{GB}$

---

### 3.3.3 Additional Improvements

Several improvements have been made in the implementation of the layout optimisation in addition to the base PSO algorithm. Firstly, a solution seeding algorithm is used to provide some valid starting solutions to the PSO algorithm. Secondly, a look-up function is defined to reduce the time to evaluate solutions within iterations of the PSO algorithm. Finally, a micro-siting function is defined, taking the best solution of the PSO algorithm and attempting to improve the solution by allowing some deviation from the

initial grid positions, as desired by some wind farm developers [10].

Seeding the initial population of solutions in a heuristic algorithm is widely conducted in academic literature. Saavedra-Moreno et al. [146] directly compare the solutions of a seeded EA (SEA) versus an unseeded version of the same EA, finding that the SEA yields better solutions in all instances. Such a seeding process must be conducted first, before the PSO is run. The look-up function, described in more detail later, enables the quick assessment of solutions within PSO iterations without the full evaluation of the wind farm model. The data set itself is compiled ‘on-the-fly’ with full evaluations of the objective function, but reduces the total number of evaluations used in the PSO algorithm. The micro-siting function is applied to the final solution from the PSO algorithm, rather than throughout the PSO in every iteration. This is to avoid increasing the computational complexity of the algorithm which, if evaluating the micro-siting function at each iteration of the PSO, would result in a greatly increased computational time. As discussed later, computational times for large wind farms ( $\geq 100$  turbines) can reach 11 hours or more on a standard desktop PC, so maintaining computational efficiency (by micro-siting only the final solution) is an important design driver in the algorithm design.

### Seeding of Initial Solutions

In order to initialise at least one particle in a region of the solution space containing reasonable solutions, a simple search procedure is employed prior to the PSO algorithm. The search procedure resembles a Pattern Search algorithm [47] and is described in Algorithm 2.

This simple pattern search is intended only to provide the reasonable seeding of one or more particles for the PSO algorithm. Given the objective function, Equation 3.13 is heavily influenced by energy capture, maximising the number of turbines in the site (by setting  $s_1$  and  $s_2$  to the minimum allowable turbine spacing,  $dist_{min}$ ) seems to be a reasonable initial step. The remaining part of the pattern search algorithm simply aims to find the best combination of angles for the rows and columns of turbines (as assessed by the objective function, Equation 3.13).

---

**Algorithm 2** Pattern search algorithm

---

Fix 6 variables of  $\phi$  ( $\Delta m_1 = \Delta m_2 = 0$ ,  $s_1 = s_2 = dist_{min}$ ,  $(x, y) = (x_{GC}, y_{GC})$ )  
 Initialise  $m_1 = 0.02\pi$  (radians)  
**while**  $m_1 \leq \pi$  **do**  
    $\theta = 0.25\pi$   
   **while**  $\theta \leq 0.75\pi$  **do**  
      $m_2 = m_1 + \theta$   
     Evaluate  $J(\phi)$   
     **if**  $J(\phi_i) > J(\phi_{GB})$  **then**  
       Update global best solution,  $\phi_{GB} = \phi_i$   
     **end if**  
     Step  $\theta$  by  $+0.02\pi$   
   **end while**  
   Step  $m_1$  by  $+0.02\pi$   
**end while**  
 Output  $\phi_{GB}$  for seeding particle in PSO

---

Here,  $\theta$  is the angle in radians between the central row and central column of the grid ( $m_2 - m_1$ );  $dist_{min}$  is the minimum allowable distance between a pair of turbines; and  $(x_{GC}, y_{GC})$  are the coordinates of the geometric centre of the wind farm site. In a classical pattern search algorithm, particles move through the solution space in a user-defined set of pattern directions. Moves are screened for constraint violations and if there is no violation the move is accepted, otherwise the step size is reduced and the process is repeated. In the approach used in this study however, the spacing of turbines (variables  $s_1$  and  $s_2$ ) are fixed so no constraints are required and therefore there is no change in the step size. In this way, the approach used here could also be considered an exhaustive search of a discrete set of user-defined points in the solution space. The globally best solution found in this process is used to seed the position of the first particle in the PSO algorithm. The remaining particles in the swarm can be seeded with user-defined values based upon empirical knowledge and experience, otherwise they are initialised randomly within the following ranges:

1.  $0 \leq m_1 \leq \pi$
2.  $m_1 + 0.45 \pi \leq m_2 \leq m_1 + 0.55 \pi$  (for  $m_1$  of the corresponding solution)
3.  $-0.02\pi \leq \Delta m_1, \Delta m_2 \leq 0.02\pi$

4.  $0.75 \text{ dist}_{min} \leq s_1, s_2 \leq 3 \text{ dist}_{min}$
5.  $x_{GC} - \text{dist}_{min} \leq x \leq x_{GC} + \text{dist}_{min}$
6.  $y_{GC} - \text{dist}_{min} \leq y \leq y_{GC} + \text{dist}_{min}$

### Look-Up Data Set

The computational load of a single evaluation of the wind farm model is reasonably low, however it is a function of the number of wind directions and the square of the number of turbines. On a standard desktop PC (3.4GHz Intel Core i7-6700, 16GB RAM), an evaluation of the model with 360 wind directions and 58 turbines takes approximately 19 seconds. The number of evaluations of the model is a function of the number of iterations and the number of particles (or potential solutions) in the PSO. Although it is not possible to reduce the number of wind directions or turbines, it is possible to reduce the number of evaluations of the model to improve the algorithm efficiency. Figure 3.2 presents a decision block in the algorithm that reduces the number of evaluations of the model to around 5% of the original number of iterations, reducing the computational load of the model by around 95%. The decision in the block is made probabilistically, as shown by the “Yes” and “No” conditions in Figure 3.2. The wind farm model is also evaluated in the condition that the number of turbines is outwith the range of the data set created up to that point.

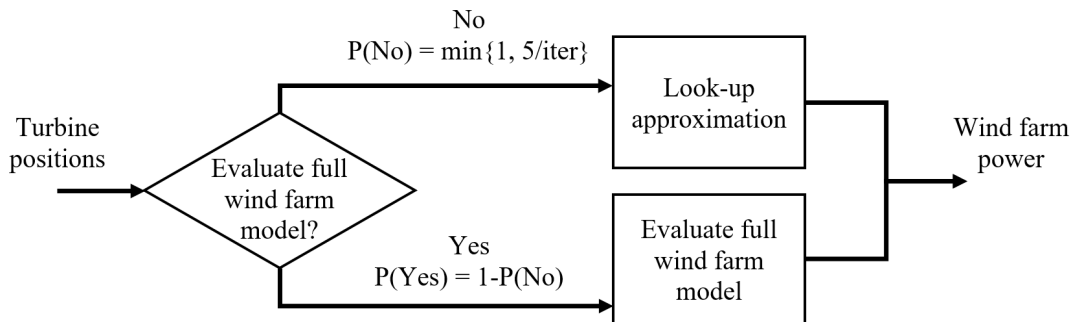


Figure 3.2: Decision block to evaluate the full wind farm model or to use an approximation.

When the wind farm model is evaluated for a given solution, the average wind farm

power for the site (averaged over one year, for all wind directions and speeds) is recorded against the number of turbines and appended to the look-up data set. This is repeated for many solutions, resulting in a relationship such as that shown in Figure 3.3. Since the orientation of the grid layout of turbines will play an important factor in the average wind farm power output, different layouts may yield a different average power (and annual energy yield) than other sites that contain the same number of turbines. However, it can be seen for this site that this is not the case, Figure 3.3; there is little variation in average wind farm power for sites containing the same number of turbines. This is due to considering all wind directions and speeds (and their frequencies of occurrence). Little variation in wind farm power, across different turbine layouts, would be expected for sites with a more uniformly distributed wind rose than those with a more asymmetric wind rose. Since there may be some variation, the mean of these average wind farm power values is used for that given number of turbines. For the remaining iterations, when an approximation is used, this data set is used as a look-up table for wind farm power. This approximation method allows the algorithm to quickly assess the wind farm power, including wake effects (specific to the site, turbines, and wind profile), without evaluating the full wind farm model.

The probability of the full model being evaluated is shown in Figure 3.2 as:

$$P(Yes) = 1 - P(No) = 1 - \min\{1, 5/iter\}$$

where *iter* is the iteration number. This formulation ensures that the first 5 iterations are used to sufficiently populate the data set, and that the probability of the full model being evaluated decreases as the algorithm progresses and the data set is increasingly well described. Additionally, the full model is evaluated for solutions that are outwith the existing range of the data set to ensure that the full range of solutions are described by the look-up curve.

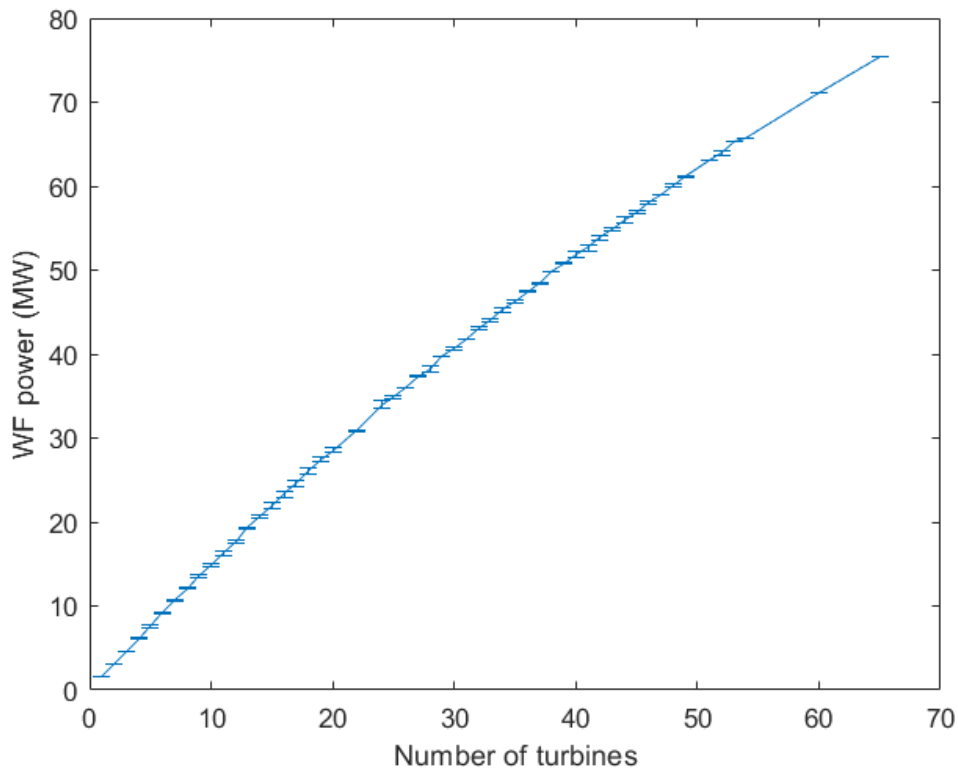


Figure 3.3: An example of average wind farm power data set created by the optimisation process during a case study of the Lillgrund Offshore Wind Farm site. (Error bars represent the maximum and minimum values of average wind farm power for a given number of turbines.)

### Micro-Siting Function

This function allows for up to one rotor radius of micro-siting of turbines away from their ‘designated’ grid-based position. This allows for two major benefits: (1) turbines that are placed less than one rotor radius outside of the wind farm boundary can be moved inside the boundary to be built, and (2) the built turbines can be spread apart to reduce the wake losses and increase energy capture. To reduce the computational complexity of the micro-siting function, two assumptions are made inline with the above, (1) a greater number of turbines will increase the wind farm power, and (2) increasing the distance between turbines will reduce the wake losses. Allowing some small deviation, linked to the size of the turbines, ensures that layouts do not deviate too far from that

permitted by navigational guidelines, but also opens up the opportunity of increased energy capture and reduced wake effects.

The function assesses each of the grid positions of possible turbine locations (including those outside of the wind farm area) to determine whether it is within the micro-siting distance of the buildable area. If it is, then a new possible turbine location is considered, that is up to one rotor radius away from the initial grid position. Positions are considered along the vector, from the grid point being considered, in the direction of the average position of the grid point's nearest neighbours. If a new position is found that is within the buildable area, then this position is used to build a turbine. If no valid position is found then no turbine is built for that grid point and the next grid position is considered. These movements move turbines just outside of the wind farm (less than one rotor radius) in to it, to be built. Once all grid positions have been assessed in this way, turbines are selected randomly, with a uniform probability, to be moved away from their nearest neighbours by up to the micro-siting distance. Incremental distances of approximately one tenth of the rotor radius are used at each iteration, reducing the impact of the order in which turbines are considered. Irrespective of the order of selection, turbines will be incentivised to 'spread out' from the centre of the wind farm to increase the distance between them, reducing wake effects and increasing energy capture. This process is repeated for many iterations such that each turbine is visited an average of five times. This second movement phase increases the spacing between turbines reducing the wake effect.

### 3.3.4 Summary of Optimisation Process

Figure 3.4 shows the key processes within the optimisation. Boundaries of the PSO algorithm and objective function have been outlined to highlight the processes involved in these sections respectively. The particle seeding method, look-up approximation method, and micro-siting function have all been included to better demonstrate where these fit into the whole optimisation process.

An initial particle is seeded in a suitable point in the 8-dimensional solution space and the remaining solutions are randomly seeded. Velocity vectors of the particles are

### Chapter 3. Turbine Placement Optimisation

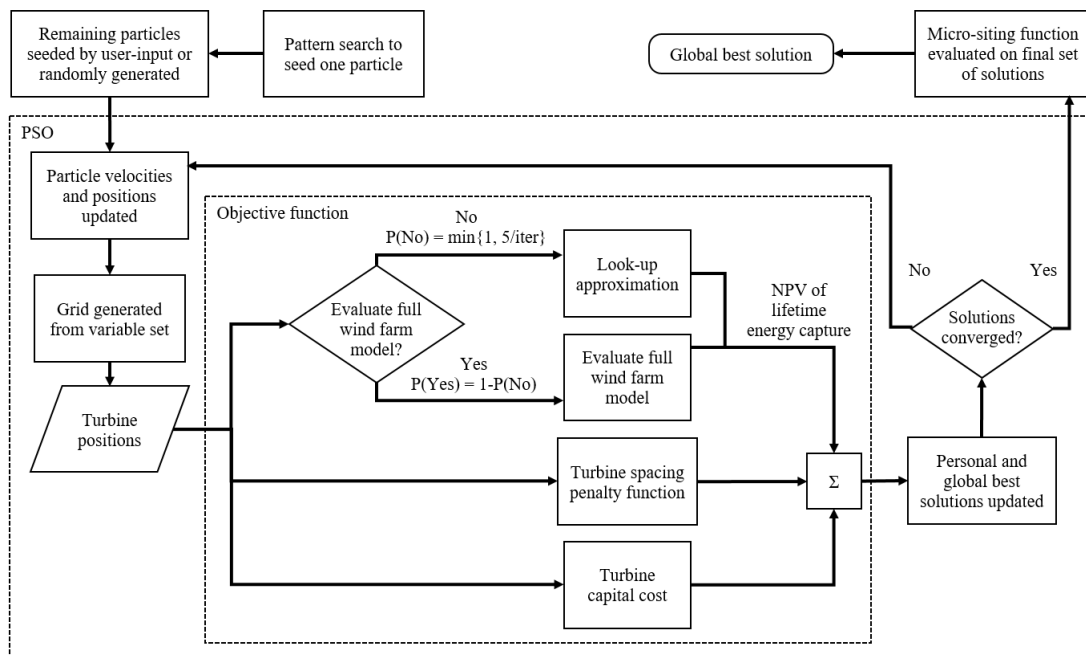


Figure 3.4: Flowchart of the key optimisation processes.

randomly generated and the positions are updated by moving the particles along these vectors. The grid of turbine positions is created from the variables for each of the proposed solutions in the swarm, as described in Section 3.2. A decision is made to evaluate the wind farm model or to look up an approximation, as described previously, providing a value of the lifetime energy capture of the site. This is summed with the cost of turbines (negative cost), and the turbine spacing penalty cost (negative cost). The record of the personal best and the global best solutions of the swarm are updated where applicable, and the particle velocities are updated. The velocities of the particles are generated from three components: the particle’s current direction of travel, towards it’s personal best solution, and towards the swarm’s global best solution. This process then repeats from updating the particle positions until the particles converge and/or the velocities have reduced to a sufficiently small value. On the final set of solutions, the micro-siting function is evaluated to improve energy capture and the best solution of the swarm is kept.

### 3.4 Validation

This section outlines the validation of the proposed wind farm model (the combination of the Larsen wake model, rotor-effective wind speed, and root-sum-square summation method) and verification of the implementation of the PSO optimisation process. This is conducted in three steps, firstly, the wind farm model was given a set of real turbine positions and the calculated wind farm power was compared against the known, real-world, power of the wind farm with the objective of matching the real wind farm power. Secondly, the operation of the PSO algorithm was investigated to determine if it operates as desired, and producing increasingly good quality solutions over iterations. Finally, the optimisation process was applied to a case study of a real-world site. The solution was compared against the actual turbine positions to determine if the optimisation process can generate solutions close to that used in the real world site.

#### 3.4.1 Wind Farm Model Validation

Prior to evaluating the whole wind farm model, it was important to establish a number of point wind speeds to calculate per rotor in order to achieve a sufficiently accurate rotor-effective wind speed. A sensitivity study was carried out by changing the resolution of the points per rotor and evaluating the rotor-effective wind speed over the range from 8 to approximately 13700 points per rotor. It was assumed that a greater resolution of points across the rotor swept area will result in a more accurate rotor-effective wind speed with the wake model. Indeed, it was found that with an increasing number of points per rotor, the rotor-effective wind speed approaches the high-resolution result. However, the quality of solutions with a low number of points was also sufficient. For one free stream wind speed, the rotor effective wind speed calculated using 8 points per rotor was 8.438m/s. This increased slightly as the resolution was increased, resulting in 8.446m/s rotor-effective wind speed with 13700 points per rotor. Since the computational time is directly proportional to the number of points per rotor to be assessed, and the error in wind speed between the lower and higher resolution cases was negligible, 8 wind speed points per rotor was chosen as sufficient for the model calculation.

The input data provided to the proposed wind farm model included the turbine positions of the real Lillgrund offshore wind farm (measured from the Vattenfall report "Technical Description Lillgrund Wind Power Plant" [147]) and the wind conditions of the site (from "Meteorological Conditions at Lillgrund" report [148]). The real turbine positions at Lillgrund can be seen in the left plot in Figure 3.5. Also indicated, is the North bearing, and one of the significant wind directions, at  $222.7^\circ$ , which is parallel to the angle of the columns of turbines. The proposed wind farm model was evaluated for the full set of wind directions at the site, and the capacity factor of the wind farm for each wind direction was recorded for comparison with the true measured values at the site. The true capacity factor measured at the site is provided as a mean value for the different power levels and wind directions [147, 148], and is the data against which this validation is conducted.

Focusing on a section of the wind directions, the right-hand plot of Figure 3.5 shows the average capacity factor of the three highlighted turbines (highlighted in Figure 3.5, left) for both the model evaluation and the real site SCADA data [149]. The real world measured data was 'binned' into four groups based on the power of the upstream turbines: 300-600kW, 700-1000kW, 1100-1400kW and 1500-1800kW. The upper and lower bounds of these binned data were used to create the upper and lower bounds of the shaded regions in Figure 3.5 (right), using the proposed wind farm model. This was achieved by back-calculating the wind speeds at which this power would be generated (for a turbine in free stream wind, i.e. not in a turbine wake) and this wind speed was then used in the wind farm model to predict the downstream turbines' mean capacity factor.

It can be seen in Figure 3.5, that the model was able to estimate wake effects close to that observed in the real world data, by a reduction in the capacity factor of similar magnitude. However, there is an offset between the angles of the peak wake effect of the two data sets of approximately  $4^\circ$ . In the model, the angle of the wind direction was defined and the model was evaluated at  $1^\circ$  increments and does not consider wake deviation or any wind direction changes through the site. The wind direction in the real data was recorded as the median yaw angle of the three upstream turbines (those

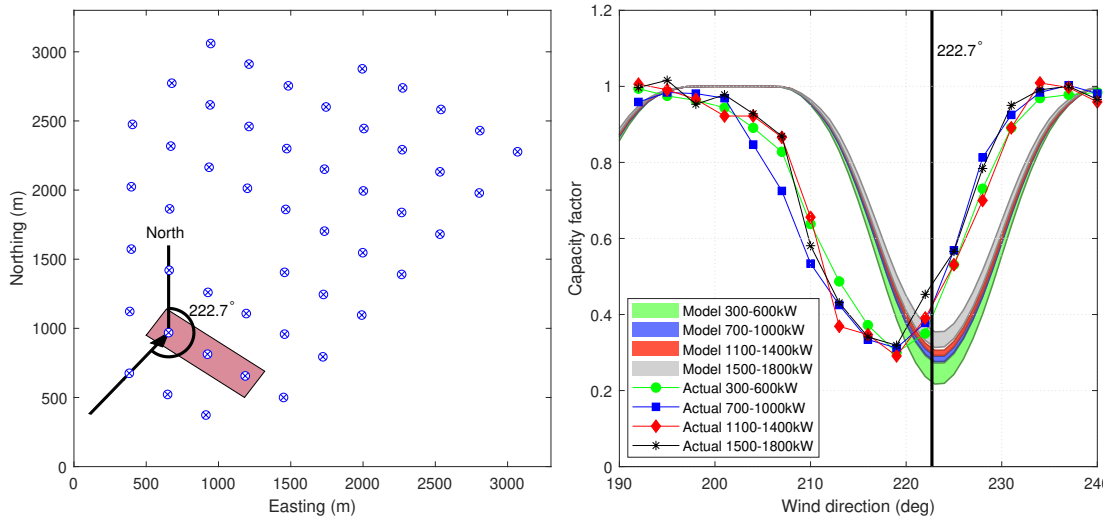


Figure 3.5: (Left) Real Lillgrund turbine positions, three highlight turbines under consideration, and the significant wind direction being considered. (Right) Mean capacity factor of the three turbines under consideration from the model evaluation and real Lillgrund SCADA data. Data is grouped into four bins based on the power level of the upstream turbines, not affected by wakes. The significant wind direction from the left-hand plot at  $222.7^\circ$  is indicated for ease of comparison.

to the South-West of the three highlighted turbines in Figure 3.5, left). The average errors between the real data set and the model predictions are given in Table 3.1, for the four power bins. Both capacity factor error and the difference in energy capture in the segment ( $190^\circ - 240^\circ$ ) are presented. A range of errors is provided for each power level bin as the real data gives a single value for each wind direction, while the model calculates an upper- and lower-bound value.

Table 3.1: Mean absolute error of capacity factor and energy capture between model evaluation and SCADA data for three turbines. Maximum and minimum values of the power bin are used by the model for comparison to the single value provided by the SCADA data; error as a percentage of SCADA values.

Power level (kW)	Mean error between capacity factors (%)	Mean error between energy capture (%)
300-600	25.65-26.15	0.98-3.54
700-1000	31.74-31.82	4.22-4.97
1100-1400	29.79-30.12	4.32-4.89
1500-1800	29.34-29.44	2.77-4.84

As shown in Table 3.1, errors between the model and real data capacity factors

range from 25.65-31.82%, in large part due to the angle shift mentioned previously. The difference in energy capture for the two data sets in the  $190^\circ - 240^\circ$  segment is far lower, between 0.98-4.97% showing good model prediction of reality. Shifting the real data by  $+3.7^\circ$  to remove any possible yaw-measurement inaccuracy reduces the errors between the model and the real data to 7.12-13.15%. Errors in the capacity factor when the real data is shifted by  $+3.7^\circ$ , is shown in Table 3.2.

Table 3.2: Mean absolute error of capacity factor between the model evaluation and SCADA data for three turbines, with original and shifted SCADA data. Maximum and minimum values of the power bin are used by the model for comparison to the single value provided by the SCADA data; error as a percentage of SCADA values.

Power level (kW)	Mean error between capacity factors (%)	
	Unshifted	Shifted by $3.7^\circ$
300-600	25.65-26.15	7.12-9.29
700-1000	31.74-31.82	13.04-13.15
1100-1400	29.79-30.12	10.06-10.25
1500-1800	29.34-29.44	10.62-11.55

Figure 3.6 shows the capacity factor of the whole Lillgrund wind farm [29] and the model prediction across the full  $360^\circ$  range for below rated wind speed. Including all turbines in the wind farm and all possible wind directions allows for the effectiveness of the summation of multiple wake effects to be assessed. Data for the  $360^\circ$  efficiency of the wind farm is also available in Dahlberg (2009) [149], however as seen in Figure 3.5 there was a misalignment between the capacity factor data and the geometric positions of the turbines (angle of turbine rows) and so this was not used for comparison. The error between the capacity factor of the real site and the model, Figure 3.6, was reasonably small, averaging 5.58% using  $15^\circ$  wind direction bins. The error in annual energy capture was even lower, at 0.72%, showing a close matching of power generation between the model and the real data.

As mentioned previously, wake models can tolerate large errors ( $>8\%$  [36]) depending on the width of the bins used to group wind directions. As such, errors demonstrated by the combination of the models shown here in the range of 5.58% are certainly acceptable for use in the optimisation algorithm. Further, the assessment of the fitness of solutions

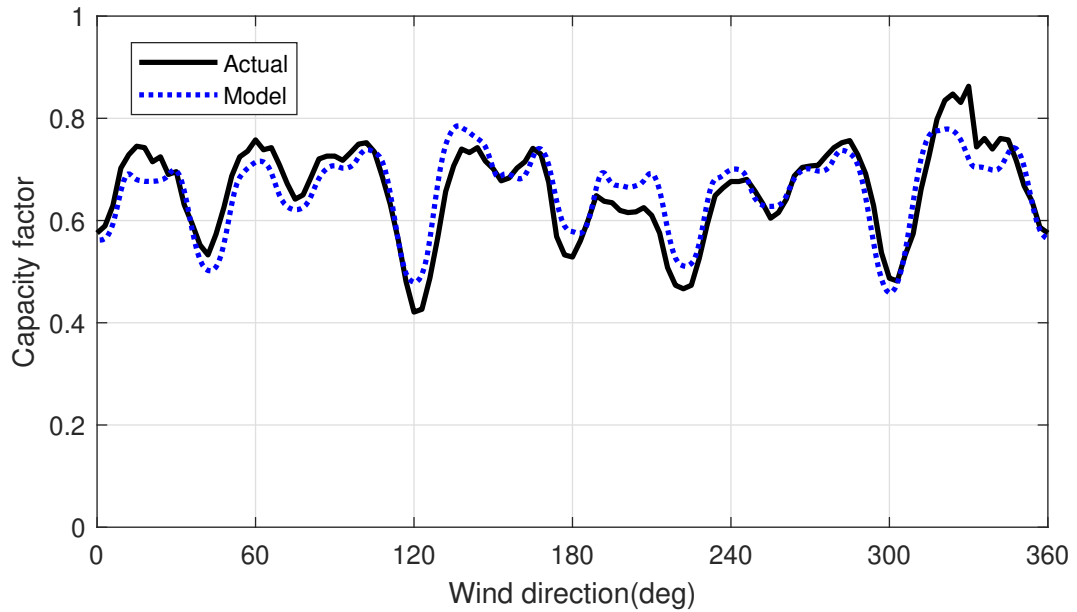


Figure 3.6: Wind farm capacity factor across wind directions for the Lillgrund offshore wind farm. Model evaluation and real Lillgrund SCADA data for below-rated wind speed.

generated by the optimisation algorithm are measured by the annual energy capture, as a function of wind farm power output, which showed an error as low as 0.72% compared to the real wind farm data - more than sufficiently accurate for use in the algorithm.

### 3.4.2 Implementation of the Algorithm

In order to validate that the PSO algorithm is implemented correctly and finds increasingly good quality solutions for this maximisation problem, an example case is run, described further in the following section. Figure 3.7 shows the range of objective function values found by the particles in the swarm, for a case study problem described in the following section. The maximum, mean and minimum values are shown, from top to bottom respectively. It can be seen that the performance index values increase and converge over iterations, which proves the functionality of the PSO algorithm. For an optimisation problem such as this, with approximately 48-50 turbines, 360 wind conditions (wind speed and direction combinations), a PSO population size of 20, and up to 500 iterations, the computational time was approximately 35 minutes on a standard

desktop PC (3.4GHz Intel Core i7-6700, 16GB RAM).

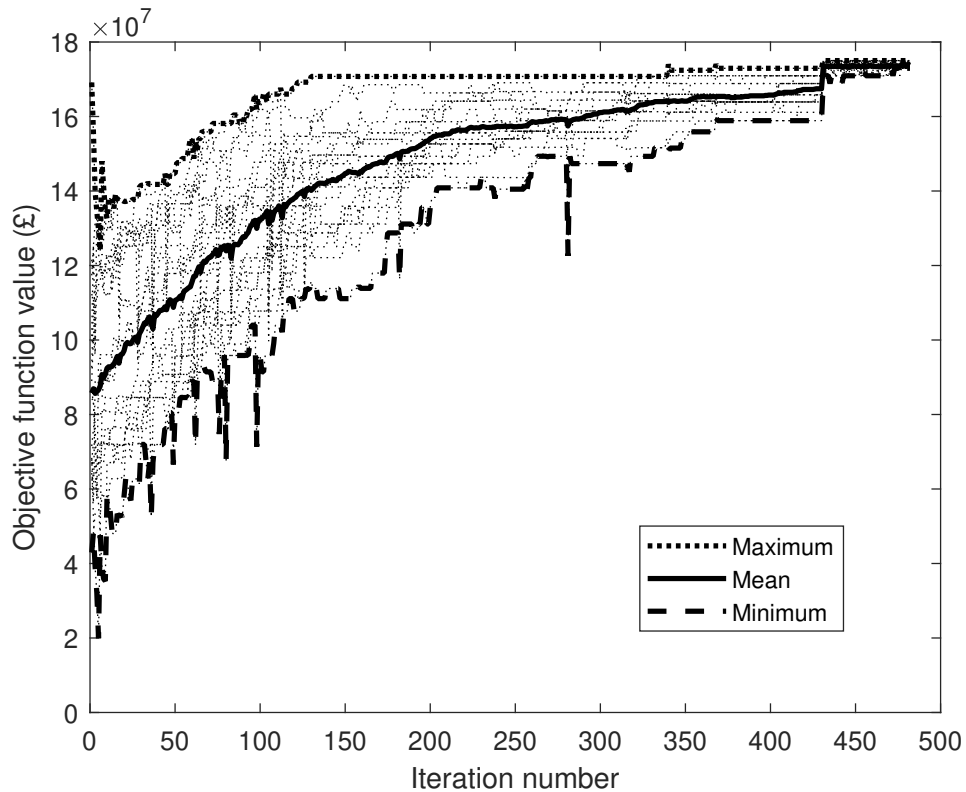


Figure 3.7: Minimum, maximum and mean objective function values in the swarm across iterations.

### 3.4.3 Real Site Case Study

Having demonstrated the wind farm model and the functionality of the optimisation algorithm, a final test was considered to examine whether the generated solutions are useful, practical solutions for a real site design. This was achieved by evaluating the performance of a real site case study using the objective function proposed in this thesis and comparing it to an optimised solution generated by the algorithm, with the goal of demonstrating a comparable (or better) objective value and similar layout. The Lillgrund offshore wind farm site was also used for this case study. Figure 3.8 shows both the real Lillgrund turbine layout (left) and the layout optimisation result (right). The wind farm boundary is outlined and the obstruction where no turbines may be

### Chapter 3. Turbine Placement Optimisation

built, in the middle of the wind farm, is shown by the shaded red region. In order to make a fair comparison, the model was restricted to generate solutions with a minimum row and column spacing of 3.3 and 4.3 times the rotor diameter respectively, as is seen in the real site, however it was free to determine the orientation of the rows and columns (through setting the variables  $m_1$  and  $m_2$ ). The real site has 48 turbines and generates an average wind farm power output of 33.6MW (294,336MWh per year) as assessed by the wind farm model proposed in this work. The optimised layout has 52 turbines and generates an average of 36.0MW (315,360MWh per year). Although the losses due to wake effects increase in the optimised layout due to the presence of 4 more turbines, the net present value of lifetime energy capture increases by £17.98M and the increase in the capital cost of turbines increases by £9.2M leading to a net gain of £8.78M (NPV) over the lifetime of the project (25 years). This demonstrates that the layout optimisation algorithm is capable of generating solutions of similar quality to real world solutions and in this case has been shown to out-perform the real site of the case study.

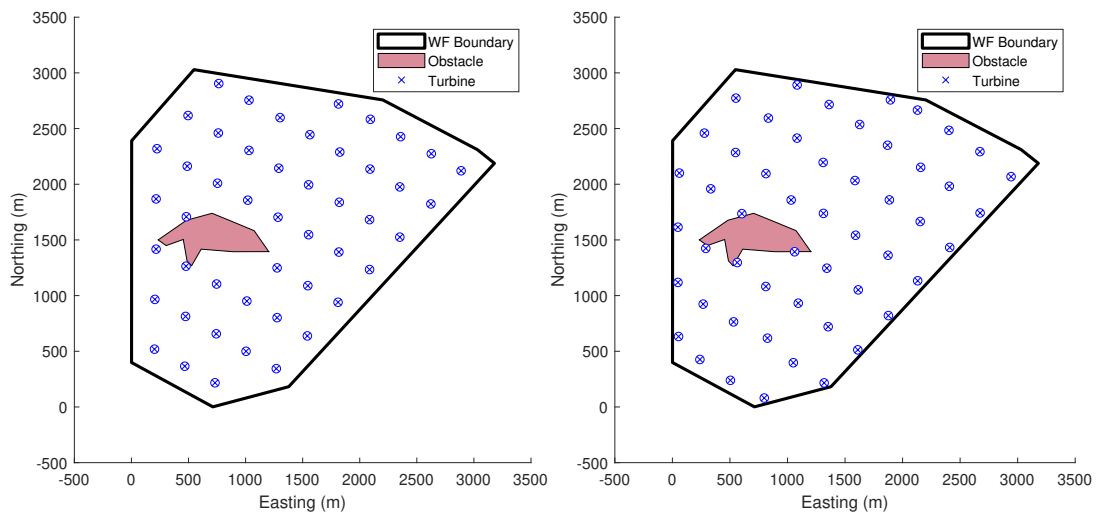


Figure 3.8: (Left) Turbine positions of the real Lillgrund site of 48 turbines generating an average of 33.6MW, and (right) optimisation algorithm result containing 52 turbines generating an average of 36.0MW.

## 3.5 Case Studies

### 3.5.1 Hypothetical Offshore Wind Farm

This section presents an updated hypothetical wind farm test case that is more representative of large-scale real-world offshore wind farms, covering the site description, wind conditions, and turbine description. All data used is publicly available and, where possible, provided in the appendices.

#### Site Description

The proposed hypothetical site has an irregular shape including a concave edge, Figure 3.9, and covers a large area sufficient to contain GW-scale projects. Two obstacles are included of different shapes, sizes and positions, marked by the red shaded regions. Turbines are restricted from ‘overhanging’ the wind farm boundary and so cannot be built within one rotor-radius of the wind farm boundary. These aspects are included in order to provide realistic constraints and complications to the model being tested. For example, the irregularly shaped wind farm boundary may lead to an irregularly shaped layout of turbines, as opposed to a ‘complete’ grid of turbines, creating a less uniform sum wake effect over the wind farm and providing a more challenging optimisation problem. Coordinates for the wind farm region and both obstacles can be found in the Appendix, Table A.4.

#### Wind Conditions

The wind conditions used in this work are taken from those described first by Mosetti et al. (1994) [37]. In their study, the authors propose three sets of wind conditions: (1) a single-direction, single-wind speed case, (2) multiple-direction, single-wind speed case, and (3) non-uniform distribution of wind speed and direction. This study used wind scenario 3, shown in Figure 3.10, as it is the most representative of real wind conditions. On inspection, it can be seen that this covers 56.36% of wind conditions, with the remaining 43.64% outside of the wind rose bins presented, representing time with no wind power generation. This represents a site with an average wind speed of

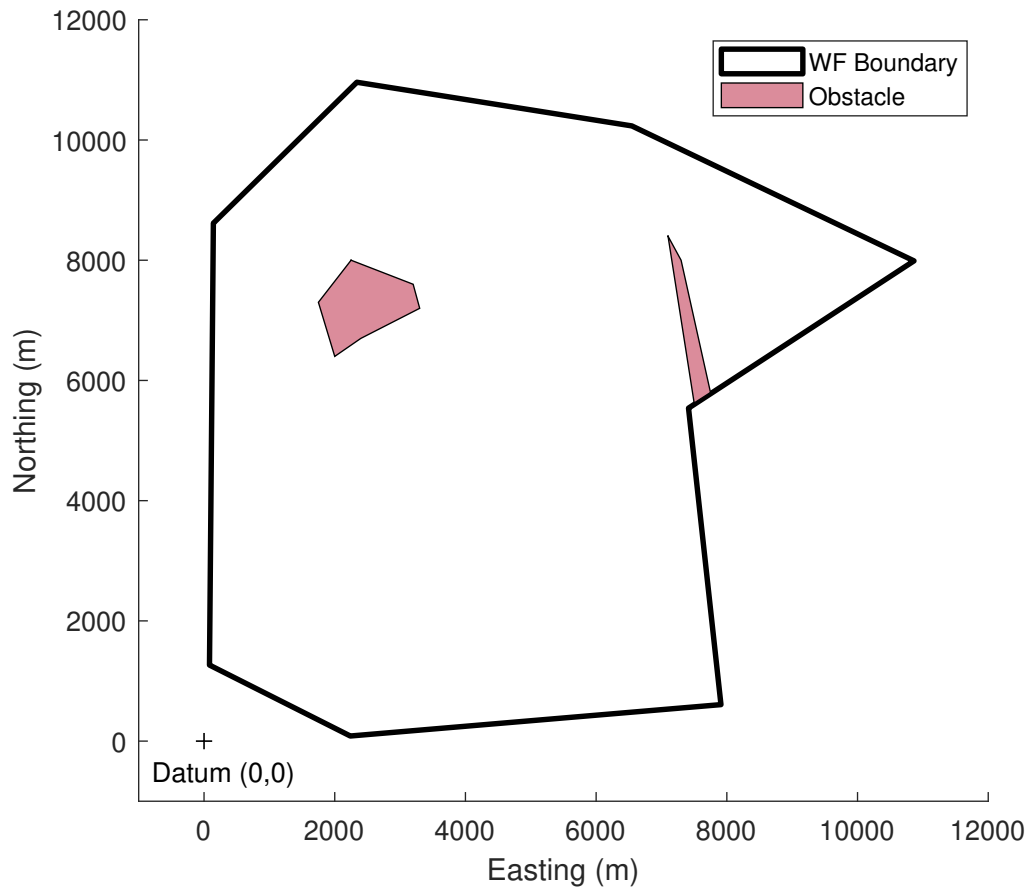


Figure 3.9: Proposed hypothetical offshore wind farm site.

$6.00ms^{-1}$ , which is very low for a typical offshore wind farm site. In order to bring this wind distribution more in-line with modern offshore wind farm conditions, the probabilities of all wind speed and direction combinations were uniformly increased by a factor of  $100/56.36$ . The resulting wind rose therefore, characterises 100% of wind conditions at the site, now with an average wind speed of  $10.64ms^{-1}$ , without impacting the distribution. As wind turbine capital cost is considered in the objective function, it is important that a representative wind field is used to ensure that the net present value of lifetime revenue from a turbine is high enough to offset the capital cost of the turbine (resulting in a positive objective value). If the mean wind speed is too low, the optimisation may be incentivised to remove all turbines from the site as they incur a

### Chapter 3. Turbine Placement Optimisation

cost higher than the net present value of income. While this is subject to parameters such as turbine cost, price of energy, and discount rate, negative objective values were found in some preliminary investigations necessitating the scaling of the wind rose in this study. The modified wind rose data can be found in the Appendix, Table A.5.

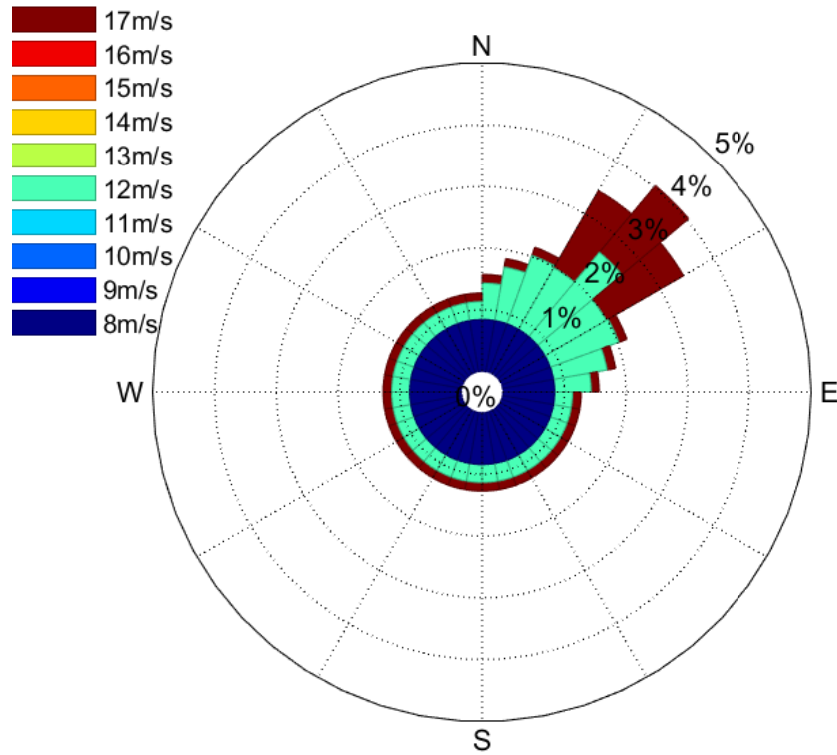


Figure 3.10: Non-uniform distribution of wind speed and direction [37]. (North 0/360 degrees, East 90 degrees).

#### Turbine Description

The turbine used was an 8MW reference wind turbine by Desmond et al. (2016) [150]. Some of the key turbine parameters are: rotor diameter 164m, hub height 110m,  $C_{Pmax}$  0.44, minimum spacing of 5 times the rotor diameter, and turbine cost £8M. More complete data can be found in the referenced study [150] including the power coefficient curve and thrust coefficient curve used by the wake model.

### 3.5.2 Berwick Bank Offshore Wind Farm

The second case study considered SSE’s Berwick Bank offshore wind farm, using representative data provided by SSE. This study was conducted as part of a layout design comparison between this thesis work and the in-house method used commercially at SSE. The objective of this comparison was to benchmark the model proposed in this thesis against a commercial tool used in the industry for the design of real offshore wind farms. Descriptions of the site, the representative wind field, and the reference wind turbine are presented in the following sections. Several optimisation constraints were required by SSE that were not considered in the case study described previously. Therefore, some amendments were made to the pre-processing phase and optimisation method, detailed later, including (1) changing the objective function to maximise AEY, (2) restricting rows and columns of turbines to be parallel, and (3) fixing the number of turbines in the site.

#### Site Description

The Berwick Bank site is a large offshore wind farm site in the North Sea, in the outer Firth of Forth, Scotland. Figure 3.11 shows the site boundary in the Cartesian coordinate system used by the optimisation algorithm. The site boundary presented in Figure 3.11 is correct as of April 2021, before it was altered to include the neighbouring Marr Bank site later in 2021. The site was designed for a 2.3GW wind farm (increased to 4.1GW with the inclusion of the Marr Bank site) and is located approximately 40-50km offshore. Wind farm boundary coordinates can be found in the Appendix, Table A.6.

#### Wind Conditions

The wind conditions of the Berwick Bank site are presented in the wind rose in Figure 3.12. Representative time series data of wind speed and direction were provided for the site and binned into  $5^\circ$  direction bins and 6 wind speed bins. Full data of the wind conditions used in the case study can be found in the Appendix, Tables A.7 and A.8, showing direction sectors and bin-centre wind speeds.

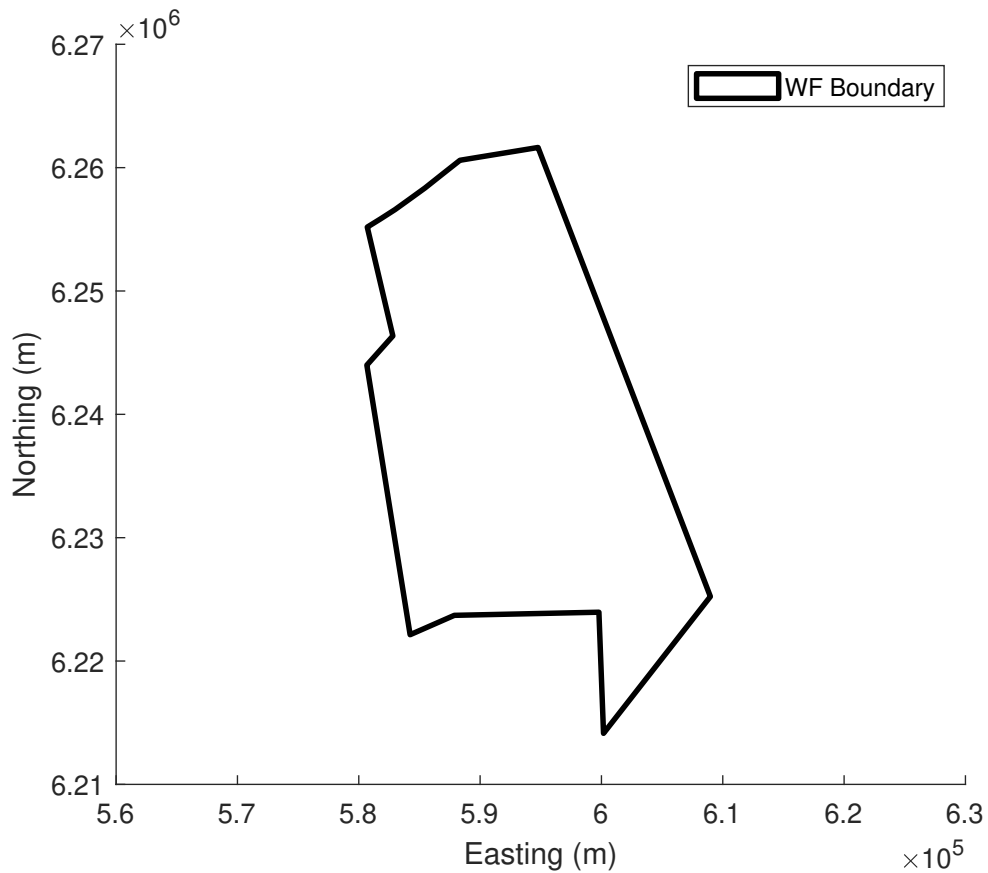


Figure 3.11: SSE's Berwick Bank offshore wind farm site (correct as of April 2021).

### Turbine Description

The turbine used in the case study was a representative 18MW wind turbine provided by SSE. This turbine has a rotor radius of 125m and a hub height of 170m. The power curve and thrust curve of the turbine are provided in the Appendix, Table A.9.

### Case Study Requirements

The requirements of this case study are different to the previous hypothetical case study. Most significantly the objective of the optimisation is to maximise annual energy yield. Equation (3.13), describing the objective function, can be adapted to maximise annual energy yield by setting the cost of turbines to zero ( $C_{turbines} = 0$ ), project lifetime is one year ( $LT = 1$ ), the sales price per unit energy is set to unity ( $k_{MWh} = 1$ ), and

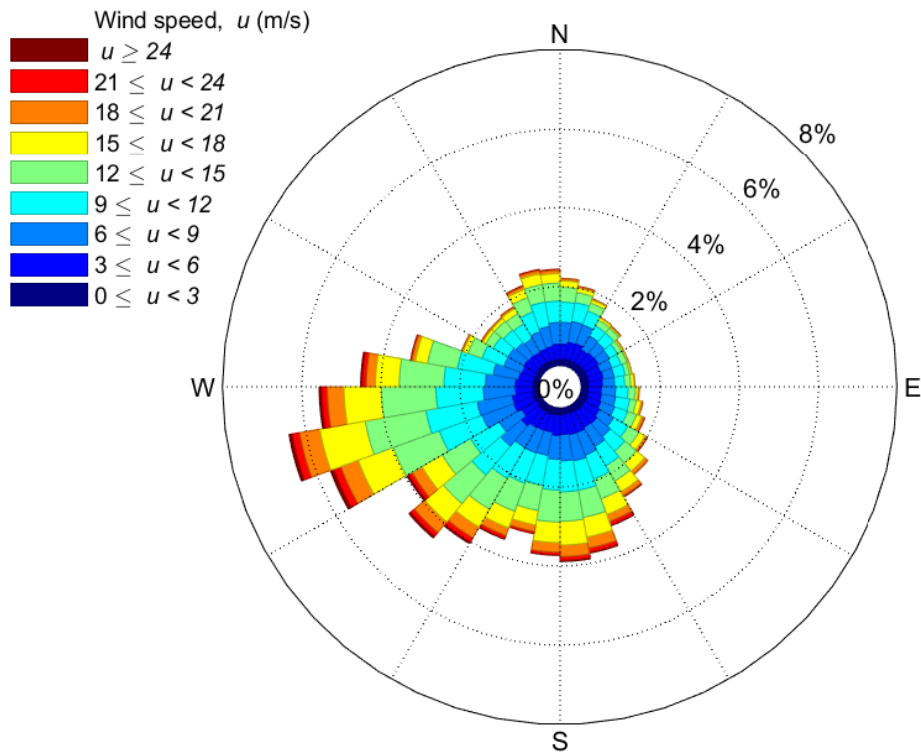


Figure 3.12: Wind rose for SSE’s Berwick Bank offshore wind farm site (using representative data).

the discount rate is zero ( $d = 0\%$ ). Further, the rows and columns of turbines were restricted to be parallel ( $\Delta m_1 = \Delta m_2 = 0$ ), no micro-siting was allowed away from the turbines’ grid positions, and the number of turbines was fixed at 128. Finally, minimum turbine spacing could be no less than six rotor radii ( $s_1, s_2 \geq 7 \times$  rotor diameter ( $6+1$  as  $s_1$  and  $s_2$  are measured between rotor centres)).

**Fixed Number of Turbines:** Since the proposed algorithm used all valid grid points on which to build turbines, it was necessary to introduce an amendment to select exactly 128 grid points to build the required number of turbines. A simple algorithm was used that assesses each grid point starting with the central node (central row and central column crossing) and, working outwards, would determine if the grid point was within the buildable area. If the grid point could be built on, a turbine was placed

there and the next grid point would be considered. This process repeated until 128 turbines had been built. It might be expected that this filling from the centre of the grid approach could lead to under-utilisation of space near the edges of the wind farm. However, for a tightly packed grid with large losses due to wake effects, the solution would be incentivised to spread out to reduce wake effects and increase energy capture. Grids, or solutions, that make better use of the space will perform better from an energy capture perspective, driving other solutions towards a more spread out layout.

As the on-the-fly look-up function considers the wind farm power as a function of the number of turbines, this was not used for the Berwick Bank case study since the number of turbines was fixed at 128.

**Improved Solution Seeding:** The original method for seeding solutions described in Algorithm 2 is similar to an exhaustive search of a discrete set of feasible solutions, selecting the best performing solution as a seed for the first particle in the PSO. However, many assessments of the wind farm model leads to a longer computational time than might not be necessary for seed generation. For the SSE case study, this solution seeding process was adapted to reduce computational time. The new method considers the weighted average wind speed for each direction without assessment of the wind farm model, greatly reducing computational complexity. As before, the best combination of wind directions can be chosen for the angle of the rows and columns of the turbines, while ensuring that constraints such as turbine proximity and minimum angle between the rows and columns are obeyed. Algorithm 3 shows this process.

In this solution seeding process, the wind speed,  $u$ , of a given direction,  $\theta$ , (and opposite direction,  $\theta + 180^\circ$ ) is summed, weighted by it's probability of occurrence,  $P_\theta^u$ . The two directions with the lowest weighted wind speed - that are  $\geq 45^\circ$  and  $\leq 135^\circ$  apart - are chosen for the angle of the rows and columns of turbine respectively. A small range of turbine spacings are included to define  $s_1$  and  $s_2$ . This generates nine particles to seed the PSO, with the remaining population seeded randomly as described previously in Section 3.3.3.

**Algorithm 3** Improved solution seeding

---

```

for  $\theta = 0 : \pi/180 : \pi$  do
  Sum relative wind strength,  $u_{rel,\theta} = \sum_{u=0}^{u_{max}} (P_{\theta}^u u + P_{\theta+\pi}^u u)$ 
end for
Initialise wind strength matrix as all infinite,  $U(:, :) = inf$ 
for  $i = 0 : \pi/180 : \pi$  do
  for  $j = 0 : \pi/180 : \pi$  do
    if  $abs(i - j) \geq \pi/4$  and  $abs(i - j) \leq 3\pi/4$  then
       $U(i, j) = u_{rel,i} + u_{rel,j}$ 
    end if
  end for
end for
Find lowest strength wind directions,  $i, j$  where  $U(i, j) = min(U)$ 
Initialise particle index,  $idx = 0$ 
for  $n = 1:0.25:1.5$  do
  for  $m = 1:0.25:1.5$  do
     $idx = idx + 1$ 
    For particle  $idx$ , set variables of  $\phi_{idx}$  as:  $m_1 = i, m_2 = j, \Delta m_1 = \Delta m_2 = 0,$ 
     $s_1 = n \cdot dist_{min}, s_2 = m \cdot dist_{min}, (x, y) = (x_{GC}, y_{GC})$ 
  end for
end for
Output  $\phi_{1:idx}$  for seeding the first nine particles in the PSO

```

---

**3.5.3 Summary of Optimisation Process Amendments**

Figure 3.13 shows an updated flowchart summarising the key optimisation processes and the amendments made for the Berwick Bank case study, from the original optimisation process, Figure 3.4.

The changes, described in the above sections, can be summarised as follows. (1) An alternative solution seeding approach is used, Algorithm 3; (2) turbine positions are determined by selecting those closest to the centre of the grid, rather than using all grid positions; (3) the look-up function is no longer used as it relies on a variable number of turbines; (4) the wind farm model is used to evaluate annual energy capture, rather than NPV lifetime energy yield, and the turbine capital cost is ignored; and (5) no micro-siting function is used. These changes are made for this case study to enable a direct comparison with SSE's turbine layout optimisation approach.

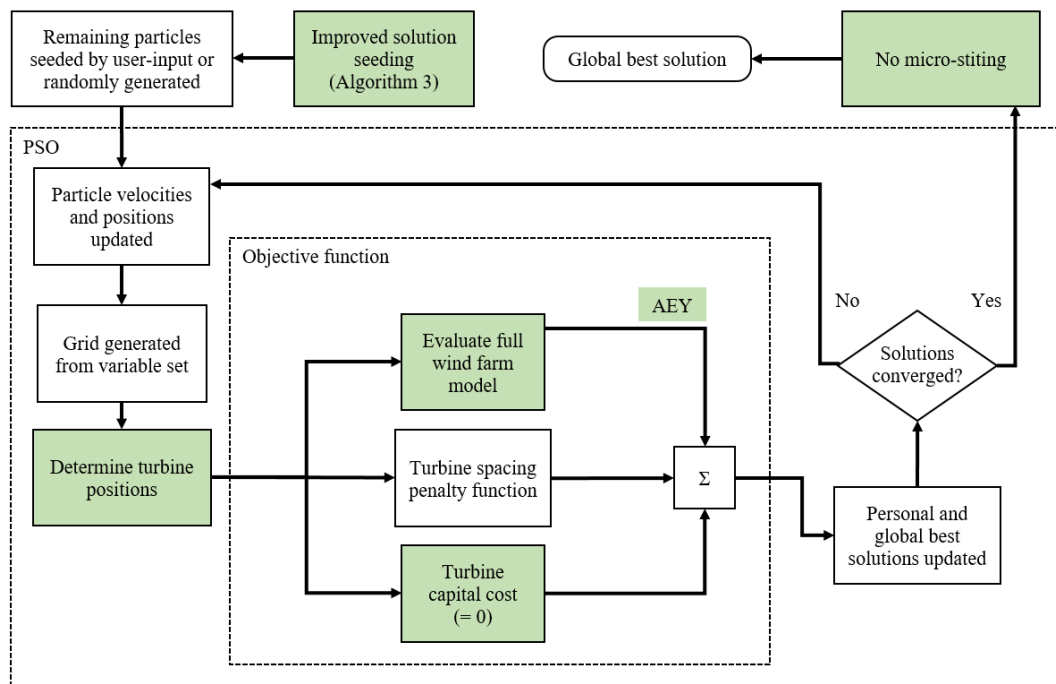


Figure 3.13: Flowchart of the amended optimisation processes (with changes from the original proposed algorithm, Figure 3.4, highlighted in green).

## 3.6 Results & Discussion

### 3.6.1 Hypothetical Offshore Wind Farm Case Study

Ten intuitively designed layouts were created by manually adjusting the grid variables to generate good quality layouts, through intuition and engineering experience. This, rather manual approach, is a common practice in early design phase work of offshore wind farms and several hours were spent on the generation of these to ensure good quality solutions were found. No additional micro-siting (deviation from the defined grid points) was considered for these ten layouts. A further ten layouts were created by the proposed optimisation algorithm. Figure 3.14 shows the turbine layouts of the best solution of each of these two sets of solutions, with the best intuitively designed result in the left plot, and the best model-based optimisation result in the right plot. The process of generating solutions manually requires appreciation of the trade-offs inherent in the problem, including but not limited to:

### Chapter 3. Turbine Placement Optimisation

- achieving an orientation relative to the predominant wind direction beneficial for energy capture, whilst ensuring net energy capture from other wind directions isn't reduced by a greater amount,
- increasing the spacing between turbines to reduce wake effects and increase energy capture, without 'pushing' turbines outside of the wind farm boundary, and
- orienting the grid to optimise the use of the space available (i.e., placing turbines near the wind farm boundary), without negatively impacting energy capture or reducing turbine numbers.

Although manually generating turbine layouts can be quicker, these complications mean that generating good quality solutions can be very difficult and can often be outperformed by solutions created by the layout optimisation algorithm. This can be seen in the objective function values of the two sets of solutions in Table 3.3.

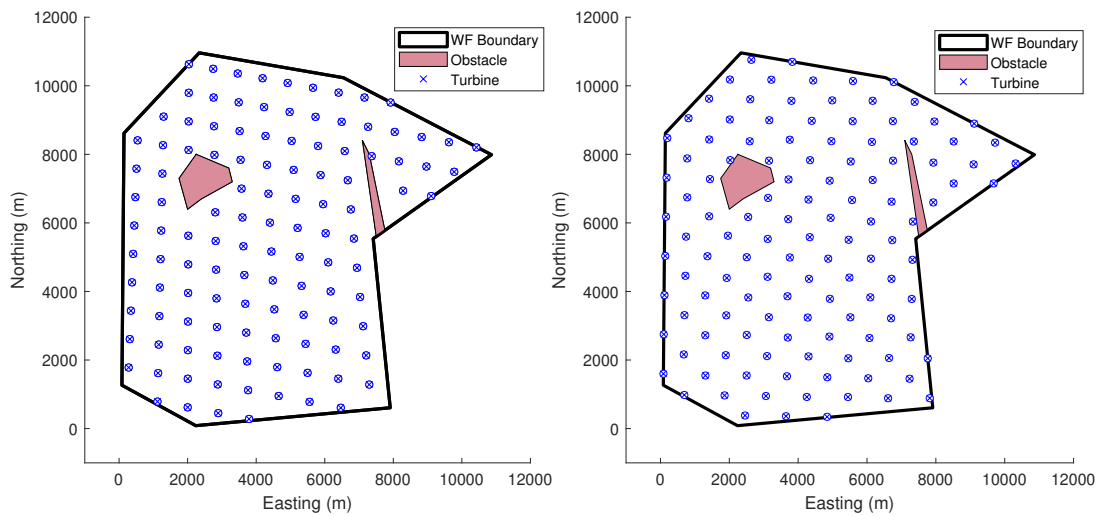


Figure 3.14: Best solutions of the intuitively designed layouts (left) and optimisation algorithm layouts (right) as assessed by the objective function, Equation (3.13).

Figure 3.15, shows a box plot of the fitness of the two sets of solutions, the manually generated layouts and the optimisation algorithm layouts, as assessed by the objective function, Equation (3.13). The intuitively created solutions have an objective function value, or fitness, in the range of £1,041M - £1,165M and a mean value of £1,117.8M

(see Table 3.3). The layouts generated by the optimisation algorithm have values of £1,198M - £1,204M and a mean value of £1,202.3M. It is clear from Figure 3.15 that the optimisation results not only outperform the intuitively designed solutions in every instance but are also more consistent. It can be seen in Table 3.3 that the intuitively designed solutions have a range of £123.2m and a standard deviation of £39.9m. Whereas the optimised solutions all occur within a range of £6.2m and have a standard deviation of £2.0m., which highlights the advantages of layout optimisation considering the aforementioned trade-offs.

Table 3.3: Objective function value of the 10 intuitively generated solutions and the 10 optimised solutions.

Solution no.	Objective function value (£M)	
	Intuitive solution	Optimised solution
1	1126.2	1204.0
2	1144.1	1203.1
3	1072.4	1198.1
4	1066.2	1203.2
5	1140.8	1202.9
6	1127.7	1198.8
7	1041.4	1203.6
8	1146.1	1202.8
9	1148.6	1204.3
10	1164.6	1201.6
<b>Mean</b>	<b>1117.8</b>	<b>1202.3</b>

From Table 3.3 it can be seen that the mean fitness of the optimised solutions is £1,202.3M relative to the mean of the intuitive solutions at £1,117.8M, which is an increase of 7.55%. This corresponds to an increase in the net present value of £84.4M as assessed by the objective function. The optimisation solutions were generated on a standard desktop PC (3.4GHz Intel Core i7-6700, 16GB RAM) in an average time of 39,495 seconds (approximately 11 hours). This computational time is considered a relatively small investment of computational time and resources for an important design phase study. The proposed algorithm can also be used as a practical design tool for sensitivity analysis.

As the turbine placement optimisation algorithm comprises two main functions, the PSO algorithm and the micro-siting function, solutions are also assessed between

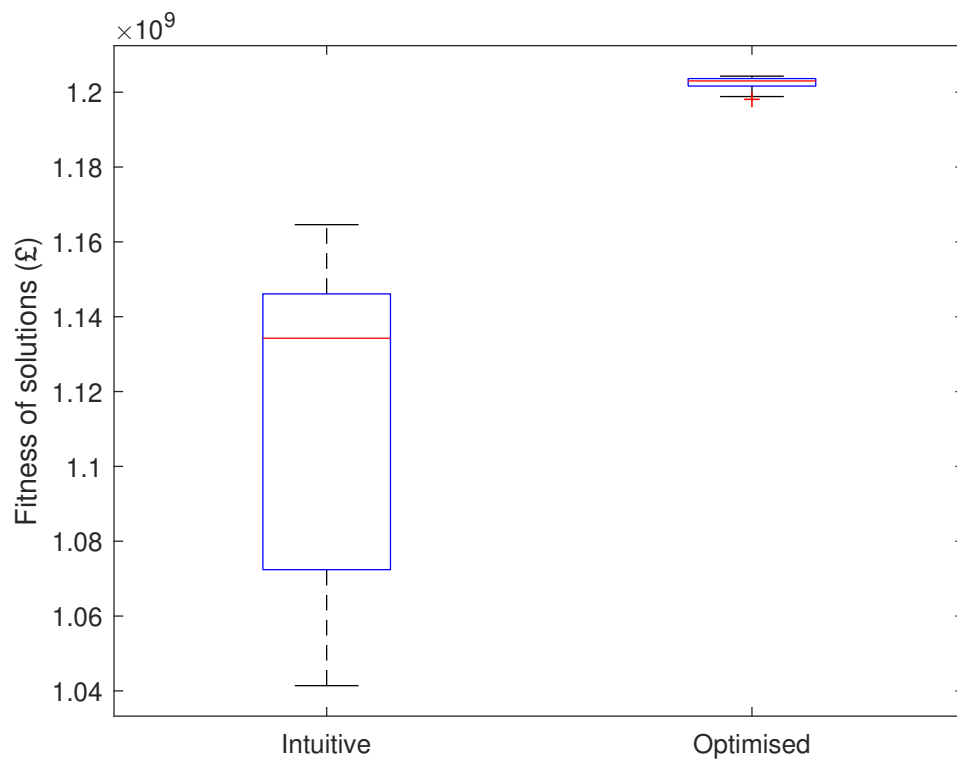


Figure 3.15: Box plot of the fitness of two sets of solutions, generated manually and by the optimisation algorithm, for the hypothetical offshore wind farm case study.

these two phases to determine the relative contribution of each. It was found that the solutions, after the completion of the PSO algorithm, had an average fitness of 6.44% greater than the average intuitively designed solution (an increase of £72.0m). The micro-siting function, which took an average of 3484 seconds (approximately 1 hour), increased this by a further £12.5 (1.11% of the mean intuitively designed solutions).

### 3.6.2 Berwick Bank Offshore Wind Farm Case Study

A single optimised turbine layout was produced by each of the SSE in-house method and the model proposed in this work. Figure 3.16 shows the two optimised layouts, with SSE's on the left, and the proposed model solution on the right. Distinct similarities can be seen between the two layouts, specifically the orientation of the rows and columns of turbines. The row and column spacing of the SSE solution have vastly different values, clearly prioritising a larger separation distance in the predominant wind direction. However, the solution of the proposed optimisation algorithm has row and column spacings that are not too different from one another, despite being oriented similarly to the SSE layout.

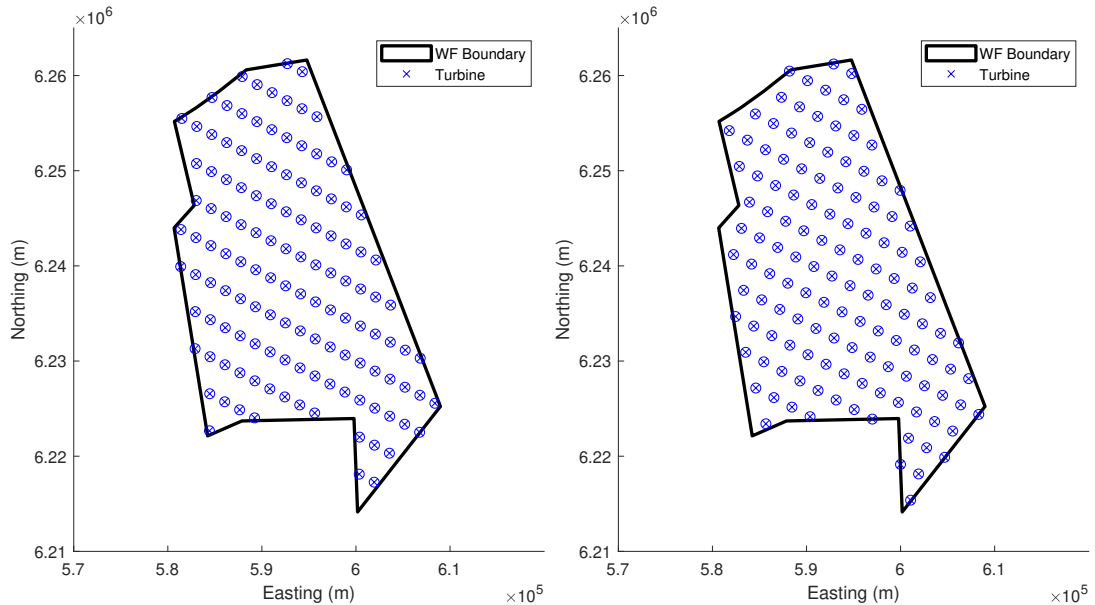


Figure 3.16: Optimised turbine layouts of the Berwick Bank offshore wind farm site generated by SSE (left) and the method proposed in this chapter (right)

While the inputs to the optimisation were shared, no knowledge or information about the algorithm or objective function was shared. Therefore an assessment of both solutions was conducted by both parties independently. Table 3.4 shows the estimated annual energy yield of both solutions as assessed by each party. The leftmost column lists the two solutions, one by SSE, one by the algorithm presented in this work, and the difference between the two. The second column shows the objective value (AEP) of both layout solutions as assessed by SSE, and the difference between the two values. The third column shows the objective value (AEP) of both layout solutions as assessed by the objective value used in this work, and the difference between the two. There are therefore two layouts, and two methods of assessment, used in this comparison.

Table 3.4: Annual energy yield for the SSE solution and proposed model solution, as assessed by SSE’s in house method and the proposed objective function, Equation (3.13).

Solution	SSE Assessment (TWh)	Adapted Objective Function, Eq. 3.13 (TWh)
SSE Solution	12.2719	11.6722
Proposed Optimisation Solution	12.2290	11.6589
<b>Difference</b>	<b>-0.35%</b>	<b>-0.11%</b>

It can be seen in Table 3.4 that for both assessments (one by SSE’s model and the other by the proposed objective function) that the difference between the two layouts is very small. SSE estimated that the proposed layout optimisation solution produced an annual energy yield (AEY) 0.35% less than the SSE layout, while this difference is calculated to be 0.11% less AEY according to the objective function in this work. The most significant difference in the results can be seen between the AEY values of the two assessment methods. For the SSE layout, the proposed model estimates AEY to be 4.89% less than the SSE assessment; and for the proposed optimisation algorithm solution the difference is 4.66%. With no knowledge of the SSE model it is impossible to know exactly what is contributing to this difference. It is expected that the difference is due to different bin widths for the wind speed and direction, differences in the wind farm modelling method (e.g. wake summation), and the inaccuracies of the wake models themselves. The resulting layout solutions are very close however, which

gives confidence that both models are identifying the region in the solution space close to the optimal layout.

### 3.7 Summary

A new approach for turbine layout optimisation of GW-scale offshore wind farms has been proposed using a combination of existing models and methods. The formulation of the grid-based framework improves on previous grid-based layout studies that often have many empty grid spaces [66] or do not allow for the rows or columns of turbines to spread out by changing the angle between them [49]. The addition of two novel components, an on-the-fly look-up dataset and micro-siting function, provides further benefits in both computational resource and the quality of solutions. Creating and using the look-up dataset of average wind farm power output reduces the number of evaluations of the wind farm model by 95%, reducing the computational time commensurately, but introduces uncertainty into the optimality of solutions (completeness of the search of the solution space) and cannot be used in cases with a fixed number of turbines. The micro-siting function, which further improves the final solutions of the PSO, increased the quality of solutions by an additional 1.11%. As this function is completed after the main PSO algorithm, it is benchmarked against the solutions from the PSO phase (immediately prior to the micro-siting function). The second case study, benchmarking the PSO-phase solutions against SSE's in-house optimisation tool, provides a high-degree of confidence in the quality of solutions generated by the proposed PSO algorithm (the solutions against which the micro-siting function solutions are benchmarked).

A comparison of the wake model against real data from the Lillgrund offshore wind farm shows that the model can correctly predict the average wake effect of a single turbine to an error range within 7.12%–13.15% and the energy capture of the downwind turbine to an error range within 0.98%–4.84%. When considering all turbines in the Lillgrund wind farm, and therefore the summation of multiple wake effects, the wind farm model predicted wind farm capacity factor for different wind directions to an error range within 5.93%–11.63%, with an energy capture error of 0.17%. The optimisation algorithm, on a case study of the Lillgrund site, has been shown to produce good quality

solutions increasing the NPV of the site by £8.78 M. This error between the measured data and the analytical wake model, must be taken into account when discussing the uncertainty of the optimised solutions. As shown here, the overall energy capture of a full wind farm is very closely predicted by the wind farm model, however the local effect of a single wake has a much larger error. Therefore, while there can be a reasonably good level of confidence in the quality of the overall layout solution, there remains some uncertainty on the exact performance of an individual wind turbine in a wake, when using analytical wake models.

A hypothetical GW-scale site was proposed to consider more complicated scenarios, and a set of 10 intuitively designed solutions were compared against 10 results generated by the proposed layout optimisation algorithm. Compared to the average fitness of the intuitively designed results, the optimisation algorithm was able to produce solutions with an average fitness 7.55% higher. The proposed algorithm showed consistency in the quality of results (and improved robustness of the approach relative to an intuitive approach), with all solutions within 0.52% of the mean (mean £1,202.3m, standard deviation £6.2m), compared to the more variable solutions created intuitively with a range of 11.02% of the mean value (mean £1,117.8m, standard deviation £39.9m). The computational resource required for the optimisation algorithm was considered acceptable for such an important design phase study (approximately 11hr on a standard desktop PC, which is suitable for running overnight [10]), and so this approach could be used as a practical design engineering tool.

An additional case study was conducted comparing the solution of the proposed model to that of SSE's in-house method on a site being developed by SSE. Theirs is based on an industry standard tool [10] and while no detailed information of the algorithm was provided, the layout solutions of the two methods are very similar. By SSE's assessment, the difference in annual energy yield between the two layouts was 0.35%, and using the proposed objective function, Equation (3.13), the difference was 0.11%. The difference in the predicted AEY for SSE's layout (using SSE's assessment and the objective function proposed in this work) was 4.89%, and for the layout generated with the proposed optimisation framework was 4.66%. It is expected that this difference in

the assessments of AEP (objective) could be due to adopting a different wind speed and direction binning structure, different wind farm models (e.g. wake summation method), and inaccuracies in the wake models themselves. However, without knowledge of the SSE in-house tool it is not possible to identify the source of this difference nor the accuracy of the SSE model. While the SSE benchmarking study provides a good level of confidence in the quality of solutions generated by the proposed PSO-based algorithm, the comparison was conducted for a single wind farm site. Therefore, some uncertainty remains in the quality of solutions when applied to other wind farm sites. During the study, SSE was not able to provide any additional sites for comparison.

Several aspects of the proposed optimisation approach described in this chapter could be explored further to improve the design process and possibly the quality of solutions. First, the micro-siting function was only used on the final set of PSO solutions; however, this could also be evaluated throughout all iterations of the PSO algorithm. If computational resource and time are not a consideration, this may yield improvements to the quality of solutions - but at the price of a large increase in computational time. Second, generating solutions intuitively and evaluating the micro-siting function only, would likely lead to better solutions with respect to manually generated solutions alone. Although it is expected that the solutions would not be as good as those generated by the proposed algorithm, it could provide a method for the quick creation of reasonable quality solutions. Thirdly, while the look-up function provided computational time savings for the hypothetical site, it was not possible to use this for the Berwick Bank site with a fixed-number of turbines. Approximating the objective value within iterations of an optimisation algorithm introduces uncertainty in the completeness of the search in the solution space. As such, this aspect will not be considered for further studies in this thesis but may offer routes for further investigation in other studies interested in reducing computational time. Finally, additional costs such as the capital expenditure of the required electrical infrastructure could be considered. The wind farm model shows diminishing returns for every additional turbine placed in the site (Figure 3.3), therefore including a more complete set of cost considerations - such as array cable cost - may lead to solutions with fewer turbines or affect the spacing and positioning of

### Chapter 3. Turbine Placement Optimisation

turbines.

In conclusion, the turbine layout optimisation approach proposed in this chapter meets the first objective of the thesis which was to develop a turbine layout optimisation that is capable of considering modern large-scale offshore wind farms (over 100 turbines) using a standard desktop computer. Improvements in computational time and quality of solutions was found through the employment of two novel components, the look-up method and micro-siting function. Comparison to SSE's in-house tool shows this method is not only applicable to large sites, but also capable of generating solutions on a standard desktop PC of similar quality to those generated by industry tools.

## Chapter 4

# Cable Layout Optimisation

This chapter considers the cable routing optimisation problem within offshore wind farm design. The problem formulation is based on a radial string array allowing for branched connections and multiple substations, as this was the strong preference of all industrial interviews when compared to looped string layouts [10]. The computationally complex constraint for crossing cables is handled in an efficient way and many other real world constraints are considered, including jointing costs, cable capacity limits, and bathymetry obstacles. An adapted ant-colony optimisation (ACO) algorithm is proposed using a decomposition technique and is used for two case studies. The first case study applies the proposed algorithm to the hypothetical site, proposed in Section 3.5.1, with comparison to a classical ACO algorithm and benchmarking against a mixed-integer linear programming (MILP) approach. The second case study investigates the effect of conductor material on the array cable layout of SSE’s Berwick Bank offshore wind farm to help determine the sensitivity to input parameters such as cable capacity and cost.

### 4.1 Formulation of the Cable Layout Problem

As mentioned in Chapter 2, the topology of array cable layouts in offshore wind farms has not converged to a single configuration. Many wind farm developers choose simple radial string connections, while others prefer to include redundancy through ‘looped’

connections.

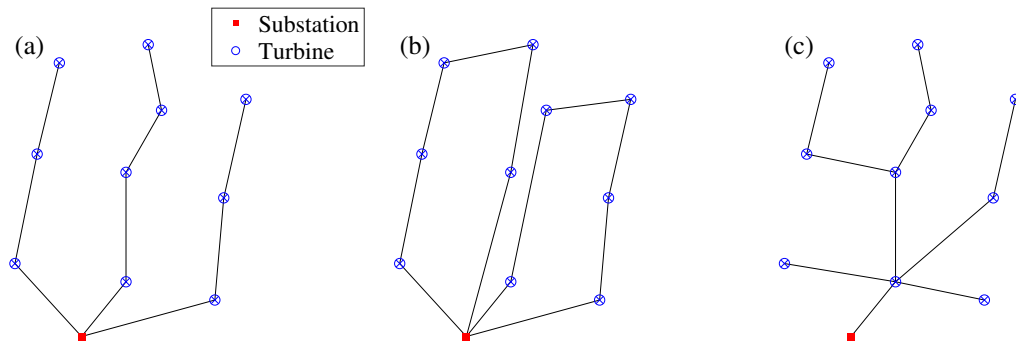


Figure 4.1: Examples of different array cable layout typologies including (a) radial strings, (b) redundant or ‘looped’ connections, and (c) star or ‘branched’ connections.

Figure 4.1 shows the three main categories of array cable layouts, where (a) shows a radial string layout, (b) shows a ‘looped’ or ring layout with redundant connections, and (c) shows a ‘star’ layout [72, 103]. The radial string layout is the simplest and is widely used in offshore wind farms currently. Typically, cable sizes and capacities increase towards the substation as more power is carried from the turbines in the string to the substation [71, 88]. Ring-based layouts, using redundant connections, are often further broken down into single sided- and double sided- rings. This differentiation describes whether the redundant connection is between the end of a string and the substation, or connects the ends of two strings [103, 105]. Additional complexity can be introduced for ‘looped’ layouts as the cable selection of the redundant connection is not trivial. Options include rating all sections of the string to be capable of handling the rated power of all turbines in the string or using a smaller cable capable of carrying the power of only some turbines in the string. This decision is inherently linked to the probability of cable failures, the mean time to repair, and the associated lost revenue to offset the additional cable cost. Branched or ‘star’ layouts are a set of layouts that include multiple connections into a single turbine. This increases the complexity of the joints [85, 103] in the turbine being connected to and therefore increasing the jointing cost, but can offer savings by reducing overall cable length.

From the perspective of optimisation design, the different categories of cable layout

can require significantly different approaches, most notably the looped layouts whose performance relies more heavily on the condition of the system. Radial and branched layouts can account for lost revenue based on cable failure probability and time to repair losing 100% of the revenue (from turbines beyond the fault) while in the ‘failed’ state. In looped layouts, this lost revenue is also a function of the composition/cable sizes in the working section of the string depending on where the fault occurs, resulting in a more complex assessment of the objective function [83]. In some looped layouts, every cable section can support the rated power of all turbines in the string in the event of a fault, others can only support some of the power generated, depending on the selection of the cable sizes [103]. In discussions with industry, including SSE prior to the layout comparison study, it was clear that current industry interest lied with radial string layouts and the possibility of branched connections rather than redundancy and looped layouts [10]. Further, radial strings and branched connections can be formulated in the same way within optimisation algorithms. The latter requires a few additional variables to capture the additional cost of complex jointing within turbines [85], and if this cost is prohibitively high will result in non-branched (radial) string solutions. As such a branched cable routing approach was taken forward for the optimisation development described in the following sections.

### 4.2 Optimisation Design Methodology

This section outlines the three optimisation algorithms used in the study, introduced in Chapter 2. These include a classical ACO algorithm, the adapted ACO-based algorithm (ACOSP), and the widely used MILP model against which the two former algorithms will be benchmarked. The following sub-sections detail the common pre-processing phase including problem formulation, electrical loss calculation, and creation of the available cable set. Detailed descriptions of the three algorithms are presented including constraints, the common objective function, and the procedures in the algorithms.

### 4.2.1 Algorithm Selection

Several algorithms are highlighted in the literature review, presented in Chapter 2. Much is dominated by the mixed-integer linear programming (MILP) approach based on the work first presented by Fischetti et al. [60]. This MILP method does not scale well - in terms of both computational time and memory - for larger sites, where function evaluations can be expensive, and so does not necessarily offer the best solution for optimising the array cable layout of GW-scale offshore wind farms. However, given enough computational time and memory, the MILP method is able to determine the proven optimal solution and so is an appropriate tool for the purposes of benchmarking the ACO and ACOsp methods. Heuristic methods and/or decomposition techniques offer an alternative approach that may better cope with these large-scale optimisation problems with expensive function evaluations [53]. The ACO algorithm is highlighted as a viable heuristic algorithm that has only been considered in a handful of academic studies for this application of array cable routing optimisation [40, 100, 101]. While the MILP algorithm is able to find the mathematically optimal solution, heuristics cannot guarantee this. For this reason the ACO method is adapted to include a simple decomposition technique. Problem decomposition essentially relies on breaking a large problem into a set of smaller problems to solve. These smaller problems could be generated by randomly selecting a small subset of the decision variables, however in this application, it is possible to use the formulation of the array cable layout problem to inform the sub-problem selection (i.e. specifically selecting the variables associated with two or more of the strings in the incumbent solution). The proposed decomposition algorithm selects pairs of strings (provided by an initial solution seed) and the turbines they support, and re-optimises the array cable layout for this subset of turbines. This process is repeated in a recursive decomposition until the stopping criteria are met. More detail of the decomposition strategy is provided later in the chapter. In order to determine the efficacy of the ACO and ACOsp approaches, the MILP algorithm is employed for comparison and benchmarking.

### 4.2.2 Pre-Processing

In order to define the problem for optimisation, the coordinates of the wind farm boundary, obstacles, and turbine positions are required in addition to the available cable parameters. A description of the wind field and turbine performance curves are also necessary for the calculation of electrical losses.

For each of the available cable sizes, a subset of cables is created considering different electrical loading scenarios (different numbers of turbines being supported) in line with the method proposed by Fischetti et al. in 2017 [77]. The net present value (NPV) of the electrical losses per unit length is calculated as follows for each of the available cables, under each of the loading scenarios.

$$loss_n^t = 8760 I_n^2 R^t k_{MWh} \sum_{yr=1}^{LT} \frac{1}{(1+d)^{yr}} \quad (4.1)$$

where  $loss_n^t$  is the NPV electrical losses per unit length for a cable of type  $t$  supporting  $n$  turbines,  $I_n$  is the current profile in an arc supporting  $n$  turbines,  $R^t$  is the resistance per unit length of cable type  $t$ ,  $k_{MWh}$  is the price per MWh,  $LT$  is the project lifetime in years, and  $d$  ( $0 < d < 1$ ) is the discount rate. An example set of cables and their associated costs are shown in Table 4.1 (representative values generated for the purpose of demonstration).

In order to reduce the complexity of the design problem and improve performance of the algorithm, the set of available cables can be reduced, simplifying the cable selection process. In the algorithms in the following sections, the cable routing and cable sizes must be determined. Cables will be supporting a given number of turbines for each connection and it is important that the cheapest overall cable is chosen (whilst obeying capacity constraints). Table 4.2 shows a reduced subset of cables, keeping only the cheapest cable (by total cost) for each number of turbines to be supported. For example, each of the three cable sizes shown in Table 4.1 (95/180/240mm<sup>2</sup>) is able to support three turbines, however only the cheapest option will be used in the algorithm solutions. Therefore, the two more expensive options are removed, keeping only the cheapest (180mm<sup>2</sup>) as can be seen in Table 4.2. This process is repeated for cables supporting 1,

Table 4.1: Example set of cable types (conductor sizes under different electrical loading scenarios), with the associated costs and net present value (NPV) of electrical losses per unit length. (Representative values for the purpose of demonstration).

Cable conductor size (mm <sup>2</sup> )	No. turbines supported	Capital cost (£/m)	Electrical losses (NPV £/m)	Total cost (£/m)
95	1	120	20	140
95	2	120	40	160
95	3	120	75	195
180	1	150	10	160
180	2	150	20	170
180	3	150	40	190
180	4	150	80	230
240	1	175	5	180
240	2	175	10	185
240	3	175	20	195
240	4	175	40	215
240	5	175	75	250

2, . . . , up to N (in this example five) turbines with the resulting cable subset shown in Table 4.2. This reduced set of cables is made available to the algorithms and allows for the selection of cable rating based solely on the number of turbines being supported. Maintaining costs in a per-unit-length format ensures the selected cable sizes are of the lowest cost, regardless of connection length. This approach has been used in academic literature, becoming a relatively standard method of considering electrical losses [77].

Table 4.2: Example of a reduced set of cables with associated costs, from the larger set of cables presented in Table 4.1, keeping only one cable per number of turbines to be supported.

Cable conductor size (mm <sup>2</sup> )	No. turbines supported	Capital cost (£/m)	Electrical losses (NPV £/m)	Total cost (£/m)
95	1	120	20	140
95	2	120	40	160
180	3	150	40	190
240	4	175	40	215
240	5	175	75	250

In order to further simplify the optimisation design, the number of possible connections - or arcs - are limited. Figure 4.2 shows an example containing 12 turbines and one substation, with Figure 4.2(a) containing all possible arcs and Figure 4.2(b)

containing only the arcs from every turbine to its closest four turbines and the substation (four chosen here for demonstration purposes only). As each arc represents a variable to be optimised by the optimisation algorithm, this method can greatly reduce the problem complexity, and for regular grid-based turbine layouts removing the longest arcs is highly unlikely to affect the optimal solution. Ensuring each turbine has an arc connecting it to a substation (regardless of the arc length) reduces the probability of infeasible solutions being generated and the risk of the optimal solution being affected or removed.

Before the longest arcs are removed, each arc route is checked to determine if it crosses the boundary of the wind farm, or an obstacle. If the arc does cross either of these, the length of that arc is artificially increased by a factor of ten to penalise it. These arcs are then highly likely to be removed during the reduction of the arc variables described previously.

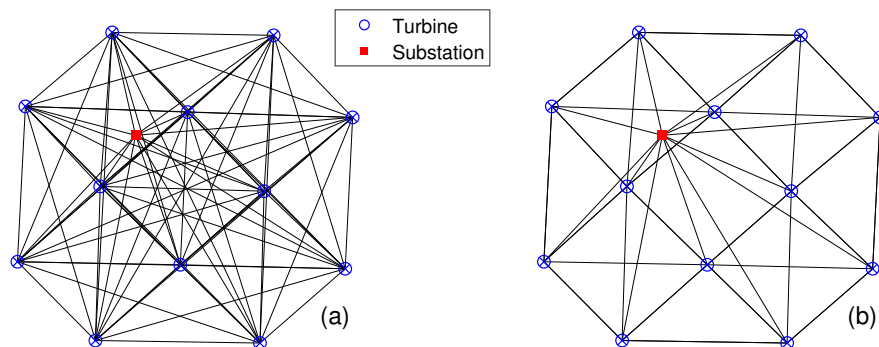


Figure 4.2: Example case of 12 turbines and one substation, with (a) all possible cable connections and (b) cable connections limited from each turbine to the nearest four turbines and the substation.

Additionally, a simple Steiner node (‘empty’ node) generation method is used to allow for the navigation of cables around obstacles. During pre-processing, Steiner nodes are included at each of the concave vertices of the wind farm boundary and any obstacles in the site. These nodes are then used in the optimisation algorithms, described further later, enabling cables to navigate around an obstacle if the straight line con-

nection between two nodes passes through the wind farm boundary or an obstacle. An example of Steiner node placement can be seen in Figure 4.5.

Once all nodes and routes are defined, the cost variables,  $c$  (discussed further later), can be calculated by considering the route length, cable type (and cost per unit length), and loading scenario (for electrical losses) for the associated variable. These costs can then be used as coefficients for some of the decision variables discussed in the following section.

### 4.2.3 Mixed-Integer Linear Programming (MILP)

The MILP method used in this study is based upon the methods proposed in [71] and [85]. In this method, binary variables are used to indicate whether a specific cable type on a specific arc is present (=1) in the layout solution or not (=0), and other non-binary variables are included describing the power flow and branching costs. The following provides a description of the decision variables used in the optimisation, with the following sections describing the objective function and constraints.

- $x_{i,j}^{t,n}$  - Binary variable, coupling power flow and cable type, describing whether a specific cable type/size,  $t$ , supporting the power flow of  $n$  turbines, using the route from node  $i$  to node  $j$  is built or not (1/0).
- $y_{i,j}$  - Binary variable describing if any cable type/size, supporting any number of turbines, is built on the route from node  $i$  to node  $j$  or not (1/0).
- $p_{i,j}$  - Continuous non-negative variable describing the power flow in the cable (if built) on the route from node  $i$  to node  $j$ .
- $w_j^h$  - Binary variable describing if the cost of  $h$  connections into a turbine node,  $\gamma_h$ , must be included or not (1/0).

where  $(i, j)$  is a route in the set of routes,  $A$ , connecting node  $i$  to node  $j$ . The  $x$  variables couple the cable route  $(i, j)$ , cable type  $(t)$ , and power flow in the cable  $(n)$  resulting in a large number of combinations,  $i, j \times t \times n$ , and therefore a large number of variables. Similarly,  $y$  and  $p$  variables exist for each of the routes,  $i, j$ , describing if any cable type

is built and the power flow in the route respectively. Finally,  $w$  variables are created for each of the turbine nodes and possible number of connections, describing if turbine  $j$  has  $h$  cable connections connecting into it. This allows the algorithm to attribute the appropriate jointing cost to the objective value.

Interestingly, it appears that both the  $y$  and  $p$  variables may be redundant in this formulation. The information stored in the  $y$  variables describes if any cable supporting any number of turbines is built on the route  $i, j$ . This information is already stored in the  $x$  variables ( $y_{i,j} = \sum_{t \in T} \sum_{n \in 1:k_{max}} x_{i,j}^{t,n}$ ) and so may be increasing the variable count unnecessarily. Similarly, the information stored in the  $p$  variables describes the power flow in a given route,  $i, j$ . While not explicitly stored in the  $x$  variables, information on the number of turbines,  $n$ , being supported by a cable connection is stored in the  $x$  variables and so information on the power flow could easily be derived. While there is no mention of this in the studies from which the model is taken [71, 85], it is assumed that these variables are included to aid the creation of the constraint equations, described further later. However, the constraint equations considering  $y$  variables, could easily be replaced with the corresponding  $x$  variables if desired, reducing the variable count of the optimisation and improving computational efficiency. Constraint equations considering the power flow variables,  $p$ , require some minor reworking, but could be replaced with corresponding  $x$  variables by using a coefficient representing the peak power produced by  $n$  turbines, say  $\Psi$ , thus considering variables in the form  $\Psi_n x_{i,j}^{t,n}$  (where  $p_{i,j} = \sum_{n \in 1:k_{max}} \Psi_n \sum_{t \in T} x_{i,j}^{t,n}$ ). Although this formulation could be amended, it - and similar formulations - are widely accepted as a robust tool for cable layout optimisation studies in the literature [75, 78, 92, 99, 108, 109], and so is replicated here for the purposes of benchmarking and comparison to the ACO and ACOsp methods.

The optimisation problem was solved using Matlab R2018b and the built-in *intlinprog* function. The key processes used by the solver include: reducing the problem size with linear programming (LP) pre-processing; solving an initial relaxed (non-integer) problem with LP; tightening the LP relaxation with mixed-integer pre-processing; cut generation; heuristic methods to find an integer-feasible solution; and a branch-and-bound algorithm to solve the restricted formulation of the LP relaxation. The following

sections outline the mathematical formulation of the objective function and the constraint equations.

### Objective Function

The objective function, Equation (4.2), aims to minimise the total lifetime cost of the installed network for all arcs (connections between nodes  $i$  and nodes  $j$ ) in the set of possible connections or arcs,  $(i, j) \in A$ , with the set of available cables,  $T$ . Denoting the cost as  $F$ , the optimisation problem is written as:

$$\min F = \min \sum_{(i,j) \in A} \sum_{t \in T} \sum_{n \in \{1:k_{max}\}} c_{i,j}^{t,n} x_{i,j}^{t,n} \quad (4.2)$$

where  $c_{i,j}^{t,n}$  is the cost of using a cable type  $t$ , with the associated losses from supporting  $n$  turbines, in the arc connecting nodes  $i$  and  $j$  (where cable type refers to cable cross-sectional area), and  $x_{i,j}^{t,n}$  is a binary variable describing if cable type  $t$  is used, to support  $n$  turbines, using the arc connection  $i, j$ . An arc connection  $i, j$  represents a cable connection, with power flow from node  $i$  to node  $j$ .

### Constraints

**No reverse power flow:** In order to facilitate constraints, the power flow in each arc must be calculated. An additional decision variable,  $p_{i,j}$ , describes the power flow in the arc  $(i, j)$  for all arcs in the set of arcs,  $A$ , whose value is determined for each intermediate solution by the *intlinprog* solver concurrently with the remaining decision variables. Equation (4.3) applies a constraint to ensure that the power flow in a given cable section is greater than or equal to zero (implying directionality of connections). While, in reality, power may flow in either direction along a cable, the formulation presented in this study treats cables as having a ‘direction’. This means that a cable connecting turbine WT1 to turbine WT2 will be considered separately to a cable connecting turbine WT2 to turbine WT1, even though practically they are the same cable.

$$p_{i,j} \geq 0, \quad \{i, j\} \in A \quad (4.3)$$

**Kirchhoff's Current Law:** A constraint must be applied in line with Kirchhoff's current law, stating that the current flowing into a node  $i$  must equal the current leaving the node, for all nodes in the set of nodes,  $V$ . This is implemented as seen in Equation (4.4), which states the power entering a node,  $p_{k,i}$  (from all other nodes,  $k$ ), plus the power generated at the node,  $p_{gen_i}$ , must equal the power leaving the node,  $p_{i,j}$  (going to all other nodes,  $j$ ).

$$\sum_{k \in V} p_{k,i} + p_{gen_i} - \sum_{j \in V} p_{i,j} = 0, \quad i \in V \quad (4.4)$$

**Cable rating:** In order to prevent the overloading of cables, the rated capacity of a cable of type  $t$ ,  $k_t$ , multiplied by the binary variable  $x_{i,j}^{t,n}$  must be greater than or equal to the power flow in the arc,  $p_{i,j}$ , for all cable types in the set of cable types,  $t \in T$ .

$$\sum_{t \in T} k_t x_{i,j}^{t,n} \geq p_{i,j}, \quad \{i, j\} \in A \quad (4.5)$$

**Up to one cable can be used per route:** Equation (4.6) introduces a new binary decision variable,  $y$ , that describes if a route is used by any cable type ( $y = 1$ ) or remains unused ( $y = 0$ ). By stipulating that  $y$  is equal to the sum of  $x$  variables associated with the same route, this constraint restricts the maximum number of cables types that can be used to one per route:

$$\sum_{t \in T} x_{i,j}^{t,n} = y_{i,j}, \quad y \in \{0, 1\}, \quad \{i, j\} \in A \quad (4.6)$$

**No cables can leave and re-enter the same node:** For simplicity, any arcs (straight-line connections) that leave and re-enter the same node ( $x_{i,j}^{t,n}$  where  $i = j$ ) are removed in pre-processing to avoid zero-length arcs being used and to reduce the number of constraint equations.

**Exactly one cable must leave a turbine:** As the power leaving a turbine node cannot be split, and to ensure the power from a turbine is connected to a substation, Equation (4.7) stipulates that exactly one arc leaving a turbine must be used, for all

turbine nodes,  $i \in V_T$ :

$$\sum_{j \in V: i \neq j} y_{i,j} = 1, \quad i \in V_T \quad (4.7)$$

**No cables may leave a substation:** As this optimisation is not considering export cable routing, a constraint may be applied to avoid any cables leaving a substation node, in a similar form to Equation (4.7). However, to reduce the number of constraint equations and redundant variables, any arcs leaving a substation node can be removed during pre-processing.

**Up to one cable may leave/enter a Steiner node:** For any ‘empty’ (Steiner) nodes that are used to navigate around obstacles, it is important that only up to one cable is allowed to enter and leave the node. This is to avoid branched connections being employed at an effectively empty node rather than at a turbine node - resulting in unrealistic layouts, since developers typically aim to joint cables at a turbine or substation rather than an arbitrary location on the seabed [88]. Equations (4.8) and (4.9) limit the number of connections entering and leaving Steiner nodes respectively, to less than or equal to one. In conjunction with Equation (4.4), if a cable enters a Steiner node, exactly one cable must leave the node. This is applied to all Steiner nodes in the set of Steiner nodes,  $V_0$ .

$$\sum_{i \in V: i \neq j} y_{i,j} \leq 1, \quad j \in V_0 \quad (4.8)$$

$$\sum_{i \in V: j \neq i} y_{j,i} \leq 1, \quad j \in V_0 \quad (4.9)$$

**Limit connections into turbines/substation(s):** Equations (4.10) and (4.11) limit the number of connections into substations and turbines to  $C$  and  $H$  respectively, where  $C$  and  $H$  are user-defined constants describing the maximum number of allowed connections (in addition to cables leaving the turbine, Equation 4.7). These constraints are useful to restrict solutions to use a realistic number of connections into a turbine,

or avoid branched layouts altogether. Equations (4.10) and (4.11) are applied to all nodes in the set of substation nodes,  $V_{SS}$ , and all nodes in the set of turbine nodes,  $V_T$ , respectively.

$$\sum_{i \in V: i \neq j} y_{i,j} \leq C, \quad j \in V_{SS} \quad (4.10)$$

$$\sum_{i \in V: i \neq j} y_{i,j} \leq H, \quad j \in V_T \quad (4.11)$$

**Cost of branched connections:** As the connection of multiple strings into a single turbine requires more complex switch-gear and cable jointing, it is useful to be able to capture these costs in the optimisation process. Equation (4.12) introduces a binary variable,  $w_j^h$ , that describes whether  $h$  ( $h \in \mathbb{Z}^+$ ) connections are connected into turbine  $j$ , (where  $w_j^h = 1$  if this condition is true, i.e. at turbine  $j$ , there are  $h$  cable connections, for  $j \in V_T$  and  $h \in H$ ). By including a cost coefficient,  $\gamma_h$ , for  $h$  connections, this branching cost can be accounted for in the optimisation.

$$w_j^h \in \{0, 1\} \quad (4.12)$$

An additional constraint equation is required to ensure the correct cost for the number of connections is attributed to the objective value, based on the formulation presented by Fischetti et al. [85]. Equation (4.13) shows the sum of cables entering (i.e. power ‘into’ the turbine, since there is directionality) a turbine node must be equal to the sum of the binary jointing variable multiplied by the associated number of connections.

$$\sum_{i \in V: i \neq j} y_{i,j} - \sum_{h=1}^H h w_j^h = 0, \quad j \in V_T \quad (4.13)$$

### Updating the Objective Function

In the previous section, several decision variables were included for use in constraint equations, including:  $y_{i,j}$  to describe if any cable is used in a given arc or connection,  $p_{i,j}$  to describe the power flow in a given arc,  $w_j^h$  to describe if  $h$  connections enter turbine

$j$ , and  $\gamma_h$  to account for the cost of  $h$  connections into a turbine. As such, the objective function must be updated to include these terms. The cost of branched connections must be included, as shown in Equation (4.14), by summing the cost of  $h$  connections in the range of  $H$  (the limit of the number of connections) across all turbines in the set of turbines,  $V_T$ .

$$\min \bar{F} = \min \left[ \sum_{(i,j) \in A} \sum_{t \in T} \sum_{n \in \{1:k_{max}\}} c_{i,j}^{t,n} x_{i,j}^{t,n} + \sum_{h \in H} \gamma_h \sum_{j \in V_T} w_j^h \right] \quad (4.14)$$

#### 4.2.4 Classical Ant Colony Optimisation (ACO)

The ant colony optimisation (ACO) algorithm mimics a colony of ants as they walk between their nest and a food source, as first described in the works by Dorigo et al. [100]. Many different paths are taken by the ants as they search for food, depositing pheromones as they walk which can be detected by other ants. For destinations close to the nest, it will take less time for the ants to walk between the two sites and so the pheromone deposits are added more regularly, leading to a stronger concentration of the pheromone on that path. For an ant about to leave the nest, the probability that it will take a given path is proportional to the strength of the pheromone scent. Since the pheromones evaporate over time, the longer paths (on which pheromones are deposited less frequently) will be a less favourable option for other ants to take, resulting in a convergence to the most efficient path.

The ACO algorithm is used to solve optimisation problems that can be formulated as a topological graph, which makes it well-suited to an array cable layout optimisation problem. In this study, based on the work by Dorigo et al. and its applications in the academic literature [100, 101], an ‘ant’ starts from the (unconnected) turbine that is furthest from a substation and undertakes a pseudo ‘random walk’ until it reaches a substation node. Another ant then starts at the unconnected turbine next-furthest from a substation, and undertakes a walk until it reaches a substation node or a turbine on an existing string. This is repeated until there are no turbines left unconnected. The available paths for the ants to take are constrained to reduce the number of decision

## Chapter 4. Cable Layout Optimisation

variables in the optimisation. At each node, ants are able to walk (in a straight line) to the nearest eight nodes (although another number of nodes may be chosen), or directly to any substation node. The paths directly linked to substations are included to avoid an ant having no available path left to walk on - which may otherwise happen if all neighbouring turbines have been connected using a cable that has no remaining capacity to support an additional turbine.

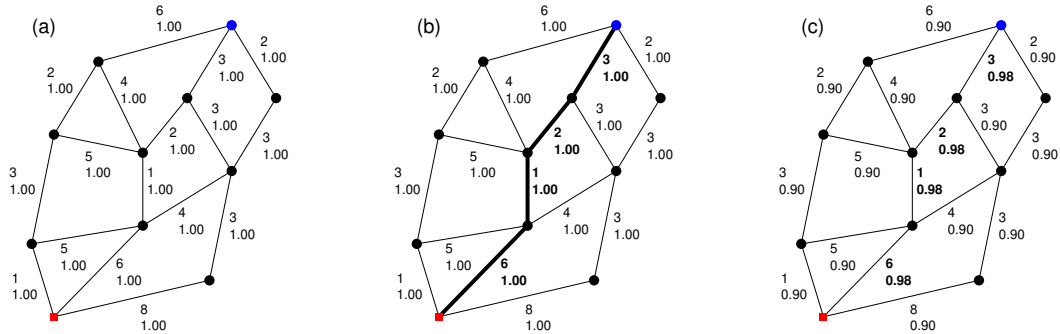


Figure 4.3: Example of a path taken by an ‘ant’ during an iteration of an ACO algorithm, from the start point (blue circle), via nodes (black circles), to the end point (red square). Path lengths and pheromone concentration are labelled for each path as the top and bottom numbers respectively, with (a) initial conditions, (b) the path taken in bold, and (c) updated pheromone concentrations.

An illustrative example of one iteration in a classical ACO algorithm is shown in Figure 4.3 to demonstrate the underlying processes of the ACO algorithm (a simple small graph is used for clarity, rather than a more complex graph as would be present in the described cable layout problem). Here the starting point (blue circle) can be considered a turbine node, the end point (red square) can be considered a substation node, and the remaining connecting nodes (black circles) can be considered ‘empty’/Steiner nodes. Figure 4.3(a) shows the initial conditions of the topological graph, with path lengths (or costs) and pheromone concentrations labelled for each path as the top and bottom number respectively. For an ant standing on node  $i$ , the probability of it walking to a connecting node  $j$ , via the path (or arc)  $x_{i,j}$  is given by:

$$P_{i,j} = \frac{pher_{i,j} \cdot weight_{i,j}}{\sum_{j \in J} (pher_{i,j} \cdot weight_{i,j})} \quad (4.15)$$

where  $pher_{i,j}$  is the pheromone concentration of the path ( $x$ ) between nodes  $i$  and  $j$ ,  $weight_{i,j}$  is equal to the reciprocal of the cost of path  $x_{i,j}$ , and  $J$  is the set of nodes available to walk to from node  $i$ . At each node, a random number is generated and used in conjunction with the probabilities of connected nodes ( $P_{i,j}$ ) for Roulette-wheel selection of the next node [48]. The ant steps to the chosen next node and the process is repeated. Figure 4.3(b) shows an example completed path from the start node to the end node, with the paths that were used shown in bold. Once a completed graph (connecting all turbines to a substation) has been generated, the pheromone concentrations must be updated. The pheromones on all paths are updated proportionally after each iteration ( $k$ ).

$$pher_{i,j}(k+1) = evap \times pher_{i,j}(k) \quad (4.16)$$

where  $evap$  is the evaporation constant (90% is used for Figure 4.3). The objective value is then calculated and used to determine the pheromone deposit. In the example in Figure 4.3(b) the objective value (total cost of the route in this example) is equal to  $12 \cdot (3+2+1+6)$ . The pheromone deposited on the used routes,  $\Delta pher$ , is equal to the reciprocal of the objective value, approximately 0.08.

$$\Delta pher = \frac{1}{F(x)} \quad (4.17)$$

Figure 4.3(c) shows the updated pheromone concentrations after the evaporation and deposit processes have taken place and the route has been cleared to begin the next iteration.

To adapt the algorithm to the optimisation problem under consideration and to improve convergence behaviour, two adaptive parameters are introduced into Equation (4.15) yielding Equation (4.18) [100] :

$$P_{i,j} = \frac{pher_{i,j}^{\alpha} \cdot weight_{i,j}^{\beta}}{\sum_{j \in J} (pher_{i,j}^{\alpha} \cdot weight_{i,j}^{\beta})} \quad (4.18)$$

where  $\alpha$  and  $\beta$  are exponents (both real non-negative numbers) describing the pheromone constant and exploratory constant respectively. These two parameters weight the relative importance of the cost and pheromone strength of the paths and can be adjusted in the algorithm to reduce the time to convergence or increase the probability of new routes being explored [100]. The overall ACO algorithm is summarised in Algorithm 4, where  $T_u$  is the set of unconnected turbines;  $dist_{t_u,SS}$  is the distance between an unconnected turbine,  $t_u$ , and the closest substation,  $SS$ ;  $loc_{ant}$  is the location of the ant;  $N_v$  is the set of nodes that have been visited by an ant in the current iteration;  $J$  is the set of nodes available to walk to from the current location,  $i$ ;  $i, j$  are two nodes connected by a path (or arc)  $x_{i,j}$  in the set of usable arcs  $A$ ;  $A_{used}$  is the subset of arcs that were used in a given iteration;  $\bar{F}(x)$  is the updated objective function, Equation (4.14); and  $avgF$  is the average of the objective function over  $m$  iterations and used to define the stopping criteria.

The values of the key parameters used in the ACO algorithm were initialised as: 1.00 for the pheromone concentration on all paths,  $pher_{i,j}$ ; 0.50 for the pheromone exponent,  $\alpha$ ; and 1.50 for the exploratory exponent,  $\beta$ . An evaporation constant of 0.99 was used. Initialising uniform pheromone concentrations avoids premature convergence on a non-optimal solution, while the ratio of exponents is found initially by Dorigo et al. [100] and adjusted for the specific test case to reduce the exploratory component slightly and reduce computational time. Tuning of parameters may be useful for application to different optimisation problems. The optimisation algorithm is directly coded, as described here, and solved in MATLAB R2018b.

#### 4.2.5 ACO with Decomposition into Sub-Problems (ACOsp)

Since the ACO algorithm creates an entirely new cable layout solution on each iteration, it is possible that improvements in one string, or area of the wind farm, go unnoticed due to a poor quality section of the solution in other strings. This becomes increasingly true

**Algorithm 4** Ant colony optimisation algorithm

---

```

Initialise stopping criteria, STOP = 0, n = 0, m = length(nodes)
while STOP == 0 do
  n = n+1
  while length( $T_u$ ) > 0 do
    Initialise ant at  $loc_{ant} = t_u$ , where  $dist_{t_u, SS} = \max(dist)$ ,  $t_u \in T_u$ 
    while not( $loc_{ant} \in N_v$ ) do
      Calculate  $P_{i,j}$  for  $j \in J$ 
      Roulette wheel selection to determine destination node,  $j \in J$ 
      Update ant location,  $x_{i,j} = 1$ ,  $N_v \cup \{loc_{ant}\}$ ,  $loc_{ant} = j$ 
    end while
  end while
  Evaporate pheromone,  $pher_{i,j} = pher_{i,j} * evap$ , for  $\{i, j\} \in A$ 
  Evaluate  $\bar{F}(x)$ 
  Calculate pheromone deposit,  $\Delta pher = 1 / \sum_{x \in A} x_{i,j}$ 
  Deposit pheromone,  $pher_{i,j} = pher_{i,j} + \Delta pher$ , for  $\{i, j\} \in A_{used}$ 
  Clear all routes,  $x_{i,j} = 0$  for  $x_{i,j} \in A$ 
  if  $n > m$  then
     $avg\bar{F}_n = \text{mean}(\bar{F}(x)_{n-m} : \bar{F}(x)_n)$ 
    if  $n > 100m$  and  $avg\bar{F}_{n-10m} \leq 1.01 * avg\bar{F}_{n-m}$  then
      STOP = 1
    end if
  end if
end while
Return best layout,  $\min(\bar{F})$ 

```

---

for larger problems where each string represents a smaller contribution to the total cost and therefore less influence on the pheromone to be deposited. The pheromone deposit is calculated from the total cost of the solution (objective value) and deposited equally on all of the paths used in an iteration. Therefore, the incentive (pheromone deposit) to use sections that have improved will be increased by the same amount as for those that have been made worse. To address this potential limitation in the ACO method, this section proposes an improved ACO algorithm, ACOSP, that considers small sub-problems of the larger optimisation problem, in a similar approach to simple decomposition techniques. In doing so, the algorithm is better able to notice improvements and apply more specific incentives (pheromones) for those routes to be used again.

To create smaller sections of the full optimisation problem, a subset of the optimisation variables must be selected for consideration as a sub-problem. Some decomposition

methods conduct a similar process by randomly selecting a subset of decision variables. However, with knowledge of an incumbent solution, this thesis proposes that the selection of variables can be done in a more intelligent and useful way. The arcs used to connect turbines in a string, are related in the fact that they currently connect turbines; in a reasonable solution these turbines will be relatively close to each other (not connecting from opposite ends of the wind farm). Selecting the decision variables associated with the selected arcs (those that are related to the incumbent string), creates a sub-problem to be solved. Selecting related variables is expected to provide more flexibility for the optimisation than selecting random variables, which could, for example, result in the selection of one arc from each string in the incumbent solution, creating a very disparate set of options for re-routing the cable connections. However, selecting the variables associated with a single string (for consideration as a sub-problem) could still somewhat limit the algorithm's ability to search the solution space for improved routes/solutions. As such, it is not only the variables associated with one incumbent string that are selected to form the sub-problem. Firstly, variables connecting the selected string to other strings (variables associated with routes that connect one of the turbines in the selected string to turbines not in the selected string) are included in the subset of variables forming the sub-problem to allow turbines to connect to another string if that yields an improved solution. Secondly, two strings are selected to form the sub-problem to allow the algorithm to explore improved routes/solutions. In a later phase of the algorithm, sub-problems are created using the variables from three strings. This again provides greater flexibility in the routes that can be explored by the algorithm, but does increase computational time. This second phase (considering three strings within a sub-problem) reduces the risk that the algorithm has got 'stuck' in a local optima, improving confidence in the solutions. Extending this to its limit, one could imagine increasing number of cables until all cables are considered in a sub-problem, and the algorithm is left with the full solution space to search. For this work, a limit of two strings is chosen in the first phase to generate quicker results to smaller sub-problems, with a later phase of three strings adding confidence that the algorithm is avoiding getting stuck in local optima.

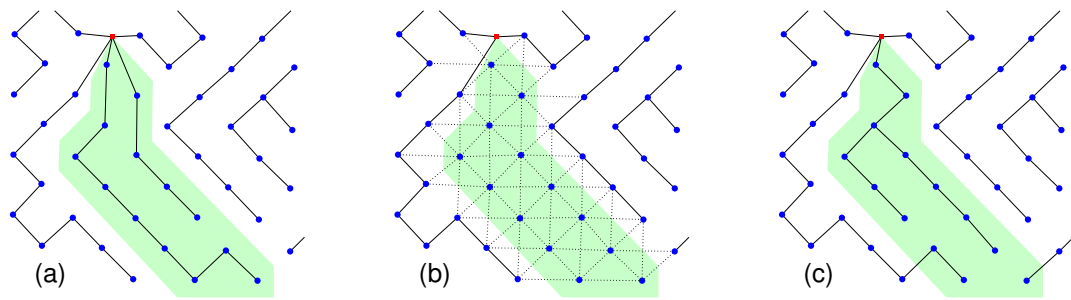


Figure 4.4: Example of a sub-problem in the improved ACOsp algorithm, with (a) two strings selected to be considered as a sub-problem of the cable layout, (b) two original strings removed and the possible paths for the ACO algorithm shown by dotted lines (omitting connections to substation for clarity), and (c) the new solution comprising a single string and several turbines joining existing neighboring strings.

Figure 4.4 shows how sub-problems are considered in this method. A section of a cable layout solution is shown, with turbine nodes (blue circles) and a substation node (red square) marked. Figure 4.4(a) contains an incumbent solution generated by a previous iteration, where two strings have been selected for consideration as a sub-problem, highlighted by the green region. The cable layout for turbines contained in the sub-problem is solved using Algorithm 4. The layout as a whole is considered in the objective function, Equation (4.14), however cables outside of the sub-problem region are fixed, and therefore the decision variables are limited to only those connections within the sub-problem region. Figure 4.4(b) shows the incumbent solution with the cables in the sub-problem removed and all the possible connections to be considered, shown by the dotted lines, where the probability of a given path being selected is described in Equation (4.18). Connections are also present between the unconnected turbines and the substation, but have been omitted from the figure for clarity. It is important to note that the subset of decision variables to be considered in the sub-problem contains routes from the turbines in the sub-problem to all of their available connections, including other turbines outwith the sub-problem. Therefore, connections to neighbouring strings are also allowed to ensure turbines do not get stuck in one sub-problem region and that coupling between sub-problems is properly captured. Randomly selecting strings to create different sub-problems also helps to facilitate this improved search process. Figure 4.4(c) shows the best result found by the algorithm after the sub-problem has been

optimised. It can be seen that several turbines have been connected to neighbouring strings outside of the sub-problem region and that one branched string connects the remaining turbines.

A new iteration begins by selecting random strings to form a sub-problem. The first string is selected randomly, then the remaining string(s) have a probability of being selected inversely proportional to their distance to the first string. This reduces the number of less-useful iterations where two strings at opposite ends of the wind farm are considered together as a sub-problem. String positions are defined as the average coordinate position of the turbines supported in that string,  $(x_s, y_s)$ . The probability that a string,  $s_2$ , will be selected, following the random selection of the first string,  $s_1$  is given by,

$$P_{s_2} = \frac{1/dist(s_1, s_2)}{\sum_{n \in S} (1/dist(s_1, s_n))} \quad (4.19)$$

The algorithm is repeated twice, with the first loop selecting string pairs to create a sub-problem, and the second loop selecting string triplets to create sub-problems. This method is proposed to avoid premature convergence and ensure greater exploration of the solutions space. Selecting larger three-string sub-problems enables the algorithm to explore more routing options, while the initial two-string sub-problems facilitates the algorithm in finding reasonable quality solutions more quickly.

The overall optimisation algorithm is summarised in Algorithm 5, where  $S_{rand}$  is the set of randomly selected string numbers used to create the sub-problem (and is a subset of the set of all strings  $S$ );  $T_{rand}$  is the set of turbine numbers in the sub-problem;  $s$  is a string number in the set  $S_{rand}$ ; and  $S_u$  is the set of binary values for all strings describing if a string has been ‘unimproved’ ( $S_u(s) = 1$ ) or improved/not-yet-considered ( $S_u(s) = 0$ ) by a sub-problem. Similarly to the ACO algorithm, this optimisation algorithm is coded and solved in MATLAB R2018b.

---

**Algorithm 5** Ant colony optimisation algorithm with decomposition strategy

---

```

Initialise stopping criteria,  $STOP = 0$ 
while  $length(T_u) > 0$  do
  Initialise ant at  $loc_{ant} = t_u$ , where  $dist_{t_u,SS} = max(dist)$ ,  $t_u \in T_u$ 
  while  $not(loc_{ant} \in N_v)$  do
    Calculate  $P_{x_{i,j}}$  for  $j \in J$ 
    Roulette wheel selection to determine destination node,  $j \in J$ 
    Update ant location,  $x_{i,j} = 1$ ,  $N_v \cup \{loc_{ant}\}$ ,  $loc_{ant} = j$ 
  end while
end while
for  $n = 2:3$  do
  while  $STOP = 0$  do
    Randomly select  $n$  strings,  $S_{rand}$ , (connecting turbines,  $T_{rand}$ )
    Clear cables in the selected strings,  $x_{i,j} = 0$  for  $i \in T_{rand}$ 
    Run Algorithm 4 (considering all  $T$ , but clearing only  $x_{i,j}$  for  $i \in T_{rand}$ )
    Record best layout to date,  $min(\bar{F})$ 
    for  $S \in S_{rand}$  do
      if String S is unimproved,  $cost(S) > min(cost(S))$  then
         $S_u(S) = 1$ 
      end if
    end for
    if  $\sum S_u = length(S_u)$  then
       $STOP = 1$ 
    end if
  end while
   $S_u = 0$ 
   $STOP = 0$ 
end for
Return best layout,  $min(\bar{F})$ 

```

---

### 4.3 Case Studies

This section details the case studies used for the comparison of the three optimisation algorithms described in Section 4.2. Details of the large, hypothetical offshore wind farm site is provided and the six cases studies based on the site are defined. Cost components used in the three optimisation approaches are presented including cable unit costs and additional key parameters necessary for the three algorithms.

### 4.3.1 Hypothetical Offshore Wind Farm

The offshore wind farm site under consideration is a large hypothetical site, proposed in Section 3.5.1 where full details of the wind farm boundary, obstacles and turbines can be found. Figure 4.5 shows the hypothetical site, including the wind farm boundary, obstacles to be avoided by cables, and turbine and substation positions. The site contains 122 turbines to be connected through the array cable network. Full details of the turbine coordinates can be found in the Appendix, Table A.10.

The proposed site contains several aspects designed to be challenging for the cable layout optimisation algorithms. Firstly, the wind farm boundary is an irregular shape including concave edges for cables to navigate around, which incurs a penalty cost if crossed by cables. Secondly, obstacles are included in the site (Figure 4.5 red shaded regions), which also incur a penalty cost if cables cross any obstacle boundary. Steiner nodes are included at some of the convex vertices of the obstacles to allow cables to navigate around them (Figure 4.5 green circles). Thirdly, two substations are employed (Figure 4.5 red squares) due to the large number of turbines which adds complexity to the cable network calculation. Finally, one substation is placed very close to the eastmost obstacle, resulting in a difficult connection to turbines on the opposite side of the obstacle. The Easting-Northing coordinates of the two substations are (2000m, 5000m) and (7000m, 6000m).

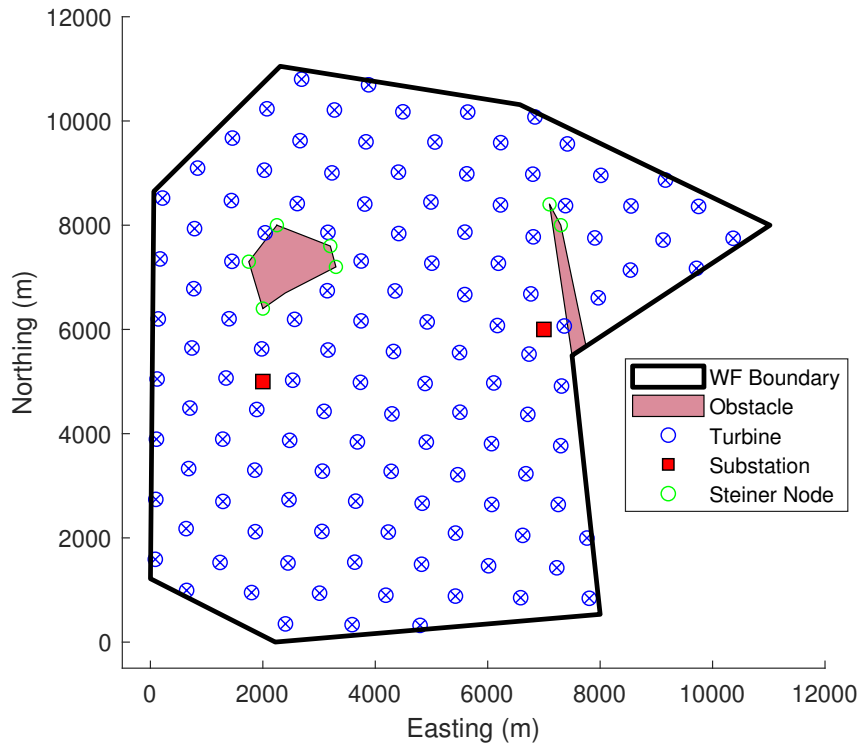


Figure 4.5: The hypothetical GW-scale offshore wind farm test case.

### 4.3.2 Definition of the Six Case Studies

Six test cases are created from the hypothetical site, containing 10, 15, 25, 40, 61, and 122 turbines respectively. Figure 4.6 shows the turbine positions used for these six test cases. Including case studies on various numbers of turbines allows for the assessment of the algorithms' performance and how this scales with problem complexity. Although the cases with fewer turbines may appear simple, and possibly unrealistic, beginning with those in the north-east section requires the algorithm to consider the wind farm boundary, obstacles, and Steiner nodes for all problem cases. Using randomly or evenly distributed turbine positions in the site may not necessarily involve all the aspects of the site, such as the wind farm boundary and obstacles, and result in an unfair comparison for the different scales of test case. Both substations are kept for all cases.

## Chapter 4. Cable Layout Optimisation

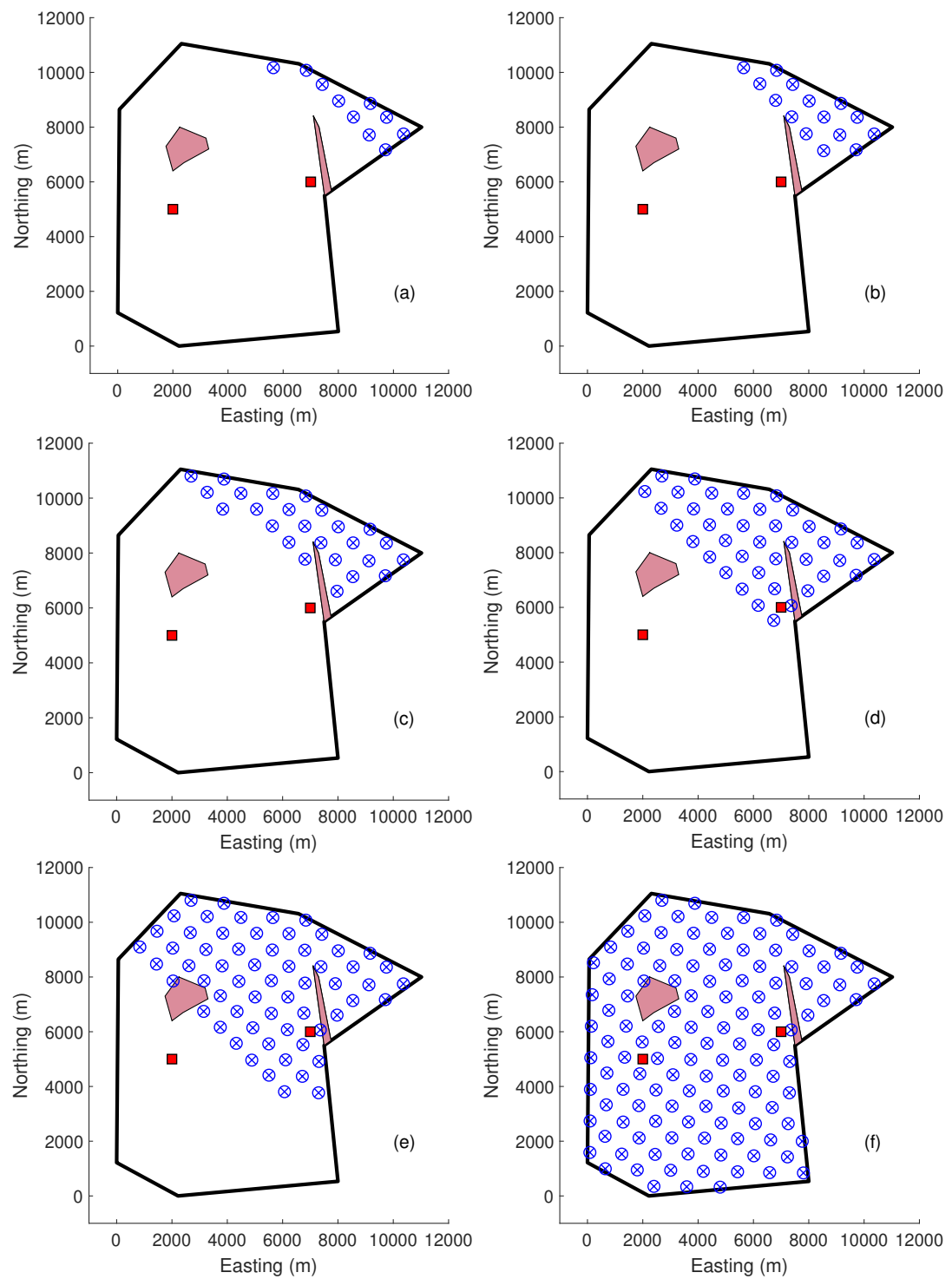


Figure 4.6: Test cases of the hypothetical offshore wind farm site, with (a) 10 turbines, (b) 15 turbines, (c) 25 turbines, (d) 40 turbines, (e) 61 turbines, (f) 122 turbines. Steiner nodes omitted for clarity.

### 4.3.3 Cost Components & Parameters

Table 4.3 contains the key parameters of the three cables that are available for the optimisation algorithm to use, with costs calculated in line with the work by Dicorato et al. [79] and representative resistance values. Cable power capacity is used to limit the number of turbines supported by a cable and is a restating of the current carrying capacity. The capacity, unit cost, and resistance per unit length of each cable are representative values used for this hypothetical wind farm study and are not taken from specific real cables.

Table 4.3: Key cable parameters.

Cable number	Cable power capacity (MW)	Unit cost (£/m)	Resistance ( $\Omega$ /m)
1	60	1400	0.00120
2	90	1750	0.00056
3	100	1870	0.00044

Table 4.4 contains further parameters for the optimisation algorithm. Similarly to cable cost information in Table 4.3, the values described in Table 4.4 are also representative values used for this study. The crossing penalty represents an increase in cost due to cables crossing other cables and is discussed further in the following section. A jointing cost is included for multiple connections into turbines. While one connection into turbines incurs zero additional cost, every additional connection increases the network cost by £13.8k [85]. Although this cost function is linear, it can be easily expanded to include a more realistic non-linear cost function in future studies. The price of energy, discount rate, and project lifetime are used to calculate the electrical losses in the pre-computation phase, described in Section 4.2.2. Additionally, in the pre-processing phase, the set of arcs is reduced by considering only connections between the nearest  $N$  neighbouring turbines. For this study the connections between the closest eight neighbours were kept in the set of possible connections. In addition, all connections directly to substations were also retained in the set of arcs.

Table 4.4: Key parameters and values used in the comparison of the cable layout optimisation algorithms.

Parameter	Value
Array voltage	66kV
Crossing penalty	£1m
Jointing cost (turbines)	£13.8k
Price of energy	£50/MWh
Discount rate	10%
Project lifetime	25 years
Nearest N nodes of allowable connections	8

#### 4.3.4 Berwick Bank Offshore Wind Farm

Following the SSE design comparison study of the turbine layout optimisation in Chapter 3, it was planned that a similar comparison could be conducted for the cable routing optimisation. Unfortunately, due to SSE's work commitments at the time and the very manual nature of their cable routing design process, it was not possible for SSE to provide a cable layout for comparison. As such, this section describes a case study of the Berwick Bank site, considering different cable conductor materials. Three cases are considered using different conductor materials; aluminium, copper, and both aluminium and copper together.

Figure 4.7 shows the Berwick Bank site with the turbine and substation positions used in the cable routing study. The site contains 128 turbines and a single substation with Easting-Northing coordinates of (593119m, 6238992m). Full details of the turbine coordinates can be found in the Appendix, Table A.11.

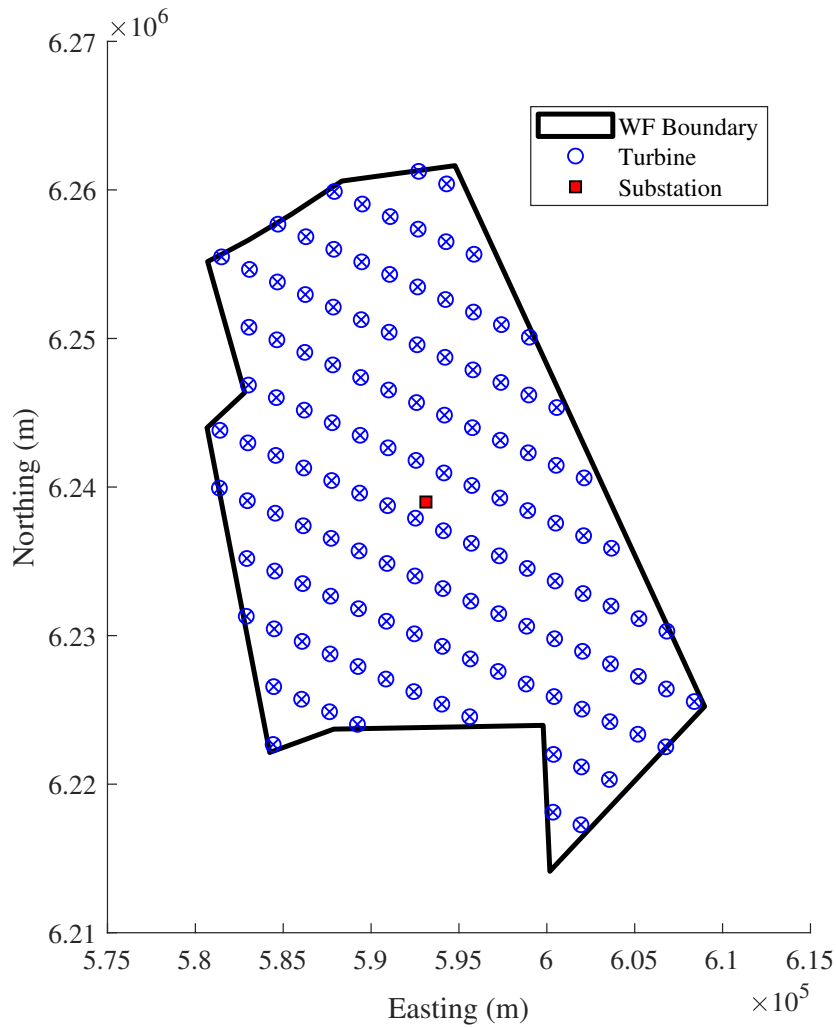


Figure 4.7: The Berwick Bank site with turbine and substation positions.

Representative data was provided by SSE for the case study, including cable parameters for aluminium and copper conductors. Table 4.5 shows the conductor material, size, cost, and electrical properties of the set of available cables. For the first case, the aluminium cables were made available to the model. For the second case, only the copper cables were available for the model to use. In the final case, all cables in Table 4.5 were available to use.

Table 4.6 contains the remaining necessary parameters for the optimisation algorithm. These parameters are similar to the previous case study parameters presented in

Table 4.5: Representative key cable parameters provided by SSE [10].

Conductor material	Cross-sectional area (mm <sup>2</sup> )	Unit cost (3 phase) (£/m)	Resistance (1 phase @ 90°C) ( $\Omega$ /km)	Capacity (1 phase) (A)
Al	100	17.7	0.392	266.8
Al	125	18.6	0.313	299.5
Al	150	19.5	0.261	329.2
Al	175	20.4	0.224	356.6
Al	200	21.3	0.196	382.1
Al	500	32.1	0.078	614.6
Al	1000	50.2	0.039	880.5
Al	1500	68.2	0.026	1086.5
Cu	100	30.4	0.226	340.6
Cu	125	34.8	0.181	381.4
Cu	150	39.2	0.151	418.2
Cu	175	43.7	0.129	452.2
Cu	200	48.1	0.113	483.8
Cu	500	101.3	0.045	769.4
Cu	1000	190.0	0.023	1092.9
Cu	1500	278.7	0.015	1341.9

Table 4.4. Following initial consultation with SSE, many of the values were updated to be more representative for modern offshore wind farm developments. Notably missing from this case study is the cost of additional joints into turbines and substations. In-line with the originally proposed cable layout comparison with SSE, this case study was to focus only on solutions of radial strings with no branching connections.

Table 4.6: Key parameters and values used in the Berwick Bank cable layout case study (representative values generated between the author and SSE [10]).

Parameter	Value
Array voltage	66kV
Crossing penalty	£100k
Price of energy	£40/MWh
Discount rate	7%
Project lifetime	30 years
Nearest N nodes of allowable connections	8

## 4.4 Results & Discussion

This section presents the results of the case studies described in Section 4.3. The first part presents the results of the the three optimisation algorithms applied to the hypothetical offshore wind farm with comparison of the solutions and computational time. Consideration of crossing cables is presented for one site with a crossing cable in the optimal solution before the penalty cost and/or constraint is applied. The second part considers the Berwick Bank site comparing the solutions of the two different cable conductor materials, aluminium and copper.

### 4.4.1 Hypothetical Offshore Wind Farm

#### Comparison of the Three Algorithms

The three optimisation algorithms were run on a standard desktop computer (3.4GHz Intel Core i7-6700, 16GB RAM) and ten simulations were conducted for each of the six case studies with different numbers of turbines. Table 4.7 contains the averaged results of each algorithm for each of the six case studies. Objective values are presented with the optimality ratio (which is a ratio between the objective value of a solution and the optimal objective value) and the average computational time is shown for each case. The optimal solution for comparison is obtained through the MILP algorithm with the final ‘branch & bound’ section of the algorithm running until optimality is reached. This is not reached for the case of 122 turbines but the obtained value at the end of the calculation is assumed to be optimal, discussed further later. A complete set of results can be found in the Appendix, Table A.12 and Table A.13.

It can be seen in Table 4.7 that the MILP algorithm finds the mathematically optimal solution (optimality ratio equal to 1) for almost all cases. However the computational time increases significantly as the number of turbines (and therefore number of possible cable connections) increases. For the largest case study, containing 122 turbines, the MILP algorithm is unable to prove the optimality of the solution due to the large memory requirements of the branch-and-bound solver. Large memory is required because, during the branch-and-bound solver, all ‘relaxed’ solutions (those with some

integer variables not yet constrained to integer values) must be stored. Only when a solution explicitly violates one of the active constraints, as they are incrementally activated, can it be discarded. The total memory available to hold data on the standard desktop computer was 37101MB. This was sufficient to record all intermediate solutions for the case of 61 turbines, but not for the case of 122 turbines. The relative gap for all ten simulations of this largest case was 2.32%. It is therefore assumed that the MILP solution had indeed found the optimal solution for this case.

Table 4.7: Average results of the three optimisation methods for the six hypothetical test cases. (Results in italics indicate an unfinished result).

No. turbines	Objective value (£) and Optimality ratio			Computational time (s)		
	MILP	ACO	ACOSP	MILP	ACO	ACOSP
10	22,064,833 (1.000)	22,667,188 (1.027)	22,068,446 (1.000)	3	5	53
15	30,945,049 (1.000)	31,075,301 (1.004)	30,945,049 (1.000)	9	8	46
25	50,235,935 (1.000)	51,473,967 (1.025)	50,750,255 (1.010)	31	18	133
40	68,683,109 (1.000)	69,693,934 (1.015)	69,678,545 (1.014)	204	51	489
61	103,255,681 (1.000)	110,766,917 (1.073)	104,651,892 (1.014)	951	164	1517
122	<i>197,401,005</i> (1.000)	212,339,986 (1.076)	199,301,590 (1.010)	<i>13717</i>	833	9991

The results from the classical ACO algorithm are between 0.4% and 7.6% more expensive than the optimal solution as assessed by the objective function, averaging 3.7% greater cost than the optimal solutions across the six case studies. The proposed ACOSP solutions are between 0.0% and 1.4% more expensive than the optimal solutions and 0.8% greater cost than the optimal solutions on average across the six case studies. There is some indication that as the problem complexity increases, the average optimality ratios of the ACO and ACOSP solutions increase. This can be seen most significantly in the classical ACO solutions, suggesting that the proposed ACOSP method is better at handling larger problems than the classical ACO method.

The computational time for the ACO and ACOSP methods increases less quickly

than the MILP algorithm as the number of turbines increases. For all six cases, except for the smallest (ten turbines), the classical ACO method is the quickest to converge to a solution. However, since all the computational times are reasonably low (of the order of a few hours), the ACOSp algorithm is considered to be an appropriate method for solving large scale problems using standard desktop computing. Clearly for smaller problems, the MILP algorithm performs the best - yielding optimal solutions in reasonable computational time. For design phase studies, computational time is not the most important factor. However, while these solutions may be run once to design the cable layout for a given site, developers may often run the studies multiple times to investigate the impact of variables such as discount rate or possibly substation location on the final layout solution. It is therefore somewhat important to have a reasonable computational time as decided by the developer/engineer using the tool [10].

Figure 4.8 shows the cable routing solutions of the three methods, for the case containing all 122 turbines. Some similarities can be seen between the three layouts, however they are largely different. This is due to the regular spacing of the turbines resulting in very different layouts with near-optimal total cost, and algorithms reaching a local-minimum before the stopping criteria are met. Information on the cable types used in the layout are omitted from Figure 4.8 for clarity. All three algorithms shared a common pre-optimisation computing phase and cable selection process. As such, cable ratings for sections supporting the same number of turbines are the same across solutions.

Table 4.7 shows that the major limitation of the MILP method is the large increase in computational time and memory with increasing number of turbines. Both ACO approaches offer a quicker alternative to this MILP approach. However, the average optimality of all ACO solutions is 1.037, meaning solutions are 3.7% more expensive than the optimal solutions on average. This compromise for quicker computational time is still present in the ACOSp algorithm, however it has an average optimality across all solutions of 1.008, which translates to an increase in cost of 0.8% relative to the optimal solutions. Therefore, the simulation results show the proposed ACOSp algorithm is a promising tool for solving large cable layout optimisation problems in a reasonable time

period.

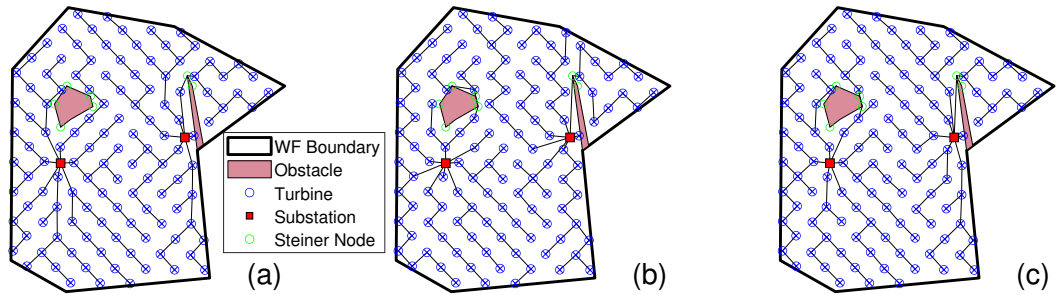


Figure 4.8: Optimised cable layouts from (a) the MILP algorithm, (b) the classical ACO algorithm, and (c) the ACO algorithm with sub-problems (ACOsp). All MILP layouts were identical, while some variation in layouts was present in the set of ACO and ACOsp layout solutions.

Initially, only the arcs crossing the wind farm boundary and/or an obstacle are penalised as described previously in the pre-processing phase. Cables crossing other cables are handled differently as they may or may not be present in a given solution. Figure 4.9 shows the optimal cable routing for the case of 25 turbines when cable crossings are not considered, with Figure 4.9(a) showing the whole solution and Figure 4.9(b) showing a zoomed-in section to identify the crossing connections. Cables crossing other cables are to be avoided as the relative motion of subsea cables against one another can lead to increased wear-and-tear and/or damage to the cable armouring and result in an increased likelihood of cable failure [10, 75]. In order to avoid such crossing sections, constraints must be applied to the solution space containing the set of all possible solutions.

### Considering Crossing Cables

Since there are many possible arcs that can be used in the cable routing solution, there are a large number of possible crossing arc pairs to be avoided (of the order  $A^2$ ). This means that applying constraints for each combination in the pre-processing phase is impractical. As such, constraints are applied on-the-fly and are considered differently for the MILP algorithm and the ACO-based algorithms.

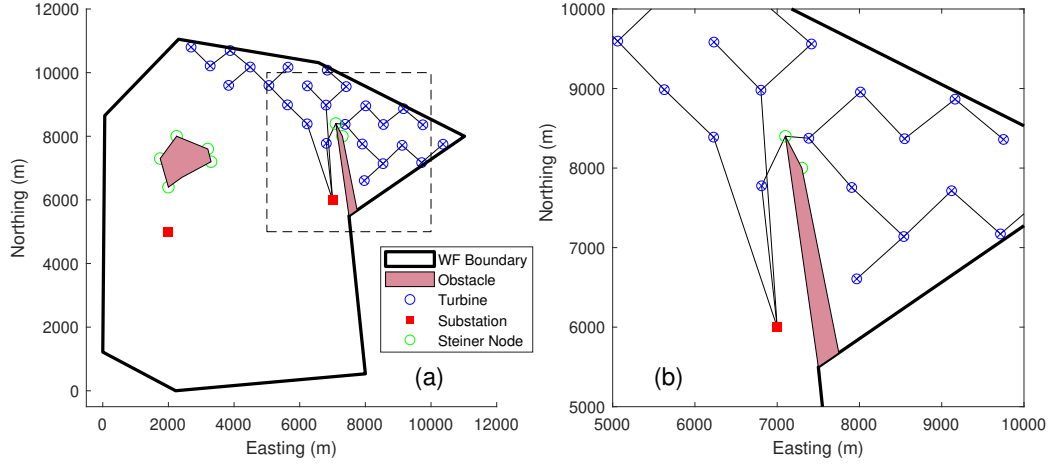


Figure 4.9: Optimal cable layout for 25 turbines (a) full cable layout, and (b) a zoomed section of the layout to show the crossing cables.

For the MILP algorithm, a solution is generated as described in Section 4.2. The solution is then checked for crossing cables by solving simultaneous equations of the two straight-line connections to determine if the intercept lies within the region covered by the two cables. This is only conducted for the cables that are used/built in the solution and not for all possible arcs. If a pair of crossing cables is present in the solution, a constraint equation is created limiting the solution to contain up to one of the pair of cables. An additional constraint equation is included for every pair of crossing cables present in the solution. This is a standard approach used in the academic literature to reduce the number of required constraint equations, with the formulation presented here based upon that by Fischetti et al. [75]. Equation (4.20) describes the constraint equation used in the MILP algorithm.

$$y_{i,j} + y_{j,i} + y_{k,l} + y_{l,k} \leq 1, \quad (\{i, j\}, \{k, l\}) \in B \quad (4.20)$$

where  $y_{i,j}$  and  $y_{j,i}$  are the two arcs between nodes  $i$  and  $j$ ,  $y_{k,l}$  and  $y_{l,k}$  are the two arcs between nodes  $k$  and  $l$ , and  $B$  is the set of crossing arc pairs. The sum of the number of connections used for a given pair of crossing arcs, considered in both directions, must be less than or equal to one, for all arc pairs within the set of crossing arc pairs. Once all required constraint equations are included, the MILP algorithm is re-run to generate

a solution that obeys the new constraint equation(s).

The two ACO-based algorithms also describe a set of crossing arcs,  $B$ , which is initialised as an all-zero matrix. There is a complementary matrix of the same size,  $B_{idx}$ , that describes whether pairs of arcs have been assessed to determine if they cross, all values of which are also initialised to be zero. For every iteration of both algorithms, the quality of the solution is assessed as outlined in Section 4.2. During this assessment, all arcs are checked for crossing cables and marked in the index matrix,  $B_{idx}$ , to record that they have been checked (cell value = 1). If the pair of cables that are being checked do cross, then the penalty cost is recorded in the corresponding cell in the matrix of crossing arcs,  $B$ , and the penalty cost is added to the cost of the solution. Since the objective of this penalty cost is to avoid crossing cable connections, it is given an arbitrary but relatively high value of £1M, Table 4.4. This is repeated for all cable pairs in the current solution. For future iterations, if a cable pair have previously been checked, any penalty cost can be found in the matrix  $B$ . This avoids repeating the calculations required to check if pairs of cables cross, avoiding unnecessary computational expense. The objective values and computational time of the solutions from the three algorithms - with and without the cable crossing constraint/penalty - is shown in Table 4.8. A complete set of results is provided in the Appendix, Table A.14.

Table 4.8: Average results of the three optimisation methods for the hypothetical test case of 25 turbines, (a) without the cable crossing constraint, (b) with the cable crossing constraint.

No. turbines	Objective value (£) (Optimality ratio)			Comp. time (s)		
	MILP	ACO	ACOSP	MILP	ACO	ACOSP
25 (a)	50,235,935 (1.000)	51,473,967 (1.025)	50,750,255 (1.010)	31	18	133
25 (b)	50,268,994 (1.000)	51,307,620 (1.021)	50,826,954 (1.011)	78	31	243

Including the crossing cables constraint increased the computational time of the MILP algorithm by a factor of more than 2. This increase shows that, upon including the constraint to avoid the crossing pair of cables, the optimal solution in the newly constrained case did not contain any further crossing cables. This is a site specific result

and it is possible for other cases that further crossing cables would be present and require additional constraint equations. The optimal solution of the constrained case increased costs by £33,059 compared to that with no cable crossing constraint. Both ACO-based algorithms demonstrated an increase in computational time, with the crossing constraint considered. The optimality ratios of both ACO-based methods also remain relatively unchanged when the crossing constraint is applied, providing confidence in the handling of the crossing cables and the effectiveness of the penalty function. The ACOsp algorithm remained the lowest cost solution of the two ACO-based approaches, being 1.1% higher cost than the cost of the optimal cable routing.

#### 4.4.2 Berwick Bank Offshore Wind Farm

Three cases were run for the Berwick Bank offshore wind farm with a set of aluminium cables, copper cables, and both aluminium and copper cables. Both types of cable had the same set of conductor cross-sectional areas available but with different electrical properties, capacities, and costs, Table 4.5. Figure 4.10 shows the optimised cable layout solutions using only aluminium cables (left) and only copper cables (right). The aluminium solution uses the full set of cable sizes in the layout, with the exception of the 175mm<sup>2</sup> cable. The copper layout uses only four sizes of cables in its solution (100mm<sup>2</sup>, 125mm<sup>2</sup>, 200mm<sup>2</sup>, and 500mm<sup>2</sup>), with most connections using the smallest two of these. This is due, in part, to the higher rating of copper cables relative to an equivalently sized aluminium cable; the largest copper cable (although unused in this solution) can support up to 16 turbines, whereas the largest aluminium cable can support up to 14.

In the copper cable solution, Figure 4.10 (right), there is a pair of crossing cables which incurs an additional cost of £100k, as described in Section 4.3.4. Since the method is a heuristic algorithm, there remains some uncertainty in the optimality of these solutions (since heuristics cannot guarantee optimality) and therefore some uncertainty in whether the crossing section would be present in the optimal solution or not. The total costs of the aluminium and copper cable layouts were £14,884,863 and £23,417,652 respectively, Table 4.9, which includes capital costs and electrical losses.

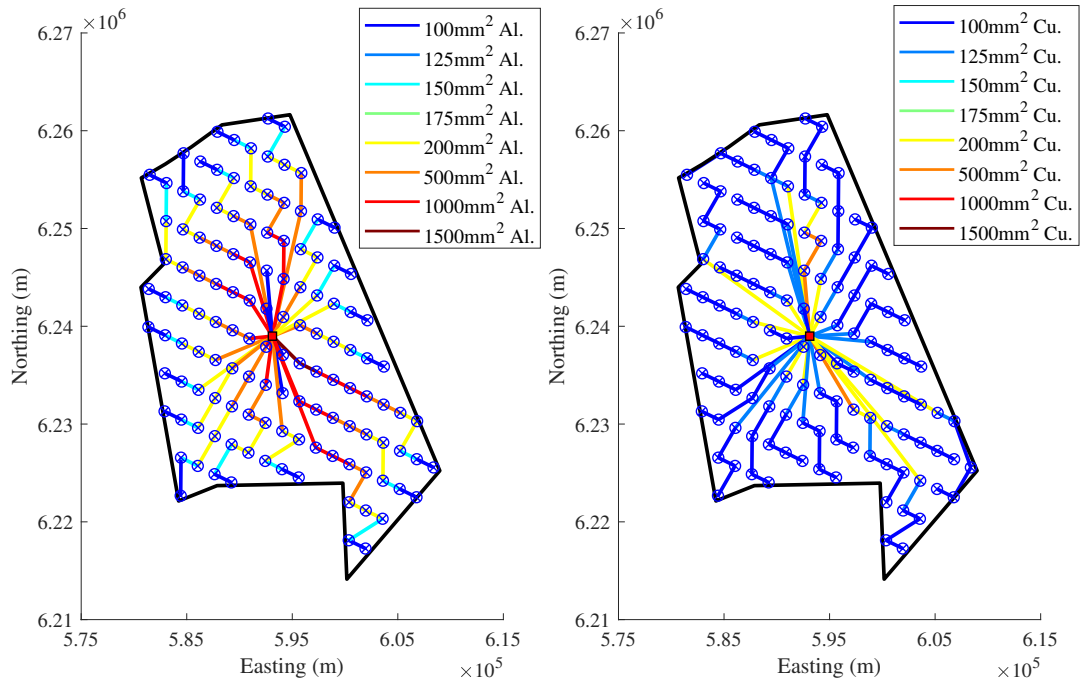


Figure 4.10: Optimised cable routing for Berwick Bank using (left) aluminium conductor cables and (right) copper conductor cables.

The copper cable layout has many more strings, 31 in total, relative to the aluminium layout containing 23. This equates to an average number of turbines per string of 5.57 and 4.13 for the aluminium and copper cables respectively (affecting electrical losses and the total cost). Additionally, the longest strings for each can be seen to support 11 and 8 turbines, with the copper case containing the lower. This is likely due to the increased capacity of the copper cables and is of course linked to the cable unit price and electrical performance and losses.

Table 4.9: Results of the three cases using different cable conductor materials for the Berwick Bank site.

Conductor material	Total cost (£)	No. strings	Avg. turbines per string	No. turbine in longest string
Aluminium	14,884,863	23	5.57	11
Copper	23,417,652	31	4.13	8
Aluminium & Copper	14,816,440	20	6.40	11

For the case with both aluminium and copper cables available to use, the resulting

solution can be seen in Figure 4.11, with the left plot showing cable size and the right plot showing conductor material. All sections in this layout use aluminium conductors as these are the cheapest cables by total cost (unit cost and electrical losses) for every electrical loading scenario up to 14 turbines, the maximum for the aluminium set. If strings of 15 or 16 turbines were to be used, some copper cable sections would be necessary, although this was not the case for the optimised layout. Since this layout used exclusively aluminium cables, there are similarities to the aluminium-only case, however the heuristic nature of the algorithm results in some differences in layout. The total cost of the new layout was £14,816,440, approximately 0.46% lower than the aluminium-only case, showing a closer-to-optimal solution was found. This may be caused by the grid-based turbine layout having many cables of similar length and cost, resulting in many different cable layout solutions being close to optimal. This makes the case study a challenging optimisation problem for the optimisation algorithms being tested. A similar number of strings is used, 20 down from 23 in the aluminium-only case, and the longest string was of the same length containing 11 turbines. It is important to note, that while the cable routing shows some small differences between the two layouts using aluminium cables, the cable selection algorithm simply chooses the best cable for the loading scenario, specific to the section being considered. As such, it is clear that the aluminium cable set is by far the better conductor material to use for this site when cable unit cost and electrical losses are taken into account, producing layouts that reduce the total cost by approximately 37% relative to the copper cable layout. Other studies in the literature have conducted similar comparisons between copper and aluminium conductors, discussing the cost benefit of aluminium versus the improved performance of copper [151]. Ultimately, this trade-off between price and performance is site specific and subject to parameters such as raw material cost and discount rate, which can vary across projects, time, and geographies.

### 4.5 Summary

With modern wind farms increasing in size (in terms of both wind farm rated power and number of turbines), the complexity of the cable routing optimisation problem is

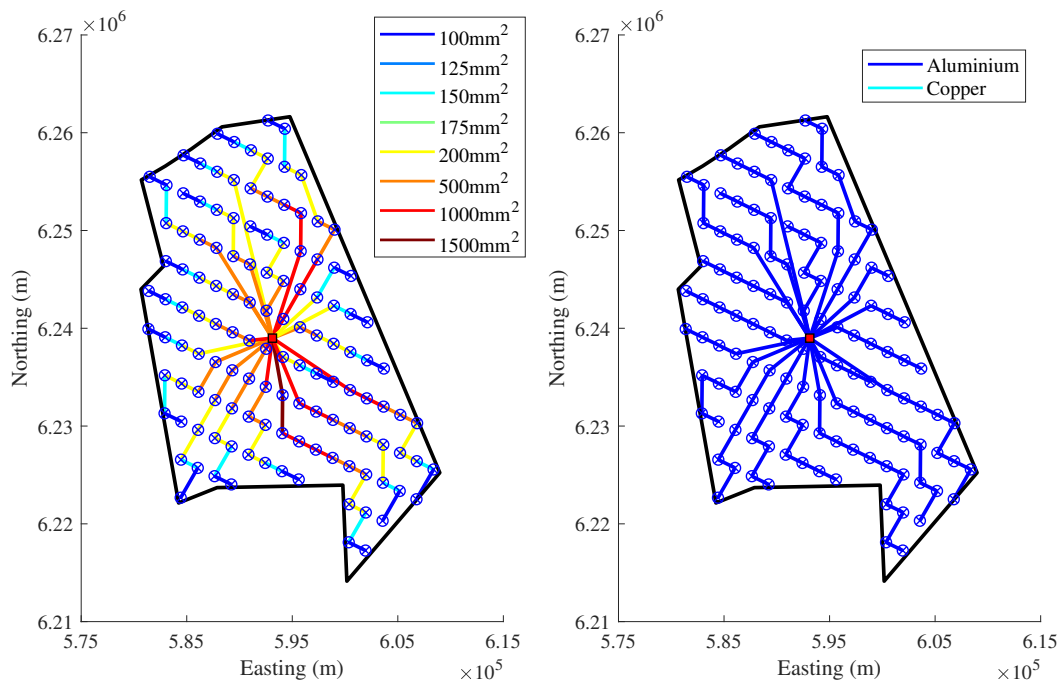


Figure 4.11: Optimised cable routing for Berwick Bank using both aluminium and copper conductor cables showing (left) conductor size and (right) conductor material.

also increasing. A new heuristic optimisation algorithm, ACOsp, is proposed based on combined techniques in ACO and decomposition of a large network, to tackle the large-scale cable layout optimisation design problem for offshore wind farms. This proposed algorithm is compared with the MILP algorithm and a standard ACO algorithm. Through the comparison of the three algorithms, the MILP method was shown to reach the optimal solution in most case study scenarios. However, as the number of turbines and possible arc connections increases, the computational time and memory requirements of the MILP algorithm increase dramatically until it is no longer possible to solve completely on a standard desktop PC using non-specialist (MATLAB) software. In the cases presented for the largest case study, 122 turbines, the MILP algorithm ran for an average of 13,717 seconds (approximately 3.8 hours), before using all of the 37,101 MB of computational memory and causing the optimisation to stop prematurely before its search of the solution space was complete. The classical ACO algorithm has shown to be a useful alternative, not suffering from the same memory and time constraints as the MILP algorithm. The classical ACO algorithm generated solutions between 0.4%

and 7.6% more expensive than the optimal solution and was the quickest of the three algorithms in all cases except for the smallest one (ten turbines). The proposed ACOSp algorithm demonstrated increased performance in the quality of solutions, with solutions between 0.0% and 1.4% more expensive than the MILP optimal solution. While the improved solutions from the ACOSp algorithm did take a longer time to run, the algorithm completed all case studies within a few hours and so the computational time appears to be a reasonable trade-off for the marked increase in the quality of the solutions. In this regard, the ACOSp algorithm should be a good alternative for very large wind farms when only standard computing facilities are available.

The case study of the Berwick Bank offshore wind farm using different conductor materials revealed that aluminium cables greatly outperformed the copper cables, with a layout that was approximately 37% more cost effective. The heuristic approach means there is some uncertainty remaining in the level of cost reduction from copper to aluminium cables (since optimal solutions are not guaranteed), so additional simulations would help to improve confidence in this number. The electrical losses, string lengths, and associated costs are a function of the site boundary shape, the local wind conditions, and the turbine performance curves and so considering different conductor materials may still be necessary for other sites. However, as was shown in the comparison of optimisation algorithms, the variability in the solutions of the ACOSp algorithm was reasonably small, giving confidence to the cost savings of the aluminium cable set.

The approach to cable layout optimisation outlined in this chapter contained several assumptions and simplifications that may be of interest to future studies in this area of research. Firstly, arcs were limited to straight-line connections, which for offshore wind farms is a reasonable simplification. However, including a path-finding algorithm to define arc routes before the optimisation (during pre-processing) would allow for more detailed bathymetry and obstacles to be included. This may also help to avoid crossing cables as was seen in the original solution of the case with 25 turbines. Secondly, crossing cables were not accepted in the solutions through the use of constraints or penalty functions. Applying a penalty function that is indicative of the actual costs associated with crossing cables would allow the algorithms to determine if the increase

in costs due to added protection at the crossing is offset by the reduction in length and capital cost. Thirdly, all turbines were assumed to generate the same electrical power regardless of their position in the array. Including a simple aerodynamic wind farm model would allow a more accurate representation of the power carried by the cables and therefore more accurate electrical losses to be determined. This would, however, increase the computational complexity of the algorithm, as the power flow and electrical losses would need to be re-calculated for each layout/iteration rather than in a pre-computation phase described earlier in this chapter. Finally, the impact of different sub-problem construction and the effect on the optimality of solutions would be a valuable future study. In this study, the decomposition was informed by the problem formulation (i.e. selecting a subset of decision variables by selecting strings of turbines to form a sub-problem). However, other methods of selecting decision variables could affect solutions, such as random selection of a given percentage of decision variables.

The key novelty introduced by the work in this chapter is the newly proposed ACOSP algorithm, including a decomposition technique informed by the incumbent solution to facilitate the algorithm in reaching optimal solutions quickly. Additionally, a hypothetical large-scale offshore wind farm site is proposed which can act as a benchmark case for future cable layout optimisation studies.

The cost associated with the array cable layouts of offshore wind farms is clearly not trivial, especially when the net present value of the lifetime electrical losses are considered. However, the layout is heavily constrained by the position of the turbines and substations that are fixed by the time detailed layout design is considered for array cables. It is possible that, by considering the cable routing earlier on in the design process, it may affect the positions of turbine and substations (and therefore also the energy capture) resulting in improved overall wind farm designs. This investigation is the focus of the following chapter.

In conclusion, the second objective of this thesis is met by this chapter; an array cable layout optimisation is developed, capable of considering large-scale problems of the same size as the turbine layout optimisation in a computationally efficient manner. The proposed ACOSP method provides improved solutions, relative to the ACO solutions,

## Chapter 4. Cable Layout Optimisation

and reduces computational complexity, relative to the MILP approach. In doing so, it is demonstrated that ACOSP is an appropriate method for the optimisation of large-scale offshore wind farm sites.

## Chapter 5

# Integrated Turbine & Cable Layout Optimisation

This chapter integrates the turbine placement optimisation design from Chapter 3 and the cable layout optimisation from Chapter 4, such that better overall solutions may be found to the wind farm layout optimisation problem. Detail of the integration of the two models is provided and a comparison is carried out between the integrated (concurrently optimised) approach and a sequential optimisation (where turbine positions are optimised followed by a separate optimisation of the cable routing). The objective of this chapter is to isolate the impact of using a sequential versus integrated approach, addressing Research Question 1 as shown in Figure 1.3. The case study of the sequential versus integrated optimisation uses the large hypothetical site proposed in Section 3.5.1 and the wind conditions provided by SSE, as outlined in Chapter 3.

### 5.1 Integration of Turbine & Cable Layout Optimisation

The turbine layout optimisation algorithm proposed in Chapter 3 can be considered as containing three key phases; (1) solution seeding, (2) particle swarm optimisation (PSO) to optimise the grid-based positions of turbines, and (3) a micro-siting function to fine-tune individual placement of turbines from grid positions. The cable routing optimisation algorithm proposed in Chapter 4 uses an ant-colony optimisation (ACO)

algorithm and recursive decomposition to solve a set of smaller sub-problems. The formulation of the three-part PSO algorithm allows for easy integration of the relevant cable layout optimisation code.

Since the cable routing optimisation requires turbine positions (and the turbine layout optimisation does not require a cable routing), it follows that the cable routing optimisation is integrated into iterations of the turbine layout optimisation as a subordinate nested algorithm. From here it may be called as a function and provide cost and route information about cables in order to influence the turbine positions. This approach is similar to that taken by Perez-Rua et al. [109], where a gradient-free turbine layout optimisation is used with a nested heuristic cable layout optimisation. This heuristic cable layout optimisation is called within each iteration of the turbine layout optimisation, providing a fast cost estimation of the array cable network. In later iterations, this heuristic is replaced with a classical MILP method to provide more accurate cost information to the turbine layout optimisation. The following subsections detail how the cable routing optimisation is integrated into the turbine layout optimisation framework.

### 5.1.1 Integration into Solution Seeding for the PSO

For the optimisation of the grid of turbine positions, eight variables are optimised that fully describe the grid. The PSO algorithm initialises many particles - or solutions - randomly in the solution space, with at least one good-quality solution (in terms of turbine layout) guaranteed by the solution seeding algorithm, proposed in Chapter 3. These initial solutions do not consider the approximated cable routing cost. This is to ensure that the PSO population contains a good quality solution, in terms of turbine layout, which is the most significant contributor to the overall objective value. As seen from the previous chapters in the studies of the hypothetical offshore wind farm site, the objective value of the turbine layout section is in the order of £1*b*, Table 3.3, while the objective value of the cable layout section is in the order of £100*m*, Table 4.7.

### 5.1.2 Integration into the PSO Algorithm Phase

Within the iterations of the PSO algorithm, particles are moved through the solution space and the quality of the solutions they find influences the next set of movements. It is here that the first influence of cable layout may be noticed. However, as the cost of cables will only affect the eight variables describing the whole grid, it is not necessary to have knowledge of the optimal cable routing exactly. An approximation of the cable cost can be used that will incentivise a denser grid, to reduce cable lengths and costs, and effect the variables such as reducing  $s_1$  and  $s_2$  that describe row and column spacing respectively.

It is proposed that the total cable network cost is proportional to the number of turbines, the spacing of the rows and columns of turbines, and the cost of cables. Investigating the true cable network costs (using a full evaluation of the ACOsp algorithm) for a range of different numbers of turbines and/or row and column spacing, it is possible to determine an approximate relationship between these parameters and the cable network cost. Figure 5.1.

Equation (5.1) shows the approximated cable network cost, used to generate the linear fit in Figure 5.1. It should be noted that this is a case specific approximation, that will be different if a different set of cables are used.

$$C_{cable\ approx} = 1.2 n_t \left( \frac{s_1 + s_2}{2} \right) \left( \frac{1}{n_{cab}} \sum_{i=1}^{n_{cab}} C_{cab^i} \right) \quad (5.1)$$

where  $C_{cable\ approx}$  is the approximated cost of the cable network,  $n_t$  is the number of turbines,  $n_{cab}$  is the number of cables in the available set, and  $C_{cab^i}$  is the unit cost of the  $i^{th}$  cable in the available set. This provides a direct cost incentive to reduce row and column spacing and may offset some of the lost revenue due to increased wake interactions. While a more complex and accurate approximation of the cable network cost could be implemented here, a simple approach such as this was assumed to be sufficient for optimising initial grid positions of turbines. Exact cable costs and routes are required when individual turbine positions are considered (as in the following subsection), rather than when optimising the eight parameters of the grid of possible turbine

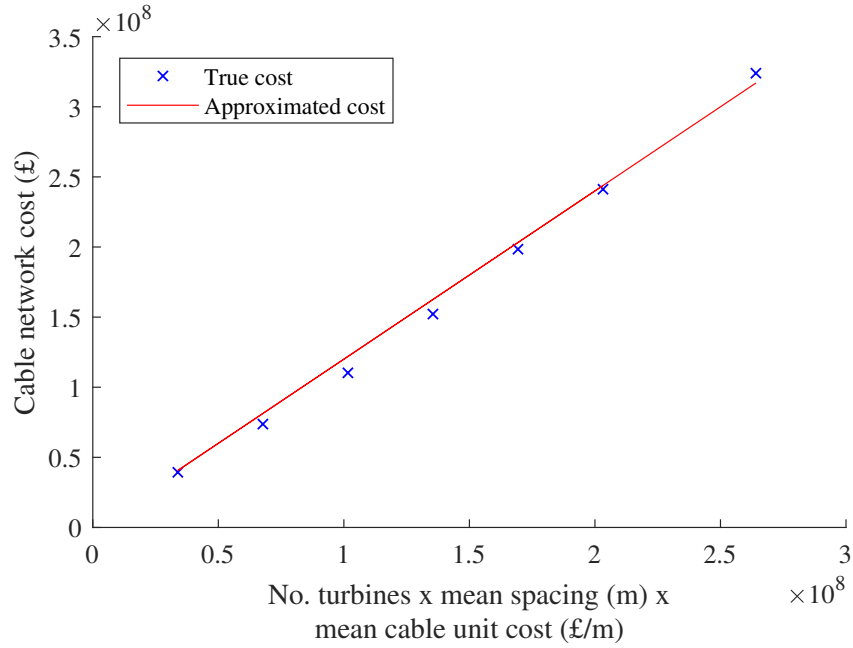


Figure 5.1: Total cable network lifetime costs (of layouts optimised by a full evaluation of the ACOsp algorithm) for a range of turbine spacings and numbers, with fitted linear approximation.

positions. This cost approximation can then be included to amend the original objective function, Equation (3.13), presented in Chapter 3. Equation (5.2) shows the amended objective function of the PSO algorithm for the integrated optimisation case.

$$J_1(\phi) = J_{rev} - C_{turbines} - P_{distance} - C_{cable\ approx} \quad (5.2)$$

where  $J_{rev}$  is the net present value of the lifetime revenue from wind farm energy capture;  $C_{turbines}$  is the capital cost of wind turbines;  $P_{distance}$  is the penalty cost associated with turbines built less than a given proximity distance apart; and  $C_{cable\ approx}$  is the approximated cost of the cable network.

### 5.1.3 Integration into the Micro-siting Phase

For the micro-siting phase, it is necessary to include a specific, optimised cable routing in order to determine the influence of turbine positions locally. From Chapter 3, the micro-siting phase contains two further sub-phases within it: firstly turbines outside of

the wind farm boundary (but close to it) are moved into the wind farm, and secondly all turbines are spaced out to reduce overall losses from wake effects. Figure 5.2 shows a flowchart of the integration of the cable layout optimisation into this micro-siting phase of the turbine layout optimisation.

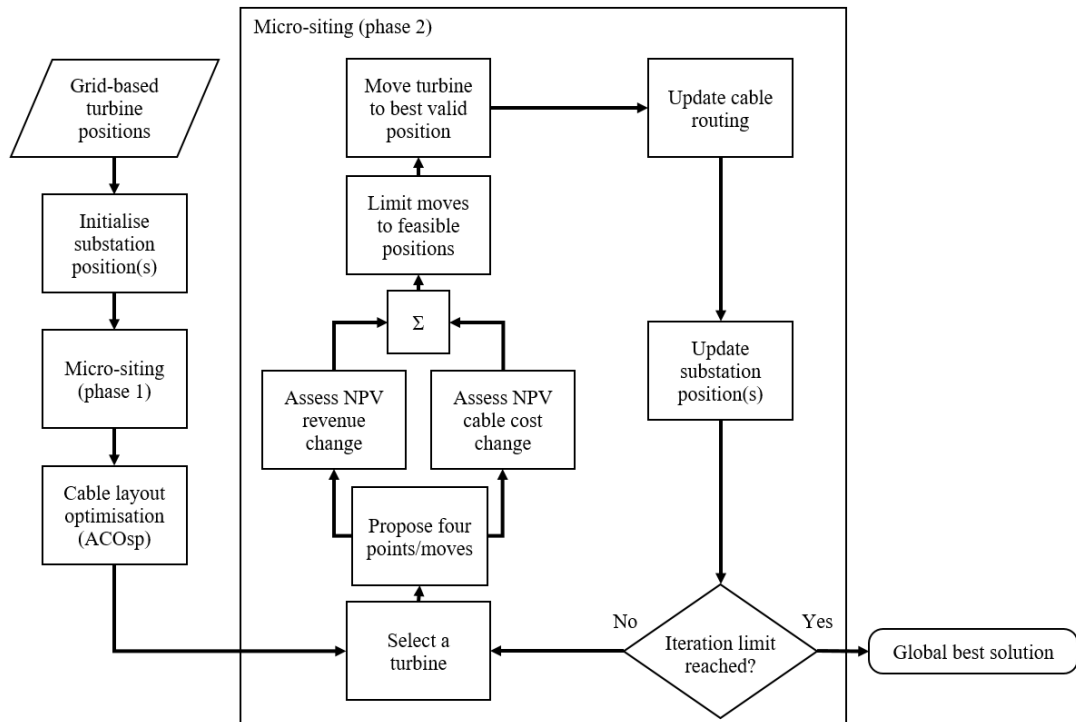


Figure 5.2: Flowchart of the integration of the cable layout optimisation into the micro-siting phase of the turbine layout optimisation.

Upon completion of the PSO phase of the turbine layout optimisation, discussed in the previous section, a grid-based set of turbine positions are provided for the micro-siting phase. Substation positions can then be initialised, discussed further later. The first micro-siting phase is unchanged in the integrated optimisation method, while the second - locally adjusting built turbines' positions - does consider cable routing costs. Therefore, the full cable layout optimisation algorithm (ACOSP, as presented in Chapter 4) is run, using the initial turbine and substation positions, to provide an initial layout solution. As solutions are incrementally changed, in the second micro-siting phase, they are assessed against the objective function, now with a specific cable network cost being

used rather than an approximation, as shown in Equation (5.3).

$$J_2(\phi) = J_{rev} - C_{turbines} - P_{distance} - C_{cable} \quad (5.3)$$

In the first stage of the micro-siting function, turbines outside of the wind farm boundary are moved inside where possible and so, from this point onward, the number of turbines will no longer change. Therefore, the capital cost of the turbines,  $C_{turbines}$ , will be fixed and the objective function need not consider it further. Additionally, turbines are limited to move to only valid locations, such as those that do not violate the proximity constraint. Therefore, assuming that the starting grid of turbine positions does not violate the proximity constraint (which should be the case given the seeding of at least one good solution), it is impossible for the proximity constraint penalty cost to be applied (to be non-zero). Therefore, the objective function can avoid considering the term  $P_{distance}$  further and now be considered as a function of only the NPV wind farm revenue and the total cable network cost, Equation (5.4).

$$J_2(\phi) = f(J_{rev}, C_{cable}) \quad (5.4)$$

As highlighted in Figure 5.2, one turbine is considered individually in each iteration, for possible micro-siting moves away from the original grid position. To determine where a turbine should be positioned locally, it is necessary to first evaluate the effect of a potential individual turbine move on the energy capture of the whole wind farm. This is achieved by evaluating the wind farm model at a discrete set of proposed new locations for a given turbine (with all other turbines remaining unmoved). These assessments of the wind farm energy capture (resulting from moving a turbine to one of a discrete set of new locations), are used to construct a cost function describing the change in wind farm energy capture over a continuous range of new possible positions (for the turbine under consideration).

For each iteration, a turbine is selected (turbine selection discussed further later) and four new possible locations for that turbine are assessed at the step-size distance ( $\approx$  rotor radius/5) away from the turbine's current location (in the North-East, North-West,

South-East, and South-West of the current grid point). For each of these four possible moves, the wind farm model is evaluated to determine the NPV of the lifetime energy capture of the whole wind farm. Considered with the turbine’s current location, giving a total of five points, a cost function of the change in NPV of lifetime energy capture can be created, Figure 5.3. An approximation such as this is used to avoid many calls for the evaluation of the wind farm model which, for a good resolution of the movable space, could result in a vastly increased computational time when multiplied by the number of micro-siting iterations. While computational time isn’t the most important factor it still must be considered. It is important to note that this cost function must describe the change in the NPV of the energy capture for the whole wind farm, not just each individual turbine, due to the interactions between the wakes of all other turbines and the turbine being considered.

Verification of the wind farm model is covered in Chapter 3, with benchmarking against SSE’s in-house wind farm planning tool. As discussed above, the wind farm model presented in this work is used to assess the wind farm energy capture for five possible locations of the turbine being considered. From these five points, the method used to create the cost surface in Figure 5.3 is Matlab’s *griddata* function, using cubic interpolation. To investigate the effectiveness and validity of this method, a full wind farm model evaluation is completed on many more locations in the range covered by the cost surface. Figure 5.4 shows the cost surface approximation (using the five points and *griddata* surface approximation), and the actual values calculated by evaluation of the full wind farm model (black dots), for 256 possible turbine moves. It can be seen that the cost surface approximation and the true calculated values show good agreement, suggesting that the cost surface generation/approximation method could be appropriate. Different methods of interpolation were investigated to generate the cost surface, and the root-mean-squared (RMS) error recorded. This revealed RMS errors of NPV£ $2.91 \times 10^4$  for linear interpolation, NPV£ $4.57 \times 10^4$  for the ‘nearest’ method, NPV£ $3.02 \times 10^4$  for the ‘natural’ method, NPV£ $2.66 \times 10^4$  for the ‘v4’ method, and NPV£ $1.11 \times 10^4$  for the cubic method. The cubic method was therefore chosen as the method of interpolation due to the low RMS error. While this method is shown to be

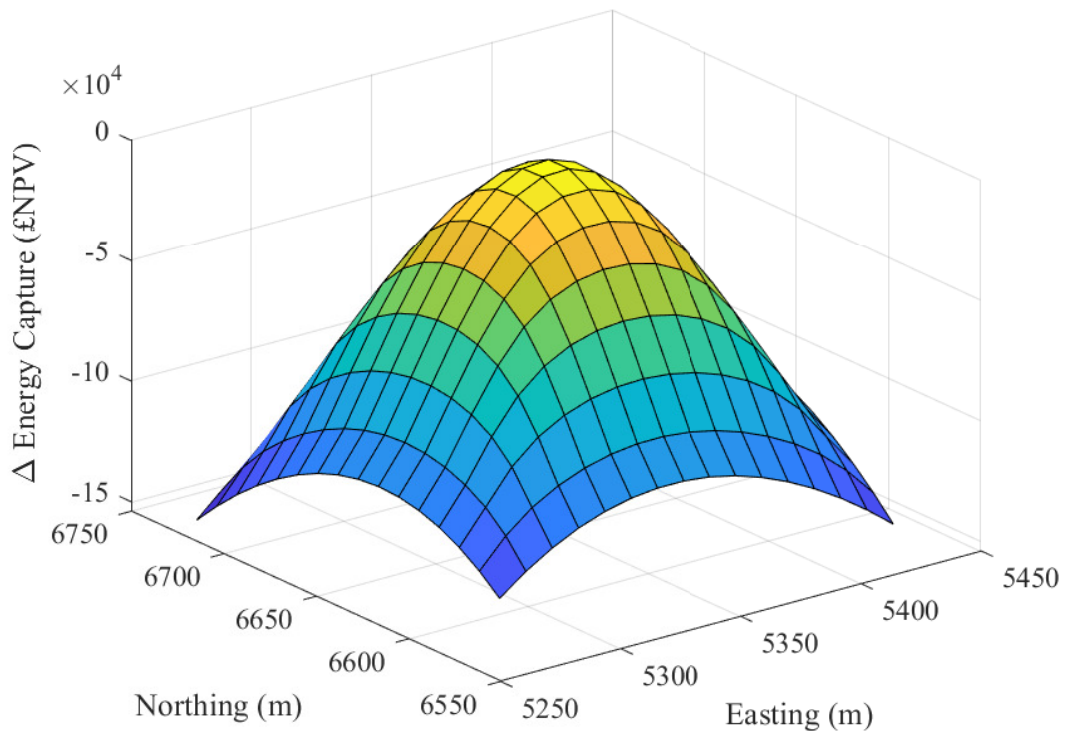


Figure 5.3: Approximated cost surface for the change in the NPV lifetime energy capture of the wind farm, for turbine locations away from the original grid position. Surface created from the evaluation of the wind farm model at five points (four corners, and the central/current location).

appropriate for the site in question, a similar comparison should be conducted if applied to other sites, to ensure confidence in the cost surface interpolation method. However, given that the underlying data (from which the cost surface is generated) is of wind farm model assessments with site-specific conditions, it is expected that this generation method for the cost surface should be applicable across sites.

Similar to the energy capture cost function, a cost function can be created for the cable network cost considering the potential moves of the selected turbine in the iteration, Figure 5.5. This function may be created from identifying the cables entering/leaving the turbine and their direction relative to the turbine. The cable(s) length, and therefore cost, will increase or decrease depending on where the turbine is moved to. The cost must be a total cost, combining cable unit cost, installation cost per unit length,

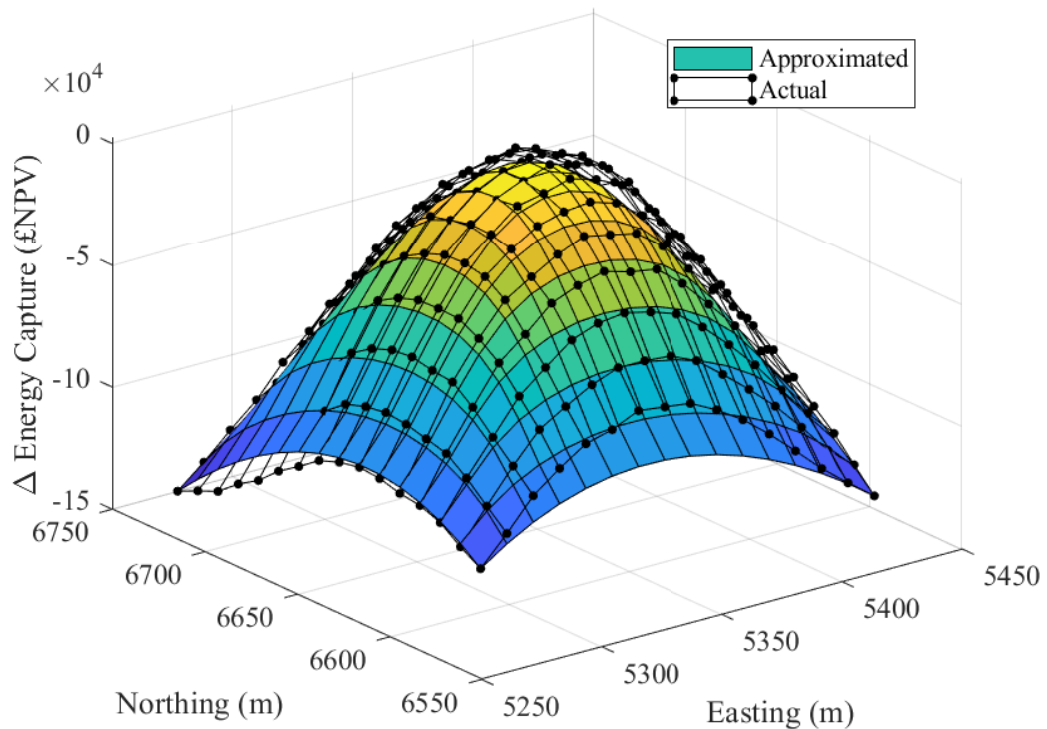


Figure 5.4: Cost surface approximation and true values for the change in the NPV lifetime energy capture of the wind farm, for turbine locations away from the original grid position.

and the NPV of lifetime electrical losses, in line with the objective function.

Having calculated these two cost functions (in common units, NPV currency) for the selected turbine, they may be combined into a single cost function, Figure 5.6, through simple summation. The resulting surface plot, shown in Figure 5.6 (left), shows the change in the objective value as a result of the possible turbine movement. As seen in the objective function, Equation (5.4), this new cost surface is created by taking the NPV energy capture cost function minus the change in the cable network cost. This subtraction explains the difference in what might be expected from the orientation of the cable network cost function, Figure 5.5. Allowing smaller incremental steps than the discrete five points tested, can lead to improved solutions in the combined optimisation considering both turbine and cable cost components. It can be seen in Figure 5.6, that

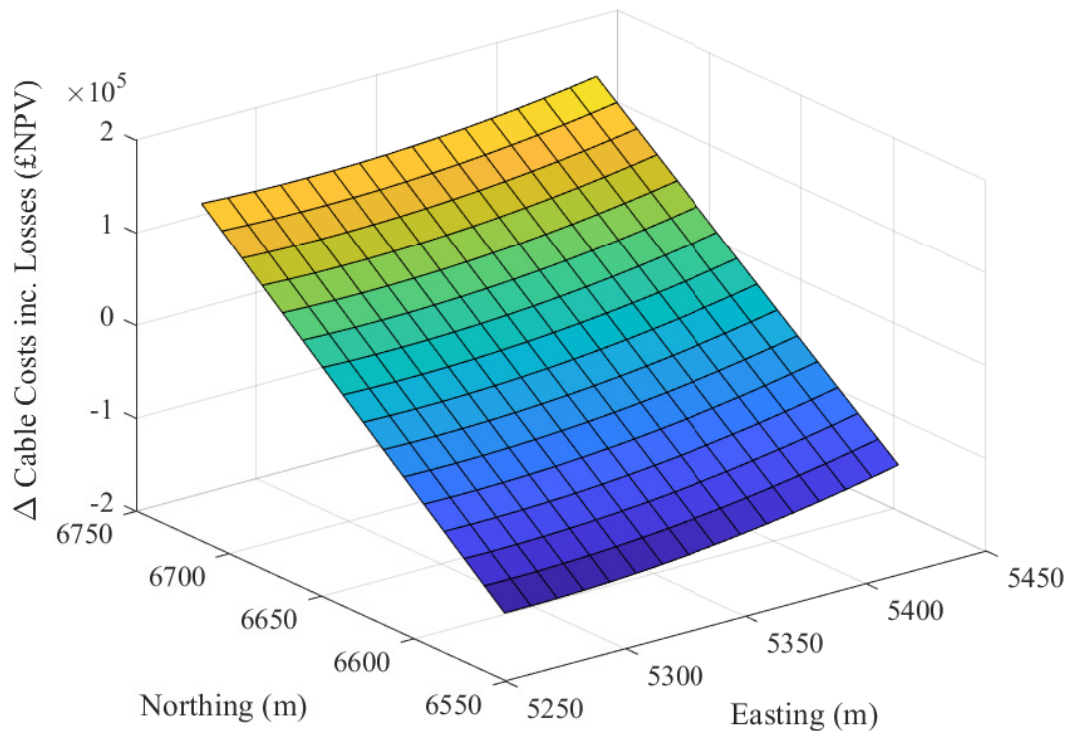


Figure 5.5: Cost surface for the change in cable costs and NPV lifetime electrical losses, for turbine locations away from the original grid position.

the best move for the turbine would be a small distance (approximately 50m) towards the south edge of the cost surface, not one of the five points tested.

With the objective function cost surface defined, it is necessary to limit turbines to valid locations only. This means restricting possible moves to only those that are within the buildable area (within the wind farm and not within an obstacle region), and to positions that are greater than the minimum turbine spacing away from neighbouring turbines. Considering the example cost surface in Figure 5.6, the corresponding constrained valid region is shown in Figure 5.7. The turbine may then be moved to the best performing region/valid position in the constrained cost surface, increasing the objective value, which may or may not be the current turbine location. In the case where no position exists with a net gain in objective value, the turbine is unmoved resulting in no change to the objective value.

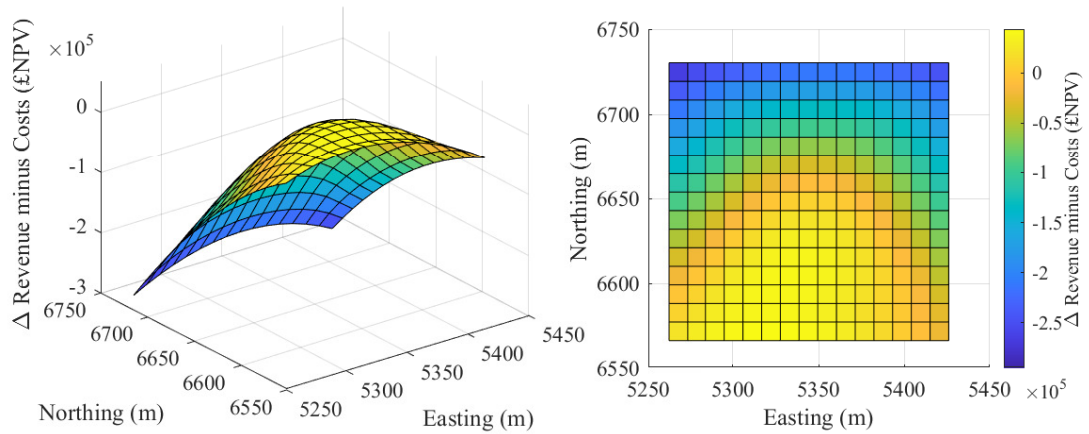


Figure 5.6: Cost surface for the combined change in NPV energy capture and cable costs (inc. NPV lifetime electrical losses), for turbine locations away from the original grid position.

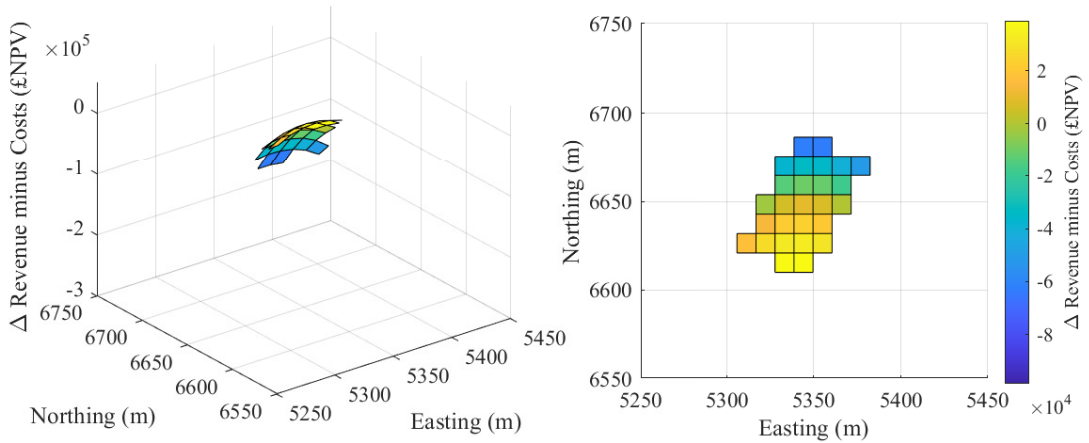


Figure 5.7: Cost surface for the combined change in NPV energy capture and cable costs (inc. NPV lifetime electrical losses), for only valid turbine locations away from the original grid position.

### 5.1.4 Updating the Cable Routing

If a turbine is moved, the optimal cable layout may have also changed. In order to capture this change in the optimal solution, if it occurs, the string connecting the moved turbine is selected - along with a random neighbouring string - to be reassessed by the ACOsp algorithm, presented in Chapter 4. The probability of the selection of the second cable is proportional to the reciprocal of the distance between it and the primary string (supporting the moved turbine). The sub-problem created by the selected pair

of strings is solved using the ACO algorithm, Algorithm 4, while continuing to consider the cost implications of all other strings. Clearly, this is analogous to the decomposition into sub-problems described in Chapter 4 and so can be thought of as a cable layout optimisation sub-problem being solved within the turbine layout micro-siting iterations.

### 5.1.5 Substation Positioning

It is not only turbines that may have their positions influenced by the layout of the collector network. Substation positions are also affected, and indeed play an important role in the solution and performance of the array cable network. In Chapter 4, substations were positioned within the wind farm in strategic locations to test aspects of the cable routing algorithm, such as obstacle avoidance. In the case study presented in this chapter, substation positions are no-longer fixed and are initialised using a *k-means clustering* algorithm [98, 152], Figure 5.2. Other approaches could be used, however, such as density- or distribution-based clustering, but the widely used *k-means clustering* was assumed to be sufficient for initialisation of substation positions, given that these positions will evolve over the iterations of the micro-siting algorithm. Initial substation positions are calculated upon completion of the PSO algorithm, when it is necessary to have an optimised cable routing to influence turbine positions.

Algorithm 6 shows the k-means clustering algorithm. Substation positions are randomly initialised in the wind farm site and turbines are each assigned to their nearest substation. Taking an average of the turbine positions for each group provides a new location, which the corresponding substation for that group is moved to. The turbines are then re-assigned to their nearest substation and the process is repeated until no further changes are made.

As shown in Figure 5.2, in each iteration of the micro-siting phase, after the turbine move is considered and the string's layout has been reassessed, the substation (connecting the string of the moved turbine) is considered for possible moves. While the substation(s) is initialised in a good position by the k-means clustering algorithm, additional moves to improve it's position are possible. Further improved positions may be found if turbines are moved that result in an altered cable layout, incentivising substa-

---

**Algorithm 6** k-means clustering algorithm for initial substation positions

---

```

Create incumbent solution,  $(x_0, y_0) = (0, 0)$ 
Initialise substation position(s) randomly in wind farm,  $(x_1, y_1)$ , where  $x_1, y_1 > 0$ 
while  $(x_0, y_0) \neq (x_1, y_1)$  do
  Update incumbent solution,  $(x_0, y_0) = (x_1, y_1)$ 
  Assign turbines,  $T$ , to their closest substation,  $S$ 
  Calculate average position of each group of turbines,  $(x_T, y_T)$ 
  Move each substation to the average positions of turbines in the corresponding
  group,  $(x_1, y_1) = (x_T, y_T)$ 
end while
Output substation coordinates,  $(x_0, y_0)$ 

```

---

tions to move towards their new/moved cable connections (moving towards the turbines directly connected to them). In the same process as described for the turbine moves, possible substation moves are assessed using the cable network cost surface only; since the energy capture cost surface is not applicable for substations. The cost surface is generated for the same range as the turbines ( $\approx$  rotor radius/5) and the substation is moved to the best (lowest cable network cost) valid position within that cost surface.

### 5.1.6 Extending the Model

This formulation of creating cost functions over the allowable range of movement may be easily adapted to include further considerations, provided they can be expressed in the same units (here NPV currency). Other such cost surfaces and/or constraint regions may include bathymetry effects such as different installation costs in different soil types, limits on the steepness of seabed gradients for installation, and water depth variation and its impact on substructure (e.g. monopile) costs. These additional cost considerations were considered beyond the scope of the investigation.

### 5.1.7 The Integrated Optimisation Algorithm

The above description of the integrated optimisation algorithm highlights that the resolution of the cable network cost is incrementally increased as the algorithm progresses, which can be summarised as follows:

1. Turbine grid seeding: No cable costs considered

2. Turbine grid optimisation (PSO): Approximated cable network cost
3. Turbine micro-siting from grid: Exact cable network cost and routing

Algorithm 7 elaborates on the exact processes taking place in the integrated optimisation algorithm, with the above Phases 1-3 highlighted for clarity.

---

**Algorithm 7** Integrated turbine and cable layout optimisation algorithm

---

**Phase 1:** Turbine layout solution seeding

Algorithm 2: Solution Seeding,  $\max(J(\phi))$ , Equation (3.13)

**Phase 2:** PSO turbine layout with approximated cable costs

Algorithm 1: PSO,  $\max(J_1(\phi))$ , Equation (5.2)

**Phase 3:** Micro-siting phase with exact cable costs

Move outside turbines into wind farm, where possible

Algorithm 6: Initial substation positioning (k-means clustering)

Algorithm 5: ACO with decomposition (ACOSP),  $\min(F)$  Equation (4.14)

$iter_{micro} = 0$

**while** Micro-siting ( $iter_{micro} < 5N_t$ ) **do**

**Phase 3a:** Micro-site turbine position

    Select random turbine,  $t$

    Generate energy capture cost function,  $J_{rev}$

    Generate cable cost function,  $C_{cable}$

    Combine cost functions,  $J_2(\phi)$ , Equation (5.3)

    Update turbine position,  $(x_t, y_t) = (x_{\max(J_2)}, y_{\max(J_2)})$

**Phase 3b:** Reassess layout of string

    Select strings,  $S_{rand}$  (containing turbine  $t$  and a random neighbouring string)

    Algorithm 4: ACO (considering all turbines,  $T$ , but only clearing routes for selected strings,  $S_{rand}$ )

**Phase 3c:** Update substation position

    Select substation supporting turbine  $t$

    Generate cable cost function,  $C_{cable}$

    Update substation position,  $(x_{SS}, y_{SS}) = (x_{\max(C_{cable})}, y_{\max(C_{cable})})$

    Re-evaluate  $J_2(\phi)$ , Equation (5.3)

$iter_{micro} = iter_{micro} + 1$

**end while**

Output  $J_2(\phi)$

---

As can be seen in Algorithm 7, Phases 1 & 2 are described by Algorithms 2 & 1 respectively, from Chapter 3. These cover, firstly, the seeding of solutions for the turbine layout and, secondly, the PSO algorithm. Important to note is the slight alteration to

the objective function used in Algorithm 1 which is updated to Equation (5.2) in order to take account of the approximated cable network cost.

Phase 3 describes the micro-siting phase which encompasses the main integration of cable layout considerations. As previously described in Chapter 3, the algorithm begins by shifting turbines that are slightly outside of the wind farm boundary, into the wind farm. Next, Algorithm 6 is employed to generate initial substation positions, required for the cable layout. Algorithm 5 is then evaluated to provide an initial cable layout solution for the site, required for micro-siting turbines.

The micro-siting loop (evaluated five times the number of turbines,  $N_t$ ) can be considered in three further sub-phases. Firstly, turbine micro-siting is considered by generating cost surfaces for the change in energy capture and change in cable network cost and moving turbines to the best overall position in the valid range. Moves are only made if they improve the objective value; if no moves provide an improvement, no move is made and the change to the objective value is zero. Secondly, the string containing the moved turbine and a neighbouring string are re-considered by the cable layout algorithm as a sub-problem to capture any changes to the optimal cable routing as a result of the turbine move. Finally, the substation positions are updated by generating a cost function from their cable connections and moving to the best position in the valid range. Upon completion of the micro-siting loop, the algorithm returns the optimised turbine positions, substation positions, and cable routing.

### 5.1.8 Turbine Selection Probability

As turbines are selected randomly in each iteration of the micro-siting function, it is possible that a turbine is selected with no move that improves the objective function. This is most likely to occur for turbines in the centre of the wind farm, where moves are limited on all sides by the proximity of neighbouring turbines.

To reduce the probability of ‘no-moves’ in the micro-siting loop, two additional elements were included into the algorithm. Firstly, a probability density function was created based on the position of turbines in the wind farm site, Equation (5.5) and, secondly, when a turbine is selected, the probability of it being selected in the next

iteration is artificially set to zero.

The proposed selection probability is presented in Equation (5.5), using the iteration number to adapt the probability of the turbine being selected. Turbines further from the centre are more likely to be picked at the start, whereas towards the end of the algorithm turbine selection probability moves towards a more uniform distribution. Figure 5.8 shows the turbine selection probability at the first and last iteration of the algorithm (left and right respectively).

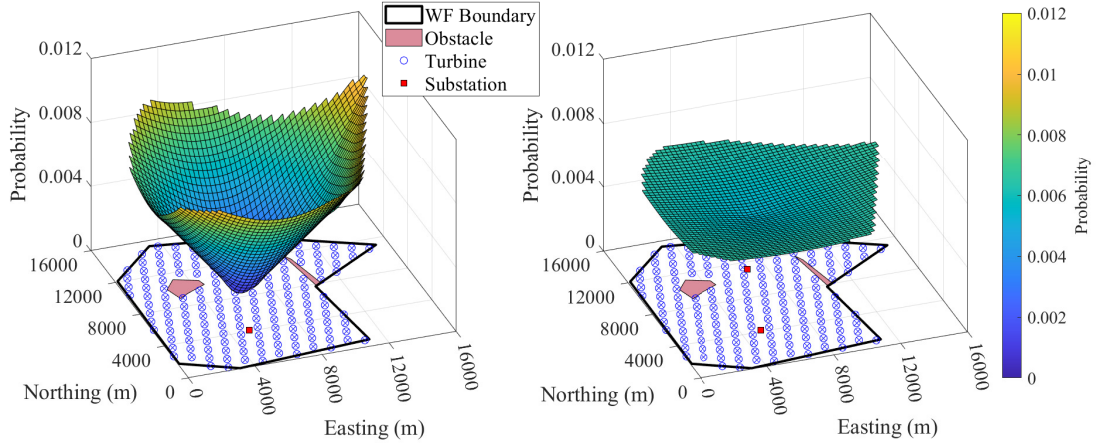


Figure 5.8: Probability density function of a turbine being selected for the micro-siting iteration for a given position in the wind farm, at (a) the first iteration and (b) the last iteration.

The probability of a turbine being selected,  $P_t$ , is given by,

$$P_t = \frac{1 + dist_{t,\tilde{t}}/(40 \text{ iter})}{\sum_{t \in T} (1 + dist_{t,\tilde{t}}/(40 \text{ iter}))} \quad (5.5)$$

where  $dist_{t,\tilde{t}}$  is the distance between the turbine,  $t$ , and the average position (average Easting and Northing position) of all turbines,  $\tilde{t}$ ; and  $iter$  is the iteration number. The denominator coefficient, 40, used for the iteration number,  $iter$ , increases the relative difference in probability between inner and outer turbines being selected. However, this is site specific term and a value appropriate for the site under consideration must be chosen when applied to other wind farms. This value was selected for this site in order to provide a large difference between probabilities in the first iteration, and little difference in the final iterations. For this site, in the first iteration, the maximum probability was

0.0113 and the minimum probability was 5.0928e-04 (a ratio of 22:1). In the last iteration, the maximum and minimum probabilities becomes 0.0068 and 0.0054 respectively (a ratio of 1.3:1). As mentioned above, for the turbine selected in the previous iteration, the probability of selection is set to zero (note: this only applies for the most recently selected turbine, which moved to its best position in the previous iteration and therefore will not find an improvement if considered immediately in consecutive iterations; in the following iterations, its probability of being selected returns to the non-zero probability calculated by Equation 5.5). Without this addition, should a turbine be selected twice consecutively, the second iteration would be guaranteed to result in a ‘no-move’ and no improvement to the objective function.

Since the micro-siting algorithm is a randomised heuristic process, there is no guarantee of reaching optimality and therefore there is potential to get stuck in a local maxima (as this is a maximisation problem). However, it is believed that this selection approach will limit this possibility by favouring the outer turbines which have more scope to move. Additionally, all iterations of the micro-siting loop result in a net improvement, or no change, to the objective function. This is because turbine moves are only made when they increase the objective value; if no improvement is found across the possible moves for a given turbine (i.e. the current turbine position is the best), then no move will be made resulting in no change to the objective value. Therefore, it was expected that the solution would tend towards the optimal solution, producing improved solutions compared to the sequentially optimised layouts.

## 5.2 Comparison of Sequential & Integrated Optimisations

A comparison of the sequential and integrated optimisation approaches was conducted on the hypothetical site proposed in Chapter 3. The case study used the wind conditions provided by SSE for the Berwick Bank site, as in Section 3.5.2, to provide a more representative description of the wind field in an offshore wind farm.

The turbines used in the case study were the same as in the previous two chapters. More detailed parameters of the 8 MW reference turbine can be found in the previously

referenced study by Desmond et al. (2016) [150]. The set of cables available to the model was also the same as that used previously, Table 4.3. Remaining miscellaneous parameters for the case study are shown in Table 5.1, and were used in both sequential and integrated optimisation approaches.

Table 5.1: Key parameters and values used in the comparison of the sequential and integrated optimisations.

Parameter	Value
Array voltage	66kV
Crossing penalty	£1m
Jointing cost (turbines)	£13.8k
Jointing cost (sub-station)	£90.7k
Price of energy	£50/MWh
Discount rate	10%
Project lifetime	25 years
Nearest N nodes of allowable connections	8

The objective function of the optimisation case study was as shown in Equation (5.3). This objective aims to maximise the NPV of the energy capture of the lifetime of the wind farm, minus the cost of turbines, minus the cost of the cable network (including the NPV of the electrical losses accrued over the life of the wind farm). The penalty cost function,  $P_{distance}$  can also be seen in the objective function, Equation (5.3), penalising solutions that place turbines too closely together. As mentioned previously, this should only be a factor within the first phase of the turbine layout optimisation, after which the penalty cost term will be equal to zero.

### 5.2.1 Sequential Optimisation Algorithm

The sequential algorithm is, as the name suggests, the turbine layout and cable layout optimisation algorithms treated separately and sequentially. Algorithm 8 shows the key processes in the sequential optimisation algorithm, with the first phase considering the turbine layout and the second phase considering the cable routing.

Similar to the integrated optimisation algorithm, Phase 1 begins by employing Algorithm 2 to provide a good quality seed solution for the PSO algorithm, Algorithm 1, which immediately follows. Upon completion of the PSO algorithm, turbines that can

be moved into the wind farm (those that are outside the wind farm area by only a small distance; this study used the rotor radius) are moved into the buildable area. Turbines are then randomly selected with the same selection probability as that presented in Section 5.1.8 and micro-sited to their best local position. While the integrated optimisation algorithm determines the best position for the turbines by assessing the impact on both wind farm energy capture and cable network cost, the sequential algorithm considers only the change to wind farm energy capture in Phase 1.

Following the completion of the micro-siting process, the turbine positions are fixed and provided as inputs to Phase 2 of the algorithm. Substation positions are calculated using the optimised turbine positions and Algorithm 6. The cable layout is then optimised using Algorithm 5 with no changes being made to either turbine positions or substation positions. The optimised solution (considering both turbine and cable layouts) is finally evaluated against the combined objective function, Equation (5.3).

---

**Algorithm 8** Sequential turbine and cable layout optimisation algorithm
 

---

**Phase 1:** Turbine layout optimisation

Algorithm 2: Solution Seeding,  $\max(J(\phi))$ , Equation (3.13)

Algorithm 1: PSO,  $\max(J_1(\phi))$ , Equation (5.2)

Move outside turbines into wind farm, where possible

**while** Micro-siting **do**

Select random turbine,  $t$

Generate energy capture cost function,  $J_{rev}$

Update turbine position,  $(x_t, y_t) = (x_{\max(J_{rev})}, y_{\max(J_{rev})})$

**end while**

**Phase 2:** Cable layout optimisation

Algorithm 6: Initial substation positioning (k-means clustering)

Algorithm 5: ACO with decomposition (ACOSP),  $\min(F)$  Equation (4.14)

Evaluate combined objective function,  $J_2(\phi)$ , Equation (5.3)

Output  $J_2(\phi)$

---

### 5.3 Results & Discussion

A set of ten optimised solutions were generated for each algorithm, sequential and integrated (Algorithms 8 & 7 respectively), for the hypothetical site case study. The

objective values of the solutions created by each approach can be seen in Table 5.2, along with the number of turbines present in each of the solutions.

Table 5.2: Full results for the sequential vs integrated optimisation methods, using representative wind data provided by SSE.

Sequential		Integrated	
No. turbines	Objective value (£)	No. turbines	Objective value (£)
164	1,128,461,489	164	1,134,932,405
164	1,129,670,889	164	1,135,131,015
165	1,135,944,345	164	1,134,478,045
164	1,129,670,889	164	1,133,935,487
164	1,129,670,889	164	1,133,801,651
164	1,129,670,889	165	1,140,878,840
164	1,129,670,889	164	1,136,765,774
164	1,129,670,889	164	1,133,466,310
164	1,129,670,889	164	1,135,888,867
164	1,129,670,889	164	1,133,174,388

Figure 5.9 shows a box plot of the objective values presented in Table 5.2. The box plot indicates the median values for each set of results, the 25<sup>th</sup> and 75<sup>th</sup> percentile, and the extreme data points in the set. Outliers are indicated with a ‘+’ symbol.

It can be seen in Figure 5.9, that the median objective value of the sequential optimisation results is £1.1297b, and the median objective value of the integrated optimisation results is £1.1347b, equating to a 0.45% increase. A Shapiro-Wilk test [153], used for testing the normality of data (particularly for small data sets), indicates that the two sets of data are non-normally distributed, with both being positively skewed and leptokurtic (long-heavy tails). Therefore, to determine if the two data sets are statistically significantly different, the common statistical significance ‘t-test’ (for normally distributed data) cannot be used, and the Mann-Whitney U Test must be used instead. This test indicates that the difference between the two data sets is significant enough to reject the null hypothesis - that the integrated optimisation had no impact on the quality of the solutions. The resulting p value, 0.001191, means that the chance of type 1 error (rejecting a correct null hypothesis) is small, 0.001191 (0.12%), and that there can be confidence that the integrated optimisation produces statistically different solutions to a sequentially optimised approach. The small sample size in this data set may

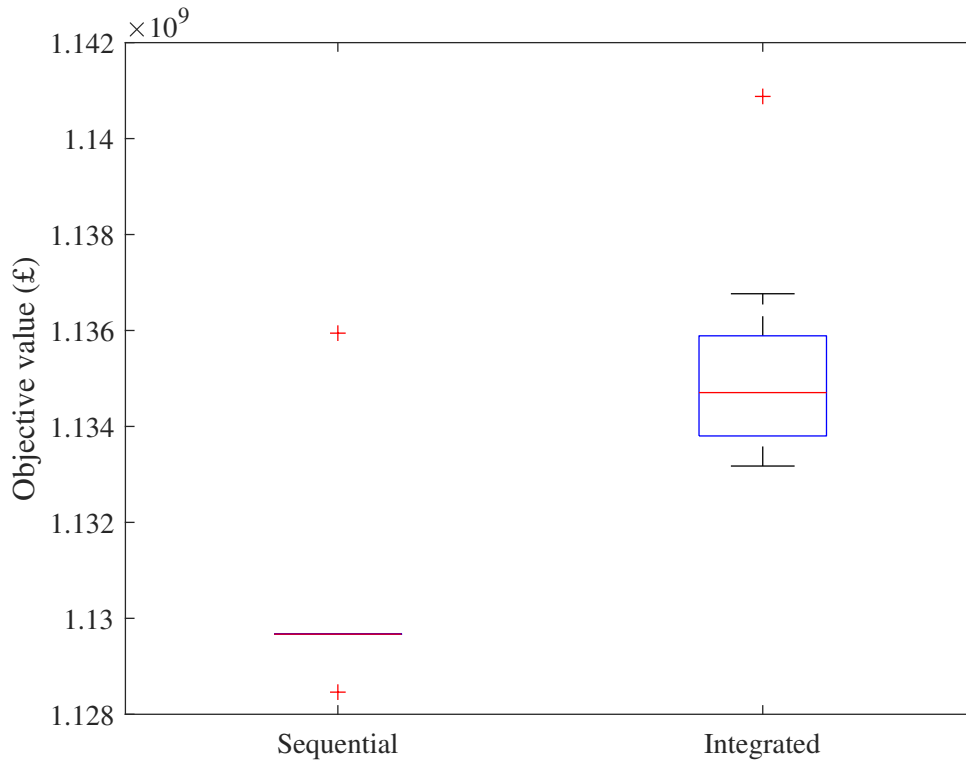


Figure 5.9: Objective values for the two sets of optimised layouts using sequential and integrated methods, with outliers marked by a red ‘+’.

introduce some uncertainty in the validity of the Mann-Whitney U test, however, it is designed for small sample sizes and non-normally distributed data and so should be appropriate for this analysis.

Since it was expected, in the alternative hypothesis, that the integrated approach improve solutions (rather than just change them), a one-tailed Mann-Whitney U test may be more appropriate. For the same data sets, a one-tailed Mann-Whitney U test indicates that the null hypothesis may be rejected, and that the integrated optimisation solutions are statistically significantly *higher* than the set of sequentially optimised solutions. The resulting p value of 0.0005953, means that there is a 0.060% chance of rejecting a correct null hypothesis.

To investigate the improvement in the integrated optimisation solutions further, the number of turbines is recorded for each solution in both data sets for comparison.

Figure 5.10 shows the objective values of the solutions plotted against the number of turbines in the solutions. Both the sequentially optimised solutions and the integrated optimisation solutions reliably produce turbine layouts containing 164 turbines, with both sets containing only one solution each that was able to site 165 turbines. This small variation is likely due to the heuristic nature of the optimisation frameworks, but shows that it is generally a reliable method. The two solutions containing 165 turbines (one sequential solution and one integrated solution), both have higher objective values than the remainder of their respective set that all contain 164 turbines. It is also clear that the integrated optimisation solutions always outperform the sequentially optimised solutions when comparing solutions with the same number of turbines.

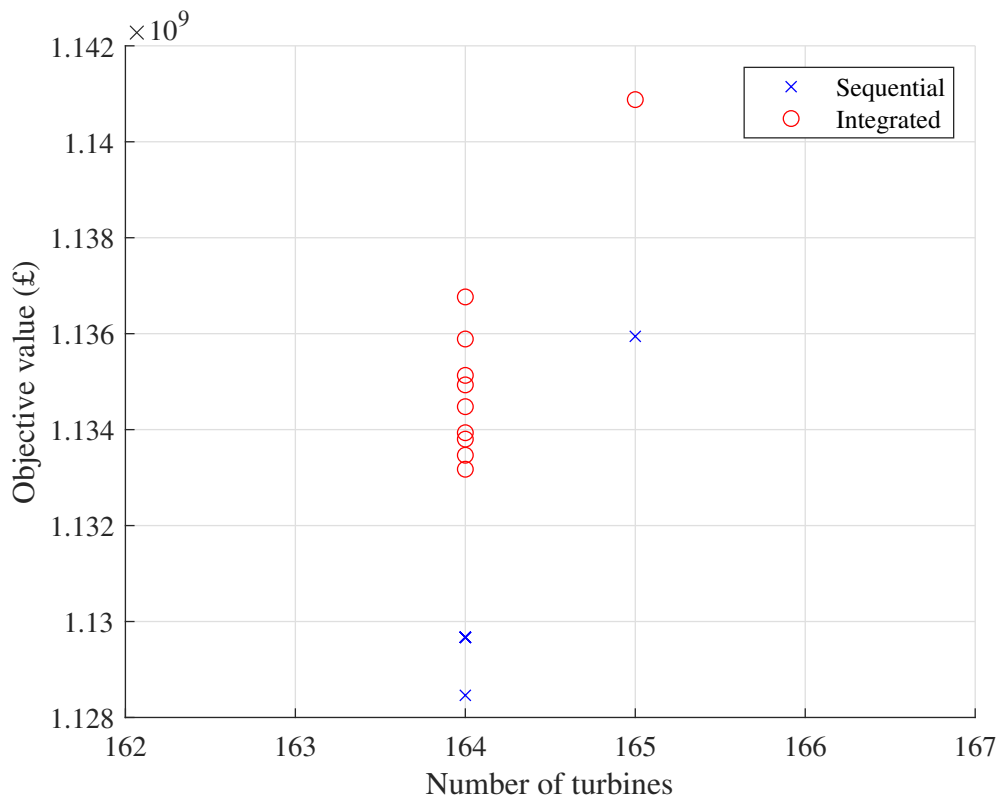


Figure 5.10: Objective values for optimised layouts using sequential and integrated optimisations with objective value against number of turbines.

In the two cases containing 165 turbines, the integrated optimisation solution has an objective value that is £4.9m higher than the sequential optimisation solution, rep-

representing an increase of 0.43%. Taking a mean of the solutions containing 164 turbines, for each set, the integrated optimisation solutions increase the objective value by £5.1m (0.45%) relative to the sequential optimisation solutions. While these increases in objective value are found through employing the integrated optimisation approach relative to the sequential approach, increases are also seen in the solutions that simply contain more turbines relative to those with fewer. For the integrated optimisation solutions set (taking the mean objective value of solutions containing 164 turbines), the average increase between the cases of 164 and 165 turbines is £6.3m (0.55%). For the sequential optimisation solutions, the increase in objective value from solutions containing 164 turbines to the solution containing 165 turbines is £6.4m (0.57%). Therefore, while the increases are modest and still contain some amount of uncertainty in the accuracy of the true performance of the site, it could be said that increasing the number of turbines in the site by one, is more impactful on the objective value than integrating the cable layout optimisation into the earlier design phases (turbine layout optimisation phase) of this large scale offshore wind farm case. The best performing solution of both optimisation approaches is that which contains the most number of turbines (165) and also employs an integrated optimisation approach, such that the cable routing may influence turbine positions.

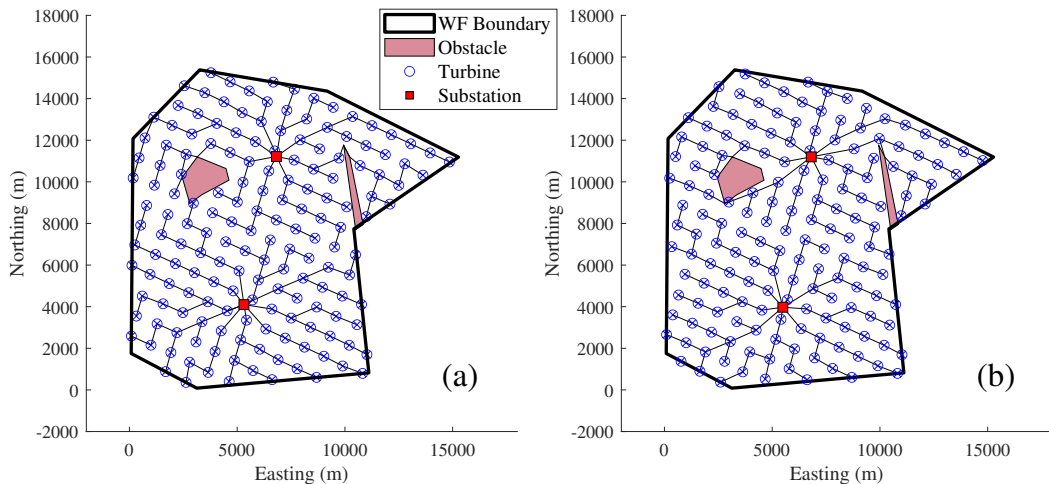


Figure 5.11: Layout solutions of the sites containing 165 turbines, using the (a) sequential optimisation approach, and (b) the integrated optimisation approach.

Figure 5.11 shows the layout solutions of the two cases containing 165 turbines, using (a) the sequential optimisation, and (b) the integrated optimisation. Both solutions appear to produce sensible layouts connecting all 165 turbines with a network of branched strings. The sequential solution is connected with a set of eight strings (81 turbines) into the north substation and 10 strings (84 turbines) into the south substation, while the integrated solution uses nine strings into each of its substations (84 turbines connected to the north substation and 81 turbines connected to the south substation). The substations are in very similar positions in both solutions, differing by only 19m and 221m, suggesting that the integrated approach does not result in significant movements in substation position within micro-siting iterations.

In both solutions, it can be seen that the cables connecting turbines near the westernmost obstacle deviate to route through a Steiner node next to the obstacle, even though this is not required and a straight line connection would suffice. This highlights a limitation of the heuristic ACO approach used within the optimisation algorithms. While the overall solutions appear to be of good quality, connecting neighbouring turbines in efficient straight-line connections, small deviations such as those near the obstacle can still occur. Adapting the tuning of the algorithm may help to re-route this non-optimal section, however, the remainder of the connector network suggests that the tuning of parameters is already reasonable and generates good quality solutions for this site.

The integration of the turbine and cable layout optimisations resulted in a much more demanding algorithm in terms of computational memory and time. As such, additional computational resource was obtained through the ARCHIE WeSt supercomputer facility hosted by the University of Strathclyde. However, with limited budget allocated to running the optimisations on the supercomputer resource, priority was given to the integrated optimisation cases that were too demanding for standard desktop PCs to run. Sequential optimisations were run on standard desktop PCs. Therefore, an accurate comparison of the computational time and memory requirements is not possible. However, the inability for the integrated case to run on a standard desktop PC, presents a significant limitation of the approach. Future development focused code optimisation and utilising different solvers may be able to rectify this issue, but this was beyond the

scope of the current work.

## 5.4 Summary

This chapter proposes a method for the integration of the cable layout optimisation with a turbine layout optimisation approach. A novel staged integration is employed, incrementally increasing the accuracy of the cable network cost contribution to the objective value, in an attempt to balance accuracy with computational efficiency. Description of this integration into the three phases covers (1) solution seeding phase, (2) the particle swarm optimisation phase, and (3) the micro-siting phase, with justification of the fidelity of the cable network contribution. During the third phase (micro-siting), a cost surface approach is taken. This considers the change to energy yield and cable costs and losses, and is easily adapted to account for additional cost considerations, if desired in future studies. Suggested additional cost surfaces that may be considered include substructure cost with water depth, seabed conditions, or bathymetry gradients.

A comparison of sequentially optimised solutions and integrated optimisation solutions was carried out on the hypothetical site proposed in Chapter 3, combining the algorithms outlined in Chapters 3 & 4. A set of ten solutions was generated for each approach, with both sets of solutions reliably producing layouts containing 164-165 turbines. On average the integrated optimisation solutions had a higher objective value by 0.45%, which was demonstrated to be a statistically significant difference through a Mann-Whitney U Test. While the integrated approach did increase the objective value in this maximisation problem, both approaches showed a larger increase between their solutions containing 165 and those containing 164 turbines (0.55% and 0.57%). The best performing solution of both approaches was that which contained 165 turbines and also adopted the integrated optimisation approach.

Some limitations were demonstrated in the ACOsp component used for the cable routing optimisation. While solutions were overall of good quality, some unnecessary small deviations to Steiner nodes remained, highlighting that the optimal solution was not found. While these are minor additional costs, it is possible that a non-heuristic

method would produce a better overall solution. Integrating an exact method in the same way should be possible, although may potentially lead to an increase in computational complexity, as outlined in the comparison in Chapter 4.

In conclusion, the third objective of this thesis - to isolate the impact of an integrated optimisation, compared to a sequential optimisation of turbine positions followed by cable routing - was met, showing a statistically significant increase in the objective value when an integrated approach is adopted. Increasing the number of the turbines in the site remains paramount in maximising the objective value, but also using an integrated approach as outlined in this chapter can provide further increase to the objective value. The level of improvement over sequentially optimised solutions will be site-specific. Since the case study presented in this work is limited to only one site (due to computational resource constraints), some uncertainty remains in the magnitude of the benefit found in the integrated approach relative to the sequential approach. However, since the micro-siting function only adjusts the solution if improvements can be found, it is known that this phase of the integrated optimisation will result in an improved solution when applied to any site, relative to a sequential optimisation. The quality of the solution is, of course, subject to the quality of the incumbent solution provided by the preceding phase of the algorithm, which considers an estimated cable network cost and does not necessarily guarantee an improved solution relative to a sequential optimisation. Overall, the approach can be used on a wide range of sites/problems and is expected to provide good quality solutions compared to sequentially optimised solutions. However, future research may want to consider additional sites for comparison, using the sequential and integrated approaches, to increase confidence in the robustness of the optimisation methodology.

## Chapter 6

# Advanced Cable Layout Optimisation

The comparison between cable layout optimisations in Chapter 4 provided insight into the performance of the ACO and proposed ACOSP methods, benchmarked against the MILP approach which is used widely in academic literature. The results of the comparison demonstrated both the utility of incorporating a decomposition method with the heuristic ACO approach, and the reliability of the MILP method. While the MILP method provides the optimal solution (provided there is sufficient computational resource), it has challenges relating to scaling up to solve larger problems. As such, the ACOSP method was used in the integrated optimisation, nested within the turbine layout optimisation, in Chapter 5, since it was targeted at large offshore wind farm sites. The integrated optimisation considered the cable layout with increasing fidelity, with the last phase of the algorithm requiring exact cable routings to influence turbine positions. The reliability of these late-stage cable layout results is therefore very important.

These considerations of the previous two chapters helped to influence an aligned project by the author, aiming to find improved methods for large scale cable layout optimisation. An alternative method was identified to expand the work of Chapter 4, aiming to combine the benefits of the decomposition technique with the reliability of the MILP method. Figure 6.1 shows the gap identified in the comparison of cable layout

optimisations. This chapter proposes a new method, MILPsp, using a classical MILP approach with a decomposition method. Constraints and additional considerations are presented with a case study of the algorithm, and comparison and benchmarking to the classical MILP method. Results of the case study are discussed to determine the efficacy of the algorithm and its limitations, and further model development is mentioned to inform future works.

## 6.1 Methodology

Three cable layout optimisation methods were presented in Chapter 4 including a MILP algorithm, ACO algorithm, and the proposed ACOSP algorithm. While the ACOSP algorithm was shown to provide a good compromise between computational time and effectiveness of solutions, a gap was identified that may provide further benefits in both the optimality of solutions and required computational resource.

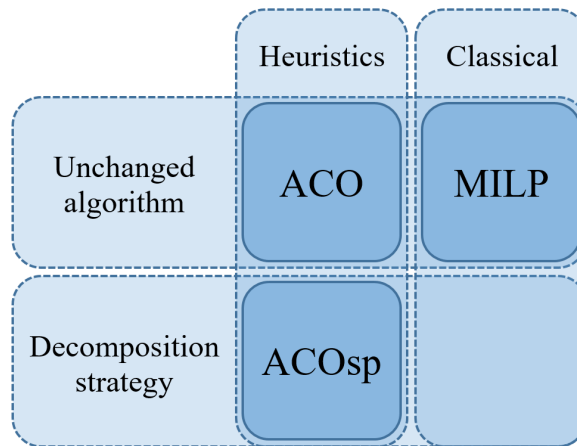


Figure 6.1: Identifying the gap in optimisation approaches at the intersection of classical methods and decomposition strategies.

Figure 6.1 shows the three algorithms used previously, highlighting the categories that each belongs to. These categories cover classical optimisation methods and heuristic approaches and, in the other axis, the standard algorithms and those with a decomposition strategy introduced. Following the review of the previous two chapters and scoping potential cable layout algorithms for an aligned project, a gap was identified

combining the previously investigated cable layout optimisation algorithms. It is clear in Figure 6.1 that there is an opportunity to explore the classical methods from Chapter 4, paired with the decomposition strategies used, in order to try and maintain the accuracy of the MILP solutions while improving computational efficiency.

This section describes the proposed algorithm to fill the identified gap, a MILP model decomposed into sub-problems (MILPsp). This dedicated cable layout optimisation method (rather than one integrated within a turbine layout optimisation framework) has several improvements over the methods described in Chapter 4. Key improvements include: a route finding algorithm for advanced obstacle avoidance; comprehensive electrical loss calculation (based on BS IEC 60287-3-2-2012 and BS IEC 60228 [154]); inclusion of substation connection costs; differentiation of the cable crossing constraint into three categories of obstacle type; inclusion of a jack-up vessel operating zone for cables to avoid; a limit to the number of cable types allowed in a solution; and an alternative sub-problem selection strategy. The following sub-sections detail the additional improvements and present the final algorithm.

### 6.1.1 The Original MILP Model

As presented in Chapter 4, the MILP model comprises both binary and continuous variables to describe a cable layout solution. The objective function is the sum of the costs associated with the cables (including electrical losses), given in Equation (4.14), and constraint equations of the previous MILP formulation can be found in Section 4.2.3.

### 6.1.2 Route Finding Algorithm

The previous model, Chapter 4, used Steiner nodes ('empty' nodes) placed on obstacle boundary vertices to enable cables to navigate around the obstacles. These could only be used by one cable and required additional constraint equations to ensure that if a cable entered the node, exactly one cable must leave the node (which would still constitute the same cable connection/route between turbines, but considered in two or more sections). The new method removes the Steiner nodes from the problem-solving

phase - reducing the number of nodes, decision variables, and constraint equations in the problem - by considering a more advanced route-finding algorithm in the pre-processing phase.

### Steiner Node Generation

As cables have limitations in the paths they can take (such as having a minimum bend radius) and will likely need to navigate around obstacles with some spacing/gap tolerance rather than following an obstacle boundary exactly, the Steiner node generation was changed from the previous model presented in Chapter 4.

A square grid of a given spacing (here the grid resolution is equal to the turbine rotor radius) is created over the whole wind farm site. Any points in the grid that are within the wind farm, not in an obstacle, and a distance between 10m and the rotor radius plus 10m ( $10 < x < rotor\ radius + 10$ ) from an obstacle vertex are kept, and the remaining grid points are removed. This results in a grid of nodes around the obstacle vertices (including the wind farm boundary) allowing for realistic routes to be found around obstacles while maintaining some small distance from obstacle edges, here 10m. These nodes are made available to a route finding algorithm, called A\*, that finds the shortest route for each connection between two nodes. For sites with small obstacles, an appropriate grid resolution must be chosen to ensure they can be effectively avoided.

Figure 6.2 shows how the Steiner node generation strategy is completed. A grid of nodes is visible, covering the whole region (except for that covered by an obstacle). Any nodes falling within the defined range from an obstacle node are kept and used as Steiner nodes.

### A\* Route Finding Algorithm

The route finding algorithm that is employed is the computationally simple and efficient A\* route finding algorithm [155]. It is similar to the ‘Dijkstra’s Shortest Path’ algorithm [156] but includes an additional heuristic to influence the search. The Dijkstra’s Shortest Path algorithm starts at the start node and recursively ‘steps’ to the next closest of the set of available connected nodes, recording the total distance taken

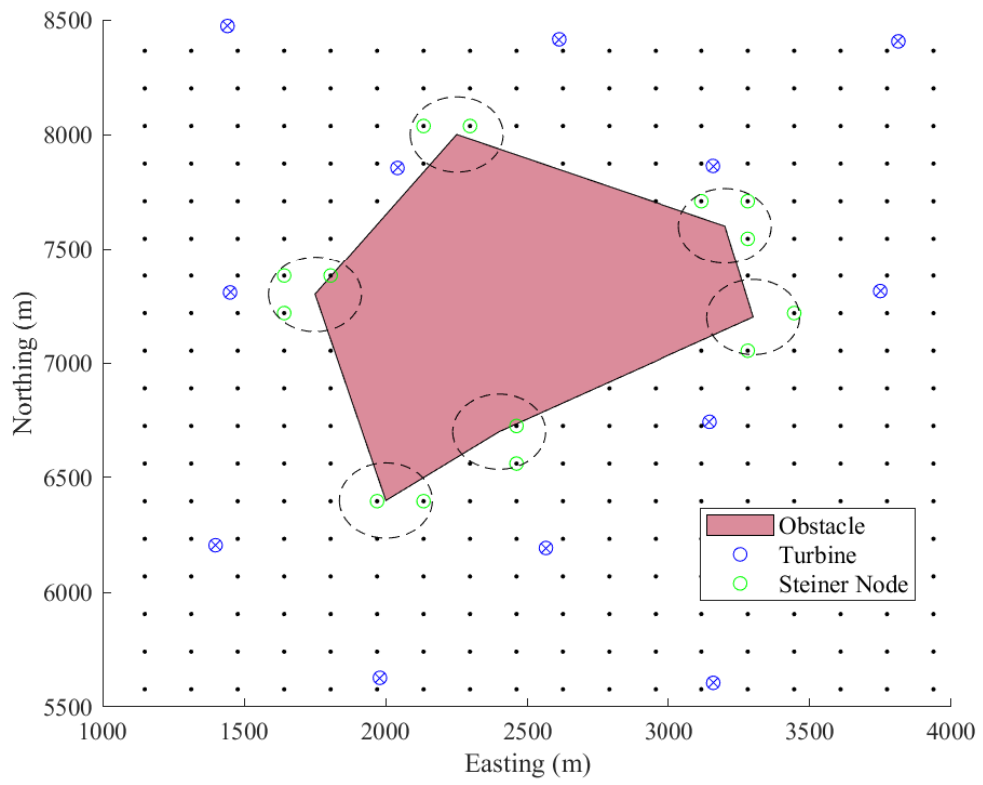


Figure 6.2: Generation of Steiner nodes for obstacle avoidance.

to reach the node in a sorted list along with the previous node from which each were connected. For the shortest total path found to date, the algorithm then expands from that node visiting each of the connected nodes and recording the total path distance (and updating the shortest path if a better route is found for an already-visited node). This continues until the node to be expanded is the end/destination node, and therefore there can be no shorter path yet to be found. The A\* algorithm progresses in a similar way, however the next node to be expanded from is determined by the total path length (so far) plus the heuristic estimate of how far is left to go to the end node from the set of next possible nodes. In this formulation, the heuristic distance is the Euclidean distance between a given node and the end node. This method helps to prioritise the more promising nodes to expand first, resulting in fewer nodes being checked and the shortest path being found more quickly. Algorithm 9 presents the key steps of the A\* route finding algorithm.

---

**Algorithm 9** A\* route finding algorithm

---

```

Initialise  $f(n)$ ,  $g(n)$ ,  $h(n) = inf$ ,  $state(n) = 0$ , and  $last(n) = []$ , for  $n \in V$ 
Calculate heuristic estimate,  $h(n)$ , for all nodes,  $n \in V$ 
Initialise algorithm at start node,  $n_{current} = n_s$ ,  $state(n_{current}) = 1$ ,  $g(n_{current}) = 0$ ,
 $f(n_{current}) = g(n_{current}) + h(n_{current})$ 
while  $not(n_{current} == n_e)$  do
  for  $n_{next} \in V_{next}$  do
    if  $g(n_{next}) \geq g(n_{current}) + dist_{current,next}$  then
       $g(n_{next}) = g(n_{current}) + dist_{current,next}$ 
       $f(n_{next}) = g(n_{next}) + h(n_{next})$ 
       $state(n_{next}) = 1$ 
       $last(n_{next}) = n_{current}$ 
    end if
  end for
   $state(n_{current}) = 0$ 
   $n_{current} = n_i$  where  $f(n_i) == \min(f(state(n) == 1))$ , for  $n \in V$ 
end while
Record the route from the end node,  $n_e$ , through the preceding nodes,  $last(n)$ , to the
start node,  $n_s$ 
Output shortest total route length,  $g(n_e)$ 

```

---

At the start of the route finding algorithm, Algorithm 9, the distance to each node,  $g(n)$ , the heuristic distance to the end from each node,  $h(n)$ , and the combined distance

estimate,  $f(n)$ , are all initialised as infinite, for all nodes. The states of all nodes,  $state(n)$ , are initialised at 0 and previous nodes from which each are connected,  $last(n)$ , are initialised as empty. The heuristic distances from each node are then calculated, which in this formulation is the Euclidean distance from a node to the end node. The search begins at the start node by setting the ‘current’ node to the start node, the state of the current/start node,  $n_{current}$ , to 1, and the distance travelled to the current node (from the start),  $g(n_{current})$ , to 0. The total estimated distance using the current node,  $f(n_{current})$ , is calculated by summing the distance travelled and heuristic estimate to the end. While the ‘current’ node under consideration is not the end node the algorithm will continue to search for the shortest path. Within each iteration, the algorithm considers each possible node,  $n_{next}$ , in the set of nodes connected to the current node,  $V_{next}$ . For each, it will check if the total distance estimate of the node is greater than or equal to the current distance travelled plus the distance between the current and next node. If the new distance is shorter, a new shortest route has been found to the next node. The distance information of the node under consideration is updated along with the record of the previous node to which it is connected,  $last(n_{next})$ , and its state is set to active ( $state_{next} = 1$ ). When all nodes in the set of next possible nodes have been checked, the state of the current node is set to 0, to mark that the routes from that node have been searched. From the set of all nodes whose state is equal to 1, the node with the minimum total distance estimate,  $min(f(n))$ , is chosen as the next node to search from - if this node is the end node the stopping criteria have been met and the algorithm will finish. Once complete, the shortest path is found by back-tracking the route from the end node, through each previous node ( $last(n)$ ), to the start node, with the shortest path length equal to the recorded distance to reach the end node,  $g(n_e)$ .

In the classical A\* approach, Algorithm 9, the full graph of connections and edge lengths are assumed to be available before running the algorithm. In the formulation used in this study, not all of the information is pre-processed, in order to reduce computational time. Here, the algorithm initialises with all the connections between all Steiner nodes, and the start and the end nodes (turbines and/or substations), but with no edge length information. When a node is expanded to search its connections for the

next node, the distance information,  $dist_{current,next}$ , is required and calculated, and the straight-line edge is checked for crossing any obstacles. If an edge crosses an obstacle, the length of the edge is set to infinite and will not be used in the shortest path. If the distance to the (next possible) node is improved (decreased), the heuristic estimate will be required and is computed. The information for the network of Steiner nodes is saved for future function calls of the route finding algorithm - which is necessary for each of the turbine connections to be made - in order to avoid re-computing the distances and checking for crossings. Conducting these checks and calculating the distances in this way greatly reduces the number of graph edges that are checked to only the necessary subset, rather than all possible edges.

### 6.1.3 Electrical Losses

The model, in Chapter 4, assumed a power factor of one (no reactive power) and considered only Joule losses, which account for the majority of the electrical losses in the cables [157]. However, to provide a more comprehensive analysis of the electrical losses, the model was amended for this chapter to include a power factor adjustment, consideration of other sources of electrical losses, and the effect of steady-state operating temperature on cable resistance.

The active power of the turbine is taken from the wind turbine power curve, describing the output power against wind speed. The apparent power,  $P_{apparent}$  is found by dividing the active power,  $P_{active}$ , by the power factor,  $P_{fac}$ .

$$P_{apparent} = P_{active}/P_{fac} \quad (6.1)$$

The electric losses of the cables are calculated in line with the British Standards for the calculation of current rating for electrical cables, BS IEC 60287 [157]. The major component of the losses is the Joule losses, Equation (6.2). Annual lost energy can be found by including terms to describe the cable length, distribution of the wind speed, and the number of hours in a year.

$$Loss_J = \sum_{u=0}^{U_{max}} N_{Turb} I^2(u) R_L(u) L W_u 8760 \quad (6.2)$$

where  $N_{Turb}$  is the number of turbines being supported by the cable,  $I$  is the current in a single phase of the cable (which is a function of wind speed,  $u$ ),  $R_L$  is the resistance per unit length of the cable (which is temperature dependent and therefore a function of the current and, by extension, wind speed),  $L$  is the cable length,  $W$  is the probability density function of wind speed ( $u$ ), and 8760 represents the number of hours in a year.

In order to calculate the charging current losses, the charging current per unit length,  $I_C$ , must first be calculated.

$$I_C = 2 \pi 50 C \frac{V}{\sqrt{3}} \quad (6.3)$$

where  $C$  is the cable capacitance and  $V$  is the array cable voltage. The charging current may then be used to calculate the associated charging current losses,  $Loss_{CC}$ , through Equation (6.4), summing across all wind conditions at the site.

$$Loss_{CC} = \sum_{u=0}^{U_{max}} \frac{1}{3} I_C^2 L^3 R_L(u) W_u 8760 \quad (6.4)$$

Di-electric losses,  $Loss_{DE}$ , are the third main component contributing to cable losses and can be calculated as follows:

$$Loss_{DE} = \sum_{u=0}^{U_{max}} 2 \pi 50 C \left( \frac{V}{\sqrt{3}} \right)^2 \tan_d L W_u 8760 \quad (6.5)$$

where  $\tan_d$  is the loss factor of the cable insulation.

Summing the three main contributors to electrical losses yields the total electrical loss experienced by a single phase and so the total loss of the 3-phase cable is found as follows:

$$Loss_T = 3 (Loss_J + Loss_{CC} + Loss_{DE}) \quad (6.6)$$

This lost energy may be converted into a monetary value by multiplying by the cost of energy,  $k_{MWh}$ . To consider the cost over the lifetime of the project in net present

value terms, another factor may be included,  $f_{NPV}$ . This term is the summation over the lifetime of the project of the effect of the discount rate on a factor of one, i.e.

$$f_{NPV} = \sum_{yr=0}^{LT} \frac{1}{(1+d)^{yr}}, \text{ where } d \text{ is the discount rate.}$$

$$Loss_{Val} = Loss_T k_{MWh} f_{NPV} \quad (6.7)$$

Additionally, it is noted that the cable temperature changes with the loading experienced by a cable at a given moment. Since the energy production of the wind farm will fluctuate with wind speed, capturing the changes in resistance at different cable temperatures will increase the accuracy of the electrical loss estimation of the array cable layout. Rather than using a fixed value of resistance as in the previous methodology, Chapter 4, a temperature dependant resistance is used, in line with the British Standards for electrical cables (BS IEC 60287) [157], capturing some of the critical influences on cable temperature. The standards consider four thermal resistances to calculate the temperature increase in buried cables. These are:  $T_1$ , the thermal resistance between the conductor and sheath;  $T_2$ , the thermal resistance between the sheath and the armour;  $T_3$ , the thermal resistance of the outer covering; and  $T_4$ , the external thermal resistance. Equation (6.8) describes the thermal resistance between the conductor and sheath (across the cable insulation),  $T_1$ .

$$T_1 = \frac{pT_1}{2\pi} \log\left(1 + 2 \frac{t_1}{d_c}\right) \quad (6.8)$$

where  $pT_1$  is the thermal resistivity of the cable insulation (K.m/W),  $t_1$  is the thickness of the insulation (mm), and  $d_c$  is the diameter of the conductor (mm). As mentioned previously, several other thermal resistances are sometimes calculated for the inner sheath, outer sheath, and soil temperature. These factors have been omitted due to the scarcity of the specific cable and material properties required for the calculations and because - before the layout optimisation has provided a result - limited information is available on the cable paths and therefore the soil types in which they will be buried.

The resistance of the cable at the maximum operating temperature (here  $90^\circ C$ ),  $R_{90}$ , can be found through Equation (6.9).

$$R_{90} = R_0(1 + \alpha_{20}(\theta_m - 20)) \quad (6.9)$$

where  $R_0$  is the resistance of the conductor (at  $20^\circ\text{C}$ ),  $\alpha_{20}$  is the temperature coefficient of resistance of the conductor material, and  $\theta_m$  is the maximum operating temperature of the cable conductor.

Taking into account the heat dissipation through the insulation, the temperature increase of the cable conductor,  $\alpha_\theta$ , may be found through Equation (6.10). Note the di-electric losses per unit length, Equation (6.5) are required.

$$\alpha_\theta = T_1 (0.5 I^2 R_{90} \text{Loss}_{DE}) \quad (6.10)$$

The resultant temperature dependent resistance,  $R_L$ , can now be calculated for the given electrical loading, Equation (6.11), and be used for the calculation of Joule losses and charging current losses.

$$R_L = R_0 (1 + \alpha_{20} \alpha_\theta) \quad (6.11)$$

Calculating the resistance and electrical losses in this way assumes a steady state temperature for a given electrical loading scenario and will miss the dynamics of the cable temperature experienced by an offshore wind farm array cable. A more complete model would also require information about the soil and burial conditions, proximity to other cables, and orientation (flat or trefoil formation). However, the method of electrical loss calculation presented here provides a much more comprehensive estimation of the true losses compared to considering only Joule losses (as in the previous model, Chapter 4).

#### 6.1.4 Substation Connection Costs

Another important addition to the considered costs is the branching or jointing costs associated with cable connections into the substation(s). This cost - different to that of the turbine jointing costs - is included into the model in exactly the same way as the turbine connection costs, presented previously in Equation (4.12) and the objective

function, Equation (4.14). Here, an additional binary variable,  $z_j^c$ , is included that describes whether  $c$  connections are made to the substation  $j$ , ( $z_j^c = 1$  if this is true). Coefficients,  $\gamma_c$ , representing the costs of  $\{1 : c\}$  connections are included into the objective function so the correct branching cost can be accounted for in the optimisation, with the maximum possible substation connections denoted by  $C$ .

$$z_j^c \in \{0, 1\} \quad (6.12)$$

As with turbine jointing costs, an additional constraint equation is required to ensure the correct cost for the number of connections to a substation is attributed to the objective value. This states, the sum of cables entering a substation node must be equal to the sum of the binary jointing variable  $z_j^c$  multiplied by the associated number of connections  $c$ .

$$\sum_{i \in V: i \neq j} y_{i,j} - \sum_{c=1}^C c z_j^c = 0, \quad j \in V_{SS} \quad (6.13)$$

### 6.1.5 Cable Crossing Constraint

In the problem formulation presented in Chapter 4, cables crossing obstacles were removed during pre-processing (noting that Steiner nodes were present in the problem to allow for navigation around them). Also, additional constraint equations were employed to prevent array cables crossing other array cables in the solution. Here, three categories of cable crossing have been employed to account for a wider range of cable crossing scenarios: obstacles, other array cables, and existing site features such as pipes or telecommunication lines that can (or must) be crossed.

#### Site Obstacles

Site obstacles are classified as fixed features that cannot be crossed by a cable. No additional constraints are required beyond the route finding algorithm, Algorithm 9, mentioned previously. This checks cables for crossings of obstacle boundaries and the wind farm boundary, and if necessary generates a route to avoid these through the use

of additional Steiner nodes.

### Array Cables

Array cables crossing other array cables is a complex constraint that depends on what other cables are present in a given solution. To avoid adding a constraint equation for every possible pair of crossing cables, this constraint is handled in the same way as presented in Chapter 4. The optimisation algorithm is run to generate a solution and, if any crossing cable pairs are present, a constraint equation is added to prevent the two specific cables from crossing in future intermediate solutions. The optimisation is then repeated to search the newly constrained solution space.

The additional constraint that must be added to prevent crossing cables is shown in Equation (4.20).

### Existing Cables/Pipes/Telecommunications-Lines

The third possibility for crossing cables to occur is in the presence of existing pipes, cables, or telecommunications lines in the wind farm site. These are handled as site features that can be crossed by the array cables but incur an additional cost in doing so; accounting for the added protection (and its installation) between the cable and the feature. The formulation of the constraint is similar to the additional branching cost at turbines and substations in that a penalty cost is applied rather than a ‘hard constraint’ being generated to prevent it from occurring.

An additional set of variables is required,  $b_q$ , with one variable for each of the existing features in the site,  $q \in Q$ . These variables are constrained to non-negative integer values, representing the number of cables that cross a given feature,  $b_q \in \mathbb{Z}^{0+}$ .

In order to capture the additional cost of a crossing in the objective function, these new  $b$  variables are assigned cost coefficients,  $\gamma_q$ , which are equal to the cost of crossing the feature. Different costs may therefore be used for crossing each different feature of the site by assigning different cost coefficients. An additional constraint equation is required, for each feature  $q$ , to ensure that the value of  $b_q$  represents the true number of cables which cross it. Equation (6.14) shows that the number of routes,  $y_{i,j}$ , that

are used (and that are present in the set of cables crossing the existing site feature,  $(\{i, j\}, q) \in B_{ex}$ ), minus the value of the  $b$  variable for the feature  $q$ , must be equal to zero. This must be true for all features,  $q$ , in the set of site features,  $Q$ .

$$\sum_{(\{i,j\},q) \in B_{ex}} y_{i,j} - b_q = 0, \quad q \in Q \quad (6.14)$$

### 6.1.6 Jack-up Vessel Exclusion Zone

One failure mechanism of subsea array cables is being compressed and damaged by the legs of jack-up vessels. To avoid this, many offshore wind farm sites stipulate that cables must enter and leave turbines at a specific set of allowable angles and travel a certain distance before being allowed to deviate from the prescribed angle and continue on the desired route. This enables jack-up vessels to operate on the sides of the turbines that are known to not have cables entering or leaving the turbine and so minimise the risk of damaging a cable. Tidal currents and a shifting seabed can move the cables over the project lifetime but this method helps to mitigate that risk to a certain extent. This approach requires a change in the cable routes close to the turbines, which was not considered in Chapter 4.

Effectively, there are a new set of obstacles around the turbines in the regions where the jack-up vessels are required to operate. As such, it could be possible to include this constraint by expanding the set of obstacle regions, and employing the route finding algorithm to avoid them. However, rather than including more obstacle regions (and therefore generate more Steiner nodes within the route finding algorithm), the constraint is included separately to minimise the number of obstacle edges and Steiner nodes in the site. A single additional Steiner node is introduced at the end of each cable corridor (from each turbine). The route finding algorithm is adjusted such that any connections to/from a turbine, must first connect to one of its associated Steiner nodes at the end of one of its cable corridors. Figure 6.3 shows an example cable routing connecting a turbine in a string with (left) no cable angle restriction and (right) the effect of the additional constraint of a cable corridor to avoid jack-up vessel operations.

While this is an efficient strategy relative to directly including the jack-up vessel

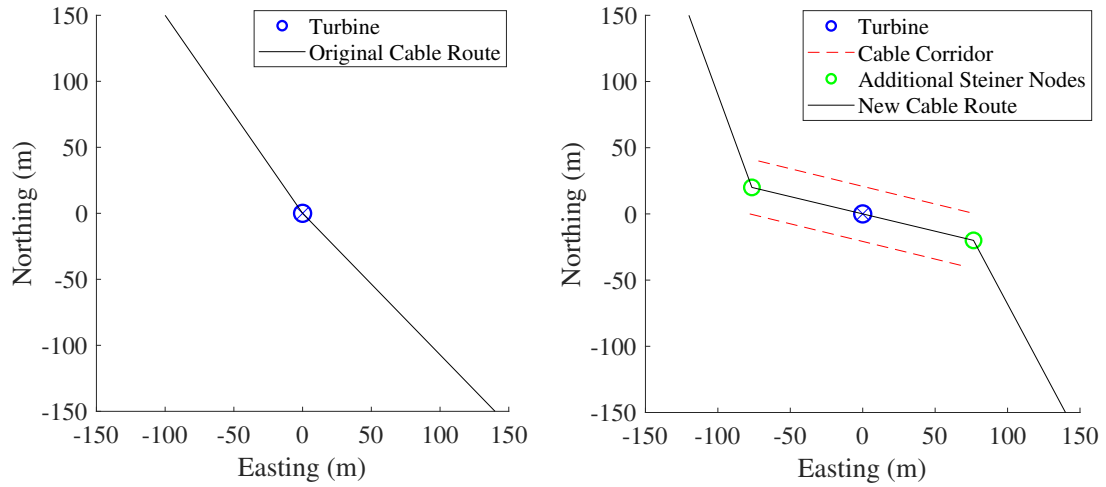


Figure 6.3: An example cable routing connecting a turbine node with (left) no restrictions on the angle of cable connections and (right) the additional cable corridor constraint to avoid jack-up vessel operations.

operating regions as obstacles, it can result in more than one cable sharing the same path through a Steiner node into a turbine node. This is also the case in the route finding algorithm used to navigate around obstacles. Electrical cables such as those used in the array cable network require a minimum spacing in order to avoid heating neighbouring cables and exceeding their thermal limit. As such, the routes generated by this approach may not be exactly suitable and some post-processing of the solution may be required to separate the real cable route to include this minimum separation distance, however this level of route detail is outside the scope of this study.

### 6.1.7 Limiting the Number of Cable Sizes

The model formulation is able to consider any number of cable sizes that may be provided, however, developers may wish to limit the number of cable sizes used in the array cable network to only a few in order to limit the number of cable laying vessels and number of vessel trips to/from the site.

One possible way of including this constraint, would be to introduce a new set of binary variables,  $\tau$ , one for each cable size/type that describes if cable type  $t$  is used anywhere in the cable layout solution ( $\tau_t = 1$ ) or not ( $\tau_t = 0$ ). A constraint

could then be added to stipulate that the sum of these binary variables must be less than or equal to the given number,  $\sum_{t \in T} \tau_t \leq N$ . In order to ensure that the new binary variables are assigned the correct value ( $\{0, 1\}$ ), additional constraint equations are included in the form of  $x_{i,j}^{t,n} \leq \tau_t$  for all routes  $(i, j) \in A$  and for each cable type  $t \in T$ . For context, a site containing 100 turbines, two substations, five cables sizes, and where turbines are allowed to connect to their eight nearest neighbours, would result in an additional 5001 constraint equations by using this formulation of the constraint ( $100 \text{ turbines} \times (8 + 2 \text{ connections}) \times 5 \text{ cable sizes} + 1 \text{ no.-of-cable-sizes constraint}$ ). For the same site, there are approximately 2000 constraints, so this additional constraint would represent a 250% increase in model complexity.

To avoid the potential increase in the number of constraint equations required, an alternative work-around solution is proposed. Here, the optimisation is run with all available cables and no restriction on the number of different cable sizes is employed. When the optimisation is completed and has provided an optimised layout solution, a different decomposition technique is used to find the best cable sizes out of a reduced set, for the given layout. All  $y$  variables, describing which routes have or have not been used by a cable, are fixed and the set of available cables is reduced. Only variables associated with the reduced set of cables are included in the optimisation. Therefore, for each combination of the reduced set of variables, the optimisation is unable to change the cable routing but rather optimises the cable size/type being employed in each section that is built. For an original set of five cables, the number of cable combinations to be tested is equal to  $5CN + 5C(N - 1) + \dots + 5C1$  (where  $C$ , in this instance, represents the mathematical ‘combination’ operator), since  $N$  or fewer cables may be used. For a constraint limiting the site to use up to two cables, this represents 15 cable combinations. Since the cable layout is fixed, it is possible that some of the cable combinations will not contain a cable size large enough to be used on the sections of the layout with a high power flow (i.e. sections closest to the substation). If this is the case, the optimisation is not run and the specific cable combination is recorded as not having sufficient capacity. Once all cable combinations have been tested, the combination with the lowest cost (that has sufficient capacity) is kept for future use and all other

combinations are discarded. Following the cable selection decomposition phase, the full problem (including the cable routing) is optimised using only the selected subset of cables identified in the previous step. The layout optimisation repeats the process of recursive decomposition, considering sub-problems until an optimised layout is found under the newly restricted cable set. More detail of the optimisation process is provided in the following sections.

### 6.1.8 Updating the Objective Function

The objective function in Chapter 4 considered the capital cost the array cable network and the additional cost of jointing branched connections into turbine nodes. This new formulation adds two key elements to the objective function, which are the additional cost of jointing branched connections at substation nodes and the additional cost of cable protection for crossing existing site features such as telecommunication lines.

Equation (6.15) shows the objective function, including the additional cost elements. Jointing costs at substation nodes,  $\gamma_c$ , are included for the corresponding number of substation joints,  $z_j^c$ , for each substation,  $j \in V_{SS}$ . The cost of crossing existing site features,  $\gamma_q$ , is multiplied by the number of crossings of a given feature,  $b_q$ , for all existing site features,  $q \in Q$ . The objective function aims to minimise overall cost, considering cable unit costs, electrical losses (included in  $c_{i,j}^{t,n}$  terms), turbine jointing costs, substation jointing costs, and protection costs for crossing existing site features.

$$\min F = \min \left[ \sum_{(i,j) \in A} \sum_{t \in T} \sum_{n \in \{1:kmax\}} c_{i,j}^{t,n} x_{i,j}^{t,n} + \sum_{h \in H} \gamma_h \sum_{j \in V_T} w_j^h + \sum_{c \in C} \gamma_c \sum_{j \in V_{SS}} z_j^c + \sum_{q \in Q} \gamma_q b_q \right] \quad (6.15)$$

### 6.1.9 The MILPsp Algorithm

The MILPsp algorithm has been split into four key phases for clarity: (1) creating a seed solution, (2) recursive decomposition, (3) cable selection, and (4) recursive decomposition with a reduced cable set. Pre- and post-processing are also included at the

start and end of the algorithm respectively. Figure 6.4 shows a flowchart representation of the four phases of the algorithm.

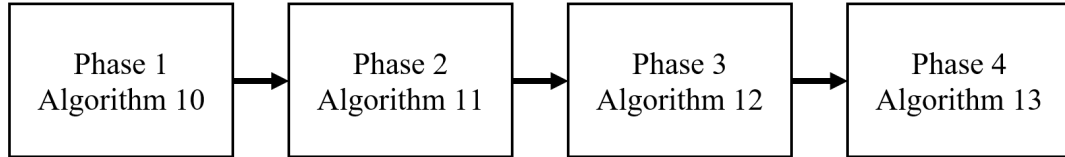


Figure 6.4: Flowchart showing the four phases of the MILP algorithm.

The MILP algorithm is logically split into the four phases out of necessity. Recursive decomposition (the MILP algorithm with decomposition strategy) is the main part of the algorithm, described in Phase 2. The cable constraint, introduced previously in Section 6.1.7, is applied in a following phase, Phase 3, to avoid a large increase in the number of constraint equations to be handled by the algorithm. Once the cable constraint has been applied, and the optimal cable sizes are selected, the recursive decomposition is repeated, Phase 4, to find the optimal cable layout solution using the reduce set of selected cable sizes. The algorithm is also provided with seed solutions, Phase 1, to ensure good quality solutions are available as a starting point for the recursive decomposition. This phase is split for clarity but is much the same as Phase 2, in that sub-problems are solved to generate a solution. However, with no incumbent solution for Phase 1, a k-means clustering algorithm is used to select turbines for sub-problems (rather than selecting strings from an incumbent solution).

### MILPsp: Phase 1

Phase 1 begins with the pre-processing phase, creating all of the variables for the cable layout design problem including the route finding algorithm, Algorithm 9, for route lengths. Next, a k-means clustering algorithm is used to group turbines based on their angle from the wind farm geometric centre,  $\theta_t$ . These groups of turbines form the initial sub-problems groups,  $V_{cut}$ , which when solved and combined, form a seed solution used to seed the MILP algorithm. For each sub-problem, the variables corresponding to that sub-problem are identified as a reduced set (or cut set) of the full set of variables. A

classical MILP model is built, including constraint equations, for the subset of variables in the given sub-problem. The cut set of variables is optimised and the solution recorded. Once all sub-problems have been optimised, the solutions are combined into a seed solution of the full problem,  $F_{incumbent}$ . This is analogous to the approach proposed in Chapter 4 for seeding the ACOsp method, where the site is broken up into a set of initial sub-problems to be solved. Figure 6.5 summarises this process in flowchart format, and Algorithm 10 provides additional detail in algorithmic format.

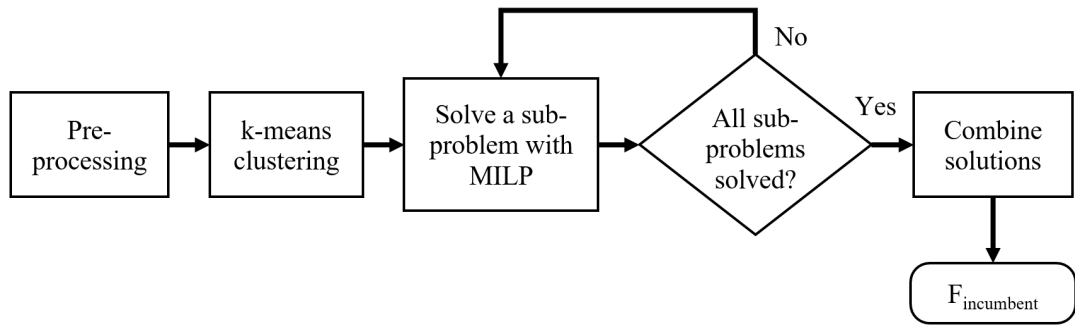


Figure 6.5: Flowchart of the key processes in Phase 1 of the MILPsp algorithm.

---

**Algorithm 10** MILPsp Phase 1: Creating a seed solution

---

Pre-processing, including Algorithm 9  
 Create incumbent solution,  $\theta_0 = 0 \text{ rad}$   
 Initialise turbine group centres,  $\theta_1 \quad 0 < \theta_1 < 2\pi$   
**while**  $\theta_0 \neq \theta_1$  **do**  
     Update incumbent solution,  $\theta_0 = \theta_1$   
     Assign turbines,  $t \in T$ , to their closest group centre,  $\theta$   
     Calculate the average angle of each group of turbines,  $\theta_t$   
     Move each group centre to the average angle of the turbines in the group,  $\theta_1 = \theta_t$   
**end while**  
 Output groups of turbines as initial sub-problems,  $V_{cut}$   
**for** Each sub-problem,  $V_{cut}$  **do**  
     Select subset,  $x_{i,j}^{t,n}, y_{i,j}, p_{i,j}, w_j, z_j, b_q, \quad i, j \in V_{cut}, t \in T, n \in N_{turb}, q \in Q$   
     Build MILP model, Sections 6.1.1 -6.1.8  
     Find  $\min F$ , Equation (6.15)  
**end for**  
 Combine solutions,  $F$ , from all sub-problems,  $V_{cut}$ , to create  $F_{incumbent}$

---

**MILPsp: Phase 2**

Phase 2 forms the recursive decomposition section of the algorithm, solving a new set of sub-problems and using the incumbent solution to seed an initial solution for the sub-problem. An all-zero square matrix, with dimensions equal to the number of strings in the incumbent solution, is created. While there are still cells in the matrix whose value is equal to zero, the algorithm will continue. A pair of strings, which have not yet been considered together, are selected to form a new sub-problem and the subset of variables required are isolated for optimisation. Only those variables with both of their corresponding turbines (i.e. start and end nodes) are kept in the sub-problem. This is a slightly different - and more constrained - version of the sub-problem creation described in Chapter 4 and therefore turbines in the sub-problem may not connect to other turbines outwith the sub-problem. This method is chosen as including variables to allow the connection to nodes outside of the sub-problem greatly increases the complexity of the formulation when using a MILP-based algorithm (as all variables would be required by the solver, with additional constraints to fix the non-sub-problem variables). Upon solving the optimisation problem for the sub-problem for the first time, a check is carried out for the presence of crossing cables in the whole site (not just the sub-problem). If crossing cables have been added, the algorithm builds a constraint equation to prevent both arcs in the crossing pair from being built and the problem is re-solved under the newly constrained condition. If no improvement

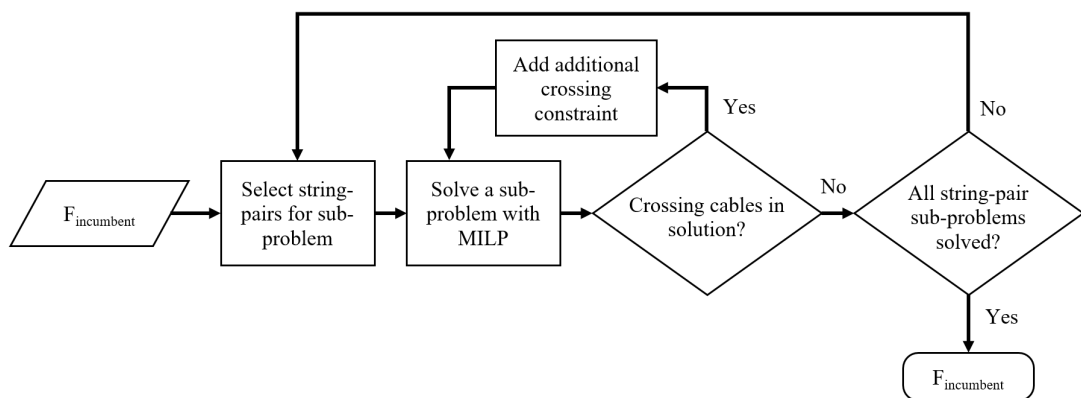


Figure 6.6: Flowchart of the key processes in Phase 2 of the MILPsp algorithm.

could be found over the incumbent solution, the string pair are recorded accordingly in the improvement matrix ( $improvement(str1, str2) = 1$ ). However, if the solution has improved, the incumbent solution is updated to the newly improved solution, and strings are renumbered if the number of strings has changed (for example, if two strings merge into a single string). When improvements cease to be found, the incumbent solution can be carried forward to the third section of the algorithm. Figure 6.6 and Algorithm 11 show the key processes of Phase 2 in flowchart format and algorithmic format respectively.

---

**Algorithm 11** MILPsp Phase 2: Recursive decomposition

---

```

Initialise string-pair improvement,  $I = zeros(N_{str}, N_{str})$ 
while  $\sum I \neq N_{str}^2$  do
    Select string pairs not yet considered,  $str1, str2$ 
    Select subset  $x_{i,j}^{t,n}, y_{i,j}, p_{i,j}, w_j, z_j, b_q, \quad i, j \in V_{str1, str2}, t \in T, n \in N_{turb}, q \in Q$ 
    Initialise  $crossing = 1$ 
    while There are crossing cables,  $crossing = 1$  do
        Build MILP model, Sections 6.1.1 -6.1.8
        Find  $min F$ , Equation (6.15)
        if The sub-problem solution has improved,  $F < F_{incumbent}$  then
             $I(str1, :) = I(:, str1) = I(str2, :) = I(:, str2) = 0$ 
            Update incumbent solution,  $F_{incumbent} = F$ 
        else
             $I(str1, str2) = 1, I(str2, str1) = 1$ 
        end if
    end while
end while

```

---

**MILPsp: Phase 3**

Phase 3 of the MILPsp algorithm considers a different formulation of the problem decomposition in order to optimise the sizes of cables to be used in the incumbent solution. This section of the algorithm is only required if a limit is applied to the number of cable sizes allowed in the final solution, which is less than the set of cables provided to the model. If a cable limit is provided, all combinations of  $N$  cables will be generated, to create the new sub-problems groups (here grouping cable sizes rather than turbines). For each combination of cables, the algorithm isolates the variables associated with the cable sizes in the subset and removes those that are associated with

other cable sizes or routes that are not used in the incumbent solution. The solver optimises the subset of variables and records the objective values. If a cable subset does not contain sufficient capacity for the layout in the incumbent solution, this cable subset will not be carried forward. The valid cable combination with the lowest objective value is chosen for the final phase of the algorithm. Figure 6.7 and Algorithm 12 show the key processes of Phase 3 in flowchart and algorithmic format respectively.

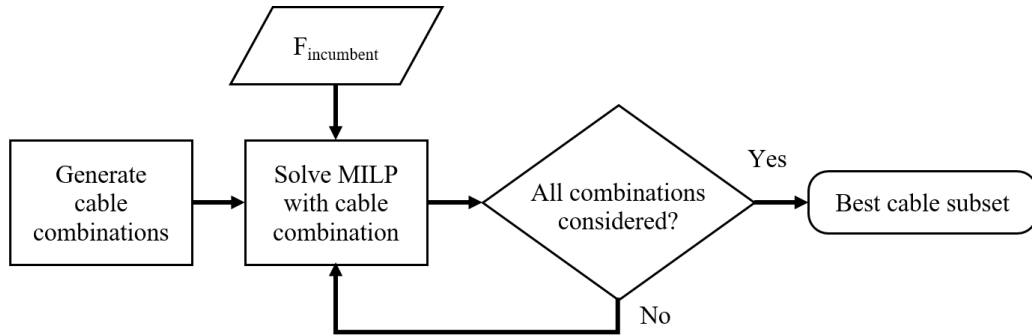


Figure 6.7: Flowchart of the key processes in Phase 3 of the MILPsp algorithm.

---

**Algorithm 12** MILPsp Phase 3: Cable selection

---

Generate cable combinations,  $T_{cut}$   
**for** Each combination of cables,  $T_{cut}$  **do**  
    Select subset  $x_{i,j}^{t,n}, y_{i,j}, p_{i,j}, w_j, z_j, b_q, \quad (i,j) \in A_{built}, t \in T_{cut}, n \in N_{turb}, q \in Q$   
    Build MILP model, Sections 6.1.1 -6.1.8  
    Find  $\min F$ , Equation (6.15)  
**end for**  
Output cable subset to use,  $T_{cut}$

---

**MILPsp: Phase 4**

Having selected the optimal cable type for the incumbent solution, it may be possible that the optimal layout using only the chosen cable subset is slightly different to the previous incumbent solution. As such, Phase 4 considers the recursive decomposition, as in phase 2 (Algorithm 11), to search for improvements in the solution. This phase is a repeat of Phase 2 with the subset of variables reduced further, to include only cables in the chosen subset,  $T_{cut}$ . Figure 6.8 shows a flowchart of the processes in Phase 4,

which can be seen to be similar to Phase 2 in Figure 6.6. Additional detail is provided in Algorithm 13.

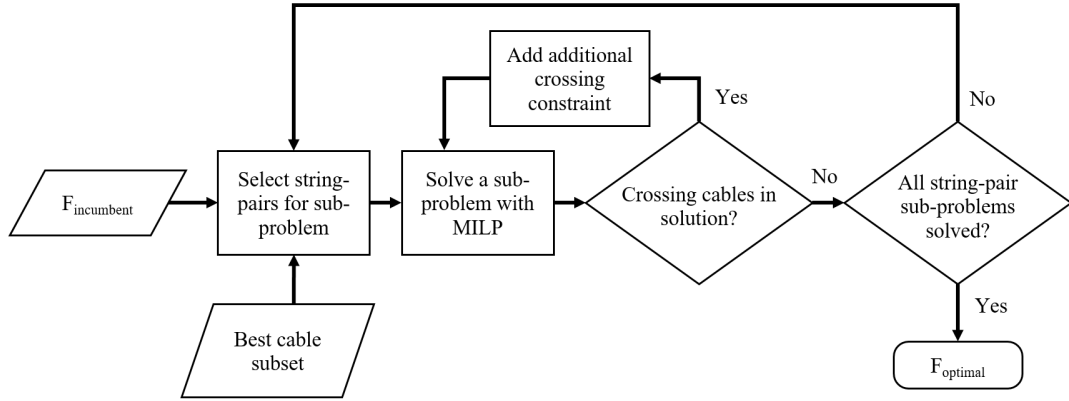


Figure 6.8: Flowchart of the key processes in Phase 4 of the MILPsp algorithm.

---

**Algorithm 13** MILPsp Phase 4: Recursive decomposition with reduced cable set

---

Initialise string-pair improvement,  $I = \text{zeros}(N_{str}, N_{str})$   
**while**  $\sum I \neq N_{str}^2$  **do**  
  Select string pairs not yet considered,  $str1, str2$   
  Select subset  $x_{i,j}^{t,n}, y_{i,j}, p_{i,j}, w_j, z_j, b_q, \quad i, j \in V_{str1, str2}, t \in T_{cut}, n \in N_{turb}, q \in Q$   
  Initialise  $crossing = 1$   
  **while** There are crossing cables,  $crossing = 1$  **do**  
    Build MILP model, Sections 6.1.1 -6.1.8  
    Find  $\min F$ , Equation (6.15)  
    **if** The sub-problem solution has improved,  $F < F_{incumbent}$  **then**  
       $I(str1, :) = I(:, str1) = I(str2, :) = I(:, str2) = 0$   
      Update incumbent solution,  $F_{incumbent} = F$   
    **else**  
       $I(str1, str2) = 1, I(str2, str1) = 1$   
    **end if**  
  **end while**  
**end while**  
Output best solution,  $\min F$   
Post-processing

---

## 6.2 Case Studies

Two case studies are conducted covering (1) the hypothetical site previously presented in Section 4.3.1, and (2) an expanded case study based on the same hypothetical site with the addition of features that the MILPsp is able to consider above and beyond those considered by the three cable layout optimisation algorithms from Chapter 4. To enable a comparison to the previous optimisation methods presented in Chapter 4, the same hypothetical offshore wind farm site is used for the first case study, with the full set of 122 turbines, and any additional parameters used by the MILPsp method set to zero (or values to nullify their impact), even if unrealistic. The second, extended version of the site is used to test the additional functionality of the MILPsp method presented in this chapter, and considers the additional parameters of the MILPsp algorithm with realistic non-zero values.

### 6.2.1 Hypothetical Offshore Wind Farm

While the first case study is the same as that presented in Section 4.3.1, the proposed MILPsp design algorithm requires some additional input parameters. These additional parameters have been set to minimise the impact on this case study to allow for a close comparison with the MILP method presented in Section 4.2.3, however some unavoidable differences will remain (such as the different method of Steiner node generation). In order to minimise the impact of the additional parameters included in the MILPsp model, many are set equal to zero which can be an unrealistic value for the given parameter, but is necessary to enable comparison with the three algorithms presented in Chapter 4. The site contains 122 turbines, with a complete set of coordinates provided in the Appendix, Table A.10.

The additional input parameters (present in the MILPsp method and not in the MILP method) and their corresponding values (which are chosen to minimise their impact) are: cable corridor angles,  $\theta_{JU}$ , in line with the rows of turbines at  $48^\circ$  and  $228^\circ$ ; cable corridor length,  $dist_{JU}$ , of  $0.001m$ ; maximum number of substation connections,  $C$ , equal to the number of turbines in the site (122); substation jointing costs,  $\gamma_{SS}$ , of

$\pounds 0$  per connection; maximum number of cable sizes allowed in a solution,  $N_{max}$ , set to 3 (of three available cables, therefore effectively no limitation); Steiner grid resolution,  $Res_{St}$ , equal to the turbine rotor diameter ( $164m$ ); cable length threshold,  $dist_{thresh}$ , of *infinity* ( $m$ ); cable length multiplier,  $L_{cab}$ , of 1; power factor,  $P_{fac}$ , of 1; cable insulation loss factors,  $tan_d$ , of 0 for all cable sizes; temperature coefficient of resistivity of the conductor,  $\alpha_{20}$ , equal to  $0 K^{-1}$  for all cable sizes; cable insulation thermal resistivity,  $pT_1$ , equal to  $0 K.m/W$  for all cable sizes; cable insulation thickness,  $t_1$ , of  $0 mm$  for all cable sizes; maximum operating temperature,  $\theta_m$ , of  $90^\circ C$  for all cable sizes; and the cost of crossing any existing site features,  $\gamma_q$ , equal to  $\pounds 0$ .

Additional cable specific values must also be included in the MILPsp model. These are summarised in Table 6.1, where cable capacity, unit cost, and resistance are set to the same values as those used in Chapter 4, and all remaining values set equal to zero to nullify their impact as they were not included in the MILP method presented in Chapter 4.2.3. (Note: These input parameters are set to representative, non-zero, values in the expanded case study presented in the following section).

Table 6.1: Representative cable parameters for hypothetical site

Capacity (MW)	Unit cost (£/m)	Capacitance per core per unit length ( $\mu F/km$ )	AC resistance per unit length ( $\Omega/m$ )	Sheath loss factor (-)	Armour loss factor (-)
60	1400	0	0.00120	0	0
90	1750	0	0.00056	0	0
100	1870	0	0.00044	0	0

### 6.2.2 Expanding the Hypothetical Offshore Wind Farm Case

The expanded hypothetical offshore wind farm site considers the additional functionality of the MILPsp method over those presented in Chapter 4. Figure 6.9 shows the hypothetical site, which is largely unchanged except for the addition of two existing site features which may be pipelines, existing cables, or telecommunication lines and which incur an additional cost if crossed by array cables. Details of the coordinates of these features is provided in the Appendix, Table A.15.

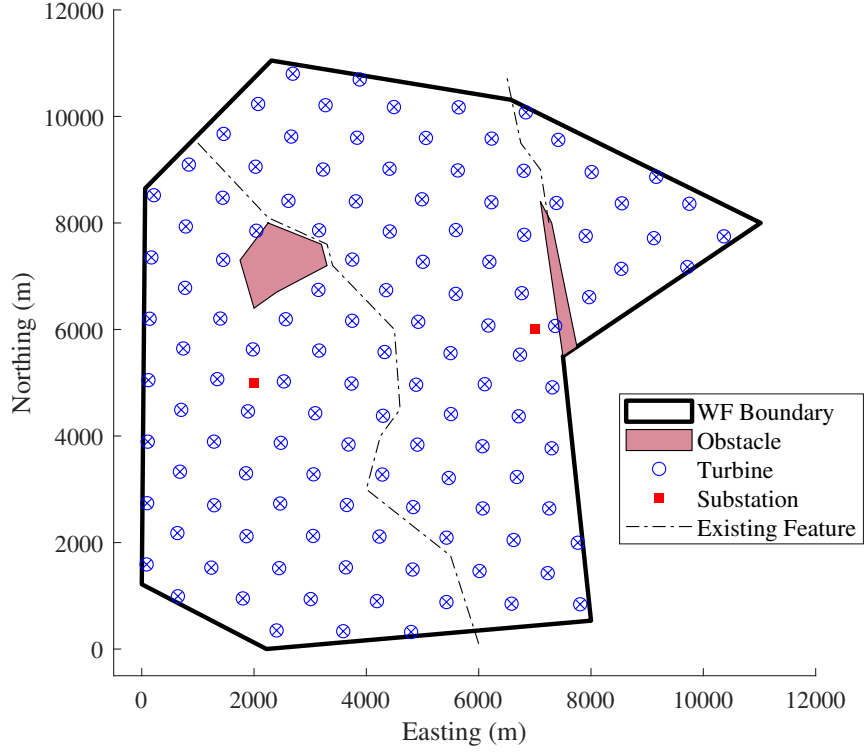


Figure 6.9: The updated hypothetical GW-scale offshore wind farm test case, including existing site features (Steiner nodes omitted for clarity).

The additional parameters for the expanded hypothetical site case study are as follows: cable corridor angles,  $\theta_{JU}$ , in line with the rows of turbines at  $48^\circ$  and  $228^\circ$ ; cable corridor length,  $dist_{JU}$ , of  $123m$  (1.5 times the rotor radius); maximum number of substation connections,  $C_{SS}$ , equal to 6; substation jointing costs,  $\gamma_{SS}$ , of  $\pounds 90.7k$  per connection [79]; maximum number of cable sizes allowed in a solution,  $N_{max}$ , set to 5 (from a set of nine provided, discussed further later); Steiner grid resolution,  $Res_{St}$ , equal to the turbine rotor diameter ( $164m$ ); cable length threshold,  $dist_{thresh}$ , of  $15km$ ; cable length multiplier,  $L_{cab}$ , of 1.05; power factor,  $P_{fac}$ , of 0.9; cable insulation loss factors,  $tan_d$ , of 0.001 for all cable sizes; temperature coefficient of resistivity of the conductor,  $\alpha_{20}$ , equal to  $0.00393 K^{-1}$  and  $0.00403 K^{-1}$  for all cable sizes of copper and aluminium conductors respectively (discussed further later); cable insulation thermal resistivity,  $pT_1$ , equal to  $3.5 K.m/W$  for all cable sizes; cable insulation thickness,  $t_1$ ,

of 11 *mm* for all cable sizes; maximum operating temperature,  $\theta_m$ , of  $90^\circ C$  for all cable sizes; and the cost of crossing any existing site features,  $\gamma_q$ , equal to  $\pounds 250k$  for both features.

The additional cable specific values required by the model, provided by Scottish Power Renewables (SPR), can be seen in Tables 6.2 & 6.3. Representative values were provided for a set of nine copper conductor cables and nine aluminium conductor cables. In addition to cable capacities, costs, and resistances, values for the capacitance and sheath and armour loss factors were also included to provide a more accurate analysis of the electrical losses. Two case studies were completed for the expanded hypothetical offshore wind farm site, one with the set of copper cables and one with the set of aluminium cables.

Table 6.2: Representative copper cable parameters.

No.	Conductor area (mm <sup>2</sup> )	Capacity (MW)	Unit cost (£/m)	Capacitance per core per unit length ( $\mu F/km$ )	AC resistance per unit length ( $\Omega/km$ )	Sheath loss factor (-)	Armour loss factor (-)
Cu1	150	44.6	447	0.1757	0.1343	0.075	0.102
Cu2	185	49.6	460	0.1866	0.1077	0.092	0.128
Cu3	240	56.3	481	0.2040	0.0824	0.117	0.169
Cu4	300	62.3	504	0.2213	0.0663	0.143	0.212
Cu5	400	69.1	542	0.2434	0.0527	0.176	0.270
Cu6	500	75.8	580	0.2619	0.0421	0.217	0.339
Cu7	630	82.8	629	0.2931	0.0340	0.262	0.421
Cu8	800	89.1	694	0.3207	0.0282	0.310	0.508
Cu9	1000	94.4	770	0.3482	0.0242	0.355	0.590

### 6.3 Results & Discussion

This section outlines the results of the two case studies, (1) the hypothetical site with comparison to the case study in Section 4.3.1, and (2) an extended version of the same problem with the set of copper cables and with the set of aluminium cables.

Table 6.3: Representative aluminium cable parameters.

No.	Conductor area (mm <sup>2</sup> )	Capacity (MW)	Unit cost (£/m)	Capacitance per core per unit length ( $\mu\text{F}/\text{km}$ )	AC resistance per unit length ( $\Omega/\text{km}$ )	Sheath loss factor (-)	Armour loss factor (-)
A11	150	35.3	407	0.1742	0.2229	0.045	0.061
A12	185	39.7	411	0.1866	0.1776	0.056	0.077
A13	240	45.4	418	0.2040	0.1357	0.071	0.102
A14	300	50.6	425	0.2191	0.1089	0.087	0.129
A15	400	56.9	436	0.2384	0.0853	0.109	0.166
A16	500	63.5	448	0.2584	0.0670	0.136	0.212
A17	630	70.6	462	0.2847	0.0529	0.169	0.270
A18	800	77.5	482	0.3143	0.0426	0.206	0.335
A19	1000	84.0	505	0.3468	0.0352	0.244	0.403

### 6.3.1 Hypothetical Offshore Wind Farm

Similarly to Chapter 4, the MILPsp algorithm was run on a range of number of turbines (from ten to the full site of 122) to explore how effectively the method performs for different size problems and to enable better comparison with the previous three methods, Section 4.2. A set of ten simulations was completed for each of the six problem sizes to explore the consistency of solutions. A full set of results of the MILPsp algorithm is provided in the Appendix, Table A.16, where it can be seen that all ten solutions were identical across all six problem sizes considered, while Table 6.4 provides a summary of the MILPsp objective values for each of the six problem sizes. Producing identical solutions was not something that the ACO and ACOSP algorithms were always able to achieve in the earlier investigation due to their heuristic nature. The MILPsp algorithm also includes heuristic components within the problem decomposition, however by informing the decomposition technique with the specific problem formulation (the string layouts in the incumbent solution), it appears that the heuristic components are not reducing the reliability of solutions.

Table 6.4 shows the results of the three optimisation algorithms presented previously (MILP, ACO, and ACOSP) and the newly proposed MILPsp algorithm. As mentioned previously, the optimisation problem is not identical due to some small changes to the problem formulation and so a direct comparison of the objective values between the

previous three algorithms and the new MILPsp algorithm cannot be made. In order to allow for a more direct comparison between the approaches, the optimality ratios can be considered, also presented in Table 6.4.

In order to determine the optimal solutions to the new formulation of the hypothetical site case study (for finding the optimality ratio of the MILPsp solutions), an adapted MILP code is used whereby an exhaustive list of constraint equations is applied to the full optimisation problem (no decomposition into sub-problems). This method is described as a potential alternative approach in Section 6.1.7 and was not used in the MILPsp algorithm due to the vast number of additional constraint equations required. The approach, while computationally inefficient, is able to determine the optimal solution for the cases smaller than 122 turbines, enabling the optimality ratio to be calculated for the MILPsp solutions. In the full case of 122 turbines, 3,161 constraint equations were required to describe the problem fully, and with the additional limit to the number of cables, this was increased to 40,572 constraint equations - an increase of 37,411 (1,184%). It is worth noting, that the optimal solution for the largest case of 122 turbines could not be found before the computational memory of the desktop PC was exceeded and the search stopped prematurely. The relative gap (the relative difference between the upper and lower bounds between which the optimal solution is known to be) at the end of the search was 1.363%, with the MILPsp solution's objective value equal to that of the upper bound. Therefore it is possible that the MILPsp solution has an optimality ratio of up to 1.014 (1.4% more expensive than the optimal solution) in the worst case scenario. All other sizes of case study can be seen in Table 6.4 to have an optimality ratio of 1.000, the optimal solution.

Figure 6.10 shows the solutions of the MILP algorithm (left) and the MILPsp algorithm (right) for the 122 turbine case. It can be seen in the figure that both solutions are largely similar in layout and cable selection, with the most similarities exhibited in strings towards the outer edges of the site. This is perhaps due to the reduced options for alternative cable routings at the edges of the site given the wind farm boundary, and because there are fewer close neighbouring strings for turbines to connect to. In the centre of the wind farm, there is slightly more variability between the two solutions,

Table 6.4: Objective values and optimality ratio of the MILPsp algorithm with comparison to the three algorithms presented in Chapter 4. (Results in italics indicate an unfinished result).

No. turbines	Objective value (£) and Optimality ratio			
	Chapter 4 approaches			Chapter 6 MILPsp
	MILP	ACO	ACOsp	
10	22,064,833 (1.000)	22,667,188 (1.027)	22,068,446 (1.000)	22,375,329 (1.000)
15	30,945,049 (1.000)	31,075,301 (1.004)	30,945,049 (1.000)	31,535,171 (1.000)
25	50,235,935 (1.000)	51,473,967 (1.025)	50,750,255 (1.010)	50,599,172 (1.000)
40	68,683,109 (1.000)	69,693,934 (1.015)	69,678,545 (1.014)	69,241,766 (1.000)
61	103,255,681 (1.000)	110,766,917 (1.073)	104,651,892 (1.014)	103,943,119 (1.000)
122	<i>197,401,005</i> (1.000)	212,339,986 (1.076)	199,301,590 (1.010)	198,199,811 (1.000 - 1.014)

possibly as there are many more neighbouring strings offering reasonable alternative connections (of very similar length and cost) to turbines in this area. This will particularly be the case in wind farms that are arranged in a regular grid-like layout, since the distance between turbines is likely to be similar, if not exactly the same. If distances between rows and columns of turbines are identical, then there will be several different optimal cable layout solutions that all share the same objective value. Towards the outer edges of the wind farm, there are fewer neighbouring turbines/strings and irregular features such as the wind farm boundary itself, which reduces the likelihood of there being multiple optimal solutions for these sections of the wind farm. Differences in the solutions, therefore, may be due to the presence of multiple solutions sharing an optimal objective value. As mentioned previously, some uncertainty remains in the optimality of the solutions to the 122 turbines case, both in the MILP solution and MILPsp solution. This variation between layouts may also therefore be due to the solutions both being close to optimal but terminating at different, near-optimal solutions.

Considering computational time, Table 6.5 shows the time for each of the four algorithms across the range of case study sizes. For the three largest cases (40, 61,

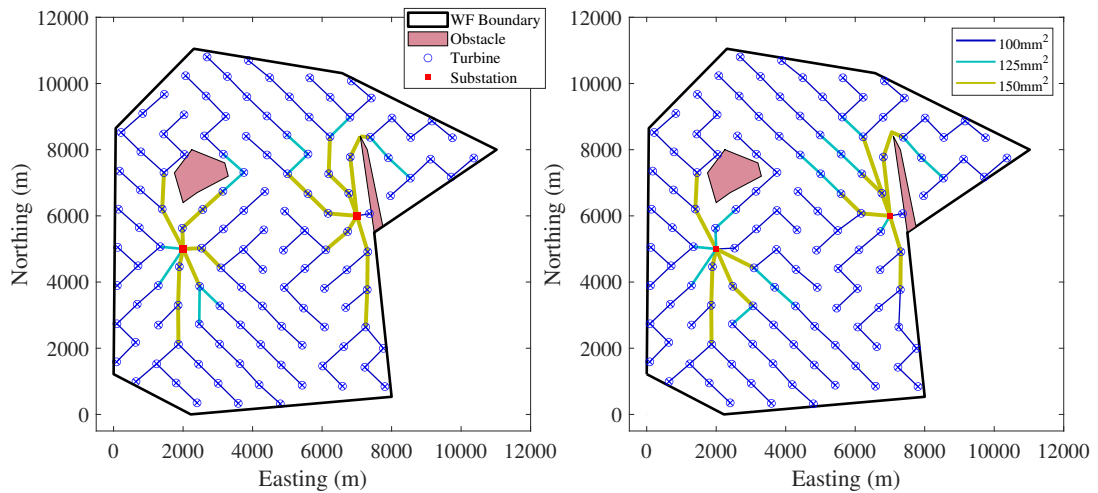


Figure 6.10: Solutions of the MILP algorithm from Chapter 4 (left) and the MILPsp algorithm (right).

and 122 turbines) the MILPsp algorithm has the second quickest computational time, beaten only by the classical ACO algorithm. Indeed, it is able to produce solutions to the largest case study in approximately 1 hour 42 minutes. These low computational times, combined with the better (lower objective value) solutions compared to the ACO-based algorithms, demonstrates that the MILPsp algorithm is a very effective tool for solving large-scale array cable layout optimisation problems on a standard desktop PC.

Table 6.5: Computational time of the MILPsp algorithm with comparison to the three algorithms presented in Chapter 4. (Results in italics indicate an unfinished result).

No. turbines	Computational time (s)			
	MILP	ACO	ACOsp	MILPsp
10	3	5	53	11
15	9	8	46	20
25	31	18	133	42
40	204	51	489	129
61	951	164	1517	606
122	<i>13717</i>	833	9991	6133

Overall, this case study demonstrates that the MILPsp method preserves the good quality of the MILP solutions but at a lower computational cost. With the computational time being non-linear with respect to the number of variables in the optimisation, decomposing the problem into many smaller sub-problems takes advantage of this scal-

ing relationship; i.e., the sum of the computational time and resource required to solve many smaller sub-problems is less than that required to solve a single large (full) optimisation problem. The formulation of the decomposition strategy - selecting sub-problems based on information of the incumbent solution (rather than a random subset of variables) - maximises the possibility of the algorithm finding improvements to the solution in each sub-problem and approaching the optimal objective value.

### 6.3.2 Expanded Hypothetical Offshore Wind Farm Case

A set of different optimisation simulations were conducted on the expanded hypothetical offshore wind farm site, similar to the hypothetical site case study, Section 6.3.1. These covered a range in the number of turbines from ten turbines to the full site of 122 turbines. The optimisation was also conducted first with a set of copper cables and again with a set of aluminium cables, with all other inputs remaining the same. The optimal solution was again found through an alternative MILP approach outlined in Section 6.1.7. Some of the cases, typically 40 turbines or more, struggled to reach a proven optimal solution and so some uncertainty remains on the efficacy of the tool solutions.

#### Copper Conductors

Table 6.6 shows the solutions of the MILPsp tool on the case using copper cables. When an optimal solution was not provable given the computational limitations, this uncertainty manifests as a ‘relative gap’ between the possible upper and lower bounds, where the upper bound is a known solution and the lower bound is the lowest possible solution in the set yet to be investigated. It can be seen in Table 6.6 that all the cases between 10-40 turbines reached the optimal solution, while the case of 61 turbines was 0.4% more expensive than the optimal solution to the problem. The optimal solution to the case of 122 turbines was not provable, leaving a relative gap between the upper and lower bound estimates, and therefore a range of optimality ratios is provided for the tool solution. Interestingly, the tool solution to the case of 122 turbines contains a large penalty cost (£1B) from violating the ‘soft constraint’ on the number of substation

connections. Despite the large incentive to avoid violating the constraint, it appears that the tool was unable to avoid this additional penalty cost. The layout solution, discussed further later, was unable to reduce the number of substation connections through the use of two-string sub-problems, despite it being technically possible to connect all 122 turbines using six connections at each substation (as the largest cable could support up to 11.8 turbines numerically). It therefore suggests that a slightly different approach to sub-problem formulation may be necessary in certain circumstances such as this where the substation connection constraint is close to the optimal solution. A possible modification may be to expand the sub-problem creation to consider the turbines of three strings rather than two when this constraint remains violated in the would-be final solution. This would increase the solution space explored by the algorithm and increase the probability of finding an improved solution that reduces the number of substation connections to within the constraint limits.

Table 6.6: Objective values of the MILPsp algorithm on the copper cable case study, for a range of number of turbines with comparison to optimal solution estimates.

No. turb.	Optimal objective value (£)		MILPsp objective value (£)	Optimality ratio range		Comp. time (s)
	Upper bound	Lower bound				
10	8,312,632	8,312,632	8,312,632	1.000	1.000	148
15	11,421,551	11,421,551	11,421,551	1.000	1.000	197
25	17,900,268	17,900,268	17,900,268	1.000	1.000	272
40	25,244,439	25,244,439	25,244,439	1.000	1.000	783
61	37,682,971	37,682,971	37,846,855	1.004	1.004	2,867
122	1,070,336,475	68,538,995	1,070,336,475 <i>70,336,475</i>	1.000	15.616 <i>1.026</i>	39,005

The last row in Table 6.6 shows the optimality ratio of the solution to the 122 turbine case if the penalty cost was not applied. Since the solution cannot have a lower cost than the optimal solution, the optimality ratio ranges from 1.000 to the worst case scenario of 1.026 (2.6% more expensive than the optimal solution). This shows that the poor (very high) optimality ratio of the penalised solution is not as bad as it might appear upon first inspection. However, if the penalty cost was avoided in the solution, the layout (and therefore cost/objective value) may be quite different from

the solution the tool produced and so this optimality ratio range must be considered to be only indicative of the tool performance. Combined with a simple visual inspection of the solution, it does appear that the tool generates good quality solutions, despite struggling with the substation connection limit.

Unlike the first case study considering the original hypothetical site, this expanded case study included a limit to the number of cable sizes allowed in the final solution (in addition to new site features and additional parameters considered by the MILPsp approach, presented in Section 6.2.2). One significant impact of this constraint is that an additional section of the algorithm is employed to determine the optimal cable subset selection (Section 6.1.9, Phase 3 of the MILPsp algorithm). Part of the impact of employing this section of the algorithm is that the computational times increase significantly with the problem size, Table 6.6. While this second case study isn't identical to the first case study, presented in the previous section, it can be seen that the computational times of the MILPsp algorithm are much larger when the cable limiting section (Phase 3) of the algorithm is employed, Table 6.6, compared to when it is not, Table 6.5, for each equivalent number of turbines. Despite this larger computational time, the largest case of 122 turbines is completed in under 11 hours, which is considered to be acceptable for such a fundamental design phase of an offshore wind farm.

### **Aluminium Conductors**

Table 6.7 shows the results of the expanded hypothetical offshore wind farm site using the aluminium cable set. Similarly to the study using copper cables, the tool solutions largely reach the optimal solution, with the exception of the 40 turbines case that costs 0.1% more than the optimal solution. The case of 122 turbines was again penalised for violating the constraint on the number of substation connections. However, when trying to determine the optimal solution for comparison, the adapted MILP solver for doing so seemed to suggest that the optimal solution to this problem also contained the same penalty. In theory, the largest aluminium cable could support up to 10.5 turbines and so if each substation had six connections to avoid the penalty, only 120 turbines could be connected. There is therefore no valid solution to this problem that avoids

the penalty cost. Considering this fact, the tool was still able to generate a solution that was, at worst, only 0.2% (or 3.6% if the penalty cost component is ignored) more expensive than the optimal solution. No better solution was found, however, and so the tool may indeed have found the optimal solution for this problem.

Table 6.7: Objective values of the MILPsp algorithm on the aluminium cable case study, for a range of number of turbines with comparison to optimal solution estimates.

No. turb.	Optimal objective value (£)		MILPsp objective value (£)	Optimality ratio range		Comp. time (s)
	Upper bound	Lower bound				
10	7,507,294	7,507,294	7,507,294	1.000	1.000	74
15	10,403,701	10,403,701	10,403,701	1.000	1.000	111
25	16,189,889	16,189,889	16,189,889	1.000	1.000	204
40	22,877,121	22,877,121	22,890,725	1.001	1.001	798
61	34,471,540	34,471,540	34,471,540	1.000	1.000	2,191
122	1,063,923,966	1,061,611,560	1,063,923,966 <i>63,923,966</i>	1.000	1.002 <i>1.000 1.036</i>	18,559

The computational times for the aluminium cable cases are very similar to the copper cable cases, which would be expected as for both problems the number of cables was limited to five out of the available nine. This meant there was the same 129 possible cable combinations for the algorithm to consider. However, the largest case of 122 turbines took approximately half as long when using aluminium cables compared to copper cables. This suggests that the algorithm, upon selecting the best cable combination to use, found further improvements in the copper cables case and therefore repeated much of the recursive decomposition with the chosen cable subset, increasing the computational time. The aluminium cables case, however, appears to have not found any improvements over the intermediate solution created by the initial recursive decomposition and cable selection phases. Therefore, the second recursive decomposition phase was computationally quick, simply confirming the already largely optimised routes and avoiding reconsidering further sub-problems.

### Comparison of Layout Solutions

Figure 6.11 shows the solutions to the full site containing all 122 turbines, with the copper cables solution on the left and the aluminium cables solution on the right. It can be seen that both layouts have the westernmost substation connecting seven strings resulting in the penalty cost. Strings on the eastern side of the site seem to be largely similar between solutions with more differences being present in the middle and west of the site. Some avoidance of the existing feature can be seen in both sites, as the strings often end close to the feature without crossing it. However, there are still four cables crossing the central existing feature in both layouts, suggesting that either this crossing penalty cost was a necessary cost in producing a good quality layout and/or the additional cost of cable protection was not a significant cost increase relative to other possible cable routes.

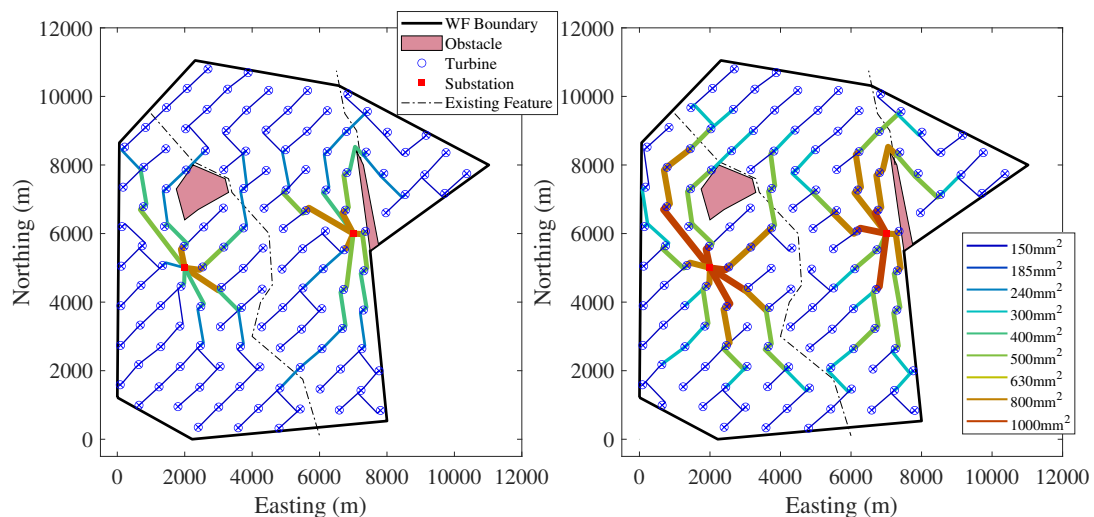


Figure 6.11: MILPsp solutions to the expanded hypothetical offshore wind farm site using (left) copper cables and (right) aluminium cables.

Overall, the copper layout uses fewer large cables but has a higher objective value (total cost), demonstrating that the aluminium cables offer a better solution to this problem. However, if the limit to the number of substation connections (6 strings per substation) is a ‘hard constraint’ that must not be violated, the copper cables must be used. This is because the largest aluminium cable has a maximum capacity equal

to 10.5 turbines and therefore, if all 122 turbines are to be connected, this would require 13 strings, with one substation receiving seven strings, violating the constraint (and/or incurring the penalty cost). Further work would be required to reduce the number of connections into substations in the aluminium cables case. The current solutions generally appear to be approaching optimality in the smaller problems (10-61 turbines) and visual inspection of this largest case, Figure 6.11, suggests good quality cable layout solutions are being found with the possible exception of the substation connection penalty cost.

## 6.4 Summary

Following the comparison of three cable layout optimisation approaches presented in Chapter 4, a gap was identified combining classical optimisation methods with a decomposition strategy. This chapter proposed a new algorithm, MILPsp, based on the combination of the classical MILP method with a decomposition strategy. In the development of the method, additional functionality was included relative to the algorithms presented in Chapter 4, including a more comprehensive set of cable crossing considerations.

The hypothetical offshore wind farm case study, used previously in Chapter 4 to assess the efficacy of the MILP, ACO, and ACOsp algorithms, was used again with comparison made between the new algorithm and the previous three. Since the problem formulation was slightly different (through a different Steiner node generation method), a direct comparison cannot be made between the three previous algorithms and the newly proposed MILPsp algorithm. The optimal values of the new slightly different site were found through an adapted MILP solver, MATLAB's *intlinprog* solver. Comparison of the optimality ratios between the four algorithms showed that the MILPsp algorithm found the optimal solution in all cases, with the exception of the 122 turbine case. In the case of 122 turbines, the optimal objective value could not be proven and therefore some uncertainty of the optimality ratio remained, such that the MILPsp solution could be up to 1.4% more expensive than the theoretical optimum result (in the worst case

scenario). Comparing the computational time of the four algorithms, it was shown that the MILPsp algorithm was the second fastest, beaten only by the classical ACO algorithm. Producing optimal values in a relatively quick computational time, it is clear that the MILPsp algorithm is a superior approach to cable layout optimisation than the MILP, ACO, and ACOsp methods. The MILPsp method maintains the good quality solutions of the MILP approach but with reduced computational expense. It achieves this by circumventing the non-linear scaling relationship between the number of optimisation variables and computational time, where the sum of the computational time for many smaller sub-problems is less than that of a single large (full) optimisation problem. The decomposition strategy that is informed by the incumbent solution helps to maximise the possibility of improving the solution during each sub-problem and approach the optimal value. Optimising the hypothetical site for a range of number of turbines helps to demonstrate the robustness of this approach, however, additional case studies with more significant differences would help to improve confidence in the proposed algorithm.

Two further cases were considered on the hypothetical site with additional site features and considerations, using copper and aluminium cables. The MILPsp algorithm performed well on the expanded cases finding solutions within 1% of the optimal solution in all but the largest case of 122 turbines. In the largest aluminium cables problem, it was not possible to avoid the penalty cost function (as the problem was over-constrained) and the algorithm found a solution within 0.2% of the optimal.

In the copper cables case, the algorithm was unable to avoid the penalty cost for too many substation connections, despite it being theoretically feasible to do so. This may be a result of operating a more constrained sub-problem creation method, as turbines were not able to connect to neighbouring strings outside of the sub-problem. Future works, may benefit from using the more complex method of sub-problem creation, that considers more variables and constraint equations, but allows for connection to neighbouring strings. This would help to avoid a situation as this, where the number of substation connections in the final solution was still greater than the defined limit.

As in Chapter 4, for the largest problems with 122 turbines, it can be difficult to

prove what the optimal solution to a problem really is, even with adapted code and allowing long computational times. As such, some uncertainty remained for some of the larger solutions and therefore a range of optimality ratios were provided for the tool solutions. Despite this, no solution was found to any problem that out-performed (i.e. had a lower objective value than) the solutions found by the MILPsp algorithm. This provides a high degree of confidence in the solutions reaching optimal, or very close to optimal, objective values.

One limitation of the proposed method, is that the optimal cable selection method is based on the optimal cable layout when all cable sizes may be used. Therefore, this may not result in the overall best cable combination. For example, a cable that is large enough to connect the largest section of an intermediate solution will definitely be picked in the optimal cable subset, regardless of if this should be used in the optimal solution when the number of cable sizes are limited. However, it appears that the correct cable sizes have been chosen in almost all - if not all - cases as the optimal solution was often found.

A second limitation to the proposed method is that the decomposition into sub-problems was not as robust as that previously presented in Chapter 4 for the ACOSp method. Since the formulation of the problem limited turbines to connect to nodes only within the sub-problem, the MILPsp algorithm struggles to reduce the number of strings (and therefore substation connections) in some of the larger problems where the optimal solution exists close to the constraint boundary. This is because each sub-problem (created by the selection of two strings) must result in a valid solution, and if there are too many turbines to be supported by a single string, even by one, the solution to that sub-problem must necessarily be made of two strings and therefore no reduction in the overall number of strings. In the previous formulation, used by ACOSp, if there was one too many turbines for a single string, this turbine could be connected to another string outwith the sub-problem if there was capacity for it. Expanding this in future works to allow connections to nodes outside of the sub-problem (as in ACOSp) would almost certainly aid the reduction in the number of strings, however with the MILP algorithm as a base this is not as straightforward as with the ACO-based method.

## Chapter 6. Advanced Cable Layout Optimisation

Despite this, the tool seems to generate good quality solutions in a relatively short time frame.

In conclusion, an effective tool for cable layout optimisation is proposed in this chapter, MILPsp, that is able to maintain the good quality solutions of a MILP approach while reducing the computational complexity.

## Chapter 7

# Influence of Energy Storage Systems

This chapter takes the MILPsp cable layout optimisation method from Chapter 6, building in capability of considering energy storage systems, to answer the second research question:

"What is the potential impact of using energy storage at the wind farm level to reduce the cable rating and lifetime losses in offshore wind farm array cable networks?"

The chapter explores what the effect might be, if any, of including energy storage systems (ESS) as a decision variable in the cable routing optimisation algorithm, MILPsp, presented in Chapter 6. Previously, the cable ratings of sections in the array cable layout have been selected based on the peak current, ensuring an appropriate cable is chosen for each connection. As wind energy is a variable resource, peak current (experienced at above-rated wind speeds) is only experienced by a given cable for a fraction of the total lifetime of the asset [15]. Therefore, for the remaining operating time, the cable may be considered to be in an overrated state. Energy storage may be able to ameliorate this by reducing the peak power and therefore the required cable rating. This is achieved by placing ESS in the turbines and operating them in a ‘peak-shaving’ capacity, where the ESS is charged at times of high power output (high wind speeds)

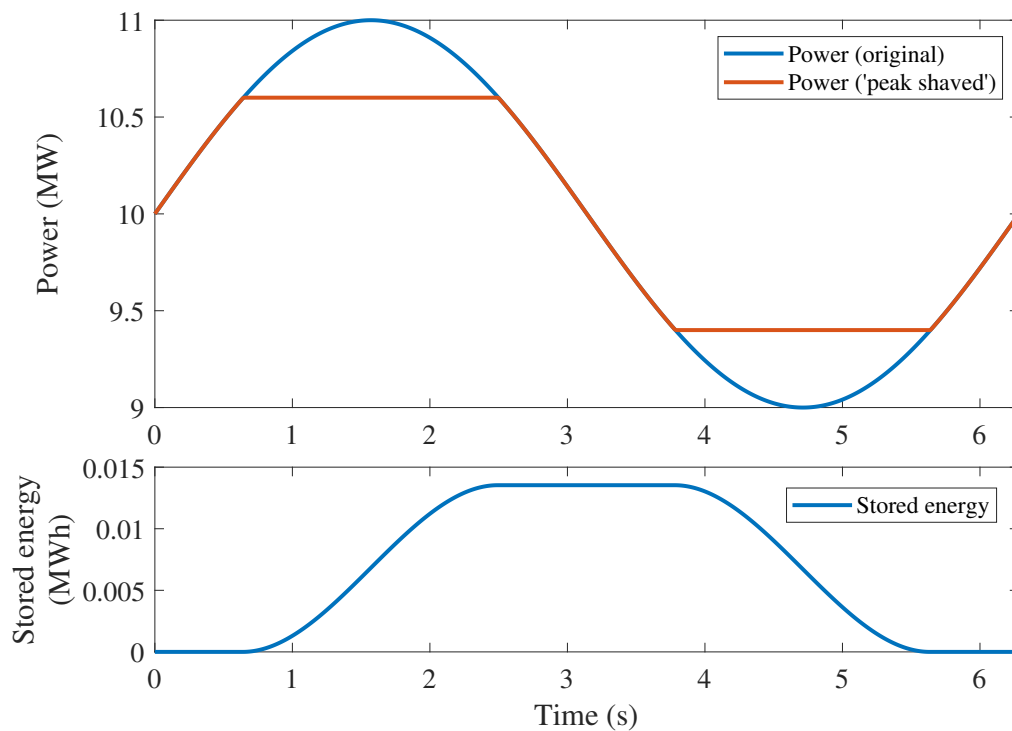


Figure 7.1: Example of ‘peak-shaving’ power using energy storage.

and discharged at times of low power output (low winds speeds). An example of this can be seen in Figure 7.1.

The formulation of the problem and the methodology of including an energy storage component into the tool are presented in the following section. This optimisation method is applied in a case study to the same hypothetical offshore wind farm site used to investigate the efficacy of the MILPsp algorithm in Chapter 6. Firstly, energy storage is allowed in all turbines at zero cost considering a range of power and energy capacities to determine the scale at which this may become a useful asset to an offshore wind farm, discussed further later. Also investigated is the charging strategy for each combination of power and energy capacity, by utilising a range of charging and discharging levels. A second study investigates if energy storage is used by the algorithm over a range of costs, enabling an analysis of what cost ESSs must be in order to be economically viable for the purpose of peak-shaving power. Finally, the hypothetical site is considered by the algorithm to determine the cable layout and selection and the optimal size and

location of ESS in the turbines. This final study allows for the investigation of the ESS placement distribution between turbines in the strings and how this may affect the overall layout.

The results of the case studies are presented and discussed to allow for an assessment of the additional functionality of ESS and whether or not it is a valuable addition to cable layout optimisation for large offshore wind farms. Future investigations in this research space are proposed in order to help guide future works.

## 7.1 Methodology

The following sections outline the changes to the decision variables, objective function, constraint equations, and algorithm that are necessary to include an ESS component into the MILPsp algorithm presented in Chapter 6. Another change is required in the pre-processing of the variables' costs, which is the change from a Weibull distribution description of the wind field to a time-series-based approach. This is necessary due to the time-displacement of energy through the use of ESS. Representative time series wind speeds for an offshore site were provided by SSE containing ten-minute mean wind speeds over the period of one year.

To effectively simplify the problem, three key assumptions are made: (1) all turbines experience the same wind speed regardless of their position in the site (wake effects are ignored), (2) all ESS uses the same charging strategy (charging and discharging levels), and (3) ESS is considered in a discrete set of incremental units where turbines may house 0 to  $E_{max}$  units. This means that all ESS across the wind farm site will be operating synchronously - in their charging and discharging activity - allowing for the location-agnostic consideration of ESS at each cable connection. For example, a cable supporting two turbines would see the exact same power profile (time series) if both turbines contained one unit of ESS, or if one turbine contained two units of ESS. Therefore, for each cable, only the total amount of 'upstream' ESS is considered in order to calculate the power flow time series, electrical losses, and peak power experienced by the cable. Here, 'upstream' of a given cable, means any ESS whose stored energy will be carried by the cable i.e. any ESS that is further away from the substation than

the cable in question. Quantities of upstream ESS and power time series experienced by a cable are calculated by a simple traversing of the network from the point/cable being considered. From a given cable section, the upstream turbine is identified, any cables entering this turbine are identified, the turbines upstream of these cables are identified, and the process repeats until the ends of all strings/branches are found. The ESS present in the selected turbines can be summed along with the power time series of the selected turbines.

### 7.1.1 Adapting the MILP Model

#### Decision Variables

The decision variables listed below are largely the same as those used previously to build the model for the MILPsp algorithm. Some changes are made to the  $x$  and  $p$  variables and two new variables are introduced,  $e1$  and  $e2$ , to enable the use of ESS in the cable layout optimisation method. The  $y$ ,  $w$ ,  $z$ , and  $b$  variables remain unchanged from the formulation presented in Chapter 6.

- $x_{i,j}^{t,n,m}$  - Binary variable describing whether a specific cable type/size,  $t$ , supporting  $n$  turbines, with  $m$  upstream ESS units, using the route between nodes  $i$  and  $j$  is built or not (1/0).
- $p_{i,j}$  - Integer non-negative variable describing the number of turbines supported by the cable (if built) on the route between nodes  $i$  and  $j$ .
- $e1_{i,j}$  - Integer non-negative variable describing the number of ESS units built upstream of the cable (if built) on the route between nodes  $i$  and  $j$ .
- $e2_i^m$  - Binary variable describing if the cost,  $\gamma_m$ , of  $m$  units of ESS built at a turbine node  $i$  must be included or not (1/0).

The set of  $x$  variables that describe if a cable,  $t$ , is used on a route,  $(i, j)$ , under a particular loading scenario, supporting  $n$  turbines, must be extended to consider the amount of upstream ESS as this will affect the electrical losses and peak power

experienced by the cable. A particular number of upstream ESS units,  $m$ , is therefore added to define  $x$ . The costs associated with the  $x$  variables are included as before in the  $c$  terms, shown in Equation 7.1. The time-varying cost components, such as electrical losses, must be calculated slightly differently to the previous MILPsp model. This is described further in Section 7.1.2.

The set of variables  $p$  was previously used to describe the power flow in a given cable connection. Since the power flow will be altered by the presence of ESS, the constraint equations for cable selection can no longer rely on using the  $p$  variables in the same way as previously. These variables are now altered to simply describe the number of turbines being supported on a route, rather than the power experienced by a cable on the given route. The peak power flow in the string is calculated by using the time series wind speed to calculate a time series sum power output of the turbines further upstream of a given cable section. The  $p$  variable, now describing the number of upstream turbines, enables constraint equations (discussed further later) to ensure the correct loading scenario is applied, i.e., supporting  $n$  turbines in the presence of  $m$  units of ESS.

The new  $e1$  variable describes the number of ESS units upstream of a cable and is an integer non-negative variable. Since there is no cost associated with these variables, they have a coefficient of zero in the objective function. The  $e1$  variables are very similar in formulation to the  $p$  variables with a variable created for each route,  $(i, j)$ , in the set of possible routes.

The new  $e2$  variable describes whether the corresponding cost,  $\gamma_m$ , of  $m$  units of ESS is to be added in a given turbine and is a binary variable. Several  $e2$  variables are created for each turbine with each one describing the cost,  $\gamma_m$ , of a certain quantity of ESS,  $m$ , in the discrete set of ESS sizes available.

### Objective Function

Equation (7.1) presents the updated objective function to be minimised using the updated set of decision variables.

$$\min F = \min \left[ \sum_{(i,j) \in A} \sum_{t \in T} \sum_{n \in \{1:k_{max}\}} \sum_{m \in E} c_{i,j}^{t,n,m} x_{i,j}^{t,n,m} + \sum_{h \in H} \gamma_h \sum_{j \in V_T} w_j^h + \sum_{c \in C} \gamma_c \sum_{j \in V_{SS}} z_j^c + \sum_{q \in Q} \gamma_q b_q + \sum_{m \in E} \gamma_m \sum_{j \in V_T} e2_j^m \right] \quad (7.1)$$

where the  $x$  variables,  $x_{i,j}^{t,n,m}$ , multiplied by their associated costs,  $c_{i,j}^{t,n,m}$ , are now also summed across all values of ESS size,  $m$ , in the set of available ESS sizes,  $E$ ; no change is made to the terms surrounding the  $w$ ,  $z$ , and  $b$  terms; and the cost of ESS is taken into account by summing the cost of  $m$  units of ESS,  $\gamma_m$ , multiplied by the binary variable  $e2_j^m$ , for all turbines,  $i \in V_T$ , and for all sizes of ESS,  $m \in E$ .

### Constraints

This section details the necessary changes to the constraint equations presented in Chapters 4 and 6 and the addition of several new constraint equations focusing on the ESS variables. The majority of constraint equations remain unchanged and so for clarity are not restated here.

**Kirchhoff's Current Law/Number of Supported Turbines:** The new formulation, Equation (7.2), is very similar to the original but with the generated power equal to one in all cases ( $p_{gen_i} = 1$ ). This now states that the number of turbines (rather than power) supported by the cable entering the node  $i$ ,  $p_{k,i}$ , plus the turbine node itself,  $p_{gen_i}$ , must equal the number of turbines being supported by the cable leaving the node,  $p_{i,j}$ ; for all nodes in the set of nodes,  $i \in V$ . (Note: This constraint now simply ensures the correct number of turbines/loading scenario is applied for a given cable. Since the peak power is now calculated separately, this does not directly impact the cable selection and any possible de-rating.)

$$\sum_{k \in V} p_{k,i} + p_{gen_i} - \sum_{j \in V} p_{i,j} = 0, \quad p_{gen_i} = 1 \quad (7.2)$$

**Cable rating:** This constraint previously used the power flow variables,  $p$ , to ensure

that the cable size,  $t$ , selected for the connection had a higher power rating than the power flow experienced by the cable, Equation (4.5). This equation is amended to state that the loading scenario,  $n$ , (number of turbines being supported), multiplied by the binary variable  $x_{i,j}^{t,n,m}$ , must be equal to the true number of turbines being supported,  $p$ , for the range of number of turbines that may be supported by a given cable type,  $n \in \{1 : k_{max}\}$ . This constraint is applied to all routes,  $(i, j) \in A$ , and all cable sizes,  $t \in T$ .

$$\sum_{n \in \{1:k_{max}\}} n x_{i,j}^{t,n,m} = p_{i,j} \quad (7.3)$$

(Note: any combinations ( $x$  variables) where the cable type,  $t$ , has a rating that is too low to support  $n$  turbines in the presence of  $m$  units of ESS peak-shaving, is removed during the creation of the variables in the pre-processing).

**Number of Upstream ESS Units:** Several new constraint equations are included to correctly describe the number of ESS units upstream of a cable. Firstly, the  $e1$  variable describing the ESS upstream of a given cable is restricted to be a non-negative integer variable,  $e1_{i,j} \in \mathbb{Z}^{0+}$ .

The variable  $e2$ , describing the number of ESS units in a given turbine node, is constrained to be a binary value. In order to ensure only one size of ESS,  $m$ , is built in a turbine node, the sum of all  $e2$  variables associated with a turbine node  $i$  must be equal to one, for all sizes of ESS in the set of possible sizes,  $m \in E$ . This constraint is applied to all turbine nodes,  $i \in V_T$ . Note: an ESS size of zero is included in the set of possible ESS sizes,  $m \in E$ , to ensure it is possible for no ESS to be built at a turbine node.

$$\sum_{m \in E} e2_i^m = 1, \quad e2_i^m \in \{0, 1\} \quad (7.4)$$

Both  $e1$  and  $e2$  variables are required for the constraint regarding the number of upstream ESS units, Equation (7.5). This constraint states that the sum of the number

of ESS units upstream of all cables entering a turbine node  $i$ ,  $e1_{k,i}$ , plus any ESS units present in the turbine node,  $m e2_i^m$ , must be equal to the number of ESS units upstream of the cable leaving the turbine node,  $e1_{i,j}$ .

$$\sum_{k \in V} e1_{k,i} + \sum_{m \in E} m e2_i^m - \sum_{j \in V} e1_{i,j} = 0 \quad (7.5)$$

**ESS Scenario Equal to ESS Built:** An additional constraint is required to ensure that the number of upstream ESS units,  $m$ , is equal to the ESS scenario for each  $x$  variable. Equation (7.6) states that the loading scenario with  $m$  upstream units of ESS, multiplied by the binary variable  $x_{i,j}^{t,n,m}$ , must be equal to the true number of upstream ESS units,  $e1_{i,j}$ , for all quantities of ESS,  $m \in E$ , applied to all routes,  $(i,j) \in A$ .

$$\sum_{m \in E} m x_{i,j}^{t,n,m} = e1_{i,j} \quad (7.6)$$

### 7.1.2 Adapting the MILPsp Algorithm

**Power Time Series Generation:** Algorithm 14 presents the charging and discharging algorithm used to generate a new power time series for each cable and loading scenario in the presence of ESS and to find the resulting peak power experienced by the cable. This location-agnostic consideration of ESS is completed for all combinations of loading scenario ( $n$  turbines), cable size ( $t$ ), and ESS ( $m$ ). The power profile (time series) of these combinations is used to determine peak power and costs such as electrical losses in the different combinations. Determination of location and sizing of ESS in the solution is then determined concurrently with cable routing/sizing in the optimisation process.

Algorithm 14 begins by initialising the state-of-charge of the ESS,  $SOC$ , at 50% of the available energy capacity. The power time series,  $P_{TS}$ , is initialised as the single-turbine power time series,  $P_{ts}$ , multiplied by the number of turbines,  $n$ , being supported by the cable. For each time step in the series, the power at time  $ts$ ,  $P_{TS}(ts)$ , is checked against the charging and discharging level,  $ESS_{ch\_lim}$  and  $ESS_{dis\_lim}$  respectively. If the power is greater than the charging level, the ESS will charge, or if the power is less than the discharging level, the ESS will discharge. In both scenarios it is necessary to

**Algorithm 14** ESS (dis)charging strategy

---

```

Initialise  $SOC = 0.5m$  and  $P_{TS} = nP_{ts}$ 
for each time step,  $ts$ , in the time series,  $P_{TS}$  do
  if  $P_{TS}(ts) > ESS_{ch\_lim}$  then
     $P_{charge} = \min\{ESS_P, (ESS_C - SOC)/(1/6), P_{TS}(ts) - ESS_{ch\_lim}\}$ 
     $P_{TS}(ts) = P_{TS}(ts) - P_{charge}$ 
     $SOC = SOC + P_{charge}/6$ 
  else if  $P_{TS}(ts) < ESS_{dis\_lim}$  then
     $P_{discharge} = \min\{ESS_P, SOC/(1/6), ESS_{dis\_lim} - P_{TS}(ts)\}$ 
     $P_{TS}(ts) = P_{TS}(ts) + P_{discharge}$ 
     $SOC = SOC - P_{discharge}/6$ 
  end if
end for
Record  $P_{TS}$  for loss calculation
Record 99th percentile peak power of  $P_{TS}$ 

```

---

calculate how much energy can be charged or discharged. The charging power is the lesser of three terms: the power rating of the ESS,  $ESS_P$ ; the energy capacity of the ESS,  $ESS_C$ , minus the SOC, divided by the time step (10 minutes, or 1/6 hours); and the difference between the power and the charging level. The power flow for the cable under consideration may be updated by negating the charging power,  $P_{charge}$ , and the SOC may be updated by the addition of the charging power multiplied by the time step.

Similarly, the discharging power is the lesser of three terms: the power rating of the ESS; the SOC divided by the time step; and the difference between the discharging level and the power at time  $ts$ . The power flow for the cable is updated by the addition of any discharged power,  $P_{discharge}$ , and the SOC may be updated by negating the discharging power multiplied by the time step. When the charging strategy has considered the full time series, the power time series is saved to be used for electrical loss calculation and the 99<sup>th</sup> percentile peak power for the cable is recorded. Rather than recording the highest value of peak power, the 99<sup>th</sup> percentile value is used to allow for some limited over-rating of the cables and to provide a slightly ‘relaxed’ formulation of the problem to help increase the probability of ESS being used.

**Electrical Loss Calculation:** The electrical losses are calculated as described previously in Chapter 6, but using each value in the power time series rather than a set of

power values with probabilities defined by the Weibull distribution. The wind speeds over the year of provided data adhered to the Weibull distribution and so no other changes were required to the electrical loss calculation method.

**Pre-processing Phase:** With the presence of ESS in some of the cable options ( $x$  variables), it is possible that a given cable may be able to support more or fewer turbines depending on how much upstream ESS is built. Therefore, when the variables are created in pre-processing with all cable/ESS/number-of-turbine combinations possible, only those that are valid may be kept, based on the peak power found for that specific combination using the charging-discharging algorithm, Algorithm 14. To clarify, any  $x$  variables whose cable size,  $t$ , has a power rating below the peak power found for the loading scenario (of  $n$  turbines and  $m$  ESS units), is removed and not used in the model.

Further, in the previous optimisation methods (ACO, ACOsp, MILP, and MILPsp) in Chapters 4 and 6, the pre-processing phase reduced the number of variables by keeping only the lowest cost cable for a given loading scenario (number of turbines) for each of the possible routes. A similar process is adopted in this formulation through a slightly adapted approach that also considers the ESS component. For every possible cable connection route, for a given number of turbines to be supported, and for a given number of upstream ESS units, only the cheapest cable option is kept for the optimisation to consider; more expensive options are ‘discarded’ as they will not be selected in the solution.

**Settings of the *intlinprog* Solver:** Initial development of the updated algorithm indicated that the solver may struggle to find a valid solution with the addition of many more variables (due to the larger set of  $x$  variables). This was caused primarily by the pre-processing phases of the built-in MATLAB solver, which was removing (cutting) valid solutions prematurely, or simply not considering regions of the solution space. Disabling these pre-processing phases, can increase the time taken to find a solution, but increases the chance of optimal solutions being found. The linear programming pre-processing phase (*LPPreprocess*) of the *intlinprog* solver and cut generation (*Cut-Generation*) were disabled, and the maximum number of nodes explored in the branch-

and-bound process (*MaxNodes*) and maximum allowable time (*MaxTime*) were both set to infinite.

## 7.2 Case Study

The turbine, wind farm, cables, and all associated inputs are taken from the GW-scale hypothetical offshore wind farm site proposed and used in the previous chapters. The wind conditions are different however, as the use of energy storage necessitates a time series approach to the power output and therefore wind speed. A representative time series of wind speed was provided by SSE which contains ten minute mean wind speeds over the period of one year. Wind speeds are converted to power through the use of the turbine power curve.

This study does not use a specific type, size, or cost of ESS. Instead, the goal is to determine what capacity ESS would be required to provide a useful level of peak-shaving for this hypothetical site, and at what cost. Once determined, the location and distribution of ESS throughout the wind farm can be investigated. For this reason, the case study is broken down into the three following sections.

### 7.2.1 ESS Sizing & Charging/Discharging Strategy

The first investigation into sizing the ESSs considers only one cable supporting a single turbine in the hypothetical site. A range of ESS power and energy capacities are considered as well as a range of charging and discharging levels. For each combination of ESS power capacity, energy capacity, charging level, and discharging level, the 99<sup>th</sup> percentile peak power is found (where power refers to the power experienced by the cable, supporting the single turbine, over the duration of the time series). This is to allow for some limited over-rating of the cables and to provide a slightly ‘relaxed’ formulation of the problem to help increase the probability of ESS being used. The power and energy capacities of the ESS range between 0-16MW and 0-160MWh respectively, and the charging and discharging levels both range between 0-8MW. Where the charging level is less than the discharging level, the ESS would clearly receive conflicting messages,

in that it would be asked to simultaneously charge and discharge when power output is between the two levels. As such, the peak power for these cases is not calculated and remains at 8MW, the rated power of the turbine. This investigation aims to determine what the best ESS size is, both in terms of power and energy capacity, and what the charging strategy should be - with this specific turbine and the provided site-specific wind conditions.

### 7.2.2 ESS Costing

Using the charging strategy and ESS size (power rating and energy capacity) identified in Section 7.2.1, this study explores the implication of the cost of the ESS. A string of 12 turbines (the maximum that can be supported by the largest cable) is used with the cable routes fixed in a single linear string such that the algorithm will optimise the cable selection and ESS sizing and location only.

The investigation of ESS cost is conducted in three phases. Firstly, the ESS is manually set to have a cost of £0 to determine if any ESS is used as expected, and if this leads to any reduction in cable rating/sizing. Secondly, an optimisation is then run applying a fixed cost (when any size of ESS is used), equal to that of the turbine jointing cost (£13,800), to take consideration of the increase in complexity of the electrical system and jointing in the presence of ESS built in the turbine. Thirdly, a further set of optimisations are run with a range of variable costs (cost per MWh), applied in addition to the fixed cost, to determine the break-even cost per MWh at which ESS becomes uneconomical.

While the power rating and energy capacity of the ESS are determined by the previous study, Section 7.2.1, turbines are allowed to build ESS in smaller incremental units. Incremental units of one quarter of the chosen power and energy capacity will be used, with turbines hosting between zero and eight units (between zero to two times the chosen power and energy). Incremental units of one quarter of the chosen power and energy capacity are chosen here to maintain a computationally efficient model, however greater resolution could be used for following studies. The limit of two times the power and energy capacity will allow the algorithm to select more ESS than might be expected

(to further reduce electrical losses for example) if it is economical to do so.

### **7.2.3 ESS Placement**

The final case study uses the ESS sizing and costing solutions from the previous case studies, Sections 7.2.1 and 7.2.2, and applies these to the hypothetical offshore wind farm site used in the previous chapters. Cable routing, ESS sizing, and ESS location are optimised concurrently to explore the placement and function of the ESS within the offshore wind farm and how this affects the cable routing and cable selection. Similar to previous chapters, the study is first carried out using only the first ten turbines in the site, then 15, 25, 40, 60, and 122 turbines, in order to explore how the solutions change and also how the model complexity and computational time increase with the number of turbines.

## **7.3 Results & Discussion**

This section presents the results of the three-part case study. Firstly, a sizing study is conducted to determine the required capacity for peak-shaving and an appropriate simple charging strategy. Secondly, the cost benefit of the ESS is investigated to find at what price ESS becomes an economically feasible option when used for peak-shaving. Finally, the location and distribution of ESS throughout the wind farm is investigated.

### **7.3.1 ESS Sizing**

Algorithm 14 (ESS (dis)charging strategy) was evaluated across a range for each of the four main parameters. These parameters are (1) ESS power capacity, (2) ESS energy capacity, (3) charging level, and (4) discharging level. The algorithm simulates a peak-shaving function for the ESS across the time series provided by SSE, determining the resulting peak power in the system. Depending on the values used for each of the four parameters, this peak power value may be reduced as a result of the peak-shaving function. The investigation yielded a four-dimensional matrix containing the resulting peak power for each combination of the four parameters. The range of ESS parameters used

were: power ratings of 0-16MW in 1MW increments, energy capacities of 0-160MWh in 8MWh increments, charging levels of 0-8MW in 0.2MW increments, and discharging levels of 0-8MW in 0.2MW increments. A large range of values was chosen to ensure that the chosen ranges did not limit the results of the algorithm. Figure 7.2 shows the peak power experienced by a cable section supporting one 8MW turbine (for the full time-series duration) over a range of charging and discharging levels for the largest possible ESS of 16MW/160MWh.

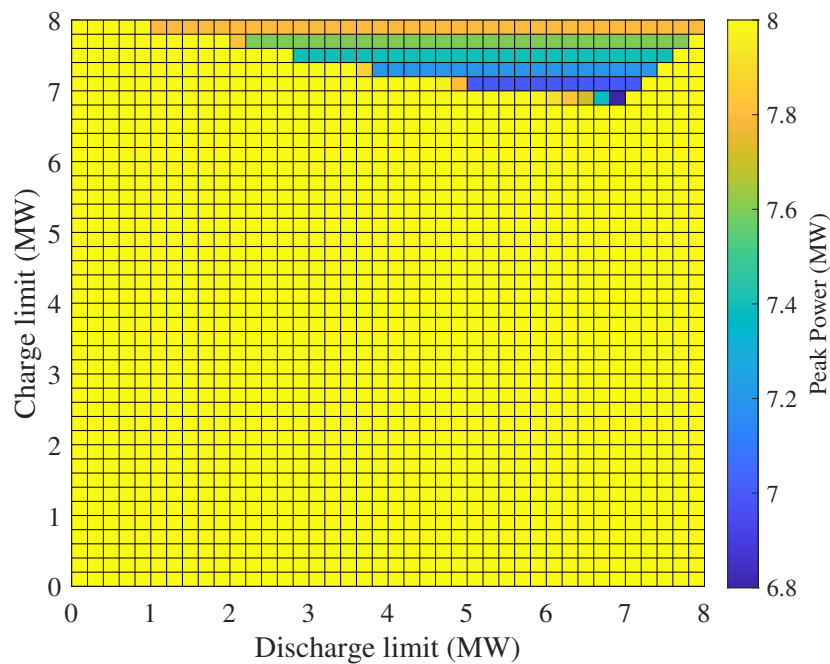


Figure 7.2: The peak power output of a turbine with 16MW/160MWh ESS over a range of charging and discharging levels.

It can be seen that very few charging strategies (charging-discharging level combinations) actually result in a reduction in the peak power below the rated power of the wind turbine, 8MW. It is important to note that the lower-right half of the plot - where the charging level is less than the discharging level - will always show no reduction in peak power. Higher charging limits are successful in peak-shaving more often than lower charging limits, Figure 7.2, in that they are more often able to provide some level of peak-shaving relative to lower charging limits. These lower charging limits potentially

offer a greater level of peak-shaving, but are only able to achieve this when high discharging limits are also used (this is shown by the peak power reducing as the charging limit is lowered from 8MW towards 6.8MW, but is only achieved at higher discharging limits no lower than 6.8MW). However, if the charging and discharging levels are too different from one-another, too much energy is required to be stored and the strategy is less likely to be successful in peak-shaving. The maximum reduction in peak power was 1.2MW, which was achieved with a charging level of 6.8MW and a discharging level of 6.8MW.

With a minority of charging strategies resulting in any peak-shaving, it suggests that large quantities of ESS are necessary to achieve any level of peak-shaving and cable size reduction. Therefore, it may be valuable to better understand what the smallest necessary size of ESS is for any reduction in cable sizes. The cable power ratings for the case study are 60MW, 90MW, and 100MW which translates to a maximum of 7, 11, and 12 supported turbines respectively. The smallest cable may not be reduced in size, since there is no smaller cable available. However, the middle and largest cables may be reduced in size if sufficient ESS is present. If the middle cable supports eight turbines in a section of the layout solution, 4MW of peak-shaving would be necessary to reduce this to the smallest cable size ((8 turbines x 8MW) - 60MW). This would require a minimum of 0.5MW of peak-shaving in each of the turbines upstream of the cable section being considered (4MW/8 turbines). Performing the same analysis on the largest cable also results in a minimum of 0.5MW of peak-shaving necessary in each of the turbines upstream. Peak-shaving of at least 0.5MW is possible for several charging strategies, as seen in Figure 7.2, suggesting cable size reduction is possible (albeit with very large ESS). To minimise the required size of the ESS, a charging level of 7.4MW is chosen to meet the 0.5MW peak-shaving requirement, Figure 7.2, and a discharging level of 7.4MW is chosen to minimise the difference between charging and discharging levels and therefore minimising the required ESS energy capacity.

Figure 7.3 shows the peak power of a range of ESS power ratings and energy capacities when using the chosen charging strategy of 7.4MW/7.4MW described above.

It can be seen in Figure 7.3 that the necessary peak-shaving of at least 0.5MW is

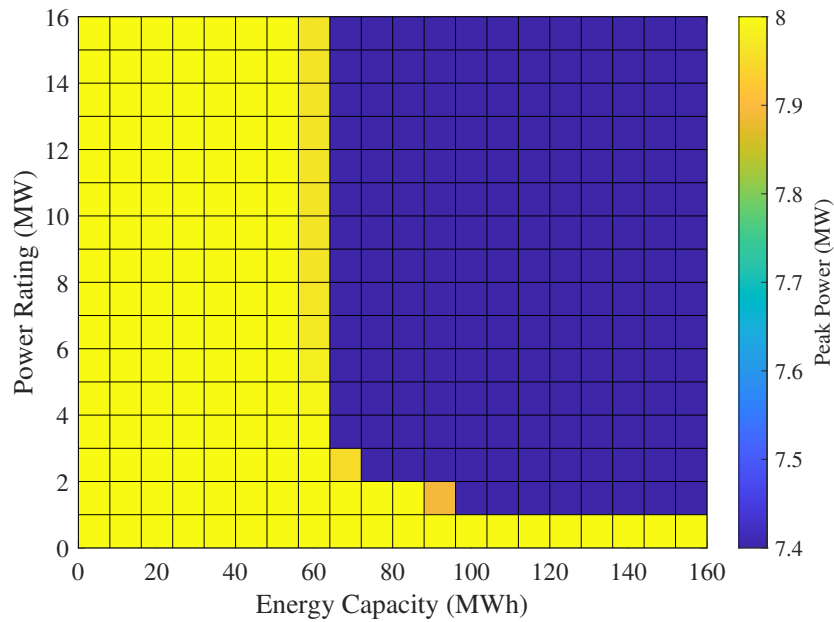


Figure 7.3: The peak power output of a turbine with a range of ESS power and energy capacities when operated with charging/discharging levels of 7.4MW/7.4MW.

achieved at many power and energy combinations between 1-16MW and 64-160MWh. Taking the minimum necessary ESS energy capacity to achieve the desired peak-shaving, results in an ESS size of 3MW/64MWh. Therefore, for this specific combination of turbine power, cable ratings, and wind conditions, an ESS of 3MW/64MWh operating with a charging strategy of 7.4MW/7.4MW will be carried forward in the case study.

### 7.3.2 ESS Costing

A small case study containing a single string of 12 turbines was created with approximately the same spacing ( $\sim 5D$ ) as seen in the hypothetical site. While the chosen ESS size was 3MW/64MWh operating with a charging strategy of 7.4MW/7.4MW, turbines were allowed to build between 0-8 smaller incremental units of 0.75MW/16MWh each (therefore, four of the possible eight units represents the chosen ESS size). Allowing more units of ESS than are necessary to achieve the desired 0.5MW peak reduction (eight rather than four), ensured that the limit would not become prohibitive for the optimisation in this investigation. With no additional cost for building ESS, Figure 7.4

shows the optimised solution - where the number and bar plot above each turbine represents the number of ESS units built at the turbine and the number below each cable section represents the total number of ESS units upstream of the cable.

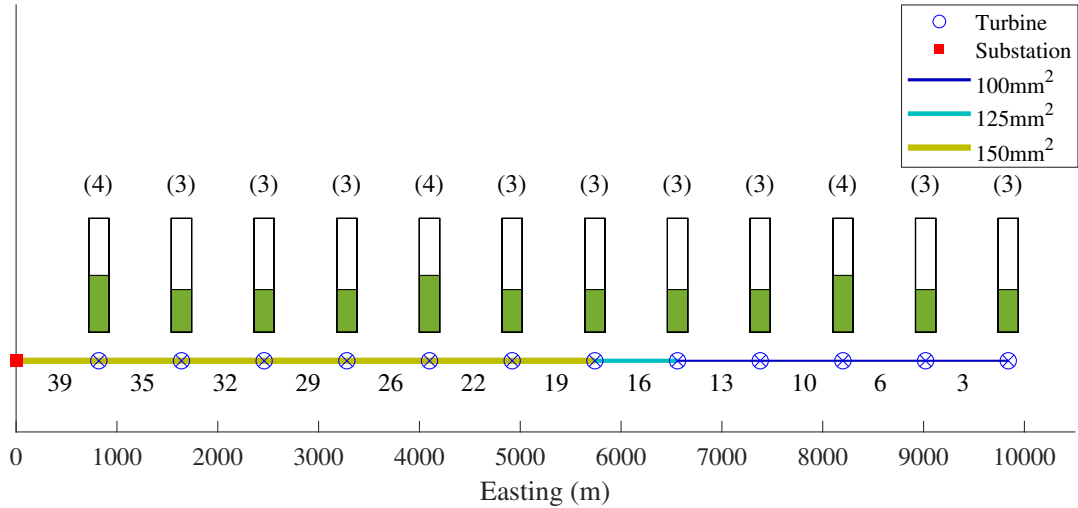


Figure 7.4: Optimised cable selection and ESS sizing and location for an ESS cost of £0. (Numbers in brackets and green bars above the turbines represent the number of ESS units built at each turbine node, numbers below each cable connection represent the number of ESS units upstream of that cable section.)

It can be seen in Figure 7.4, that at least three units of ESS (2.25MW/48MWh) were built in each turbine, with three turbines containing four units (3MW/64MWh) of ESS. The ESS appears to be relatively evenly distributed throughout the string of turbines, with the final cable section connecting to the substation showing that there is a total of 39 units (29.25MW/624MWh) of ESS in total in the string. It might be expected that, since peak-shaving will reduce the peak currents (and electrical losses are proportional to the square of the current), that the maximum amount of ESS would be used throughout the string when the ESS cost is zero.

Upon closer inspection, it can be seen that the electrical losses did not continue to reduce in the presence of an increasing amount of ESS due to the chosen charging strategy. Figure 7.5 shows the electrical losses of the smallest cable size supporting a single turbine with a varying number of ESS units present in the turbine it is supporting.

Increasing the number of ESS units to peak-shave the power output of the turbine does indeed decrease the electrical losses for the first three units of ESS (up to

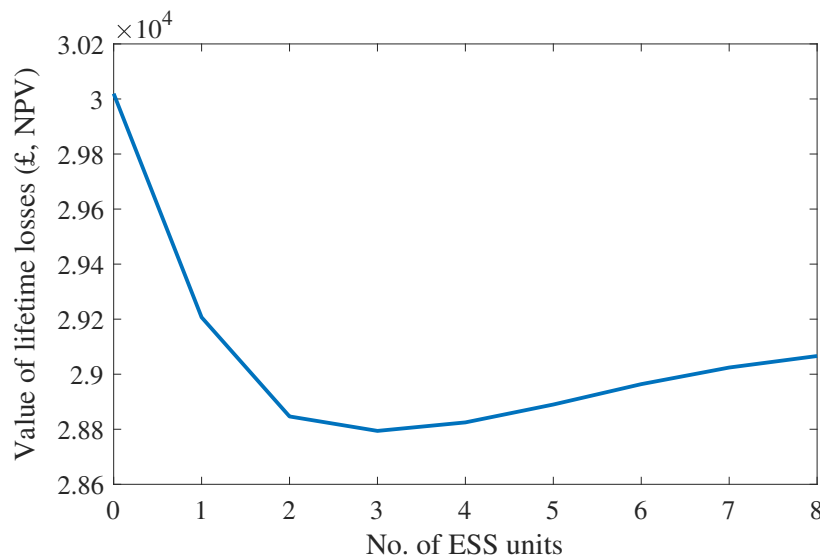


Figure 7.5: NPV lifetime electrical losses in the smallest cable size (100mm<sup>2</sup>) supporting one turbine, in the presence of varying numbers of ESS units in the turbine.

2.25MW/48MWh). After this, any additional increase in the number of ESS units actually increases the electrical losses. This is because the larger sizes of ESS (both in terms of power rating and energy capacity) are able to discharge more energy more quickly when the power output of the turbine drops just below the discharging level. Smaller ESS discharges similarly, however, with a lower power rating it is slower to discharge and still has energy to discharge as the turbine power output drops lower. Discharging the stored energy at lower power levels results in less electrical losses than discharging the energy when the turbine power output is higher (but still below the discharge threshold). This could be a potential limitation of the simple two-level charging strategy and perhaps an alternative charging strategy using proportional charging may be more suitable - where the rate of (dis)charging depends on the relative difference between the charging limit and turbine power output.

A fixed-cost of using ESS in a turbine node is applied that takes into account the additional complexity of the electrical system when ESS is built in a turbine. The cost that is applied is equal to the turbine jointing cost of £13,800 as a representative value and is applied when any amount of ESS is built in a turbine. Figure 7.6 shows the optimised solution in the presence of this additional fixed cost of installing ESS.

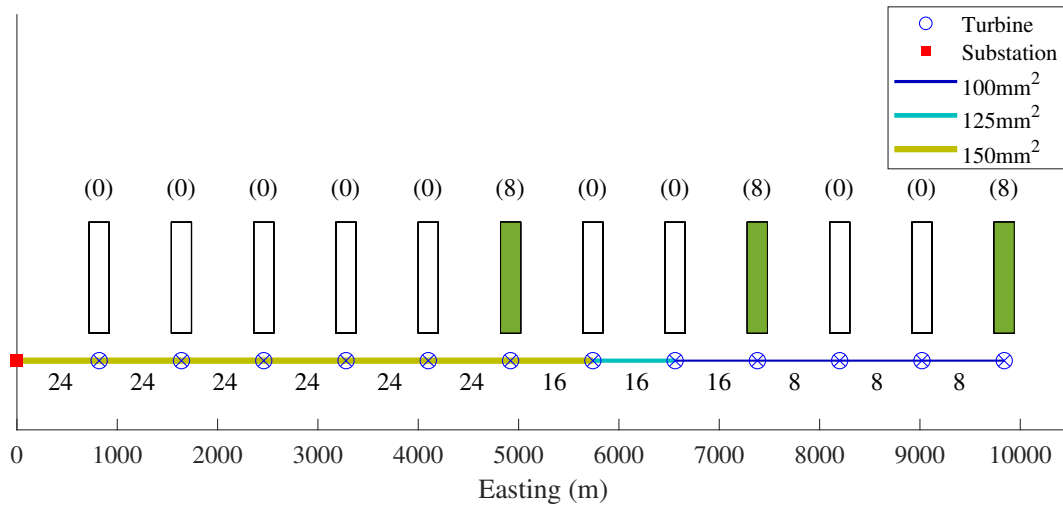


Figure 7.6: Optimised cable selection and ESS sizing and location for a fixed cost of ESS jointing of £13,800. (Numbers in brackets and green bars above the turbines represent the number of ESS units built at each turbine node, numbers below each cable connection represent the number of ESS units upstream of that cable section.)

As can be seen in Figure 7.6, ESS that was previously distributed throughout the string is aggregated into only three turbines, each containing the maximum eight units of ESS (6MW/128MWh). This is clearly to minimise the number of additional cost terms associated with including the ESS system in a turbine; here the fixed cost of £13,800 is included three times (once for each turbine containing ESS). In total, the string now only contains 24 units of ESS, down from 39 previously included at zero cost. The associated increase in the objective value (which includes cable costs, electrical losses, and ESS cost) can be seen in Table 7.1, where the addition of the fixed cost term increases the objective value by £48,359 (0.20%).

Table 7.1 shows the objective values of the single-string case study for a range of variable costs of ESS (cost per MWh), from £200/MWh to £2,000/MWh. The fixed cost remains the same for all cases except the initial zero cost case.

The objective value for the single-string case study, when the ESS has no cost (fixed or variable) is £24,241,721, whereas the objective value when no ESS is used is £24,560,859, an increase of £319,138 (1.32%). This decrease, as a result of including zero-cost ESS, is due to the reduction in electrical losses in the cable sections, discussed further later. Table 7.1 shows the objective value for a range of variable costs. It can be

Table 7.1: Objective values of the cable and ESS selection over a range of variable costs per MWh.

Fixed cost (£)	Variable cost (£/MWh)	Objective Value (£, NPV)
0	0	24,241,721
13800	0	24,290,080
13800	200	24,353,574
13800	400	24,404,774
13800	600	24,445,595
13800	800	24,471,195
13800	1000	24,496,795
13800	1200	24,519,145
13800	1400	24,537,342
13800	1600	24,551,677
13800	1700	24,557,552
13800	1750	24,559,952
13800	1800	24,560,859
13800	2000	24,560,859

seen that no ESS is used when the variable cost is greater than or equal to £1,800/MWh (as the objective value remains unchanged for costs greater than £1,800/MWh), with the ‘break-even’ point for any ESS being used between £1,750/MWh and £1,800/MWh. As the ESS cost increases from zero, a decreasing amount of ESS is built in the string until it is prohibitively expensive. Figure 7.7 shows the solutions for a range of ESS costs, £200/MWh, £800/MWh, £1,400/MWh, and £1,800/MWh.

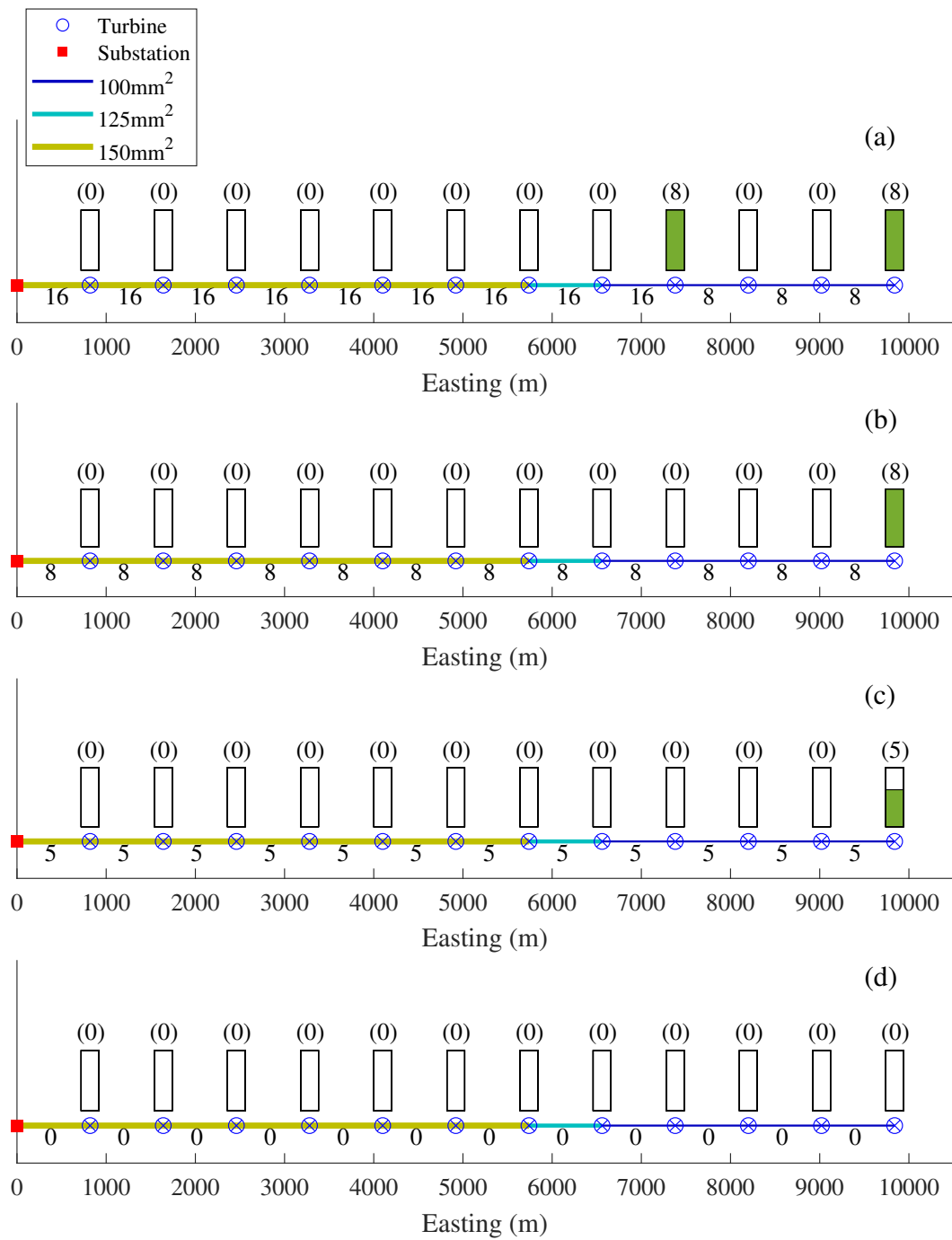


Figure 7.7: Optimised cable selection with fixed cost of ESS of £13,800 and a variable cost of (a) £200/MWh, (b) £800/MWh, (c) £1,400/MWh, and (d) £1,800/MWh. (Numbers in brackets and bars above the turbines represent the number of ESS units built at each turbine node, numbers below each cable connection represent the number of ESS units upstream of that cable section.)

With the addition of a variable cost of £200/MWh (to the fixed cost of £13,800), the total ESS built is reduced from 24 units in three turbines to 16 units in two turbines, Figure 7.7 (a). Increasing the cost further, to £800/MWh and £1,400/MWh, reduces the amount of ESS built to eight and five units respectively. Any ESS that was built in turbines in the middle of the string is removed first as the cost increases, with ESS in the end turbine (furthest from the substation) being preferred by the algorithm. This is because the ESS towards the end of the string provides peak-shaving - and therefore electrical loss reduction - for more of the string. As the cost reaches £1,800/MWh or greater, the additional cost outweighs the benefit provided by the ESS and none is built, Figure 7.7 (d).

Interestingly, the cable selection for all solutions over the range of ESS costs does not change, including the zero cost case. The smallest cable size ( $100\text{mm}^2$ ) is used to support up to four turbines, the middle cable size ( $125\text{mm}^2$ ) is used to support five turbines, and the largest cable size ( $150\text{mm}^2$ ) is used to support six to 12 turbines, irrespective of how much ESS is built in the string. As discussed previously, 0.5MW of peak-shaving is required in each upstream turbine in order to reduce the cable size of a given section of the string. Also discussed was the impact on the electrical losses of increasing amounts of ESS. Increasing the ESS present in the string provides a more rapid discharge at power levels near the discharge level, which when maximised results in slightly increasing electrical losses. This suggests that all the benefit of the ESS is observed through electrical loss reduction rather than a reduction in cable size (with the wind distribution of the site and cable sizes being instrumental in this result). It is expected that for the layout study of the full site, all three cable sizes will be used, however in the presence of branching connections it is possible that there may be different distributions of ESS further upstream in the string that may lead to a reduction in cable size.

With the introduction of an ESS cost, the limit of eight units of ESS per turbine seems to have become prohibitive to the optimisation. While the number of ESS units that can be used could be increased (which would also increase the number of decision variables), it is chosen in this initial investigation not to do so. This is to maintain

reasonable limits to the size and weights of ESS being used in solutions. Table A.2, in the Appendix, shows the energy density and power density of different types of ESS. Considering the highest energy density ESS by weight (hydrogen, up to 10,000Wh/kg), eight units of ESS (128MWh) equates to approximately 13 tonnes. On first inspection, this seems feasible for a large turbine. However, considering energy density per volume, this equates to approximately 42,667 litres. Other forms of energy storage that are less energy dense result in larger weights (for the eight units of ESS or 128MWh), such as compressed-air energy storage (CAES) at 4,267 tonnes. Increasing the eight-unit limit then, while academically interesting, is impractical for ESS co-located at a turbine. An area of interest for future studies may be to quantify the weight and volume restrictions for a given turbine model, to better define the constraints for the ESS optimisation, however that is beyond the scope of this investigation.

Since the range of ESS costs are all significantly below the lowest real cost shown in the literature review (with the lowest cost at \$2-50/kWh for compressed-air energy storage), an assumption is made to enable the following sections of the case study to be conducted. Without the following assumption, applying a real cost of any type of ESS as presented in the literature review would mean using values higher than £1,800/MWh and therefore having no ESS present in the solutions (as demonstrated by the above costing study). The assumption is that an additional ‘stacked’ revenue stream can offset the capital cost of the ESS, and that the peak-shaving service investigated in this work is an additional benefit of ESS present in the wind farm. Therefore, a variable cost of £0/MWh is chosen with a fixed cost of £13,800. This cost structure is to ensure ESS is used in the following layout study, enabling an assessment of the impact of ESS on the cable layout. While this might seem unrealistic, it is proposed that for future developments, ESS may use ‘stacked’ revenue streams [130,131] - such as black start provision - which may offset the cost of the ESS in the wind farm but allow for concurrent charging operations to provide secondary benefits. Detail of the revenue streams for such ancillary service provisions is provided in the Appendix in Table A.1. In such a context, it may be reasonable to suggest the cost of the storage need not be taken into account and as such a cost of £0/MWh may be used. However, a fixed

cost of £13,800 is still used to account for the cost of the additional electrical system complexity when ESS is built in a turbine.

### 7.3.3 ESS Placement

Optimising the hypothetical site's cable layout - allowing ESS to be built - concurrently optimises the cable routing, cable selection, ESS sizing, and ESS location. Not only does this allow for the investigation of ESS placement, but also its effect on the cable selection and routing. Similar to previous chapters, a range of case study sizes are considered by taking a subset of the turbines in the hypothetical site for cable layout optimisation. Firstly, the first ten turbines of the hypothetical site are considered, before cases considering the first 15, 25, 40, 60, and 122 turbines respectively. The layout solutions of the proposed algorithm (including ESS components) are compared to solutions of the MILPsp algorithm, presented in Chapter 6. Table 7.2 shows the objective values of the two approaches (without and with ESS) for each of the six case studies.

Table 7.2: Objective values of the cable layout solutions using the MILPsp algorithm and the amended MILPsp algorithm including ESS.

No. turbines	Objective value (£)		Difference (%)
	MILPsp	MILPsp inc. ESS	
10	23,931,903	23,847,741	-0.35
15	33,410,675	33,335,180	-0.23
25	53,555,201	52,565,747	-1.85
40	73,725,624	73,495,434	-0.31
60	109,438,341	108,511,815	-0.85
122	209,696,645	209,231,196	-0.22

It can be seen that the cases including ESS all reduce the objective value of solutions by 0.22-1.85%, which includes the capital cost of cables, electrical losses over the lifetime of the project, and the additional cost of integrating ESS into turbines. Investigating the layout solutions more closely provides a deeper insight into the method by which the cases with ESS reduce the objective value.

### Ten-Turbine Site

Figure 7.8 shows the layout solutions for the case containing ten turbines, with the MILPsp solution on the left and the solution allowing ESS on the right.

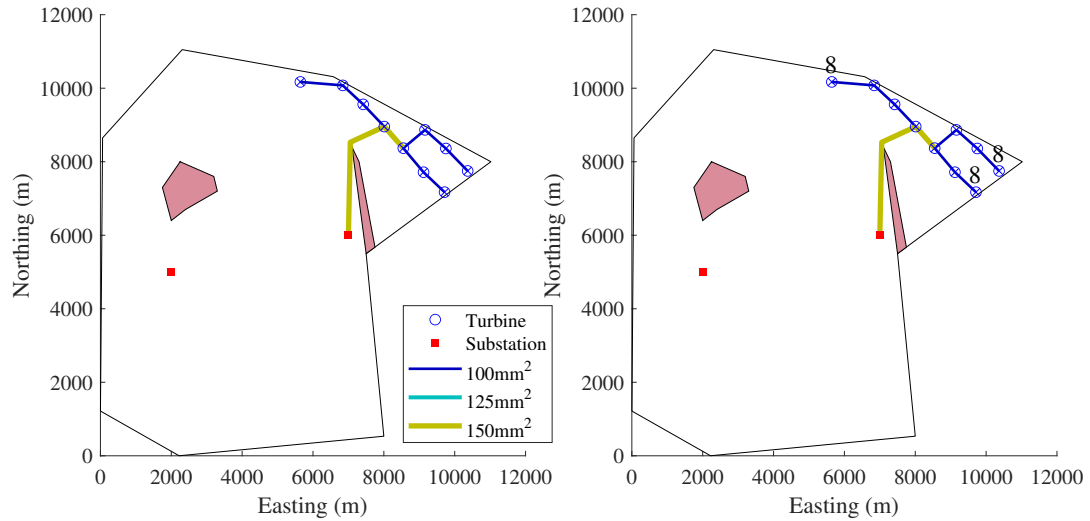


Figure 7.8: Cable layout solutions for the hypothetical site with 10 turbines, using (left) the MILPsp algorithm with no ESS and (right) the adapted MILPsp algorithm including ESS. (Numbers immediately above turbines indicate the number of ESS units built at the turbine.)

It can be seen in Figure 7.8 that the cable routing and cable sizes have not changed between the two solutions. Despite this, there is ESS included in three of the ten turbines, which is providing some benefit/reduction to the objective function through the mechanism of peak-shaving. The additional cost of the ESS in the turbines is £41,400 ( $3 \times £13,800$ ), however, the objective value is £84,162 less in the case with the ESS present (Table 7.2). Therefore, the ESS is providing £125,562 of cost reduction in the form of electrical loss reduction over the lifetime of the project (in net present value), since all cable sizes and routes have remained the same. All three instances of ESS are positioned at the ends of the string branches, furthest from the substation so as to provide the peak-shaving service to all turbines in the string. Turbines containing ESS have all maximised the number of ESS units they are able to accommodate individually, likely to minimise the number of fixed costs of integrating ESS into a turbine. Here, eight units (6MW/128MWh) are present in each of the three turbines, resulting in the

cable entering the substation having 24 units of upstream ESS (18MW/384MWh).

### 15-Turbine Site

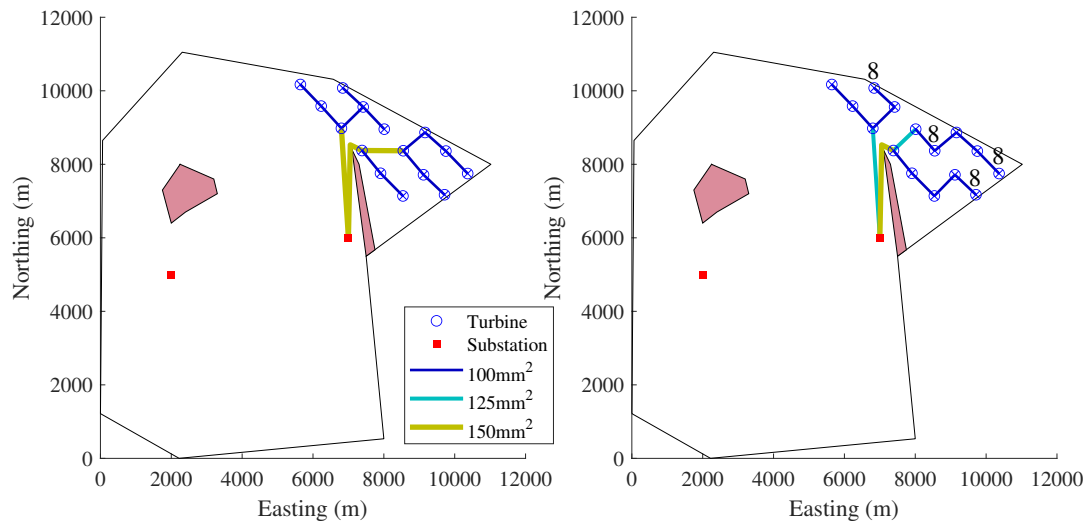


Figure 7.9: Cable layout solutions for the hypothetical site with 15 turbines, using (left) the MILPsp algorithm with no ESS and (right) the adapted MILPsp algorithm including ESS. (Numbers immediately above turbines indicate the number of ESS units built at the turbine.)

The cases containing 15 turbines, presented in Figure 7.9, do exhibit some differences when ESS is and is not included, both in terms of the cable layout and cable selection. The MILPsp solution, Figure 7.9 (left), contains two branched strings supporting six and nine turbines and using only the largest ( $150\text{mm}^2$ ) and smallest ( $100\text{mm}^2$ ) cable sections. The adapted MILPsp solution that includes ESS, Figure 7.9 (right), also comprises two branched cables, although with a different layout such that five and ten turbines are supported by the two strings. All three cable sizes are utilised in the solution and only one cable section is built using the largest cable size, down from three sections in the MILPsp solution. ESS is present in four of the 15 turbines, with all maximising their individual capacity of eight ESS units. Interestingly, three of the turbines containing ESS are at the ends of the string branches, but one is in the middle of a string.

It might be expected, that since ESS at the end of a string provides electrical loss

reduction to every cable section in the string, that all ESS would be positioned towards the end of the string, not in the middle of a string as in Figure 7.9. To better understand why ESS was built in the middle of the string, Figure 7.10 considers each of the six cable sections of the branched string (that contains ESS in the middle of the string) in the 15 turbine solution in Figure 7.9 (right). Figure 7.10 (a) corresponds to the first cable section going from the eastmost terminal turbine (containing eight units of ESS), supporting one turbine, and Figures 7.10 (b-f) consider the ‘downstream’ cable sections, with Figure 7.10 (f) corresponding to the cable section entering the substation. Each plot in Figure 7.10 shows what the electrical losses of the cable would be in the presence of different numbers of upstream ESS (solid blue line), the maximum number of upstream ESS units possible (dotted orange line), and the actual number of ESS units built upstream of each cable section (dashed black line).

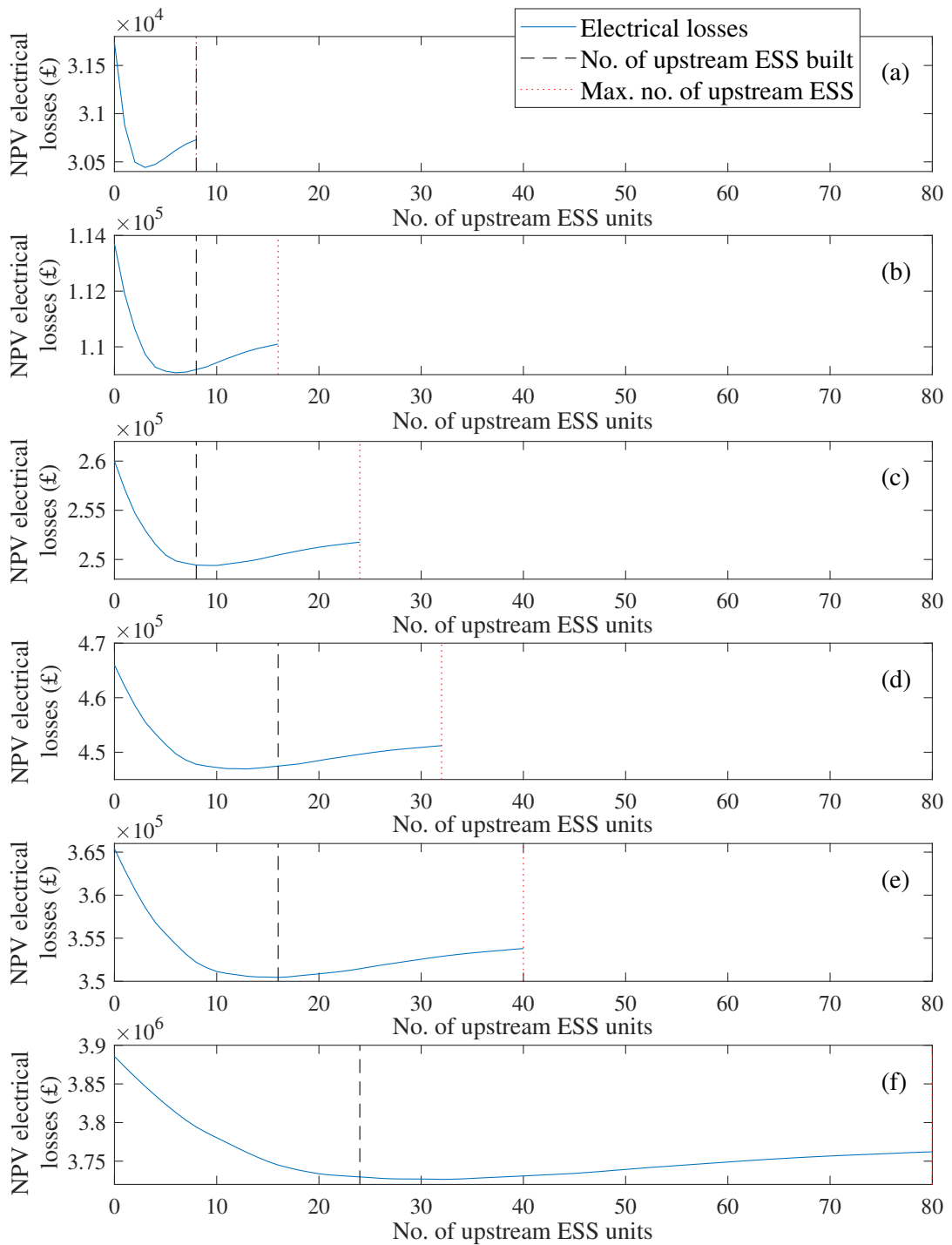


Figure 7.10: Electrical losses for a varying number of upstream ESS units, for the subset of cable sections present in the 15 turbine case study with two turbines containing eight units of ESS. Cable sections support (a) one turbine, (b) two turbines, (c) three turbines, (d) four turbines, (e) five turbines, and (f) ten turbines.

In the solution, Figure 7.9 (right), eight units of ESS are built in the end turbine under consideration, thus Figure 7.10 (a) shows eight units of upstream ESS as indicated by the vertical dashed black line. It can be seen in Figure 7.10 (a) that this does not minimise the electrical losses in the first section of the cable, which occurs at three units of ESS (the lowest point on the solid blue line). With no additional ESS built in the second turbine, the second section of cable, Figure 7.10 (b) still shows eight units of upstream ESS, while the maximum possible is 16. The same is true of the third section of cable, represented by Figure 7.10 (c), since no ESS is present in the third turbine in the string. Here the upstream ESS is eight units (black dashed line) and the maximum possible is 24 units (dotted orange line). In the fourth turbine in the string, eight additional units of ESS is built, meaning that the fourth cable section in the string, Figure 7.10 (d), shows 16 units of upstream ESS out of a possible 32 units. With no ESS in the fifth turbine, the fifth cable section, Figure 7.10 (e), shows 16 units of upstream ESS out of a possible 40 units. Finally, the sixth and final cable section, Figure 7.10 (f), shows 24 units of upstream ESS of a possible 80 units (since there are a total of ten upstream turbines on both sections of the branched string with 16 units of ESS from the above sections and an additional eight units from the other branch of the string).

The ESS is distributed in the turbines such that it minimises the sum total electrical losses in the whole string, not just the immediate next cable. This is because the ESS not only affects the losses in the next section of cable, but also all further downstream cable sections in the string. If all three of the ESSs were positioned in the three turbines at the end of the string as hypothesised, the electrical losses of sections 2-3 (Figure 7.10 (b)-(c)) would be higher than in the current positions.

### 25-Turbine Site

Figure 7.11 presents the solutions to the 25 turbine cases, with the MILPsp algorithm (left) and the adapted optimisation including ESS (right). This case study shows a significant change in the cable layout, most notably by reducing the number of strings from three to two. The MILPsp solution contains strings supporting eight, seven, and ten turbines, whereas including ESS as a decision variable has allowed the strings to

support 13 and 12 turbines. Since the largest cable is able to support up to 12 turbines, it is clear that the ESS has allowed for more turbines to be connected. Similar to the previous case studies, the ESS is all located in the end turbines and all host the maximum eight units of ESS.

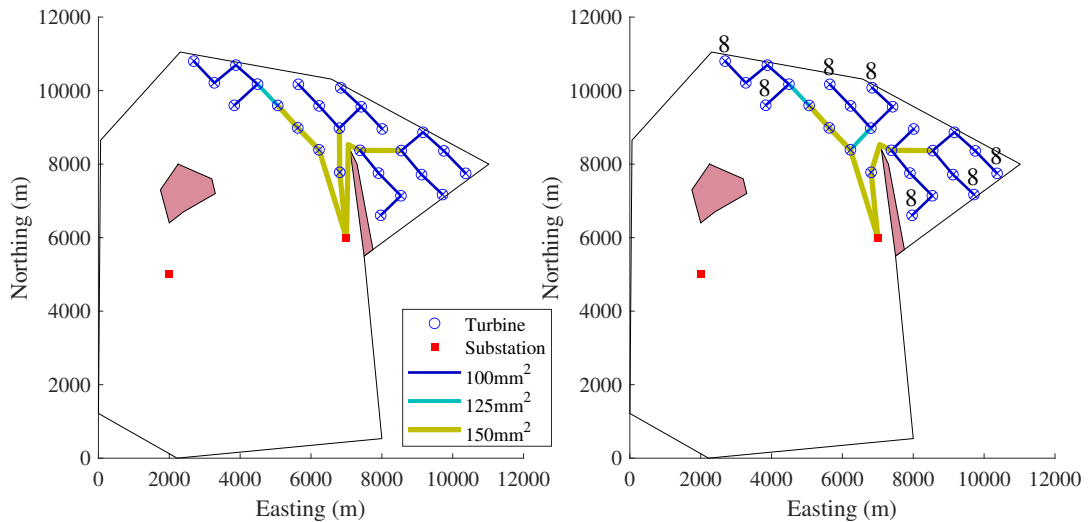


Figure 7.11: Cable layout solutions for the hypothetical site with 25 turbines, using (left) the MILPsp algorithm with no ESS and (right) the adapted MILPsp algorithm including ESS. (Numbers immediately above turbines indicate the number of ESS units built at the turbine.)

#### 40-Turbine Site

The two solutions, with and without ESS, for the case of 40 turbines shows no change to the cable layout or selection unlike the previous two cases. A total of 80 units (60MW/1,280MWh) of ESS is built however, across ten turbines, which all operate to reduce the electrical losses in the array. Eight of the turbines containing ESS are built at the ends of the strings with two located in the middle of the string, at the fourth turbine from the end. This is in line with what was described in Figure 7.10, where ESS was not necessarily all built close to the end of the string. Despite the lack of change in the layout and cable selection, the ESS in this solution was able to reduce the objective value by £230,190 (0.31%).

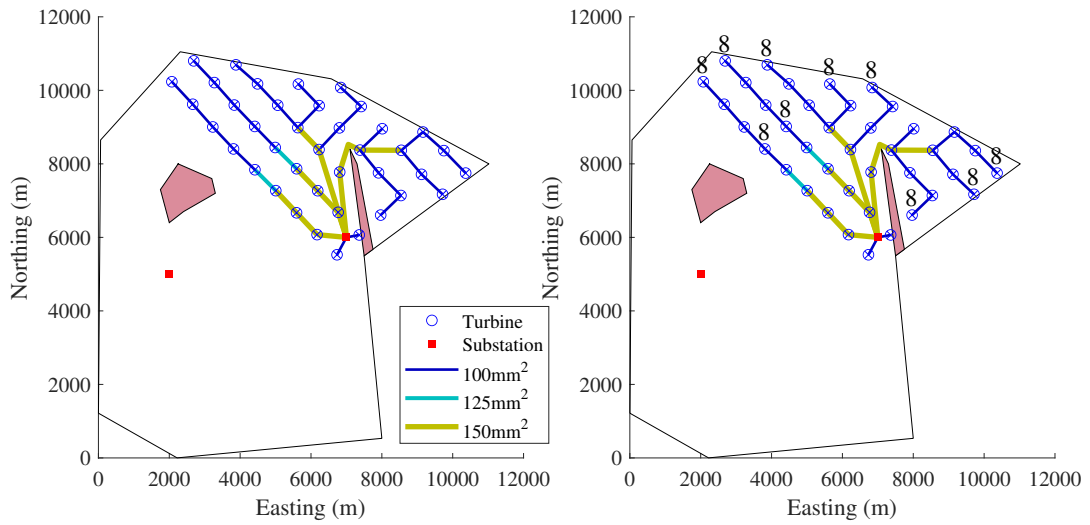


Figure 7.12: Cable layout solutions for the hypothetical site with 40 turbines, using (left) the MILPsp algorithm with no ESS and (right) the adapted MILPsp algorithm including ESS. (Numbers immediately above turbines indicate the number of ESS units built at the turbine.)

### 60-Turbine Site

Upon increasing the size of the case study site to 60 turbines, the layout between the two cases with and without ESS showed changes again. Only small differences exist between the two layouts, shown in Figure 7.13, in the southernmost strings between the two substations. Despite this, a total of 15 turbines contain ESS, all hosting the maximum possible eight units (6MW/128MWh) providing an overall objective value reduction of £926,526. Of the 15 turbines containing ESS, 13 are placed at the ends of string branches and two are in the middle of strings. The total number of strings has been affected by the small layout change, reducing from a total of eight (without ESS) to seven (with ESS), which reduces the substation connection cost. Also reduced, is the number of sections using the largest cable size (150mm<sup>2</sup>), which has changed from 17 to 16 with the addition of the ESS.

### 122-Turbine Site

Although computational time is not a focus of this ESS integration study, computational complexity increases significantly with the increase in the number of turbines (more so

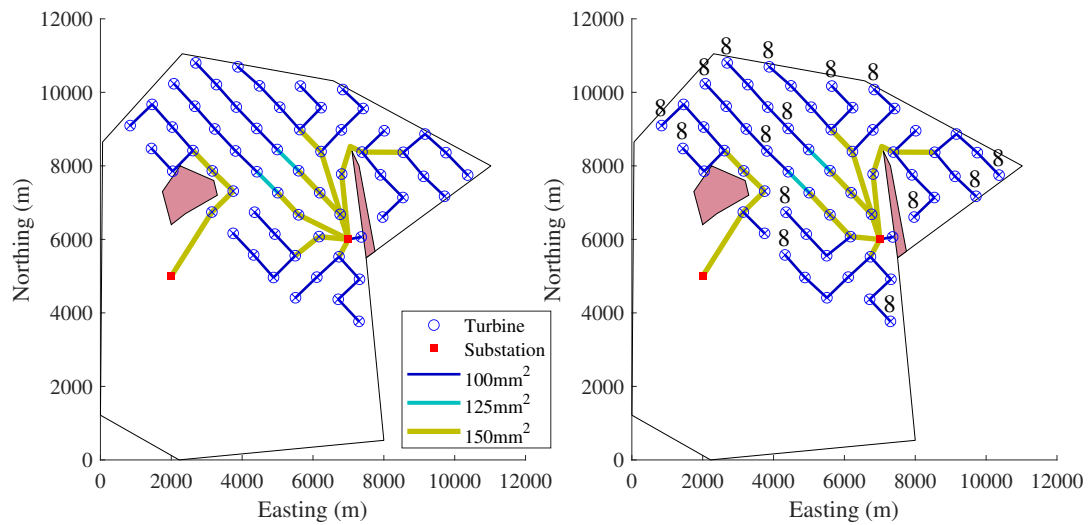


Figure 7.13: Cable layout solutions for the hypothetical site with 60 turbines, using (left) the MILPsp algorithm with no ESS and (right) the adapted MILPsp algorithm including ESS. (Numbers immediately above turbines indicate the number of ESS units built at the turbine.)

than in the cable layout optimisation without ESS). As such, the optimisation of case study sites containing 25, 40, 60, and 122 turbines was conducted on a desktop PC with higher specifications (3.5GHz Intel Core i9-10920X, 192GB RAM). Additionally, for the case of 60 and 122 turbines, the pre-processing phases were conducted in parts running in parallel on the ARCHIE WeSt supercomputer hosted by the University of Strathclyde. This greatly reduced the pre-processing time of the two solutions but means accurate computational times of the total algorithm are not possible to obtain. While the pre-processing phase may be run in parallel, MATLAB's *intlinprog* solver is not compatible with parallel processing and so no benefit would be gained by running on the ARCHIE WeSt supercomputer, which was instead run on the high-specification desktop PC mentioned previously. With the 60 turbine case taking approximately 5 days to run (excluding the pre-processing phase), it was clear that the case of 122 turbines would not be possible to run in a reasonable time period, given the exponential increase in computational time with number of turbines. However, with all previous solutions resulting in turbines containing either zero or eight units of ESS, a compromise was found in reducing the ESS set from  $\{0:1:8\}$  to  $\{0, 8\}$  which greatly reduces the number

of variables and therefore computational complexity. Solutions reaching the maximum of eight units of ESS in all solutions may represent a limitation of the optimisation study. Earlier phases of the investigation justified the sizing of ESS available, however the introduction of a fixed cost incentivised ESS to be grouped into fewer and fewer turbines until the limit was reached. Future studies, that consider a specific type of ESS, may benefit from determining the true maximum ESS capacity of a given offshore turbine to influence the maximum allowable sizing, however that was beyond the scope of this ESS-agnostic investigation. It is not unlikely (at a maximum of 6MW/128MWh of ESS) that the limit used in this work is already beyond the practical hosting capacity of even a large offshore turbine.

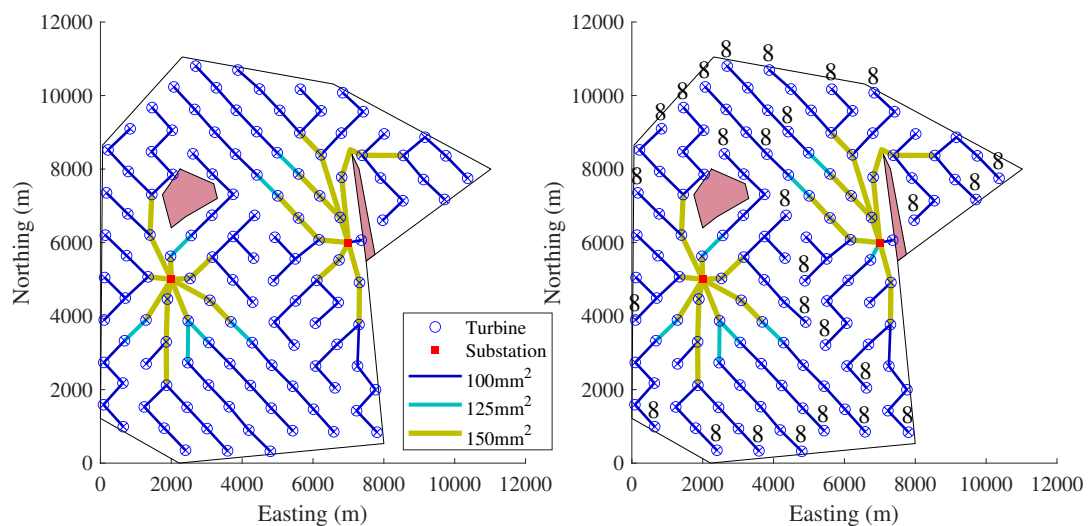


Figure 7.14: Cable layout solutions for the hypothetical site with 122 turbines, using (left) the MILPsp algorithm with no ESS and (right) the adapted MILPsp algorithm including ESS. (Numbers immediately above turbines indicate the number of ESS units built at the turbine.)

The solution to the 122 turbine case, with the reduced set of number of ESS units, is shown in Figure 7.14. The two cables layouts, (left) without ESS and (right) with ESS, are very similar with only three strings in the centre of the wind farm having changed between cases. A total of 27 turbines each contain eight units of ESS, which represents 162MW/3,456MWh in total in the site and provides £465,449 of reduction (0.22%) in the objective value. As per the previous cases, the ESS is largely placed in the turbines

at the ends of strings, however two turbines in the middle of strings also contain ESS, in the Northern half of the site. One cable section, entering the eastern substation, has reduced from the largest size (150mm<sup>2</sup>) to the medium sized cable (125mm<sup>2</sup>) but all other sections have remained the same. It is clear then, that the majority of the objective value reduction is a result of reduced electrical losses, rather than substantial changes to the layout or cable selection.

#### 7.3.4 Limitations

As a novel investigation into using co-located ESS within offshore wind turbines for the purposes of peak-shaving power, it was not possible to exhaust all areas of the study. This section discusses some of the limitations of the work, with the aim of guiding future research.

When calculating the peak power in cables in the presence of ESS, Algorithm 14, peak power over the full time series was recorded. With the Weibull distribution of wind speeds, long periods of high wind speed do not occur very regularly (to varying degrees based on the wind profile at the site). As such, the algorithm may report a high peak power but says nothing about how often this occurs. It could therefore be the case that the large quantities of ESS required to provide meaningful peak-shaving could be reduced by considering curtailing the wind farm for short periods of time. Curtailing the wind farm in this way, introduces further considerations, such as lost revenue, that were beyond the scope of this study but may enable smaller capacities of ESS to be used for peak-shaving. Additional costs, such as the ESS degradation, should also be considered in future studies, once a type of ESS has been selected (not possible in the ESS-agnostic study presented in this work).

As discussed previously, ESS capacities and the constraints in the optimisation would benefit from more detailed investigation. Many of the solutions presented in this work contain the maximum of eight units of ESS and it is possible that solutions would differ from this if more ESS was allowed to be co-located within turbines. While this may be interesting academically, determining the available capacity within a specific turbine model (with a specific type of ESS) would be useful in determining a realistic constraint

to ESS sizes. Given the very large quantities of ESS already used in this study (up to 6MW/128MWh of ESS per 8MW turbine), the author expects a likely limit to be much lower, depending on the turbine model used.

The results presented in this work show that including ESS for the purposes of peak-shaving power is able to provide improved objective values (considering the connection cost of ESS, but not capital cost). This is determined based on a single site case study, but replicated across different sizes of wind farm, from 10-122 turbines. With limitations to time and computational resource, future studies should look to replicate this result on other sites, using different wind profiles, to improve confidence in the use of ESS for this peak-shaving function.

## 7.4 Summary

This chapter aimed to investigate the potential benefits and implications of including ESS as an additional set of decision variables in the cable routing optimisation algorithm. The MILPsp model from Chapter 6 was adapted to include the additional variables describing the ESS built in turbine nodes and additional constraint equations were introduced. The chapter considered three distinct investigations regarding the ESS, which were the sizing and charging strategy, the cost, and the implications to the overall layout and cable selection.

To determine the ESS sizes to use, both in terms of power rating and energy capacity, and to determine the most appropriate charging strategy, the first study simulated a range of power ratings, energy capacities, charging limits, and discharging limits. The resulting peak-shaving capability of each combination was explored showing that a large energy capacity was required to provide any meaningful peak power reduction. While the peak power reduction is very site specific, it was found that for the combination of turbine, wind profile, and cable set presented in this chapter, an ESS of 3MW/64MWh operating a two-level charging strategy of 7.4MW/7.4MW would provide the necessary peak-shaving to allow for cable size reduction if determined economically feasible to do so by the algorithm.

A string of 12 turbines connected in a single non-branching line was used for the costing study. Turbines were allowed to contain between zero and eight units of ESS, with the individual ESS unit size equal to 0.75MW/16MWh (one quarter of the size determined in the previous study). This allowed turbines to contain a range of ESS sizes in the string between zero and twice that determined in the previous study, allowing for over-sizing if the algorithm found benefit in electrical loss reduction, for example. With zero cost associated with building the ESS units, it was found that turbines contained between three and four units of ESS each, not the expected eight. Because of the simple two-level charging strategy (or one-level charging strategy since the charging and discharging levels were the same), the electrical losses actually increased for higher power ESS in turbines as more energy was discharged closer to the discharge level at higher powers, increasing electrical losses. With a fixed cost of ESS, the ESS in the string was aggregated into three turbines each containing eight units, minimising the number of turbines with the additional fixed cost. In addition to the fixed cost, a range of variable costs (cost per MWh) were included, showing that no ESS was built in the string when the cost was £1,800 or higher. For lower costs, ESS tended to be built towards the end of the string (furthest from the substation) where the peak-shaving benefits could be utilised for the downstream cable sections. Interestingly, no cable size reduction was seen at any cost; ESS peak-shaving was used only to reduce the electrical losses. A fixed cost of £13,800 and a variable cost of £0/MWh was chosen for the following layout study. This was chosen as the break-even cost (cost per MWh) for using ESS was too low compared to real ESS costs identified in the literature review. An additional cost is still required, however, in order to account for the complexity of placing ESS in a turbine rather than grouping it all centrally in the substation for example. This assumes that the cost of the ESS (£/MWh) is accounted for by another concurrent revenue stream such as black-start provision and any peak-shaving benefits are only an additional stacked revenue stream for the operator. However, no consideration was given to the additional cost of repairs and replacements or the additional capacity required to account for degradation over the life of the ESS.

Optimising the cable layout for the hypothetical site with the ESS components

included, showed that improved solutions were found and that the benefit was largely from electrical loss reduction. However, several of the case studies also exhibited altered layouts and cable selections when ESS was included for peak-shaving. Most solutions placed ESS at the ends of the strings, however some of the solutions also included ESS in the middle of strings when non-branching sections of strings became long enough to justify it. In some cases the number of substation connections were reduced, reducing the substation connections costs. No cable sizes were directly de-rated in the same layout, but changes to the layout did allow for fewer of the larger cables to be used overall, and in one instance the largest cable that can support up to 12 turbines when no ESS is present, was actually able to support 13 turbines - which can be considered to be effectively de-rating the connection. The objective value of all instances of the hypothetical site case study were reduced by 0.22-1.85%, however, there were limitations to the approach. As the number of turbines increases, so too does the computational complexity although an exact computational time was difficult to record. This meant that the larger sites were very difficult to solve with a standard or higher specification desktop PC and the formulation was not suitable for parallel processing using a supercomputer. Reducing the set of possible ESS sizes resulted in an optimised solution for the largest case study of 122 turbines in a reasonable computational time but in a more constrained solution space than the smaller cases. Future adaptations to the proposed model may wish to optimise the computational efficiency. One possible improvement, is removing the  $e1_{i,j}$  variables, to be replaced with  $m \cdot x_{i,j}^{t,n,m}$  variables. This change would not affect the results of the optimisation, but in removing a small number of variables, may provide an incremental improvement in computational efficiency.

With the costing study assuming other stacked revenues, not taking into account additional cost components such as ESS degradation, and the large ESS sizes required to provide any meaningful peak-shaving, there is further work required in both the modelling and real-world development of energy storage before this may be a practical application for offshore wind farm developers and operators. Further work includes the detailed analysis of the ESS sizing especially in relation to the available space within a given turbine. Considering the charging activity and the SOC profile will allow the con-

sideration of not only the degradation but also what additional stacked revenue streams may be able to operate concurrently with the peak-shaving functionality. A more sophisticated charging strategy may also reduce ESS degradation relative to the simple two-level strategy proposed in this initial work. Finally, allowing ESS in the substation nodes may alter the positioning of the ESSs within the site if the cost components are favourable for siting at the substation.

In conclusion, the objective of this chapter was to integrate energy storage as a decision variable into the cable routing optimisation to determine to what extent energy storage may be able to change (or ‘loosen’) constraints and provide more cost-effective cable routing solutions. The methodology proposed in this chapter met this objective by adding additional decision variables into the MILPsp method proposed in Chapter 6. It was found that very few charging strategies were able to deliver meaningful peak-shaving to the power in the array cables and those that did, required a very large ESS capacity to do so. While this is a site-specific result, it is unlikely that variations between sites will be enough to substantially change the results shown in this work. As an initial study in this field, future works should look to build upon this, considering not only other sites and wind profiles, but also expanding the quantities of ESS available and constraining ESS capacity based on real turbine weight and volume limitations. Further, the cost of the co-located ESS was prohibitively high compared to real ESS prices at the time of writing. Ignoring cost restrictions, using ESS within the cable layout optimisation was able to reduce cable network costs by 0.22-1.85% for this specific site.

## Chapter 8

# Conclusions

This section provides a summary of the work presented in the thesis, with key conclusions and possible avenues of future research. Reference is made to the aims and objectives posed at the start of the thesis to ascertain to what extent these have been met and what the resulting findings are for the research questions.

### 8.1 Thesis Summary

In order to address the research questions posed at the start of the thesis, several objectives were identified and a chapter of work was produced to address each one. The following provides a summary of the work conducted within each chapter and the associated key findings.

#### 8.1.1 Turbine Placement Optimisation

Although there is clearly not yet a convergence on the best method for turbine layout optimisation, several areas of interest are highlighted by the literature including: the need for developing an efficient optimisation approach for larger, more complex sites; the use of more accurate wake models; and a standard benchmark wind farm with data on the wind profile, turbines, and realistic boundary shape. Many optimisation methods are also explored by works in the academic literature with heuristics offering a promising approach to large-scale optimisation problems with complex objective functions.

As such, the objective of Chapter 3 was to utilise a PSO-based approach, as identified in the literature review, to develop a turbine layout optimisation method for large-scale offshore wind farms. A new approach was proposed, built from a combination of existing models and methods as well as two novel components: the on-the-fly lookup and the micro-siting function which were able to reduce computational time by around 95% and increase the objective value by 1.11%, respectively. A comparison of the wind farm model with real data from the Lillgrund offshore wind farm showed very good correlation, matching energy capture of the site to within 0.17%, and a GW-scale hypothetical site was proposed to compare turbine layout solutions to intuitively designed solutions. The tool was able to outperform all intuitively designed solutions and maintain a more consistent set of solutions despite utilising heuristic methods.

An additional case study was carried out on the Berwick Bank offshore wind farm site (before it was joined with the Marr Bank site) being developed by SSE. Here, the solutions of the proposed method were compared to those produced by SSE and its in-house tool. The quality of the solutions, as assessed by annual energy yield, were very similar (with the proposed tool solution between 0.11-0.35% lower energy capture than the SSE solution). The results of the case studies, in terms of closely matching annual energy yield and the ability to consider large sites, gave a high degree of confidence that the proposed tool was sufficiently good and that the objective had been met. The tool was therefore acceptable for the integration of a cable layout optimisation module into this - typically much earlier - design phase.

### 8.1.2 Cable Layout Optimisation

The objective of Chapter 4 was to develop an offshore wind farm array cable layout optimisation method, capable of considering large-scale problems in a computationally efficient manner. As the MILP method, dominant in the academic literature, faces challenges with scaling up to larger problems, a comparison was conducted between the MILP approach, a heuristic ACO method, and a novel approach combining an ACO with a decomposition strategy, ACOSP. The new method, ACOSP, was compared to a classical MILP method and an unedited ACO algorithm. The MILP algorithm yielded

the best solutions but scales very poorly with increasing numbers of turbines to connect, such that for large sites with many turbines it is not possible to solve using standard desktop computing facilities. The ACO algorithm generates solutions very quickly, however being a heuristic algorithm can produce different results from each simulation and not necessarily reach the optimal solution. (Note, care must be taken when tuning the optimisation parameters to ensure robust results from heuristic approaches such as ACO, which are likely to be problem specific). Solutions of the ACO algorithm were between 0.4% and 7.6% higher total cost (as determined by the objective function) than the optimal solution. The ACOsp algorithm produced solutions more slowly than the ACO algorithm but still within a couple of hours and its solutions were only between 0.0% and 1.4% more expensive than the optimal solution, showing that it is a good method for large scale sites when standard desktop computing power is available.

The ACOsp approach was therefore determined, through the above case studies, to be a suitable tool moving forwards for integration with the turbine layout optimisation approach from Chapter 3.

### **8.1.3 Integrated Turbine & Cable Layout Optimisation**

The objective of Chapter 5 was to integrate the turbine and cable layout optimisation approaches from the two preceding chapters into a single optimisation framework to determine and quantify the impact of considering array cable network costs during early design phases of offshore wind farms. The cable layout optimisation algorithm was integrated in stages throughout the turbine layout optimisation to limit computational complexity. A set of ten simulations were carried out for the sequential optimisation and a set of ten for the integrated approach on the large-scale hypothetical site proposed in the earlier chapters. This facilitated a comparison of sequential and integrated solutions to isolate the impact of the integration of approaches.

Both sets of solutions, sequential and integrated, reliably produced layouts containing 164-165 turbines, however, the integrated optimisation solutions had a higher objective value by 0.45% on average. An appropriate statistical test, the Mann-Whitney U Test, was conducted, which determined that the objective value difference in the sets

of solutions was statistically significant. While the integrated approach did increase the objective value in this maximisation problem, both approaches showed a larger increase between their solutions containing 165 and those containing 164 turbines (0.55% and 0.57%). This demonstrates that, for this site, it is more impactful to include another turbine in the site, than to integrate the optimisation approaches. However, the best performing solution of both approaches was that which contained 165 turbines and also adopted the integrated optimisation approach.

#### 8.1.4 Advanced Cable Layout Optimisation

Following the development of the ACOSP cable layout optimisation algorithm and its integration into the turbine layout optimisation process, it became clear that there may be a need and opportunity to develop a more robust array cable layout optimisation tool through the use of classical optimisation approaches and decomposition strategies. This aimed to maintain the benefits of robust and accurate solutions of the classical MILP approach combined with the computational efficiency and speed of the decomposition proposed in the ACOSP methodology. Chapter 6 presents the methodology and development of such a method, the MILPsp algorithm.

While a direct comparison could not be made between the MILPsp algorithm and the previous methods used in Chapter 4 because of the change in the problem formulation, the MILPsp algorithm did appear to generate better quality solutions in a faster computational time. Optimal solutions were found in almost all test cases, with the worst case solution only 1.4% more expensive than the optimal. The change in problem formulation from the ACOSP method resulted in the MILPsp algorithm struggling to find good quality solutions for some problems however. Reducing the number of strings to within the substation connection limit proved difficult as sub-problems were solved in isolation with no option to join to neighbouring strings, unlike in the ACOSP method. Overall the proposed MILPsp algorithm was very effective and the problem formulation allowed for easier integration of an energy storage component into the MILP-based model; this was therefore selected for the following chapter of work.

### 8.1.5 Influence of Energy Storage Systems

The objective of Chapter 7 was to integrate energy storage as a decision variable into the cable routing optimisation to determine to what extent energy storage may be able to change (or ‘loosen’) constraints and provide more cost-effective cable routing solutions. A set of energy storage variables were included into an extended version of the MILPsp algorithm which described the quantity of energy storage in each turbine and the amount electrically ‘upstream’ of each cable section.

The first part of the three-part study investigated the required power and energy capacity of ESS to provide a peak-shaving service to the particular hypothetical case study problem. The solutions showed that very large amounts of ESS (3MW/64MWh) were required for any meaningful peak-shaving capability that might allow for cable de-rating. A simple two-level charging strategy was also determined for the range of ESS sizes which, in order to minimise the energy capacity, was ‘collapsed’ to a one-level charging strategy by setting the charging and discharging levels to the same value (7.4MW/7.4MW).

The second part of the study considered a discrete range of ESS sizes based on the sizing study and optimised the cable selection for a single linear string of 12 turbines. A fixed cost was first applied to account for the increased complexity of fitting ESS within turbines followed by the addition of a range of variable costs (£/MWh). The solutions showed that the break-even price for using any ESS fell well below that of the real ESS prices identified in the literature review. As such, it was necessary to assume that the cost of the ESS may be accounted for by another stacked revenue stream but the fixed cost would be kept to account for the increase in complexity when placed in a turbine.

The third part of the study considered the cable layout of the hypothetical offshore wind farm case study over a range of numbers of turbines. The solutions including ESS all reduced the objective value (NPV total lifetime costs), relative to solutions without ESS, by 0.22-1.85%. The ESS was typically built at the ends of the strings as this helps to peak-shaving the power over the whole string, however, not all of the sites changed the cable layout in the presence of ESS. Indeed, it was the case that most of the cost reduction provided by the ESS was through reducing the electrical losses in the cables

and only a small amount from changing the layout and/or cable selection in some cases.

## 8.2 Conclusions

Having summarised the content of the thesis with consideration of each objective, this section aims to provide a conclusion to the thesis with respect to the initial research questions.

### 8.2.1 Research Question 1

In Chapters 3 and 4, the turbine layout and cable layout optimisation tools developed in this thesis have been shown to be effective tools, even when compared to industry standard methods such as SSE's in-house turbine layout optimisation tool. For large scale offshore wind farms, good layout solutions can save large amounts of money for relatively small incremental improvements and so tools generating solutions approaching optimality can be very valuable for the industry.

Chapter 5 aimed to directly answer the research question by integrating the two optimisations into a single optimisation framework and isolate the effect relative to sequentially optimising the turbine layout followed by the cable layout. For the hypothetical site on which the case study was run, a statistically significant result was found that demonstrated a benefit of using an integrated/concurrent optimisation approach. The increase in objective value, however, was less than the increase found by adding another turbine to the site, so the benefit of this approach may be modest. The best solutions were those that had the most turbines and also used the integrated optimisation approach. The overall impact on project costs (value of energy capture minus turbine and cable capital costs) was a 0.45% increase/benefit when integrating cable layout optimisation into the earlier turbine layout optimisation phase.

A limitation of the study was the limited resources required to run the optimisations for comparison and the largely increased computational time required. Running the comparison on only one site limits the extent to which a benefit can be claimed. While nothing in the proposed approach should be a site-specific benefit, it is possible

that less (or more) benefit would be found at a different wind farm site. Further, while the number of optimisations run was a large enough sample size to detect a statistically significant result, an increased number of runs for the case study would help to increase confidence in this.

**Research Question 1:** What is the potential impact, in terms of project costs, of considering array cable network costs during early turbine layout design optimisation phases of GW-scale offshore wind farms?

**Answer:** The overall impact on project costs (value of energy capture minus turbine and cable capital costs) was a 0.45% increase/benefit when integrating cable layout optimisation into the earlier turbine layout optimisation phase. While nothing in the proposed approach should be a site-specific benefit, it is possible that less (or more) benefit would be found at a different wind farm site.

### 8.2.2 Research Question 2

The cable layout optimisation that was used to address this research question was the MILPsp algorithm proposed in Chapter 6. The MILPsp algorithm was developed following the integrated optimisation study to provide a reliable cable layout optimisation code that was able to consider large sites using a standard desktop PC.

An energy storage component can be easily integrated into the MILPsp algorithm which enabled a three-part study of the impacts of ESS relative to cable layout solutions with no ESS present. The first part revealed that large amounts of ESS are required to provide any meaningful peak shaving service and a charging strategy must be adopted to minimise the total size, which in turn impacts the number of charging cycles and degradation. Though it will be site specific, the ESS parameters required for the hypothetical site case study were a power rating of 3MW, an energy capacity of 64MWh, a charging level of 7.4MW, and a discharging level of 7.4MW. This means that, at all times, the ESS will either be charging or discharging (unless the SOC means there is no further energy capacity for charging/discharging). As the ESS degradation was not considered, the effect of this charging strategy is unknown, however, the constant oper-

ation is likely to lead to high cycling and degradation and so is unlikely to be a valid approach to the ESS charging strategy.

A costing study using the above ESS parameters as a base, showed that the price of the ESS would need to be on the very lowest end of current prices of ESS (of any type);  $< \text{£}1,800/\text{MWh}$  required with a minimum available cost of  $\text{\$}2,000/\text{MWh}$  using CAES . With a fixed cost of integrating ESS into a turbine equal to that of the cable jointing cost ( $\text{£}13,800$ ), the price per MWh at which ESS became too expensive was approximately  $\text{£}1,800$ , much lower than most of the prices shown in the review of the state of the art. This low price is required only when the costs associated with the ESS must be offset by the benefit provided in the peak-shaving function investigated in this work. Therefore, an assumption was made that, by stacking revenue streams such as black start provision, the cost of the ESS may be accounted for by another service. Making this assumption allowed for the investigation of the impacts to the cable ratings and lifetime costs as posed in the research question. However, since other ancillary services such as black start may not require the ESS to be distributed throughout the turbines, it was important to keep the fixed cost of installing ESS in a turbine to account for that cost in this study.

The third part of the study concurrently optimised the cable layout, cable selection, ESS sizes, and ESS location. Using the sizes and costs of ESS identified previously, it was found that the ESS was able to reduce the objective value of the solutions by 0.22-1.85% when the full cable layout optimisation was considered. The ESS that was built was typically at the ends of the strings, as this helps to peak-shave the power throughout the whole string, however, not all of the sites changed the cable layout in the presence of ESS. Indeed, it was the case that most of the cost reduction provided by the ESS was through reducing the electrical losses in the cables and only a small amount from changing the layout and/or cable selection in some cases. While it is clear that most of the saving came from the reduction in electrical losses, it is hard to quantify as it is very site specific and in some cases some changes to the layout were made which in turn affected the cable selection and electrical losses of other cable sections in the network.

Overall, it was shown that while the integration of ESS into the cable layout optimisation can reduce the lifetime costs of offshore wind farms, the high energy capacity and low cost required are prohibitively high and low respectively, such that it is not yet a practical application for offshore wind farm projects. The complex study required assumptions to be made that may limit the extent to which results can be said to be reliable. Separating the study into three distinct sections, while necessary to enable to study, assumes that a one-at-a-time sensitivity analysis of the parameters (capacity, cost, and location) is sufficiently similar to considering all variables in a single optimisation. While justified by enabling the case study to happen at all, this approach inevitably introduces some uncertainty into the result. Another assumption used to enable to latter part of the study is that a secondary revenue stream may be used to account for the capital cost of ESS. Further, with the study being agnostic to the type of ESS, degradation of the storage was beyond the scope of the project. Given that the study, with the enabling assumptions present, demonstrated that co-located ESS would not be a practical application for large offshore wind farms, it is unlikely that including the costs associated with degradation would change this result.

**Research Question 2:** What is the potential impact of using energy storage at the wind farm level to reduce the cable rating and lifetime losses in offshore wind farm array cable networks?

**Answer:** Co-located ESS can lower the lifetime costs of the array cable network, primarily through reducing the electrical losses in cables (rather than de-rating cable sections). However, the high energy capacity and low ESS cost required to deliver this benefit are prohibitively high and low respectively and therefore does not currently make this a practical application for large offshore wind farms.

### 8.3 Future Research

Throughout the work presented in the previous chapters, several areas have been highlighted for potential future research focuses. The below details the areas for future research in each of the main components of this thesis covering turbine layout optimi-

sation, cable layout optimisation, integrated turbine and cable layout optimisation, and integrated energy storage and cable layout optimisation.

While the turbine layout optimisation presented in Chapter 3 was shown to be a good optimisation method, some opportunities for future research were identified. The proposed micro-siting function was only used on the final solution, rather than employed throughout on the incumbent solutions generated during the PSO algorithm. Applying the micro-siting function at each step/iteration in the PSO algorithm may yield improved results. However, this would lead to a very large increase in computational time (of several orders of magnitude), so would need additional work to develop a much quicker, but equally robust, approach to micro-siting. The proposed method used an objective function considering the lifetime costs of the wind farm (NPV lifetime energy capture, minus the capital cost of turbines). This objective was appropriate for the consideration of lifetime costs, as per the research question, and the integration with a cable layout optimisation in the following chapters. However, future works may wish to investigate how the proposed methodology performs with alternative objective functions such as the maximisation of energy yield and/or the minimisation of wake interactions.

In the area of cable layout optimisation, this thesis used cable routes that were predominantly defined by straight line connections, sometimes in conjunction with a path routing algorithm to route around obstacles (always using straight line sections to form the routes). Including a more accurate model of the cables and their bending restrictions could provide a more accurate assessment of the route lengths and limitations on tight bends. For all instances of cable layout optimisation, it was assumed that all turbines generate the same electrical power regardless of their position in the site. This necessary assumption greatly reduced the complexity of what could develop into an impractical level of detail. Finding an efficient methodology to include this aspect would again increase the accuracy of the cable models and associated electrical losses. A third area of potential future cable layout research was mentioned in Chapter 6, outlining the problem with the MILPsp algorithm in its current form; turbines are not allowed to connect to neighbouring strings outside of the sub-problem. Adjusting the problem

formulation to allow turbines to connect to other strings outside of the sub-problem will most likely remove the issue of some solutions containing too many strings, as was shown in the ACOsp approach. This would require a reasonably comprehensive change to the recursive decomposition but would help to mitigate the current limitation.

While the integrated turbine and cable layout optimisation did appear to show some initial improvements, the data set was too small for these to be statistically significant. Therefore, a much larger data set may be able to determine what level of improvement can be made by this approach compared to a sequentially optimised site. To generate such a set of results, a large computational resource is required (which limited the size of the data set in this study). An alternative area of future research regarding an integrated optimisation framework, is to investigate alternatives to the heuristic elements of the algorithm, ideally that can take advantage of high-performance parallel computing facilities (unlike the MILP based solvers used in this study) such as the ARCHIE WeSt supercomputer at the University of Strathclyde. This may help to reduce the spread in the objective values of the solutions and make it easier to determine any statistical significance using a reasonably small data set.

While the integrated turbine and cable layout optimisation did show some initial improvements, the increase in objective value was modest (0.45%). The approach used a single objective function in each phase of the algorithm, evaluating all parts of the solutions based on NPV currency. Future studies may wish to consider different objective functions for the different aspects of solutions in a multi-objective approach. For example, turbine layouts may be assessed based on annual energy yield and cables may be assessed on capital cost. The objective values may then be weighted and combined to assess the overall integrated solution. This approach may change the level to which the cable routings effect the turbine positions and give a solution more in line with the focus of a given developer (if that is different from NPV currency). Future works may also wish to expand the cost components considered, such as substructure costs based on the bathymetry of the site. These may be easily integrated into the current approach, as described in Chapter 5.

Regarding the integration of ESS into cable layout optimisation, several areas could

be investigated to build on the work presented in this thesis. Firstly, for different types of ESS, an analysis of the housing capacity of a given turbine would provide a valuable constraint to the sizing section of the study. Secondly, a more advanced charging strategy may be used as opposed to the two-level charging strategy proposed in this work. Including consideration of the ESS degradation (specific to the type of ESS used) would also be valuable in determining what level of charging activity is acceptable and what the additional cost is for repairs and replacements. Within a possible future charging strategy study, another useful constraint to determine is what additional services the ESS is required to do to offset the cost, and how these impact the charging activity. For example, if black start provision is also provided, what level of ESS SOC must be maintained to meet the requirements of providing this service. Finally, future works could look to allow differentiated charging activity at each ESS, even if a uniform charging strategy is adopted but in the presence of differentiated power output (through consideration of wake effects for example). This is a much more complex optimisation problem and would require more in-depth modelling than the location agnostic consideration of ESS presented in this study.

## 8.4 Application for Industry

This section aims to provide a summary of the key information for - and recommendations for implementation of - each of the sections of this thesis, for use within industry.

### 8.4.1 Turbine Layout Optimisation

The turbine layout optimisation algorithm presented in Chapter 3 generated good quality solutions for grid-based layouts in offshore wind farms even in sites that contained irregular boundaries, obstacles, and large numbers of turbines. For a full description, see Equations (3.1 - 3.17) and Algorithms 1 and 2.

Two additional sections were included in the algorithm: an on-the-fly lookup heuristic and a micro-siting function. It is recommended that the on-the-fly lookup function is not used as this only provided benefits in reducing the computational time to determine

the optimal number of turbines to use in the site, which was later made redundant when assigning a fixed number of turbines for the SSE comparison study. The micro-siting function can be used if turbines are allowed to deviate from their grid-based positions and small improvements in AEY may be found using this function.

Overall, the tool was able to generate solutions that very closely matched the solutions of the SSE in-house tool ( $\leq 0.35\%$  difference in AEY).

### 8.4.2 Cable Layout Optimisation

Several cable layout optimisation tools are presented in this thesis. It is recommended that the MILPsp tool, presented in Chapter 6, is used as this offered the best compromise between the quality of solutions and computational time - largely reaching the optimal solution using a standard desktop PC.

Some limitations were found in the algorithm and problem formulation. Unlike the ACO and ACOSP algorithms, presented in Chapter 4, the MILPsp algorithm does not allow turbines within a sub-problem to connect to turbines outwith the sub-problem. This can lead to the number of strings remaining higher than the substation connection constraint in the final solution. A small addition to the start of the recursive decomposition phase may alleviate this limitation, whereby a small group of strings (more than two) may be solved together in a sub-problem to reduce the number of strings to within the substation connection limit.

For a full description of the model and optimisation equations, see Sections 4.2.3 and 6.1 and Algorithms 9 - 13.

### 8.4.3 Integrated Turbine & Cable Layout Optimisation

Integrating the turbine layout and cable layout optimisations into a single optimisation framework found improvements in solutions relative to considering them as separate sequential design phases. The proposed algorithm in Chapter 5 demonstrated a 0.45% improvement in project costs (NPV energy capture, minus capital costs of turbine and cables, minus electrical losses) for a large hypothetical offshore wind farm site. Exact levels of cost benefit are likely to be site specific, but it is recommended that this approach

be employed as presented in Chapter 5 for the generation of good quality solutions for large offshore wind farm layouts.

#### **8.4.4 Integrating Energy Storage**

Integrating a set of energy storage variables into the cable layout optimisation did show that ESS was able to affect the solutions largely through electrical loss reduction but also in some cases through the layout and cable selection. However, it was shown that the size (both in terms of power and energy capacity) of the ESS required was very large to be placed within an offshore turbine. Further, the cost study suggests that a prohibitively low cost would be required in order to justify the use of ESS unless accounted for by another concurrent revenue stream. This low cost also did not consider the effect of degradation of the storage device or the cost of repairs and replacements and so further work is needed before this study could be used in industry applications.

# Bibliography

- [1] United Nations, “Paris Agreement,” United Nations, Tech. Rep., 2015.
- [2] European Union, “Update of the NDC of the European Union and its Member States,” European Union, Tech. Rep., 2020.
- [3] United States Department of State, “The Long-Term Strategy of the United States: Pathways to Net-Zero Greenhouse Gas Emissions by 2050,” United States Government, Tech. Rep. November, 2021. [Online]. Available: <https://www.whitehouse.gov/wp-content/uploads/2021/10/US-Long-Term-Strategy.pdf>
- [4] Global Wind Energy Council, “Global Offshore Wind Report 2021,” Global Wind Energy Council (GWEC), Tech. Rep., 2021. [Online]. Available: <https://gwec.net/wp-content/uploads/2021/03/GWEC-Global-Wind-Report-2021.pdf>
- [5] International Energy Agency, “Key World Energy Statistics 2021,” International Energy Agency (IEA), Tech. Rep., 2021.
- [6] —, “Net Zero by 2050 - A Roadmap for the Global Energy Sector,” International Energy Agency (IEA), Tech. Rep., 2021. [Online]. Available: <https://www.iea.org/reports/net-zero-by-2050>
- [7] British Petroleum, “Statistical Review of World Energy,” British Petroleum (BP), Tech. Rep., 2021. [Online]. Available: <https://www.bp.com/content/dam/bp/business-sites/en/global/corporate/pdfs/energy-economics/statistical-review/bp-stats-review-2021-full-report.pdf>

## Bibliography

- [8] International Renewable Energy Agency, “Renewable Power Generation Costs in 2020,” International Renewable Energy Agency (IRENA), Tech. Rep., 2020.
- [9] BVG Associates, “A Guide to an Offshore Wind Farm Updated and extended,” *Published on behalf of The Crown Estate and the Offshore Renewable Energy Catapult*, no. January, pp. 1–70, 2019. [Online]. Available: 10.1016/S0029-5493(00)00422-2
- [10] P. Taylor (author) personal communications with, Atkins, Fraser Nash, K2 Management, Orsted, SSE, and UL Openwind, “Industry Interviews,” 2021.
- [11] F. M. Gonzalez-Longatt, P. Wall, P. Regulski, and V. Terzija, “Optimal Electric Network Design for a Large Offshore Wind Farm Based on a Modified Genetic Algorithm Approach,” *IEEE Systems Journal*, vol. 6, no. 1, pp. 164–172, mar 2012. [Online]. Available: 10.1109/JSYST.2011.2163027
- [12] ORE Catapult, “An innovator’s guide to The Offshore Wind Market,” Offshore Renewable Energy Catapult, Tech. Rep., 2018. [Online]. Available: [https://ore.catapult.org.uk/app/uploads/2018/10/OREC01\\_{\\_}7468-SME-Report-2-Offshore-Wind-Market-SP.pdf](https://ore.catapult.org.uk/app/uploads/2018/10/OREC01_{_}7468-SME-Report-2-Offshore-Wind-Market-SP.pdf)
- [13] P. Taylor, H. Yue, D. Campos-Gaona, O. Anaya-Lara, and C. Jia, “Turbine layout optimisation for large-scale offshore wind farms—A grid-based method,” *IET Renewable Power Generation*, no. February, pp. 1–17, oct 2021. [Online]. Available: 10.1049/rpg2.12295
- [14] —, “Wind farm array cable layout optimisation for complex offshore sites—A decomposition based heuristic approach,” *IET Renewable Power Generation*, no. May, pp. 1–17, sep 2022. [Online]. Available: 10.1049/rpg2.12593
- [15] T. Burton, D. Sharpe, N. Jenkins, and E. Bossanyi, *Wind Energy Handbook*. John Wiley & Sons Ltd, 2001.
- [16] S. H. Kim, H. K. Shin, Y. C. Joo, and K. H. Kim, “A study of the wake effects on the wind characteristics and fatigue loads for the turbines in a

## Bibliography

- wind farm,” *Renewable Energy*, vol. 74, pp. 536–543, 2015. [Online]. Available: <http://dx.doi.org/10.1016/j.renene.2014.08.054>
- [17] K. Thomsen and P. Sørensen, “Fatigue loads for wind turbines operating in wakes,” *Journal of Wind Engineering and Industrial Aerodynamics*, vol. 80, no. 1-2, pp. 121–136, 1999.
- [18] A. P. J. Stanley, J. King, and A. Ning, “Wind Farm Layout Optimization with Loads Considerations,” *Journal of Physics: Conference Series*, vol. 1452, no. 1, p. 012072, jan 2020. [Online]. Available: <https://iopscience.iop.org/article/10.1088/1742-6596/1452/1/012072>
- [19] H. Díaz and C. Guedes Soares, “Review of the current status, technology and future trends of offshore wind farms,” *Ocean Engineering*, vol. 209, no. March, p. 107381, aug 2020. [Online]. Available: <https://doi.org/10.1016/j.oceaneng.2020.107381><https://linkinghub.elsevier.com/retrieve/pii/S002980182030411X>
- [20] N. O. Jensen, *A note on wind generator interaction*. Roskilde: Risø National Laboratory, 1983. [Online]. Available: <http://www.risoe.dk/rispubl/VEA/veapdf/ris-m-2411.pdf>
- [21] F. Azlan, J. Kurnia, B. Tan, and M.-Z. Ismadi, “Review on optimisation methods of wind farm array under three classical wind condition problems,” *Renewable and Sustainable Energy Reviews*, vol. 135, no. November 2019, p. 110047, jan 2021. [Online]. Available: [doi.org/10.1016/j.rser.2020.110047](https://doi.org/10.1016/j.rser.2020.110047)<https://linkinghub.elsevier.com/retrieve/pii/S1364032120303385>
- [22] A. C. Pillai, “On the Optimization of Offshore Wind Farm Layouts,” Ph.D. dissertation, The University of Edinburgh, 2016.
- [23] I. Katic, J. Hojstrup, and N. Jensen, “A Simple Model for Cluster Efficiency,” in *EWEC’86. Proceedings*, vol. 1, 1987.

## Bibliography

- [24] G. Larsen, *A Simple Wake Calculation Procedure*. Risø National Laboratory, 1988, vol. No. 2760. [Online]. Available: [http://orbit.dtu.dk/ws/files/55567186/ris\\_{\\_}m\\_{\\_}2760.pdf](http://orbit.dtu.dk/ws/files/55567186/ris_{_}m_{_}2760.pdf)
- [25] S. Frandsen, R. Barthelmie, S. Pryor, O. Rathmann, S. Larsen, J. Højstrup, and M. Thøgersen, “Analytical modelling of wind speed deficit in large offshore wind farms,” *Wind Energy*, vol. 9, no. 1-2, pp. 39–53, jan 2006. [Online]. Available: [10.1002/we.189](https://doi.org/10.1002/we.189)
- [26] M. Ge, Y. Wu, Y. Liu, and Q. Li, “A two-dimensional model based on the expansion of physical wake boundary for wind-turbine wakes,” *Applied Energy*, vol. 233-234, no. May 2018, pp. 975–984, 2019. [Online]. Available: [10.1016/j.apenergy.2018.10.110](https://doi.org/10.1016/j.apenergy.2018.10.110)
- [27] M. Ge, Y. Wu, Y. Liu, and X. I. Yang, “A two-dimensional Jensen model with a Gaussian-shaped velocity deficit,” *Renewable Energy*, vol. 141, pp. 46–56, 2019. [Online]. Available: [doi.org/10.1016/j.renene.2019.03.127](https://doi.org/10.1016/j.renene.2019.03.127)
- [28] M. Bastankhah and F. Porté-Agel, “A new analytical model for wind-turbine wakes,” *Renewable Energy*, vol. 70, pp. 116–123, oct 2014. [Online]. Available: [doi.org/10.1016/j.renene.2014.01.002](https://doi.org/10.1016/j.renene.2014.01.002)
- [29] T. Göçmen, P. V. D. Laan, P. E. Réthoré, A. P. Diaz, G. C. Larsen, and S. Ott, “Wind turbine wake models developed at the technical university of Denmark: A review,” *Renewable and Sustainable Energy Reviews*, vol. 60, pp. 752–769, 2016. [Online]. Available: [doi.org/10.1016/j.rser.2016.01.113](https://doi.org/10.1016/j.rser.2016.01.113)
- [30] M. M. Pedersen, A. M. Forsting, P. van der Laan, R. Riva, L. A. Alcayaga Romàn, J. Criado Risco, M. Friis-Møller, J. Quick, J. P. S. Christiansen, R. V. Rodrigues, B. T. Olsen, and P.-E. Réthoré, “PyWake 2.5.0: An open-source wind farm simulation tool,” *DTU Wind, Technical University of Denmark*, 2023. [Online]. Available: <https://gitlab.windenergy.dtu.dk/TOPFARM/PyWake>

## Bibliography

- [31] S. Frandsen, “On the wind speed reduction in the center of large clusters of wind turbines,” *Journal of Wind Engineering and Industrial Aerodynamics*, vol. 39, no. 1-3, pp. 251–265, 1992.
- [32] S. Ott and M. Nielsen, “Developments of the offshore wind turbine wake model Fuga,” Technical University of Denmark, Tech. Rep., 2014.
- [33] S. Kumar, R. K. Saket, D. K. Dheer, P. Sanjeevikumar, J. B. Holm-Nielsen, and F. Blaabjerg, “Layout optimisation algorithms and reliability assessment of wind farm for microgrid integration: A comprehensive review,” *IET Renewable Power Generation*, no. October, 2021. [Online]. Available: 10.1049/rpg2.12060
- [34] B. S. Ivanell, R. Mikkelsen, J. N. Sørensen, and D. Henningson, “Validation of methods using EllipSys3D,” Linne Flow Centre, KTH Mechanics, Stockholm, Sweden/Gotland University, Tech. Rep., 2008.
- [35] G. C. Larsen, H. Madsen Aagaard, F. Bingöl, J. Mann, S. Ott, J. N. Sørensen, V. Okulov, N. Troldborg, N. M. Nielsen, K. Thomsen, T. J. Larsen, and R. Mikkelsen, “Dynamic wake meandering modeling,” Technical University of Denmark, Tech. Rep., 2007.
- [36] A. C. Pillai, J. Chick, and V. De Laleu, “Modelling wind turbine wakes at Middelgrunden wind farm,” in *European Wind Energy Conference & Exhibition 2014*. IEEE, oct 2017, pp. 1–10. [Online]. Available: <http://hdl.handle.net/10871/27759>
- [37] G. Mosetti, C. Poloni, and D. Diviacco, “Optimization of wind turbine positioning in large wind farms by means of a Genetic algorithm,” *Journal of Wind Engineering and Industrial Aerodynamics*, vol. 51, pp. 105–116, 1994.
- [38] U. Aytun Ozturk and B. A. Norman, “Heuristic methods for wind energy conversion system positioning,” *Electric Power Systems Research*, vol. 70, no. 3, pp. 179–185, aug 2004. [Online]. Available: 10.1016/j.epsr.2003.12.006

## Bibliography

- [39] G. Marmidis, S. Lazarou, and E. Pyrgioti, “Optimal placement of wind turbines in a wind park using Monte Carlo simulation,” *Renewable Energy*, vol. 33, no. 7, pp. 1455–1460, jul 2008. [Online]. Available: [10.1016/j.renene.2007.09.004](https://doi.org/10.1016/j.renene.2007.09.004)
- [40] Y.-K. Wu, C.-Y. Lee, C.-R. Chen, K.-W. Hsu, and H.-T. Tseng, “Optimization of the Wind Turbine Layout and Transmission System Planning for a Large-Scale Offshore WindFarm by AI Technology,” *IEEE Transactions on Industry Applications*, vol. 50, no. 3, pp. 2071–2080, may 2014. [Online]. Available: [10.1109/TIA.2013.2283219](https://doi.org/10.1109/TIA.2013.2283219)
- [41] H. S. Huang, “Efficient hybrid distributed genetic algorithms for wind turbine positioning in large wind farms,” *IEEE International Symposium on Industrial Electronics*, no. ISIE, pp. 2196–2201, 2009. [Online]. Available: [10.1109/ISIE.2009.5213603](https://doi.org/10.1109/ISIE.2009.5213603)
- [42] Maritime & Coastguard Agency, “Safety of Navigation: Offshore Renewable Energy Installations (OREIs) - Guidance on UK Navigational Practice, Safety and Emergency Response.” Maritime and Coastguard Agency (MCA), Tech. Rep., 2016.
- [43] Y. Wu, S. Zhang, R. Wang, Y. Wang, and X. Feng, “A design methodology for wind farm layout considering cable routing and economic benefit based on genetic algorithm and GeoSteiner,” *Renewable Energy*, vol. 146, pp. 687–698, feb 2020. [Online]. Available: [doi.org/10.1016/j.renene.2019.07.002](https://doi.org/10.1016/j.renene.2019.07.002)
- [44] J. S. González, Á. G. Rodríguez, J. C. Mora, M. Burgos Payán, and J. R. Santos, “Overall design optimization of wind farms,” *Renewable Energy*, vol. 36, no. 7, pp. 1973–1982, jul 2011. [Online]. Available: [doi.org/10.1016/j.renene.2010.10.034](https://doi.org/10.1016/j.renene.2010.10.034)
- [45] T. Kunakote, N. Sabangban, S. Kumar, G. G. Tejani, N. Panagant, N. Pholdee, S. Bureerat, and A. R. Yildiz, “Comparative Performance of Twelve Metaheuristics for Wind Farm Layout Optimisation,” *Archives of Computational Methods in Engineering*, apr 2021. [Online]. Available: [10.1007/s11831-021-09586-7](https://doi.org/10.1007/s11831-021-09586-7)

## Bibliography

- [46] M. A. Lackner and C. N. Elkinton, “An Analytical Framework for Offshore Wind Farm Layout Optimization,” *Wind Engineering*, vol. 31, no. 1, pp. 17–31, jan 2007. [Online]. Available: 10.1260/030952407780811401
- [47] B. DuPont and J. Cagan, “A hybrid extended pattern search/genetic algorithm for multi-stage wind farm optimization,” *Optimization and Engineering*, vol. 17, no. 1, pp. 77–103, mar 2016. [Online]. Available: 10.1007/s11081-016-9308-3
- [48] A. Pillai, J. Chick, L. Johanning, M. Khorasanchi, and S. Pelissier, “Optimisation of Offshore Wind Farms Using a Genetic Algorithm,” *International Journal of Offshore and Polar Engineering*, vol. 26, no. 3, pp. 225–234, sep 2016. [Online]. Available: 10.17736/ijope.2016.mmr16
- [49] J. Serrano González, Á. L. Trigo García, M. Burgos Payán, J. Riquelme Santos, and Á. G. González Rodríguez, “Optimal wind-turbine micro-siting of offshore wind farms: A grid-like layout approach,” *Applied Energy*, vol. 200, pp. 28–38, aug 2017. [Online]. Available: 10.1016/j.apenergy.2017.05.071
- [50] S. K. Swamy, S. Szklarz, R. M. Fonseca, and B. H. Bulder, “Combined wind turbine design and wind farm layout optimisation under wind resource uncertainty,” *Journal of Physics: Conference Series*, vol. 1618, no. 4, p. 042030, sep 2020. [Online]. Available: 10.1088/1742-6596/1618/4/042030
- [51] A. Stanley, O. Roberts, J. King, and C. Bay, “Objective and Algorithm Considerations When Optimizing the Number and Placement of Turbines in a Wind Power Plant,” *Wind Energy Science Discussions*, pp. 1–38, 2021. [Online]. Available: 10.5194/wes-2021-15
- [52] S. Boyd and L. Vandenberghe, *Convex optimization*. Cambridge University Press, 2004.
- [53] E. M. Hendrix and B. G.-Tóth, *Introduction to Nonlinear and Global Optimization*, ser. Springer Optimization and Its Applications. New York, NY: Springer New York, 2010, vol. 37. [Online]. Available: 10.1007/978-0-387-88670-1

## Bibliography

- [54] A. Al Shereiqi, B. Mohandes, A. Al-Hinai, M. Bakhtvar, R. Al-Abri, M. S. El Moursi, and M. Albadi, “Co-optimisation of wind farm micro-siting and cabling layouts,” *IET Renewable Power Generation*, no. July 2020, p. rpg2.12154, mar 2021. [Online]. Available: doi/10.1049/rpg2.12154
- [55] B. Gagakuma, A. P. Stanley, and A. Ning, “Reducing wind farm power variance from wind direction using wind farm layout optimization,” *Wind Engineering*, pp. 1–14, 2021. [Online]. Available: 10.1177/0309524X20988288
- [56] C. Croonenbroeck and D. Hennecke, “A comparison of optimizers in a unified standard for optimization on wind farm layout optimization,” *Energy*, vol. 216, p. 119244, 2021. [Online]. Available: doi.org/10.1016/j.energy.2020.119244
- [57] B. Gu, H. Meng, M. Ge, H. Zhang, and X. Liu, “Cooperative multiagent optimization method for wind farm power delivery maximization,” *Energy*, vol. 233, 2021. [Online]. Available: 10.1016/j.energy.2021.121076
- [58] J. W. Park, B. S. An, Y. S. Lee, H. Jung, and I. Lee, “Wind farm layout optimization using genetic algorithm and its application to Daegwallyeong wind farm,” *JMST Advances*, vol. 1, no. 4, pp. 249–257, 2019. [Online]. Available: doi.org/10.1007/s42791-019-00026-z
- [59] I. Ulku and C. Alabas-Uslu, “A new mathematical programming approach to wind farm layout problem under multiple wake effects,” *Renewable Energy*, vol. 136, pp. 1190–1201, 2019. [Online]. Available: doi.org/10.1016/j.renene.2018.09.085
- [60] M. Fischetti, M. Monaci, J. Stoustrup, J.-J. Leth, and A. B. Borchersen, “Mixed Integer Programming Models and Algorithms for Wind Farm Layout,” Ph.D. dissertation, Università Degli Studi di Padova, 2014.
- [61] J. Serrano González, M. Burgos Payán, J. M. R. Santos, and F. González-Longatt, “A review and recent developments in the optimal wind-turbine micro-siting problem,” *Renewable and Sustainable Energy Reviews*, vol. 30, pp. 133–144, feb 2014. [Online]. Available: 10.1016/j.rser.2013.09.027

## Bibliography

- [62] S. Grady, M. Hussaini, and M. Abdullah, “Placement of wind turbines using genetic algorithms,” *Renewable Energy*, vol. 30, no. 2, pp. 259–270, feb 2005. [Online]. Available: 10.1016/j.renene.2004.05.007
- [63] C. Wan, J. Wang, G. Yang, and X. Zhang, “Optimal Micro-siting of Wind Farms by Particle Swarm Optimization,” in *Lecture Notes in Computer Science*, 2010, vol. 6145 LNCS, no. PART 1, pp. 198–205. [Online]. Available: 10.1007/978-3-642-13495-1{ }25
- [64] A. C. Pillai, J. Chick, L. Johanning, and M. Khorasanchi, “Offshore wind farm layout optimization using particle swarm optimization,” *Journal of Ocean Engineering and Marine Energy*, vol. 4, no. 1, pp. 73–88, feb 2018. [Online]. Available: doi.org/10.1007/s40722-018-0108-z
- [65] D. Wilson, S. Rodrigues, C. Segura, I. Loshchilov, F. Hutter, G. L. Buenfil, A. Kheiri, E. Keedwell, M. Ocampo-Pineda, E. Özcan, S. I. V. Peña, B. Goldman, S. B. Rionda, A. Hernández-Aguirre, K. Veeramachaneni, and S. Cussat-Blanc, “Evolutionary computation for wind farm layout optimization,” *Renewable Energy*, vol. 126, pp. 681–691, 2018. [Online]. Available: 10.1016/j.renene.2018.03.052
- [66] A. C. Pillai, J. Chick, L. Johanning, M. Khorasanchi, and S. Barbouchi, “Comparison of Offshore Wind Farm Layout Optimization Using a Genetic Algorithm and a Particle Swarm Optimizer,” in *Volume 6: Ocean Space Utilization; Ocean Renewable Energy*, vol. 6. American Society of Mechanical Engineers, jun 2016, pp. 1–11. [Online]. Available: 10.1115/OMAE2016-54145
- [67] J. F. Herbert-Acero, O. Probst, P. E. Réthoré, G. C. Larsen, and K. K. Castillo-Villar, “A review of methodological approaches for the design and optimization of wind farms,” *Energies*, vol. 7, no. 11, pp. 6930–7016, 2014. [Online]. Available: 10.3390/en7116930

## Bibliography

- [68] R. C. Poudel, H. Tinnesand, and I. E. Baring-Gould, “An Evaluation of Advanced Tools for Distributed Wind Turbine Performance Estimation,” in *Journal of Physics: Conference Series*, 2019.
- [69] M. Krawczyk, N. Robinson, and S. Tyler, “Testing the Effect of Different Optimization Parameters on Layout Design Using openWind,” Royal Dutch Shell, Tech. Rep., 2011.
- [70] A. Tesauro, P. E. Réthoré, and G. C. Larsen, “State of the art of wind farm optimization,” in *Proceedings of EWEA 2012 - European Wind Energy Conference & Exhibition*, 2012.
- [71] M. Fischetti and D. Pisinger, “Optimizing wind farm cable routing considering power losses,” *European Journal of Operational Research*, vol. 270, no. 3, pp. 917–930, nov 2018. [Online]. Available: [doi.org/10.1016/j.ejor.2017.07.061](https://doi.org/10.1016/j.ejor.2017.07.061)
- [72] G. Quinonez-Varela, G. Ault, O. Anaya-Lara, and J. McDonald, “Electrical collector system options for large offshore wind farms,” *IET Renewable Power Generation*, vol. 1, no. 2, p. 107, 2007. [Online]. Available: [10.1049/iet-rpg:20060017](https://doi.org/10.1049/iet-rpg:20060017)
- [73] A. Wędzik, T. Siewierski, and M. Szymowski, “A new method for simultaneous optimizing of wind farm’s network layout and cable cross-sections by MILP optimization,” *Applied Energy*, vol. 182, pp. 525–538, 2016. [Online]. Available: [doi.org/10.1016/j.apenergy.2016.08.094](https://doi.org/10.1016/j.apenergy.2016.08.094)
- [74] M. Sedighi, M. Moradzadeh, O. Kukrer, and M. Fahrioglu, “Simultaneous optimization of electrical interconnection configuration and cable sizing in offshore wind farms,” *Journal of Modern Power Systems and Clean Energy*, pp. 1–14, jan 2018. [Online]. Available: <http://link.springer.com/10.1007/s40565-017-0366-0>
- [75] M. Fischetti and D. Pisinger, “Mathematical Optimization and Algorithms for Offshore Wind Farm Design: An Overview,” *Business & Information Systems Engineering*, no. June, pp. 0–27, 2018. [Online]. Available: [10.1007/s12599-018-0538-0](https://doi.org/10.1007/s12599-018-0538-0)

## Bibliography

- [76] A. Cerveira, A. F. de Sousa, E. J. Pires, and J. Baptista, “Optimal Cable Design of Wind Farms: The Infrastructure and Losses Cost Minimization Case,” *IEEE Transactions on Power Systems*, vol. 31, no. 6, pp. 4319–4329, 2016. [Online]. Available: 10.1109/TPWRS.2016.2521700
- [77] M. Fischetti and D. Pisinger, “On the Impact of using Mixed Integer Programming Techniques on Real-world Offshore Wind Parks,” *Proceedings of the 6th International Conference on Operations Research and Enterprise Systems (ICORES 2017)*, no. Icores, pp. 108–118, 2017. [Online]. Available: 10.5220/0006190701080118
- [78] —, “On the Impact of Considering Power Losses in Offshore Wind Farm Cable Routing,” in *Communications in Computer and Information Science*. Springer International Publishing, 2018, vol. 509, pp. 267–292. [Online]. Available: 10.1007/978-3-319-94767-9{ }14
- [79] M. Dicorato, G. Forte, M. Pisani, and M. Trovato, “Guidelines for assessment of investment cost for offshore wind generation,” *Renewable Energy*, vol. 36, no. 8, pp. 2043–2051, aug 2011. [Online]. Available: doi.org/10.1016/j.renene.2011.01.003
- [80] E. Eriksson, “Wind farm layout - a reliability and investment analysis,” Ph.D. dissertation, Uppsala Universitet, 2008.
- [81] S. Catmull, R. D. Chippendale, J. A. Pilgrim, G. Hutton, and P. Cangy, “Cyclic Load Profiles for Offshore Wind Farm Cable Rating,” *IEEE Transactions on Power Delivery*, vol. 31, no. 3, pp. 1242–1250, jun 2016. [Online]. Available: 10.1109/TPWRD.2015.2469538
- [82] A. Đorđević and Ž. Đurišić, “General mathematical model for the calculation of economic cross sections of cables for wind farms collector systems,” *IET Renewable Power Generation*, vol. 12, no. 8, pp. 901–909, jun 2018. [Online]. Available: 10.1049/iet-rpg.2017.0420
- [83] T. Pereira and R. Castro, “Comparison of internal grid topologies of offshore wind farms regarding reliability and economic performance metrics analysis,”

## Bibliography

- IET Renewable Power Generation*, vol. 13, no. 5, pp. 750–761, 2019. [Online]. Available: 10.1049/iet-rpg.2018.5474
- [84] A. Messac, *Optimization in Practice with MATLAB®*. Cambridge University Press, mar 2015. [Online]. Available: 10.1017/CBO9781316271391
- [85] M. Fischetti and D. Pisinger, “Optimal wind farm cable routing: Modeling branches and offshore transformer modules,” *Networks*, vol. 72, no. 1, pp. 42–59, jul 2018. [Online]. Available: 10.1002/net.21804
- [86] J. A. Pérez-Rúa, S. Lumbreras, A. Ramos, and N. A. Cutululis, “Reliability-based topology optimization for offshore wind farm collection system,” *Wind Energy*, no. May, pp. 1–19, 2021. [Online]. Available: 10.1002/we.2660
- [87] M. Fischetti and D. Pisinger, “Mixed Integer Linear Programming for new trends in wind farm cable routing,” *Electronic Notes in Discrete Mathematics*, vol. 64, pp. 115–124, feb 2018. [Online]. Available: doi.org/10.1016/j.endm.2018.01.013
- [88] —, “Inter-array cable routing optimization for big wind parks with obstacles,” *2016 European Control Conference, ECC 2016*, pp. 617–622, 2017. [Online]. Available: 10.1109/ECC.2016.7810357
- [89] A. C. Pillai, J. Chick, L. Johanning, M. Khorasanchi, and V. De Laleu, “Offshore wind farm electrical cable layout optimization,” *Engineering Optimization*, vol. 47, no. 12, pp. 1689–1708, 2015. [Online]. Available: doi.org/10.1080/0305215X.2014.992892
- [90] R. C. Prim, “Shortest Connection Networks And Some Generalizations,” *Bell System Technical Journal*, vol. 36, no. 6, pp. 1389–1401, nov 1957. [Online]. Available: <https://ieeexplore.ieee.org/document/6773228>
- [91] A. Hertz, O. Marcotte, A. Mdimagh, M. Carreau, and F. Welt, “Optimizing the Design of a Wind Farm Collection Network,” *INFOR: Information Systems and Operational Research*, vol. 50, no. 2, pp. 95–104, 2012. [Online]. Available: 10.3138/infor.50.2.095

## Bibliography

- [92] A. Cerveira, E. J. Pires, and J. Baptista, “Wind farm cable connection layout optimization with several substations,” *Energies*, vol. 14, no. 12, pp. 1–14, 2021. [Online]. Available: 10.3390/en14123615
- [93] J. Bauer and J. Lysgaard, “The offshore wind farm array cable layout problem: A planar open vehicle routing problem,” *Journal of the Operational Research Society*, vol. 66, no. 3, pp. 360–368, 2015. [Online]. Available: 10.1057/jors.2013.188
- [94] T. Zuo, Y. Zhang, K. Meng, Z. Tong, Z. Y. Dong, and Y. Fu, “A Two-Layer Hybrid Optimization Approach for Large-Scale Offshore Wind Farm Collector System Planning,” *IEEE Transactions on Industrial Informatics*, vol. 17, no. 11, pp. 7433–7444, 2021. [Online]. Available: 10.1109/TII.2021.3056428
- [95] D. Cazzaro and D. Pisinger, “Balanced cable routing for offshore wind farms with obstacles,” *Networks*, no. December 2021, pp. 1–21, 2022. [Online]. Available: 10.1002/net.22100
- [96] Y. Qi, P. Hou, G. Liu, R. Jin, Z. Yang, G. Yang, and Z. Dong, “Cable connection optimization for heterogeneous offshore wind farms via a voronoi diagram based adaptive particle swarm optimization with local search,” *Energies*, vol. 14, no. 3, 2021. [Online]. Available: 10.3390/en14030644
- [97] S. Dutta and T. J. Overbye, “A clustering based wind farm collector system cable layout design,” *2011 IEEE Power and Energy Conference at Illinois, PECEI 2011*, pp. 4–9, 2011. [Online]. Available: 10.1109/PECEI.2011.5740480
- [98] J.-S. Shin and J.-O. Kim, “Optimal Design for Offshore Wind Farm considering Inner Grid Layout and Offshore Substation Location,” *IEEE Transactions on Power Systems*, vol. 32, no. 3, pp. 2041–2048, may 2017. [Online]. Available: 10.1109/TPWRS.2016.2593501
- [99] P. Fagerfjäll, “Optimizing wind farm layout – more bang for the buck using mixed integer linear programming,” Ph.D. dissertation, Chalmers University

## Bibliography

- of Technology, 2010. [Online]. Available: <http://www.math.chalmers.se/Math/Research/Optimization/reports/masters/Fagerfjall-final.pdf>
- [100] M. Dorigo and G. Di Caro, “Ant colony optimization: a new meta-heuristic,” in *Proceedings of the 1999 Congress on Evolutionary Computation-CEC99 (Cat. No. 99TH8406)*, vol. 2. IEEE, 1999, pp. 1470–1477. [Online]. Available: 10.1109/CEC.1999.782657
- [101] R. Srikakulapu and U. Vinatha, “Combined approach based on ACO with MTSP for optimal internal electrical system design of large offshore wind farm,” in *2018 International Conference on Power, Instrumentation, Control and Computing (PICC)*. IEEE, jan 2018, pp. 1–6. [Online]. Available: 10.1109/PICC.2018.8384743
- [102] Y. Wu, T. Xia, Y. Wang, H. Zhang, X. Feng, X. Song, and R. Shibasaki, “A synchronization methodology for 3D offshore wind farm layout optimization with multi-type wind turbines and obstacle-avoiding cable network,” *Renewable Energy*, vol. 185, pp. 302–320, 2022. [Online]. Available: [doi.org/10.1016/j.renene.2021.12.057](https://doi.org/10.1016/j.renene.2021.12.057)
- [103] S. Lumbreras and A. Ramos, “Offshore wind farm electrical design: a review,” *Wind Energy*, vol. 16, no. 3, pp. 459–473, apr 2013. [Online]. Available: 10.1002/we.1498
- [104] —, “Optimal design of the electrical layout of an offshore wind farm applying decomposition strategies,” *IEEE Transactions on Power Systems*, vol. 28, no. 2, pp. 1434–1441, 2013. [Online]. Available: 10.1109/TPWRS.2012.2204906
- [105] L. Amaral and R. Castro, “Offshore wind farm layout optimization regarding wake effects and electrical losses,” *Engineering Applications of Artificial Intelligence*, vol. 60, no. January, pp. 26–34, 2017. [Online]. Available: 10.1016/j.engappai.2017.01.010

## Bibliography

- [106] T. Marge, S. Lumbreras, A. Ramos, and B. F. Hobbs, “Integrated offshore wind farm design: Optimizing micro-siting and cable layout simultaneously,” *Wind Energy*, vol. 22, no. 12, pp. 1684–1698, 2019. [Online]. Available: 10.1002/we.2396
- [107] S. Tao, Q. Xu, A. Feijoo, and G. Zheng, “Joint Optimization of Wind Turbine Micrositing and Cabling in an Offshore Wind Farm,” *IEEE Transactions on Smart Grid*, vol. 12, no. 1, pp. 834–844, jan 2021. [Online]. Available: 10.1109/TSG.2020.3022378
- [108] M. Fischetti and M. Fischetti, “Integrated Layout and Cable Routing in Wind Farm Optimal Design,” *Management Science*, no. May, aug 2022. [Online]. Available: 10.1287/mnsc.2022.4470
- [109] J. A. Pérez-Rúa and N. A. Cutululis, “A framework for simultaneous design of wind turbines and cable layout in offshore wind,” *Wind Energy Science*, vol. 7, no. 2, pp. 925–942, 2022. [Online]. Available: 10.5194/wes-7-925-2022
- [110] P. Hou, W. Hu, M. Soltani, C. Chen, and Z. Chen, “Combined optimization for offshore wind turbine micro siting,” *Applied Energy*, vol. 189, pp. 271–282, mar 2017. [Online]. Available: doi.org/10.1016/j.apenergy.2016.11.083
- [111] H. Chen, T. N. Cong, W. Yang, C. Tan, Y. Li, and Y. Ding, “Progress in electrical energy storage system: A critical review,” *Progress in Natural Science*, vol. 19, no. 3, pp. 291–312, mar 2009. [Online]. Available: doi.org/10.1016/j.pnsc.2008.07.014
- [112] V. Kalkhambkar, R. Kumar, and R. Bhakar, “Joint optimal allocation methodology for renewable distributed generation and energy storage for economic benefits,” *IET Renewable Power Generation*, vol. 10, no. 9, pp. 1422–1429, 2016. [Online]. Available: 10.1049/iet-rpg.2016.0014
- [113] H. Dagdougui, R. Minciardi, A. Ouammi, M. Robba, and R. Sacile, “A dynamic decision model for the real-time control of hybrid renewable energy production systems,” *IEEE Systems Journal*, vol. 4, no. 3, pp. 323–333, 2010. [Online]. Available: 10.1109/JSYST.2010.2059150

## Bibliography

- [114] K. Dvijotham, S. Backhaus, and M. Chertkov, “Operations-Based Planning for Placement and Sizing of Energy Storage in a Grid With a High Penetration of Renewables,” *Optimization and Control*, vol. 27, no. 4, pp. 547–582, jul 2011. [Online]. Available: <http://arxiv.org/abs/1107.1382><http://journals.sagepub.com/doi/10.1177/030631297027004001>
- [115] H. T. Le, S. Santoso, and T. Q. Nguyen, “Augmenting wind power penetration and grid voltage stability limits using ESS: Application design, sizing, and a case study,” *IEEE Transactions on Power Systems*, vol. 27, no. 1, pp. 161–171, 2012. [Online]. Available: [10.1109/TPWRS.2011.2165302](https://doi.org/10.1109/TPWRS.2011.2165302)
- [116] P. Wang, Z. Gao, and L. Bertling, “Operational Adequacy Studies of Power Systems With Wind Farms and Energy Storages,” *IEEE Transactions on Power Systems*, vol. 27, no. 4, pp. 2377–2384, nov 2012. [Online]. Available: [10.1109/TPWRS.2012.2201181](https://doi.org/10.1109/TPWRS.2012.2201181)
- [117] E. Castronuovo and J. Lopes, “On the Optimization of the Daily Operation of a Wind-Hydro Power Plant,” *IEEE Transactions on Power Systems*, vol. 19, no. 3, pp. 1599–1606, 2004. [Online]. Available: [10.1109/TPWRS.2004.831707](https://doi.org/10.1109/TPWRS.2004.831707)
- [118] J. P. Barton and D. G. Infield, “A probabilistic method for calculating the usefulness of a store with finite energy capacity for smoothing electricity generation from wind and solar power,” *Journal of Power Sources*, vol. 162, no. 2 SPEC. ISS., pp. 943–948, 2006. [Online]. Available: [10.1016/j.jpowsour.2005.07.006](https://doi.org/10.1016/j.jpowsour.2005.07.006)
- [119] C. Abbey, K. Strunz, and G. Joós, “A knowledge-based approach for control of two-level energy storage for wind energy systems,” *IEEE Transactions on Energy Conversion*, vol. 24, no. 2, pp. 539–547, 2009. [Online]. Available: [10.1109/TEC.2008.2001453](https://doi.org/10.1109/TEC.2008.2001453)
- [120] D. L. Yao, S. S. Choi, K. J. Tseng, and T. T. Lie, “Determination of short-term power dispatch schedule for a wind farm incorporated with dual-battery energy

## Bibliography

- storage scheme,” *IEEE Transactions on Sustainable Energy*, vol. 3, no. 1, pp. 74–84, 2012. [Online]. Available: 10.1109/TSTE.2011.2163092
- [121] Y. Kim, J. Zhao, and R. J. Harrington, “Performance analysis of energy storage systems connected to a doubly fed induction generator,” *2015 IEEE Green Energy and Systems Conference, IGESC 2015*, pp. 30–34, 2015. [Online]. Available: 10.1109/IGESC.2015.7359387
- [122] S. Venkataraman, C. Ziesler, P. Johnson, and S. Van Kempen, “Integrated Wind, Solar, and Energy Storage: Designing Plants with a Better Generation Profile and Lower Overall Cost,” *IEEE Power and Energy Magazine*, vol. 16, no. 3, pp. 74–83, 2018. [Online]. Available: 10.1109/MPE.2018.2793478
- [123] I. N. Moghaddam, B. Chowdhury, and M. Doostan, “Optimal sizing and operation of battery energy storage systems connected to wind farms participating in electricity markets,” *IEEE Transactions on Sustainable Energy*, vol. 10, no. 3, pp. 1184–1193, 2019. [Online]. Available: 10.1109/TSTE.2018.2863272
- [124] Z. Jiang and X. Yu, “Modeling and control of an integrated wind power generation and energy storage system,” *2009 IEEE Power and Energy Society General Meeting, PES '09*, pp. 1–8, 2009. [Online]. Available: 10.1109/PES.2009.5275753
- [125] Q. Li, S. S. Choi, Y. Yuan, and D. L. Yao, “On the determination of battery energy storage capacity and short-term power dispatch of a wind farm,” *IEEE Transactions on Sustainable Energy*, vol. 2, no. 2, pp. 148–158, 2011. [Online]. Available: 10.1109/TSTE.2010.2095434
- [126] F. Luo, K. Meng, Z. Y. Dong, Y. Zheng, Y. Chen, and K. P. Wong, “Coordinated operational planning for wind farm with battery energy storage system,” *IEEE Transactions on Sustainable Energy*, vol. 6, no. 1, pp. 253–262, 2015. [Online]. Available: 10.1109/TSTE.2014.2367550
- [127] Xinda Ke, Ning Lu, and Chunlian Jin, “Control and size energy storage systems for managing energy imbalance of variable generation resources,” *IEEE*

## Bibliography

- Transactions on Sustainable Energy*, vol. 6, no. 1, p. 8040, 2015. [Online]. Available: 10.1109/TSSTE.2014.2355829
- [128] R. P. Batagholi, D. V. Coury, and O. Anaya-Lara, “Full-Variable Speed Wind Generator Protection considering Energy Storage System Connection and Island Mode Operation,” Ph.D. dissertation, University of Strathclyde, 2017.
- [129] A. Berrada and K. Loudiyi, “Operation, sizing, and economic evaluation of storage for solar and wind power plants,” *Renewable and Sustainable Energy Reviews*, vol. 59, pp. 1117–1129, jun 2016. [Online]. Available: doi.org/10.1016/j.rser.2016.01.048<https://linkinghub.elsevier.com/retrieve/pii/S1364032116000782>
- [130] F. Fan, G. Zorzi, D. Campos-Gaona, G. Burt, O. Anaya-Lara, J. Nwobu, and A. Madariaga, “Sizing and coordination strategies of battery energy storage system co-located with wind farm: The uk perspective,” *Energies*, vol. 14, no. 5, 2021. [Online]. Available: 10.3390/en14051439
- [131] D. Campos-Gaona, A. Madariaga, J. Zafar, O. Anaya-Lara, and G. Burt, “Techno-Economic Analysis of Energy Storage System for Wind Farms: The UK Perspective,” in *2018 International Conference on Smart Energy Systems and Technologies (SEST)*. IEEE, sep 2018, pp. 1–6. [Online]. Available: 10.1109/SEST.2018.8495885
- [132] D. D. Banham-Hall, G. A. Taylor, C. A. Smith, and M. R. Irving, “Flow batteries for enhancing wind power integration,” *IEEE Transactions on Power Systems*, vol. 27, no. 3, pp. 1690–1697, 2012. [Online]. Available: 10.1109/TPWRS.2012.2185256
- [133] Z. Zhang, Y. Zhang, Q. Huang, and W.-J. Lee, “Market-oriented optimal dispatching strategy for a wind farm with a multiple stage hybrid energy storage system,” *CSEE Journal of Power and Energy Systems*, vol. 4, no. 4, pp. 417–424, dec 2018. [Online]. Available: 10.17775/CSEEJPES.2018.00130
- [134] M. Mahmoud, M. Ramadan, A. G. Olabi, K. Pullen, and S. Naher, “A review of mechanical energy storage systems combined with wind and solar applications,”

## Bibliography

- Energy Conversion and Management*, vol. 210, no. February, p. 112670, 2020. [Online]. Available: [doi.org/10.1016/j.enconman.2020.112670](https://doi.org/10.1016/j.enconman.2020.112670)
- [135] H. Zhao, Q. Wu, S. Hu, H. Xu, and C. N. Rasmussen, “Review of energy storage system for wind power integration support,” *Applied Energy*, vol. 137, pp. 545–553, 2015. [Online]. Available: [doi.org/10.1016/j.apenergy.2014.04.103](https://doi.org/10.1016/j.apenergy.2014.04.103)
- [136] Highview Power, “Liquid Air Energy Storage,” 2018. [Online]. Available: <https://www.highviewpower.com/>
- [137] Energy Storage Association (ESA), “Energy Storage Technologies,” 2018. [Online]. Available: <http://energystorage.org/energy-storage/energy-storage-technologies>
- [138] Energy Matters, “Cryogenic Energy Storage Plant Opens,” 2015. [Online]. Available: <https://www.energymatters.com.au/renewable-news/cryogenic-energy-storage-em5250/>
- [139] K. H. Chua, Y. S. Lim, and S. Morris, “Energy storage system for peak shaving,” *International Journal of Energy Sector Management*, vol. 10, no. 1, pp. 3–18, 2016.
- [140] A. J. Pimm, T. T. Cockerill, and P. G. Taylor, “The potential for peak shaving on low voltage distribution networks using electricity storage,” *Journal of Energy Storage*, vol. 16, pp. 231–242, 2018. [Online]. Available: <https://doi.org/10.1016/j.est.2018.02.002>
- [141] V. Kalkhambkar, R. Kumar, and R. Bhakar, “Energy loss minimization through peak shaving using energy storage,” *Perspectives in Science*, vol. 8, pp. 162–165, 2016. [Online]. Available: <http://dx.doi.org/10.1016/j.pisc.2016.04.022>
- [142] G. C. Larsen, “A simple stationary semi-analytical wake model,” *Denmark. Forskningscenter Risoe. Risoe-R*, vol. 1713, no. August, pp. 1–21, 2009.
- [143] M. N. Soltani, T. Knudsen, M. Svenstrup, R. Wisniewski, P. Brath, R. Ortega, and K. Johnson, “Estimation of rotor effective wind speed: A comparison,” *IEEE*

## Bibliography

- Transactions on Control Systems Technology*, vol. 21, no. 4, pp. 1155–1167, 2013. [Online]. Available: 10.1109/TCST.2013.2260751
- [144] W. G. Van Sark, H. C. Van der Velde, J. P. Coelingh, and W. A. Bierbooms, “Do we really need rotor equivalent wind speed?” *Wind Energy*, vol. 22, no. 6, pp. 745–763, jun 2019. [Online]. Available: <https://onlinelibrary.wiley.com/doi/10.1002/we.2319>
- [145] K. Balasubramanian, S. B. Thanikanti, U. Subramaniam, S. N., and S. Sichelalu, “A novel review on optimization techniques used in wind farm modelling,” *Renewable Energy Focus*, vol. 35, no. December, pp. 84–96, dec 2020. [Online]. Available: [doi.org/10.1016/j.ref.2020.09.001](https://doi.org/10.1016/j.ref.2020.09.001)
- [146] B. Saavedra-Moreno, S. Salcedo-Sanz, A. Paniagua-Tineo, L. Prieto, and A. Portilla-Figueras, “Seeding evolutionary algorithms with heuristics for optimal wind turbines positioning in wind farms,” *Renewable Energy*, vol. 36, no. 11, pp. 2838–2844, 2011. [Online]. Available: <http://dx.doi.org/10.1016/j.renene.2011.04.018>
- [147] J. Jeppsson, P. E. Larsen, and A. Larsson, “Technical Description Lillgrund Wind Power Plant,” *Vattenfall Vindkraft AB*, no. September, p. 79, 2008.
- [148] H. Bergstrom, “Meteorological conditions at Lillgrund,” *Swedish Energy Agency*, no. March, pp. 1–26, 2009.
- [149] J.-Å. Dahlberg, “Assessment of the Lillgrund Windfarm Power Performance Wake Effects Lillgrund,” Vattenfall, Tech. Rep. September, 2009.
- [150] C. Desmond, J. Murphy, L. Blonk, and W. Haans, “Description of an 8 MW reference wind turbine,” *Journal of Physics: Conference Series*, vol. 753, no. 9, 2016. [Online]. Available: 10.1088/1742-6596/753/9/092013
- [151] W. Boone, R. Bal, and D. N. V. Gl, “Copper or Aluminium cable conductors , broadly compared in a life cycle perspective TYPICAL PROPERTIES OF COPPER AND,” *Jicable 2015*, pp. 1–5, 2015.

## Bibliography

- [152] D. Arthur and S. Vassilvitskii, “K-means++: The advantages of careful seeding,” *Proceedings of the Annual ACM-SIAM Symposium on Discrete Algorithms*, 2007.
- [153] S. S. Shapiro and M. B. Wilk, “An Analysis of Variance Test for Normality (Complete Samples),” *Biometrika*, vol. 52, no. 3/4, p. 591, dec 1965. [Online]. Available: <https://www.jstor.org/stable/2333709?origin=crossref>
- [154] International Electrotechnical Commission (IEC), “BS IEC 60228,” International Electrotechnical Commission (IEC), Tech. Rep., 2004.
- [155] P. Hart, N. Nilsson, and B. Raphael, “A Formal Basis for the Heuristic Determination of Minimum Cost Paths,” *IEEE Transactions on Systems Science and Cybernetics*, vol. 4, no. 2, pp. 100–107, 1968. [Online]. Available: <http://ieeexplore.ieee.org/document/4082128/>
- [156] E. W. Dijkstra, “A Note on Two Problems in Connexion with Graphs,” in *Edsger Wybe Dijkstra*. New York, NY, USA: ACM, jul 2022, pp. 287–290. [Online]. Available: <https://dl.acm.org/doi/10.1145/3544585.3544600>
- [157] International Electrotechnical Commission (IEC), “BS IEC 60287-3-2:2012,” International Electrotechnical Commission (IEC), Tech. Rep., 2012.
- [158] Z. G. Yang, “Is this the ultimate grid battery?” *IEEE Spectrum*, vol. 54, no. 11, pp. 36–41, nov 2017. [Online]. Available: [10.1109/MSPEC.2017.8093799](https://doi.org/10.1109/MSPEC.2017.8093799)
- [159] UniEnergy Technologies, “UET Chemistry,” 2018. [Online]. Available: <http://www.uettechnologies.com/technology>
- [160] Forbes, “Vanadium-Flow Batteries: The Energy Storage Breakthrough We’ve Needed,” pp. 2016–2019, 2016. [Online]. Available: <https://www.forbes.com/sites/jamesconca/2016/12/13/vanadium-flow-batteries-the-energy-storage-breakthrough-weve-needed/>
- [161] Gravity Power, “Gravity Power Module Technology,” 2017. [Online]. Available: <http://www.gravitypower.net/technology-gravity-power-energy-storage/>

[162] Heindl Energy, “Hydraulic Potential Energy: Basic Concept.” [Online]. Available:  
<https://heindl-energy.com/technical-concept/basic-concept/>

# Appendix A: Industry Engagement

In order to guide the work in this thesis and ensure relevance for industry, engagement with industry was sought and a variety of topics and questions were discussed [10]. The format was generally an open discussion, with somewhat of a focus on the work that was being conducted in the thesis at the time of the discussion. Outcomes of the discussion were collated and summarised and used to guide the thesis work. This section highlights some of the key findings from these discussions without providing the specific responses/viewpoints of companies.

**Discussions conducted by:** Peter Taylor

**Dates of discussions:** Apr-May 2020, Feb-Apr 2021

**Companies:** Atkins, Fraser Nash, K2 Management, SSE, Orsted, and UL Openwind.

## A.1: Turbine Layout Optimisation

### Formulations

- Irregular vs grid-based layouts
  - Maritime & Coast Guard Agency (MCA) recommend grid-based structure therefore it is best to keep a gridded layout, however some deviation is ok.
  - It is good to have some flexibility in the positions of turbines.
  - Projects are always designed to be MCA compliant.
  - Regulations vary around the world.
- Some sites use a ‘perimeter and grid’ layout.

- A site can probably remove a lot of turbines from the initial grid and still be a reasonably acceptable layout.
- Single line of orientation may be worth looking into.
- ‘Overplanting’ turbines may be a benefit when co-located ESS is present.
- Curved rows/columns of turbines may be of interest.
- For onshore, a ‘greedy turbine’ approach is often used (individual turbines aim to maximise own power output with no consideration of downstream wake effects).

### **Objectives**

- Onshore wind farms tend to optimise for maximising energy capture.
- Lifetime costs/benefits are important to include with CAPEX.
- It is good to focus on lifetime costs/revenue.
- Can be useful to consider O&M costs.
- Unscheduled O&M is not a large cost driver.
- Reducing wake interaction with turbines will help to reduce turbine fatigue loads.

### **Constraints & Considerations**

- Bathymetry constraints should be included.
- Avoiding ‘oversail’ (blades overhanging the seabed lease area) is important to include.
- Export capacity is what typically limits the number of turbines.
- Large turbine spacings are required to increase wake recovery (typically 5x3 or 8x6 rotor diameters).
- Set back distance from existing wind farms (typically 1 km) is a constraint to include, if more than one wind farm is present.

- Developers are starting to have an increased appetite for risk.
- Sea depths will impact substructure costs.
- Larger sites may need to consider wind variation across the site.
- Developers are constrained by what is ‘buildable’ in reality.
- Jensen model does not consider upstream effects (no blockage effect).
- Ideally a turbine layout design tool will run on standard desktop computing. Developers don’t always want to invest or pay for high-powered computing facilities if it can be avoided.
- Tools need to be useful for an engineer; wouldn’t want to be waiting hours for a solution, running things overnight would probably be ok but is not desired as simulations will be run many times using varying input parameters.

## A.2: Cable Layout Optimisation

### Formulations

- Looped cable layouts may be able to improve reliability, but are not of interest due to the higher costs. Radial (including branched) layouts are more than sufficient and are what is intended to be used for current/future layout designs.
- Could investigate ‘double cables’ rather than looped layouts to increase reliability.
- Very large (GW-scale) sites are increasingly targeted to be developed.
- Important to be capable of handling multiple substations.
- There are projects looking into using the turbine power output to directly power hydrogen generation.
- Typically requires fixed turbine and substation positions as inputs.

- Proposed A\* algorithm (or similar simple route-finding algorithm) is a reasonable method for finding possible paths.
- An approximate cost of the cable network may be sufficient when used as part of an integrated concurrent optimisation with turbine positions. A more detailed cost approximation could be found by running the cable layout optimisation algorithm a few times in the macro turbine layout optimisation.
- Peak shaving could come from ‘spilling’ power, in order to enable cable size and/or electrical loss reduction.

### **Objectives**

- It is good to focus on lifetime costs/losses as well as cable CAPEX.
- Existing in-house tools are being developed that are looking to include electrical losses, bathymetry constraints, and O&M in the future.
- There is interest in the effect of reducing/changing load profiles in the cable as a result of curtailment and/or co-located ESS.

### **Constraints & Considerations**

- The impact of fixed vs floating wind would be an interesting future development for the tool.
- Bathymetry may be important e.g. cables ‘slipping’ downhill on the seabed.
- Thickness of the cables may need to be considered for things like bend radius – more important for floating offshore wind farms.
- Seabed movement could be considered.
- Consider what stage(s) the tool is intended to be used for - is a detailed cable layout needed at all stages, from wind farm layout concept to detailed design?
- Typically considered after the turbine layout design phase.

- Cable failure rates may be of interest.
- Effect of co-located ESS on cable constraints would be interesting.
- As turbine layout optimisation tools; computational resource is standard desktop computing and computational time should be reduced where possible to allow the simulation of many cases by a design engineer.

# Appendix B: ESS & Ancillary Services

Revenue Stream	Description	Suitable Storage	Approx. Value UK (£/MW/yr)
Enhanced Freq Response (EFR)	Fastest freq. response - Avoid 1% deviation from nominal freq.	Li-Ion Battery Flow Battery Flywheel Capacitor	60k-105k
Firm Freq Response (FFR)	Static - responds with specified power at set freq. deviation Dynamic - power response proportional to deviation	Li-Ion Battery Flow Battery Flywheel Capacitor Pumped-Hydro	50k-145k
Fast Reserve	Protects security of supply from increase in demand/loss of generation	Flow Battery Pumped-Hydro	50k-70k
Short Term Operating Reserve (STOR)	Similar to 'Fast Reserve' with a significantly slower response time ( $\geq 2$ hr duration)	Flow Battery Pumped-Hydro CAES/LAES	20k-35k
Capacity Market (CM)	Ensures sufficient generation capacity during system stress	Li-Ion Battery Flow Battery CAES/LAES	22.5k
Triad Avoidance	Section of annual transmission costs that generators/users of elec. pay for generating/importing during peak demand	Li-Ion Battery Pumped-Hydro CAES/LAES	Region dependent $\sim 30$ k (S. Scotland)
Capacity Split Energy	Storing energy when the grid export capacity reached, exporting when capacity is available	Li-Ion Battery Flow Battery Flywheel Capacitor CAES/LAES	Site dependent
Managing Imbalance Risk	Avoiding disparity between contractual generation/consumption and actual gen/con	Li-Ion Battery Flow Battery	7k-30k
Wholesale Price Arbitrage	Exploits wholesale price change (buy cheap, sell expensive)	Li-Ion Battery Flow Battery LAES	20k
Black Start	Aids recovery of transmission system in total/partial shutdown	Pumped-Hydro CAES/LAES	Undisclosed
Peak-Shaving	'Smoothing' power output to use (cheaper) cables of lower rating	-	-

Table A.1: Revenue streams for energy storage projects in the UK [131]

System	Rating & Response		Energy & Power Density				Capital Cost			Ref.
	Power Rating (kW)	Discharge Time	Wh/kg	W/kg	Wh/l	W/l	\$/kW	\$/kWh	¢/kWh/cycle	
Capacitor	0-50	ms-60 min	0.05-5	~100,000	2-10	100,000+	200-400	500-1,000	-	[111]
Super-Capacitor	0-300	ms-60 min	2.5-15	500-5,000	10-30	100,000+	100-300	300-2,000	2-20	[111]
SMES	100-10,000	ms-8 s	0.5-5	500-2,000	0.2-2.5	1,000-4,000	200-300	1,000-10,000	-	[111, 135]
Li-Ion Bat.	0-100	s-4.5hrs	75-200	150-315	200-500	-	1,200-4,000	600-2,500	15-100	[111, 131, 135]
Ni-Cad Bat.	0-40,000	s-hr	50-75	150-300	60-150	-	500-1,500	800-1,500	20-100	[111]
Lead-Acid Bat.	0-20,000	s-hr	30-50	75-300	50-80	10-400	300-600	200-400	20-100	[111]
Na-S Bat.	50-8,000	s-hr	150-240	150-230	150-250	-	1,000-3,000	300-500	8-20	[111]
ZEBRA	0-300	s-hr	100-120	150-200	150-180	220-300	150-300	100-200	5-10	[111]
VRFB	30-3,000	ms-10 hr	10-30	-	16-33	-	600-1,500	150-1,000	5-80	[111, 158-160]
Zn-Br Bat.	50-2,000	s-10 hr	30-50	-	30-60	-	700-2,500	150-1,000	5-80	[111]
Zn-Air Bat.	0-10	s-24+ hr	150-3,000	-	500-10,000	-	100-250	10-60	-	[111]
PSB	1,000-15,000	s-10 hr	-	-	-	-	700-2,500	150-1,000	5-80	[111]
Hydrogen	0-50,000	s-24+ hr	800-10,000	500+	500-3,000	500+	10,000+	-	6,000-20,000	[111]
Pumped-Hydro	100-5,000 (MW)	1-24+ hr	0.5-1.5	-	0.5-1.5	-	600-2,000	5-100	0.1-1.4	[111, 135]
Hydraulic	-	-	-	-	-	-	-	-	-	[161, 162]
CAES	5-300 (MW)	1-24+ hr	30-60	-	3-6	0.5-2	400-8000	2-50	2-4	[111, 135]
Flywheel	0-250	ms-15 min	10-30	400-1,500	20-80	1,000-2,000	250-350	1,000-5,000	3-25	[111]
LAES	100-300,000	1-8 hr	150-250	10-30	120-200	-	200-300	3-30	2-4	[111, 136-138]

Table A.2: Comparison of ESSs - Rating &amp; Response, Energy &amp; Power Density and Capital Costs

System	Storage Duration		Life Time		Environmental Impact	Ref.
	Self Discharge per Day (%)	Suitable Storage Duration	Life Time (yrs)	Cycle Life (cycles)		
Capacitor	40	s-hr	~5	50,000+	Little amount of remains	[111]
Super-Capacitor	20-40	s-hr	20+	100,000+	Little amount of remains	[111]
SMES	10-15	min-hr	20+	100,000+	Strong mag fields	[111]
Li-Ion Bat.	0.1-0.3	min-day	5-15	1,000-10,000+	-	[111, 158]
Ni-Cad Bat.	0.2-0.6	min-day	10-20	2,000-2,500	-	[111, 135]
Lead-Acid Bat.	0.1-0.3	min-day	5-15	500-1,000	Toxic remains	[111]
Na-S Bat.	~20	s-hr	10-15	2,500	-	[111]
ZEBRA	~15	s-hr	10-14	2,500+	-	[111]
VRFB	Small	hr-mnth	5-20+	12,000-14,000+	Toxic remains	[111, 158–160]
Zn-Br Bat.	Small	hr-mnth	5-10	2,000+	-	[111]
Zn-Air Bat.	V. Small	hr-mnth	-	100-300	Little amount of remains	[111]
PSB	Small	hr-mnth	10-15	-	-	[111]
Hydrogen	~0	hr-mnth	5-15	1,000+	Little amount of remains	[111]
Pumped-Hydro	V. Small	hr-mnth	40-60	-	Large areas flooded	[111]
Hydraulic	-	-	-	-	-	[161, 162]
CAES	Small	hr-yr	20-40	-	-	[111, 135]
Flywheel	100	s-min	~15+	20,000+	Almost none	[111]
LAES	0.5-1	min-day	20-40	-	Removes contaminants from air during charging	[111, 136–138]

Table A.3: Comparison of ESSs - Storage Duration, Life Time and Environmental Impact

# Appendix C: Turbine Layout Optimisation Case Studies

Information for the two turbine layout optimisation case studies in Chapter 3, a large hypothetical offshore wind farm and representative data for the Berwick Bank offshore wind farm.

## C.1 Case Study 1: Hypothetical Wind Farm

Table A.4: Coordinates for the hypothetical wind farm boundary and obstacles

Wind farm boundary		Obstacle 1		Obstacle 2	
Easting (m)	Northing (m)	Easting (m)	Northing (m)	Easting (m)	Northing (m)
1	1217	7100	8400	2250	8000
61	8649	7500	5625	3200	7600
2309	11049	7750	5800	3300	7200
6573	10313	7300	8000	2400	6700
11021	8000			2000	6400
7500	5500			1750	7300
8000	533				
2221	1				

Table A.5: Non-uniform distribution of wind speed and direction probabilities, from wind scenario 3 by [37] (probability values given in %)

Wind direction (deg)	8 ms <sup>-1</sup>	12 ms <sup>-1</sup>	17 ms <sup>-1</sup>
0<deg≤10	1.49	1.05	0.25
10<deg≤20	1.49	1.56	0.25
20<deg≤30	1.49	2.09	0.25
30<deg≤40	1.49	2.04	2.56
40<deg≤50	1.49	3.16	2.50
50<deg≤60	1.49	2.04	2.56
60<deg≤70	1.49	2.09	0.25
70<deg≤80	1.49	1.56	0.25
80<deg≤90	1.49	1.05	0.25
90<deg≤100	1.49	0.51	0.25
...	1.49	0.51	0.25
10 deg increments	1.49	0.51	0.25
...	1.49	0.51	0.25
350<deg≤360	1.49	0.51	0.25

## C.2 Case Study 2: Berwick Bank Offshore Wind Farm

Table A.6: Coordinates for the Berwick Bank offshore wind farm boundary

Wind farm boundary	
Easting (m)	Northing (m)
605970	6221440
600172	6214137
599791	6223958
587874	6223704
584231	6222134
580665	6243990
582808	6246355
581328	6252545
580699	6255179
581778	6255835
582985	6256597
583556	6257001
584212	6257465
584951	6257991
584975	6258008
585461	6258354
586922	6259497
586999	6259556
588340	6260597
589569	6260796
592835	6261322
594774	6261635
595656	6259381
595691	6259291
596637	6256872
601287	6244949
602218	6242562
608977	6225228
606201	6221731

Table A.7: Representative wind speed and direction probabilities for the Berwick Bank offshore wind farm site (probability values given in %) (Part 1: 0 deg - 205 deg)

Wind direction (deg)	1.5ms <sup>-1</sup>	5ms <sup>-1</sup>	9ms <sup>-1</sup>	13ms <sup>-1</sup>	17ms <sup>-1</sup>	22ms <sup>-1</sup>
0<deg≤5	0.071	0.245	0.352	0.249	0.109	0.020
5<deg≤10	0.084	0.280	0.352	0.234	0.068	0.017
10<deg≤15	0.090	0.279	0.353	0.216	0.059	0.016
15<deg≤20	0.083	0.317	0.346	0.202	0.067	0.021
20<deg≤25	0.085	0.321	0.337	0.183	0.058	0.014
25<deg≤30	0.079	0.308	0.267	0.139	0.041	0.005
30<deg≤35	0.081	0.263	0.230	0.138	0.039	0.004
35<deg≤40	0.086	0.243	0.261	0.111	0.034	0.008
40<deg≤45	0.093	0.262	0.233	0.132	0.021	0.011
45<deg≤50	0.093	0.256	0.217	0.118	0.025	0.011
50<deg≤55	0.094	0.248	0.191	0.109	0.027	0.005
55<deg≤60	0.101	0.253	0.174	0.091	0.025	0.007
60<deg≤65	0.084	0.236	0.165	0.116	0.023	0.008
65<deg≤70	0.095	0.246	0.214	0.104	0.019	0.003
70<deg≤75	0.098	0.236	0.207	0.102	0.030	0.003
75<deg≤80	0.093	0.230	0.197	0.088	0.023	0.006
80<deg≤85	0.096	0.222	0.180	0.097	0.048	0.002
85<deg≤90	0.097	0.219	0.205	0.133	0.052	0.008
90<deg≤95	0.084	0.219	0.228	0.137	0.037	0.006
95<deg≤100	0.085	0.224	0.257	0.137	0.048	0.011
100<deg≤105	0.090	0.227	0.265	0.130	0.056	0.013
105<deg≤110	0.091	0.228	0.261	0.129	0.095	0.010
110<deg≤115	0.096	0.236	0.270	0.154	0.082	0.029
115<deg≤120	0.096	0.244	0.242	0.182	0.079	0.032
120<deg≤125	0.091	0.279	0.285	0.211	0.091	0.025
125<deg≤130	0.091	0.286	0.289	0.232	0.115	0.027
130<deg≤135	0.098	0.292	0.296	0.273	0.150	0.027
135<deg≤140	0.098	0.335	0.309	0.284	0.170	0.033
140<deg≤145	0.087	0.322	0.363	0.310	0.181	0.038
145<deg≤150	0.091	0.332	0.389	0.324	0.190	0.048
150<deg≤155	0.085	0.354	0.427	0.375	0.226	0.087
155<deg≤160	0.084	0.359	0.428	0.369	0.277	0.127
160<deg≤165	0.079	0.360	0.459	0.450	0.301	0.134
165<deg≤170	0.079	0.389	0.503	0.502	0.327	0.145
170<deg≤175	0.089	0.335	0.518	0.516	0.368	0.134
175<deg≤180	0.086	0.374	0.480	0.470	0.361	0.140
180<deg≤185	0.082	0.352	0.472	0.530	0.332	0.121
185<deg≤190	0.095	0.348	0.462	0.546	0.293	0.094
190<deg≤195	0.089	0.315	0.466	0.472	0.241	0.075
195<deg≤200	0.088	0.317	0.477	0.422	0.200	0.071
200<deg≤205	0.097	0.305	0.504	0.479	0.236	0.084

Table A.8: Representative wind speed and direction probabilities for the Berwick Bank offshore wind farm site (probability values given in %) (Part 2: 205 deg - 360 deg)

Wind direction (deg)	1.5ms <sup>-1</sup>	5ms <sup>-1</sup>	9ms <sup>-1</sup>	13ms <sup>-1</sup>	17ms <sup>-1</sup>	22ms <sup>-1</sup>
205<deg≤210	0.099	0.314	0.476	0.545	0.300	0.125
210<deg≤215	0.098	0.316	0.501	0.620	0.311	0.164
215<deg≤220	0.090	0.338	0.481	0.598	0.339	0.166
220<deg≤225	0.087	0.341	0.480	0.583	0.355	0.148
225<deg≤230	0.089	0.340	0.506	0.575	0.344	0.147
230<deg≤235	0.079	0.358	0.552	0.566	0.347	0.148
235<deg≤240	0.082	0.357	0.584	0.656	0.436	0.169
240<deg≤245	0.085	0.381	0.656	0.750	0.509	0.234
245<deg≤250	0.085	0.413	0.695	0.892	0.624	0.261
250<deg≤255	0.085	0.407	0.747	1.066	0.725	0.276
255<deg≤260	0.083	0.378	0.717	0.989	0.655	0.248
260<deg≤265	0.068	0.339	0.677	0.930	0.619	0.204
265<deg≤270	0.077	0.353	0.655	0.888	0.496	0.206
270<deg≤275	0.084	0.340	0.604	0.773	0.389	0.164
275<deg≤280	0.073	0.314	0.624	0.723	0.305	0.095
280<deg≤285	0.071	0.299	0.587	0.646	0.226	0.059
285<deg≤290	0.078	0.278	0.470	0.440	0.127	0.025
290<deg≤295	0.065	0.248	0.384	0.334	0.086	0.015
295<deg≤300	0.073	0.256	0.346	0.239	0.060	0.008
300<deg≤305	0.070	0.260	0.325	0.187	0.047	0.016
305<deg≤310	0.080	0.257	0.293	0.169	0.055	0.013
310<deg≤315	0.080	0.250	0.287	0.208	0.047	0.011
315<deg≤320	0.079	0.233	0.281	0.215	0.058	0.013
320<deg≤325	0.084	0.216	0.280	0.217	0.070	0.015
325<deg≤330	0.079	0.208	0.305	0.213	0.100	0.024
330<deg≤335	0.076	0.224	0.337	0.267	0.122	0.033
335<deg≤340	0.080	0.249	0.340	0.293	0.132	0.034
340<deg≤345	0.083	0.245	0.391	0.338	0.162	0.026
345<deg≤350	0.073	0.247	0.398	0.317	0.161	0.043
350<deg≤355	0.087	0.276	0.385	0.304	0.153	0.035
355<deg≤360	0.066	0.284	0.368	0.320	0.124	0.039

Table A.9: Electrical power output and thrust coefficients of the representative turbine, provided by SSE.

Wind speed ( $\text{ms}^{-1}$ )	Power (kW)	Thrust coefficient
1	0	0.00
2	0	0.00
3	0	0.00
4	620	0.92
5	1580	0.80
6	2920	0.80
7	4740	0.80
8	7090	0.80
9	10020	0.80
10	13290	0.80
11	15920	0.75
12	17310	0.57
13	17810	0.45
14	17950	0.36
15	17990	0.29
16	18000	0.24
17	18000	0.20
18	18000	0.17
19	18000	0.14
20	18000	0.12
21	18000	0.11
22	18000	0.09
23	18000	0.08
24	18000	0.07
25	18000	0.06
26	0	0.00
27	0	0.00
28	0	0.00
29	0	0.00
30	0	0.00

# Appendix D: Cable Layout Optimisation Comparison

This section contains turbine positions for the hypothetical offshore wind farm case study and Berwick Bank site study. The full set of results for the cable routing optimisation study are also included.

## D.1 Hypothetical Wind Farm Turbine Positions

Turbine positions and full set of results for the cable layout optimisation algorithm comparison in Chapter 4.

Table A.10: Turbine positions for cable layout optimisation comparison.

No.	x-coord. (m)	y-coord. (m)	No.	x-coord. (m)	y-coord. (m)	No.	x-coord. (m)	y-coord. (m)
1	9162	8866	42	1459	9672	83	3089	4428
2	9751	8360	43	2027	9056	84	3682	3842
3	10366	7749	44	2612	8415	85	4283	3277
4	6840	10077	45	3158	7863	86	4834	2665
5	7417	9560	46	3749	7313	87	5427	2092
6	8012	8956	47	4352	6739	88	6015	1465
7	8549	8369	48	4923	6144	89	6586	852
8	9120	7715	49	5499	5556	90	140	6202
9	9714	7172	50	6108	4973	91	739	5644
10	5644	10171	51	6713	4370	92	1345	5068
11	6231	9584	52	7299	3769	93	1892	4464
12	6802	8979	53	839	9096	94	2477	3872
13	7384	8375	54	1441	8473	95	3059	3281
14	7906	7756	55	2041	7854	96	3652	2705
15	8539	7139	56	3146	6743	97	4232	2112
16	3881	10694	57	3747	6164	98	4823	1494
17	4491	10176	58	4324	5577	99	5426	883
18	5061	9596	59	4886	4963	100	119	5049
19	5628	8986	60	5506	4412	101	703	4491
20	6227	8389	61	6068	3808	102	1287	3895
21	6810	7777	62	6679	3231	103	1857	3300
22	7967	6607	63	7255	2641	104	2465	2733
23	2690	10802	64	7765	1997	105	3051	2124
24	3273	10211	65	216	8521	106	3635	1534
25	3835	9600	66	785	7934	107	4188	900
26	4412	9018	67	1450	7307	108	4797	321
27	4990	8445	68	2565	6193	109	107	3894
28	5594	7867	69	3159	5605	110	680	3330
29	6190	7270	70	3736	4985	111	1290	2700
30	6767	6682	71	4296	4380	112	1866	2119
31	7362	6066	72	4908	3838	113	2447	1519
32	2073	10234	73	5467	3212	114	3009	939
33	2662	9622	74	6072	2641	115	3588	335
34	3229	9004	75	6622	2048	116	96	2739
35	3813	8406	76	7229	1426	117	635	2178
36	4417	7840	77	7807	841	118	1239	1529
37	5006	7271	78	172	7353	119	1800	951
38	5592	6669	79	772	6782	120	2402	350
39	6172	6075	80	1399	6205	121	87	1589
40	6735	5527	81	1979	5627	122	644	992
41	7313	4914	82	2531	5025			

## D.2 Berwick Bank Offshore Wind Farm Turbine Positions

Table A.11: Turbine positions for the Berwick Bank cable layout study.

No.	x-coord. (m)	y-coord. (m)	No.	x-coord. (m)	y-coord. (m)	No.	x-coord. (m)	y-coord. (m)
1	581491	6255492	44	586137	6237392	87	592464	6230121
2	584700	6257694	45	584518	6234346	88	590844	6227075
3	583080	6254647	46	582898	6231300	89	589225	6224029
4	587909	6259895	47	595825	6251778	90	600532	6241461
5	586289	6256848	48	594205	6248732	91	598912	6238414
6	584669	6253802	49	592586	6245686	92	597293	6235368
7	583050	6250756	50	590966	6242640	93	595673	6232322
8	589498	6259050	51	589346	6239593	94	594053	6229276
9	587878	6256003	52	587727	6236547	95	592434	6226230
10	586259	6252957	53	586107	6233501	96	602121	6240616
11	584639	6249911	54	584487	6230455	97	600502	6237569
12	583019	6246865	55	597414	6250933	98	598882	6234523
13	581400	6243819	56	595795	6247887	99	597262	6231477
14	592707	6261251	57	594175	6244841	100	595643	6228431
15	591087	6258205	58	592555	6241795	101	594023	6225385
16	589468	6255158	59	590936	6238748	102	602091	6236724
17	587848	6252112	60	589316	6235702	103	600471	6233678
18	586228	6249066	61	587696	6232656	104	598852	6230632
19	584609	6246020	62	586076	6229610	105	597232	6227586
20	582989	6242974	63	584457	6226564	106	595612	6224540
21	581369	6239928	64	599004	6250088	107	603680	6235879
22	594296	6260406	65	597384	6247042	108	602061	6232833
23	592677	6257359	66	595764	6243996	109	600441	6229787
24	591057	6254313	67	594144	6240950	110	598821	6226741
25	589437	6251267	68	592525	6237903	111	603650	6231988
26	587818	6248221	69	590905	6234857	112	602030	6228942
27	586198	6245175	70	589285	6231811	113	600411	6225896
28	584578	6242129	71	587666	6228765	114	605239	6231143
29	582959	6239082	72	586046	6225719	115	603620	6228097
30	594266	6256514	73	584426	6222673	116	602000	6225051
31	592646	6253468	74	598973	6246197	117	600380	6222004
32	591027	6250422	75	597353	6243151	118	606829	6230298
33	589407	6247376	76	595734	6240105	119	605209	6227252
34	587787	6244330	77	594114	6237058	120	603589	6224206
35	586168	6241284	78	592494	6234012	121	601970	6221159
36	584548	6238237	79	590875	6230966	122	600350	6218113
37	582928	6235191	80	589255	6227920	123	606798	6226407
38	595855	6255669	81	587635	6224874	124	605179	6223361
39	594236	6252623	82	600562	6245352	125	603559	6220314
40	592616	6249577	83	598943	6242306	126	601939	6217268
41	590996	6246531	84	597323	6239259	127	608387	6225562
42	589377	6243485	85	595703	6236213	128	606768	6222516
43	587757	6240439	86	594084	6233167			

### D.3 Full Set of Results

Table A.12: Full results of the 3 cable layout optimisation methods for the hypothetical test cases of 10, 15, and 25 turbines.

No. turbines	Objective value (£) (Optimality ratio)			Comp. time (s)		
	MILP	ACO	ACOsp	MILP	ACO	ACOsp
10	22,064,833	22,408,394	22,064,833	2	5	56
10	22,064,833	22,218,796	22,064,833	3	5	62
10	22,064,833	22,818,266	22,064,833	3	5	43
10	22,064,833	23,390,878	22,064,833	2	5	56
10	22,064,833	22,082,901	22,082,901	3	5	59
10	22,064,833	23,065,385	22,064,833	3	5	52
10	22,064,833	22,064,833	22,064,833	3	5	44
10	22,064,833	23,688,668	22,064,833	3	5	34
10	22,064,833	22,850,863	22,082,901	3	5	59
10	22,064,833	22,082,901	22,064,833	3	5	65
15	30,945,049	30,945,049	30,945,049	9	8	46
15	30,945,049	30,962,130	30,945,049	9	8	42
15	30,945,049	30,945,049	30,945,049	9	8	48
15	30,945,049	30,945,049	30,945,049	9	8	44
15	30,945,049	30,945,049	30,945,049	9	8	37
15	30,945,049	30,945,049	30,945,049	9	8	36
15	30,945,049	30,981,350	30,945,049	9	8	42
15	30,945,049	31,473,244	30,945,049	9	8	84
15	30,945,049	31,318,610	30,945,049	9	8	33
15	30,945,049	31,292,432	30,945,049	9	8	46
25	50,235,935	51,400,208	50,726,894	32	18	184
25	50,235,935	51,082,109	50,517,433	31	18	184
25	50,235,935	51,435,071	50,906,992	32	19	117
25	50,235,935	50,726,894	50,638,853	30	19	130
25	50,235,935	50,986,235	51,120,941	31	19	84
25	50,235,935	52,211,013	50,863,738	31	19	153
25	50,235,935	52,834,868	50,638,853	31	19	152
25	50,235,935	51,298,347	51,002,778	31	18	114
25	50,235,935	50,986,235	50,254,400	31	19	96
25	50,235,935	51,778,689	50,831,666	31	18	118

Table A.13: Full results of the 3 cable layout optimisation methods for the hypothetical test cases of 40, 61, and 122 turbines. (Results in italics indicate an unfinished result).

No. turbines	Objective value (£) (Optimality ratio)			Comp. time (s)		
	MILP	ACO	ACOSP	MILP	ACO	ACOSP
40	68,683,109	69,616,813	68,773,414	211	55	533
40	68,683,109	69,438,084	68,683,109	203	49	461
40	68,683,109	69,840,373	68,780,011	202	53	504
40	68,683,109	69,727,906	68,860,675	202	53	503
40	68,683,109	68,792,808	69,588,458	203	45	374
40	68,683,109	69,935,585	69,099,361	202	45	641
40	68,683,109	69,621,046	68,683,109	205	54	733
40	68,683,109	69,817,395	73,987,050	204	54	261
40	68,683,109	69,686,863	68,938,338	205	54	508
40	68,683,109	70,462,463	71,391,926	204	45	371
61	103,255,681	108,888,532	104,495,408	1001	166	918
61	103,255,681	109,304,565	105,255,466	946	168	1531
61	103,255,681	107,852,746	104,171,024	948	169	1454
61	103,255,681	109,067,619	104,156,885	949	169	2056
61	103,255,681	108,366,035	104,939,532	950	166	1264
61	103,255,681	107,900,829	105,021,094	943	148	1379
61	103,255,681	111,998,888	105,113,423	943	156	773
61	103,255,681	111,298,981	104,874,937	948	173	1660
61	103,255,681	125,194,485	104,634,856	942	158	1909
61	103,255,681	107,796,489	103,856,300	941	164	2226
122	<i>197,401,005</i>	211,786,176	198,257,682	<i>16850</i>	843	12024
122	<i>197,401,005</i>	211,201,872	198,321,383	<i>12280</i>	849	11400
122	<i>197,401,005</i>	211,399,235	200,539,889	<i>12249</i>	865	10012
122	<i>197,401,005</i>	212,635,115	200,543,388	<i>12319</i>	773	7077
122	<i>197,401,005</i>	209,805,860	198,410,360	<i>12391</i>	846	11103
122	<i>197,401,005</i>	222,826,513	201,505,632	<i>14781</i>	822	9261
122	<i>197,401,005</i>	210,545,252	198,037,874	<i>13303</i>	826	9856
122	<i>197,401,005</i>	211,575,736	198,195,071	<i>13159</i>	865	12906
122	<i>197,401,005</i>	209,910,343	199,846,143	<i>13201</i>	833	9126
122	<i>197,401,005</i>	211,713,753	199,358,479	<i>16639</i>	804	7149

Table A.14: Full results of the 3 optimisation methods for the hypothetical test case of 25 turbines, including the cable crossing constraint.

No. turbines	Objective value (£) (Optimality ratio)			Comp. time (s)		
	MILP	ACO	ACOsp	MILP	ACO	ACOsp
25	50,268,994	52,871,395	50,358,286	79	31	232
25	50,268,994	51,476,879	50,664,055	79	32	169
25	50,268,994	51,444,607	52,079,903	78	31	202
25	50,268,994	51,194,029	50,664,055	78	31	306
25	50,268,994	51,287,461	50,662,610	78	30	180
25	50,268,994	50,638,853	52,128,744	78	30	286
25	50,268,994	51,082,109	50,638,853	78	30	465
25	50,268,994	50,760,320	50,319,503	78	30	163
25	50,268,994	50,664,055	50,465,140	79	30	212
25	50,268,994	51,656,498	50,288,389	79	30	219

# Appendix E: Advanced Cable Layout Optimisation

## Expanded Hypothetical Offshore Wind Farm Site

Table A.15: Coordinates for the existing features in the expanded hypothetical offshore wind farm site.

Existing feature 1		Existing feature 2	
Easting (m)	Northing (m)	Easting (m)	Northing (m)
7250	8000	1000	9500
7100	9000	2250	8100
6750	9500	3300	7600
6500	10750	3400	7200
		4500	6000
		4600	4500
		4250	4000
		4000	3000
		5500	1750
		6000	100

Table A.16: Full set of results for the MILPsp cable layout optimisation of the hypothetical offshore wind farm site.

No. turbines	Objective value (£)	Comp. time (s)	No. turbines	Objective value (£)	Comp. time (s)
10	22,375,329	11	40	69,241,766	129
10	22,375,329	9	40	69,241,766	111
10	22,375,329	10	40	69,241,766	112
10	22,375,329	8	40	69,241,766	113
10	22,375,329	7	40	69,241,766	112
10	22,375,329	7	40	69,241,766	111
10	22,375,329	7	40	69,241,766	111
10	22,375,329	7	40	69,241,766	112
10	22,375,329	7	40	69,241,766	111
10	22,375,329	7	40	69,241,766	111
15	31,535,171	20	61	103,943,119	606
15	31,535,171	18	61	103,943,119	539
15	31,535,171	18	61	103,943,119	537
15	31,535,171	18	61	103,943,119	539
15	31,535,171	18	61	103,943,119	533
15	31,535,171	19	61	103,943,119	532
15	31,535,171	19	61	103,943,119	530
15	31,535,171	19	61	103,943,119	537
15	31,535,171	19	61	103,943,119	533
15	31,535,171	19	61	103,943,119	625
25	50,599,172	42	122	198,199,811	6133
25	50,599,172	40	122	198,199,811	5948
25	50,599,172	41	122	198,199,811	5907
25	50,599,172	40	122	198,199,811	5897
25	50,599,172	39	122	198,199,811	5882
25	50,599,172	39	122	198,199,811	6001
25	50,599,172	39	122	198,199,811	6340
25	50,599,172	39	122	198,199,811	6228
25	50,599,172	41	122	198,199,811	6766
25	50,599,172	40	122	198,199,811	6823